

Identification and use of novel vasodilators in the prevention of cisplatin-induced acute kidney injury

By **Kristen Renee McSweeney, B. Sc. (Hons)**

In total fulfilment of the requirements for the degree of

Doctor of Philosophy

Victoria University, Australia

Institute for Health and Sport (IHES)

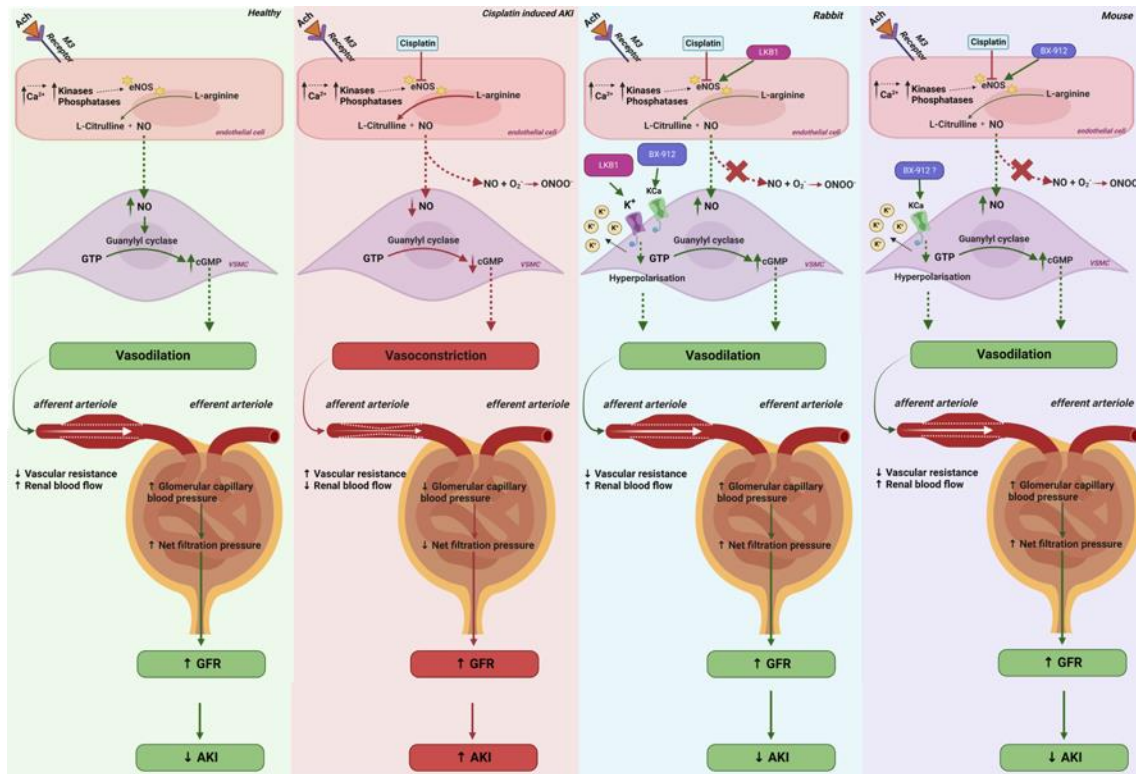
February 2023

Abstract

Background: Cisplatin (CDDP) is a potent chemotherapy; however, its use is limited by its dose-limiting side effect, nephrotoxicity, which primarily manifests as acute kidney injury (AKI) and occurs in 20-30% of patients. Cisplatin-induced acute kidney injury (CIAKI) is characterised by afferent arteriole vasoconstriction stimulated by CDDP-induced endothelial dysfunction. Endothelial dysfunction is characterised by impaired endothelial nitric oxide synthase (eNOS) phosphorylation, reduced nitric oxide (NO) bioavailability, and increased renal microvasculature vasoconstriction. This subsequently reduces renal blood flow, increases vascular resistance, and decreases glomerular capillary blood pressure and net filtration pressure, resulting in a reduced glomerular filtration rate (GFR). When untreated reduced GFR can quickly worsen and manifest in the clinical presentation of CIAKI. This decreases patient quality of life and increases the risk of mortality, thus, novel vasodilators are required. The direction of this thesis was split into three studies: *Chapters 3 and 4*, identification of novel pharmaceutical vasodilators (LKB1 and BX); *Chapter 5*, establishing a dose of CDDP without causing irreversible kidney pathologies in an animal model and *Chapter 6*, assessment of the identified novel vasodilator with the most significant potential determined in Chapters 3 and 4. **Method:** *In chapters 3 and 4*, New Zealand White (male) rabbit blood vessels (thoracic aorta, interlobar arteries, and mesenteric arteries) were assessed for vascular function using isometric tension analysis to determine a novel vasodilator to be used in a CIAKI model. *Chapter 5*, A clinical and physiologically relevant model of CIAKI, was used to determine the efficacy of two clinically relevant doses of CDDP (6.25 and 12.5 mg/kg) to induce reversible pathological kidney damage. Mice were euthanised 72 hours after CDDP administration. *Chapter 6*, This regimen (12.5 mg/kg) was chosen to assess BX in the prevention of CIAKI. Mice received a daily dose of BX (5, 0.5 or 0.05 mg/kg) on days 0-3 and a single dose of 12.5mg/kg of CDDP on day one via IP injection. Mice were euthanised for *ex vivo* experiments, including isometric tension for vascular function analysis, histology to determine kidney damage via periodic acid Schiff's (PAS) stain and immunohistochemistry (IHC) to investigate protein expression of kidney injury, ER stress and pro-inflammatory biomarkers associated with CIAKI. RT² profiler PCR was used analyse gene up/down-regulation of genes associated with nephrotoxicity, and SEM was used to investigate the effects of platinum accumulation. **Significant Results and Conclusions:** *Chapters 3 and 4*, LKB1 and BX were direct vasodilators. Both drugs partly mediated their effects through K⁺ channels; however, LKB1-induced relaxation was also partly endothelial-dependent. BX was chosen to progress within the

model of CIAKI. This was justified due to the ability of BX to induce vasodilation mainly through non-endothelial-dependent mechanisms. **Chapter 5**, the results of the CIAKI dose-finding study showed that CDDP 12.5 mg/kg induced a more clinically relevant degree of damage to both the kidney and the vasculature compared to 6.25 mg/kg, suggesting it is a more suitable dose for use in this CIAKI model. **Chapter 6**, BX improved acetylcholine (ACH)-induced relaxation suggesting it may influence endothelial function. Surprisingly, BX reduced angiotensin II (ANGII)-induced vasoconstriction, suggesting it may display ARB properties. BX significantly reduced protein expression of key biomarkers associated with CIAKI, including kidney injury molecular 1 (KIM-1), glucose-regulated protein 78 (GRP78), intracellular adhesion molecule 1 (ICAM-1), vascular cell adhesion molecule 1 (VCAM-1) and E-Selectin. This pilot study provides evidence that BX could inhibit CIAKI. A more extensive animal study is warranted to confirm these results.

Graphical abstract: Prevention of CDDP-induced endothelial dysfunction and the associated reduced renal blood flow.



Graphical Abstract. Representation of enhanced vasodilation of LKB1 and BX as a therapeutic target to restore renal blood flow and reduce glomerular filtration rate associated with CIAKI. Figure Created with BioRender.com. CDDP treatment results in decreased eNOS, reduced NO bioavailability and reduced afferent arteriole vasodilation. This results in reduced RBF, decreased glomerular capillary blood pressure, impaired net filtration pressure, and ultimately reduced GFR. If left untreated reduced GFR can rapidly worsen and be diagnosed clinically as AKI. This diagram represents **A. Healthy function**, **B. endothelial dysfunction triggered by CDDP** and the signalling cascade leading to reduced GFR **C. the hypothesized role of LKB1 and BX in reducing impaired RBF based on its mechanisms in rabbits to prevent the development of CIAKI** and **D. proposed effects of BX-912 in the prevention of CIAKI through increased vasodilation and subsequent increase in GFR.**

Doctor of Philosophy Student Declaration

“I, Kristen Renee McSweeney, declare that the PhD thesis entitled “*Identification and use of novel vasodilators in the prevention of cisplatin-induced acute kidney injury*” is no more than 80,000 words in length including quotes and exclusive of tables, figures, appendices, bibliography, references, and footnotes. This thesis contains no material that has been submitted previously, in whole or in part, for the award of any other academic degree or diploma. Except where otherwise indicated, this thesis is my own work”.

“I have conducted my research in alignment with the Australian Code for the Responsible Conduct of Research and Victoria University’s Higher Degree by Research Policy and Procedures.

Signature



Date: 03/02/2023

Institute for Health and Sport (IHES), Victoria University,

Melbourne, Victoria, 8001, Australia

Ethics Declaration

“All research procedures reported in the thesis were approved by the Victoria University Animal ethics committee”, AEC project 20/003.

Signature



Date: 03/02/2023

Acknowledgements

This list of thank-yous is extensive, and I cannot possibly name everyone, however,

Firstly, I would like to thank my supervisors, Associate Professor Anthony Zulli and Professor Vasso Apostolopoulos who have been excellent mentors and have supported and encouraged me throughout my PhD. Notably, Anthony, you have not only taught me how to be a scientist and a researcher but have contributed to helping me grow as a person that will help me in the future. I cannot thank you both enough.

To Laura, your friendship and support throughout these past few years will never be forgotten, and I will miss our 3 am giggling sessions on long experiment days when the overtiredness kicked in. I could not have gotten through the past few years had I not had you to lean on and help; I will forever be grateful for that.

To Tawar, I will always cherish the time you took to teach me; no matter how many times I asked you to re-explain how to calculate drug doses, your patience was profound. I vow to display your enthusiasm for science and positivity towards life. Your memory will live on, and I am forever grateful to have been touched by your presence, rest in eternal peace. We will beat cancers butt for you!

To mention a few others, Renee, Alex, and Balu, thank you for teaching me to help build my fundamental research skills. Anne, Kelly, Steve (our AWO) and all the technical staff, thank you for your guidance and support and for monitoring my animals when you could start to see how exhausted I was getting.

To all the students I helped supervise, thank you for letting me teach the things I learned from those who preceded me. It was a pleasure getting to know every one of you.

My family, Mum, Dad, Brooke and Blake, thank you for dealing with my never-ending meltdowns, random breakthrough babbles, and your endless support through my PhD and my entire educational journey. I will forever cherish your love for always encouraging my passion for learning. Tony, thank you for always showing enthusiasm towards what I do. You may not understand much of what I talk about but thank you for always being enthusiastic about my graphs, being emotional support, and helping me see the positives. Megan, we lived together for a short time; however, I will forever be grateful for your support throughout the pandemic and the most challenging part of my PhD and for showing me that it is okay to have fun at the same time as doing postgraduate studies. To David, thank you for allowing me to have such a flexible work schedule, always allowing me to put my education first, and always being so gracious when things arise at Uni.

Lastly, I want to dedicate this to everyone who has ever doubted what they can accomplish and remind them that no matter their potential is infinite if they work hard.

DETAILS OF INCLUDED PAPERS: THESIS WITH PUBLICATION

Please list details of each scholarly publication and/or manuscript included in the thesis submission. Copies of published scholarly publications and/or manuscripts submitted and/or final draft manuscripts should also be included in the thesis submission.

This table must be incorporated in the thesis before the Table of Contents.

Chapter No.	Publication Title	Publication Status <ul style="list-style-type: none"> Published Accepted for publication In revised and resubmit stage Under review Manuscript ready for submission 	Publication Details <ul style="list-style-type: none"> Citation, if published Title, Journal, Date of acceptance letter and Corresponding editor's email address Title, Journal, Date of submission
Chapter 1	Mechanisms of Cisplatin-Induced Acute Kidney Injury: Pathological Mechanisms, Pharmacological Interventions, and Genetic Mitigations	Published	McSweeney, K.R.; Gadanec, L.K.; Qaradakhi, T.; Ali, B.A.; Zulli, A.; Apostolopoulos, V. Mechanisms of Cisplatin-Induced Acute Kidney Injury: Pathological Mechanisms, Pharmacological Interventions, and Genetic Mitigations. <i>Cancers</i> 2021, 13, 1572.

Declaration by [candidate name]:

Kristen McSweeney

Signature:

Kristen

Digitally signed by
Kristen McSweeney

McSweeney

Date: 2023.02.03
04:04:50 +11'00'

Date:

03/02/2023

PRIVACY STATEMENT Victoria University (VU) values your privacy and is committed to handling your personal information in accordance with the Privacy and Data Protection Act 2014 (Vic) and other applicable privacy legislation. The personal information collected on this form will be used primarily for the purposes of assessing and processing this application. VU may also use and disclose your personal information to verify the information provided by you, to comply with government and other reporting requirements and/or to carry out associated activities connected with this application. Your personal information may also be disclosed to Commonwealth and State agencies such as the Department of Education and Training and the Department of Home Affairs in accordance with VU's obligations under the Education Services for Overseas Students Act 2000 (Cth) (ESOS Act), the National Code of Practice for Providers of Education and Training to Overseas Students 2018 (National Code) and other applicable legislation. Your personal information will not otherwise be used or disclosed without your consent, unless permitted by law. By completing and submitting this application, you agree to VU collecting, using and disclosing your personal information as described above and in accordance with VU's Privacy Policy and Student Information Privacy Collection Statement (which provides further detail about the types of personal information VU may collect from you and how it is managed) available on the Privacy page on our website vu.edu.au/privacy You have a right to access your personal information held by VU. If you have any questions regarding privacy, please refer to the Privacy page on our website, our frequently asked questions at ASKVU or phone us on 9919 6100 or 1300 VIC UNI (or 1300 842 864).

PRIVACY INFORMATION: We collect and protect your personal information in accordance with our Privacy Policy vu.edu.au/privacy.

Victoria University CRICOS Provider No. 00124K (Melbourne) and CRICOS Provider No. 02475D (Sydney). RTO Code: 3113. ABN: 83 776 954 731

Table of Contents

Abstract	2
Graphical abstract: Prevention of CDDP-induced endothelial dysfunction and the associated reduced renal blood flow.	4
Doctor of Philosophy Student Declaration.....	5
Acknowledgements.....	6
Table of figures.....	12
List of tables	15
List of abbreviations	16
List of symbols	20
Chapter 1: Cisplatin-induced acute kidney injury: Up to date.	21
1.1 Introduction	21
1.2 Targeted drug delivery	21
1.3 Ferroptosis.....	23
1.4 Genetics/Epigenetics.....	24
1.5 Inflammation	28
1.6 Cell stress	28
1.7 Apoptosis.....	29
1.8 Natural Supplements.....	30
1.9 Conclusion.....	31
Chapter 2: General Methods.....	32
2.1 Animals / experimental regimens	32
2.1.1 Healthy and atherogenic rabbit model (AEC project 12/013).....	32
2.1.2 Cisplatin-induced AKI (5-day model) (AEC Project 20/003)	32
2.2 Monitoring.....	33
2.2.1 Mice monitoring	33
2.3 Anesthesia and culling	34
2.3.1 Rabbit.....	34
2.3.2 2.3.2 Mouse	34
2.4 Dissection	34
2.4.1 Rabbit dissection.....	34
2.4.2 Mouse dissection	35
2.5 2.5 EchoMRI	35
2.6 Isometric tension analysis	35
2.6.1 Rabbit drug stimulations	36
2.6.2 Mouse drug stimulations.....	37
2.7 Tissue processing.....	38

2.8	Histology	38
2.8.1	Immunohistochemistry	38
2.8.2	PAS stain.....	39
2.9	Semi-Quantification of immunohistochemistry slides	40
2.10	SEM metal composition analysis.....	42
2.11	Nephrotoxicity real-time (RT ²) profiler PCR.....	43
2.11.1	RNA isolation protocol.....	43
2.11.2	cDNA synthesis protocol	43
2.11.3	RT ² profiler PCR arrays protocol.....	44
2.12	Statistical analysis	44
2.12.1	ANOVA	44
2.12.2	Cohen's d	45
2.13	Solutions	45
2.13.1	Drug formulations.....	45
2.14	General chemicals	47
Chapter 3:	LKB1, identification as a novel vasodilator.....	49
3.1	Abstract	49
3.2	Introduction.....	50
3.3	Methods.....	52
3.3.1	Materials.....	52
3.3.2	Animals	52
3.4	Isometric tension.....	52
3.5	Data/Statistical Analysis	52
3.6	Results	53
3.6.1	LKB1 induces vasodilation in a vessel-specific manner.	53
3.6.2	Effects of vehicle and Atherogenesis on LKB1-induced vasodilation.	55
3.6.3	Mechanistic evaluation of the vasodilatory effects of LKB1.....	59
3.7	Discussion	68
a)	LKB1-induced vasodilation	68
b)	PIM1 kinase as a target for CIAKI treatment	68
c)	Mechanisms of action: KPSS reduced vasodilation in mesenteric arteries. 69	
d)	An AD did not affect LKB1-induced relaxation	70
e)	ODQ does not affect LKB1-induced vasorelaxation.....	70
f)	Pan-PIM kinase inhibitor AZD1208 did not induce relaxation.	70
3.8	Future directions.....	71
3.9	Conclusion.....	71

Chapter 4: BX-912: a potential treatment for reduced renal blood flow and vascular resistance in cisplatin-induced acute kidney injury through its function as a vasodilator.

72

4.1	Abstract	72
4.2	Introduction	73
4.3	Methods.....	75
4.3.1	Materials.....	75
4.3.2	Animals	75
4.3.3	Isometric tension.....	75
4.3.4	Data/Statistical Analysis	76
4.4	Results	76
4.4.1	BX-induced vasodilation is vessel specific.....	76
4.4.2	An AD does not reduce BX-induced relaxation.....	78
4.4.3	BX Mechanistic Analysis.....	82
4.5	Discussion	95
4.6	Limitations	99
4.7	Future studies.....	99
4.8	Conclusion.....	99

Chapter 5: Identification of a CDDP dose that induces vascular dysfunction and pathological kidney damage. 100

5.1	Abstract	100
5.2	Introduction	101
5.3	Methods.....	103
5.3.1	Materials/Chemicals	103
5.3.2	Animals/Experimental Protocol	104
5.3.3	Isometric tension analysis	104
5.3.4	Tissue Processing/Histological and Immunohistochemical analysis	104
5.3.5	Data/Statistical Analysis	104
5.4	Results	105
5.4.1	CDDP 6.25 and 12.5 mg/kg has opposing effects on aortic relaxation. .	105
5.4.2	CDDP does not affect SNP-stimulated vasodilation.	107
5.4.3	Effect of CDDP on ANGII-induced vasoconstriction compared to SHAM mice	108
5.4.4	Weight differences.....	109
5.4.5	CDDP-induced pathological damage.....	111
5.4.6	Immunohistochemical analysis determined that CDDP treatment enhances tubular expression of TNF- α , GRP78 and Tim-1/Kim-1.....	113
5.4.7	Pro-inflammatory markers ICAM-1, VCAM-1 and E-Selectin expression are upregulated by CDDP.	115

5.4.8	VCAM-1 was upregulated in the tubules, glomeruli, and interlobar arteries of CDDP-treated mice.....	117
5.4.9	CDDP-induced E-Selectin upregulation following CDDP treatment. ...	119
5.5	Discussion	121
	a) The CDDP 12.5 group demonstrated an effect (Cohen's d) in reduced ACH-mediated relaxation compared to the SHAM group.	121
5.6	Limitations	126
5.7	Future directions.....	127
5.8	Conclusion.....	127
Chapter 6: BX-912 mitigates cisplatin-induced AKI through improved renal blood flow and reduced inflammation: A pilot study.....		
6.1	Abstract	128
6.2	Introduction	130
6.3	Materials.....	131
6.4	Methods.....	132
	6.4.1 Animals/Experimental Protocol	132
	6.4.2 EchoMRI.....	132
	6.4.3 Isometric Tension	132
	6.4.4 Tissue Processing/Histochemical and Immunohistochemical staining/Analysis.....	132
	6.4.5 SEM analysis.....	133
	6.4.6 RT ² -PCR Analysis	133
	6.4.7 Data/Statistical Analysis	133
6.5	Results	133
	6.5.1 BX, increased ACH and SNP-mediated relaxation compared to CDDP treatment alone.	133
	6.5.2 BX reduced ANGII-induced vasoconstriction in CDDP-treated mice...	137
	6.5.3 Effect of CDDP and CDDP + BX on body composition.....	138
	6.5.4 BX reduces tubular PAS staining.....	139
	6.5.5 BX reduces KIM-1 in tubules and glomeruli of CDDP-treated mice. ...	141
	6.5.6 Inflammatory biomarkers are reduced in BX compared to CDDP treated mice. 143	
	6.5.7 Tubular GRP78 expression is reduced following concomitant administration of BX at various doses.....	150
	6.5.8 Effect of BX on the platinum accumulation in renal glomeruli following CDDP treatment.....	152
	6.5.9 Mouse nephrotoxicity gene expression in CDDP + BX0.05 treated mice. 152	
6.6	Discussion	155
6.7	Future Studies.....	162

6.8	Limitations	162
6.9	Conclusion.....	163
Chapter 7:	General Discussion and Conclusions.....	164
7.1	Major Findings	164
7.1.1	Chapter 3. LKB1, identification as a novel vasodilator.....	165
7.1.2	Chapter 4. BX-912: a potential treatment for reduced renal blood flow and vascular resistance in cisplatin-induced acute kidney injury through its function as a vasodilator.	166
7.1.3	Chapter 5. Identification of a CDDP dose that induces vascular dysfunction and pathological kidney damage.	167
7.1.4	Chapter 6. BX-912 mitigates cisplatin-induced AKI through improved renal blood flow and reduced inflammation: A pilot study.	168
7.2	Future Directions	170
7.2.1	Chapter 3. LKB1, identification as a novel vasodilator.....	170
7.2.2	Chapter 4. BX-912: a potential treatment for reduced renal blood flow and vascular resistance in cisplatin-induced acute kidney injury through its function as a vasodilator.	171
7.2.3	Chapter 5. Identification of a CDDP dose that induces vascular dysfunction and pathological kidney damage.	171
7.2.4	Chapter 6. BX-912 mitigates cisplatin-induced AKI through improved renal blood flow and reduced inflammation: A pilot study.	171
7.3	Limitations of the thesis.....	172
7.3.1	Scanning Electron Microscopy.....	173
7.3.2	Real-time polymerase chain reaction.....	173
7.4	Conclusions:	174
References	176
Appendix A:	Establishing the method- Renal Perfusion	198
Appendix B:	Genes unaffected by BX-912 administration in RT ² profiler PCR experiments in Chapter 6.....	202

Table of figures

Graphical Abstract. Representation of enhanced vasodilation of LKB1 and BX as a therapeutic target to restore renal blood flow and reduce glomerular filtration rate associated with CIAKI.	4
Figure 1.1 Renoprotective mechanisms associated with CIAKI mitigation.	23
Figure 2.1. Treatment timeline for the CIAKI mouse model.	33
Figure 2.2. Schematic diagram of the isometric tension process to assess vascular relaxation. Created with BioRender.com	37
Figure 2.3. Tubule Analysis method using MCID.....	40
Figure 2.4. Immunohistochemical analysis using MCID analysis of DAB-stained Glomeruli.....	40
Figure 2.5. MCID Analysis of Interlobar arteries.....	41
Figure 2.6. Pt analysis area of glomeruli.....	42
Figure 2.7. Mouse Nephrotoxicity RT ² profiler PCR Array Program.....	44
Figure 3.1. LKB1-induced vasodilation is vessel-specific, (n=4-13).....	54
Figure 3.2. LKB1 Dose-response curves and AUC graphs of vehicle vs LKB1 and LKB1 vs AD in TA, ILA, and MA isolated from Male, white New Zealand rabbits (n=4-13).....	57
Figure 3.3. Mechanistic evaluation of eNOS inhibition by L-NAME on LKB1 induced relaxation (n=7-13).	61
Figure 3.4. Effect of mechanical denudation of vessels on LKB1 induced relaxation (n=4-13).....	63
Figure 3.5. LKB1 induced relaxation DRC graphs of CD and AD in TA, ILA, and MA pre-incubated with the sGC inhibitor ODQ (n=8-13).....	64
Figure 3.6. LKB1 DRC graphs of CD and AD in TA, ILA, and MA pre-constricted with 40mM KPSS to non-selectively inhibit potassium channels (n=7-13).	66
Figure 3.7. Vasorelaxation response to cumulative doses of AZD1208 in TA, ILA, and MA of white New Zealand (male) rabbits (n=2-4).....	67
Figure 4.1. BX directly induces vascular relaxation in mesenteric and interlobar arteries but not in thoracic aorta (n=15).	77
Figure 4.3. Graphical illustration of targeted pathways by each drug used to identify the signalling cascade BX uses to induce vascular relaxation.	83
Figure 4.4. Mechanistic evaluation of endothelial dependency via mechanical denudation on BX-induced vasodilation (n=4-15).	84
Figure 4.5. Mechanistic evaluation of BX-induced vasodilation in the presence of eNOS- inhibition, L-NAME (n=5-15).	86
Figure 4.6. BX dose-response curve graphs of CD and AD, thoracic aorta, interlobar arteries, and mesenteric arteries incubated with ODQ (n=5-15).....	87
Figure 4.7. BX dose-response curve graphs of CD and AD, thoracic aorta, interlobar arteries, and mesenteric arteries pre-constricted with 40mM KPSS, (n=4-15).....	89
Figure 4.8. BX dose-response curve graphs of CD, interlobar arteries pre-incubated with various K ⁺ channel inhibitors (n=3-15).....	91
Figure 4.9. BX dose-response curve graphs of CD, mesenteric arteries pre-incubated with various K ⁺ channel inhibitors (n=3-15).....	93
Figure 4.10. Effect of COX-2 inhibition by Indomethacin on BX-induced relaxation DRC, (n=3-15).....	94

Figure 5.1. CDDP effect on vasodilation to cumulative doses of ACH and SNP (10^{-8} to 10^{-5} [M]), (n=4).....	106
Figure 5.2. Effect of Angiotensin II-induced vasoconstriction in the SHAM and CDDP12.5 groups (n=3-4)	109
Figure 5.3. Percentage (%) weight loss of CDDP (6.25 and 12.5) treated mice (n=3-4).	110
Figure 5.4. Histochemical analysis using periodic acid Schiff (PAS) stain of kidney structures, including tubules, glomeruli and interlobar arteries in mice treated with SHAM, CDDP (6.25 or 12.5), (n=3-4).	112
Figure 5.5. Immunohistochemical tubular expression of TNF- α , a pro-inflammatory biomarker, GRP78, an ER stress marker and TIM-1/KIM-1, a kidney injury biomarker (n=3-4).....	114
Figure 5.6. Immunohistochemical staining analysis of ICAM-1 expression in kidney structures, including tubules, glomeruli and interlobar arteries in mice treated with SHAM, CDDP (6.25 or 12.5), (n=3-4).	116
Figure 5.7. Immunohistochemical staining analysis of VCAM-1 expression in renal structures, including tubules, glomeruli and interlobar arteries in mice treated with SHAM, CDDP (6.25 or 12.5), (n=3-4).	118
Figure 5.8. Immunohistochemical staining analysis of E-Selectin expression in kidney structures, including tubules, glomeruli and interlobar arteries in mice treated with SHAM, CDDP (6.25 or 12.5), (n=3-4).	120
Figure 6.1. Isometric tension analysis results of CDDP and CDPP + BX treated mice (n=3-4).....	134
Figure 6.2. BX reduced ANGII-induced vasoconstriction in CDDP + BX treated mice compared to CDDP alone (n=4).	137
Figure 6.3. Effect of CDDP and BX + CDDP on mouse body composition analysis, (n=3-4).....	139
Figure 6.4. Histological analysis of PAS-stained mouse kidney tubules, glomeruli and interlobar arteries, (n=3-4).	140
Figure 6.5. Immunohistochemical Analysis of KIM-1-stained mouse kidney tubules, glomeruli and interlobar arteries (n=3-4).	142
Figure 6.6. Immunohistochemical Analysis of ICAM-1-stained mouse kidney tubules, glomeruli and interlobar arteries (n=3-4).	144
Figure 6.7. Immunohistochemical analysis of kidneys stained for VCAM-1 of mouse kidney tubules, glomeruli and interlobar arteries (n=3-4).	146
Figure 6.8. Immunohistochemical analysis of kidneys stained for E-Selectin of mouse kidney tubules, glomeruli and interlobar arteries (n=3-4).	149
Figure 6.9. Immunohistochemical analysis of kidneys stained for GRP78 stained mouse kidney tubules, glomeruli and interlobar arteries (n=3-4).	151
Figure 6.10. Element Identification (EID) X-Ray analysis using SEM of Glomeruli from CDDP and BX + CDDP treated mice (n=3).	152
Figure 6.11. Relative fold regulation of genetic response using RT ² Profiler PCR in kidneys of mice treated with either CDDP or CDDP + BX0.05, (n=3).....	153
Figure 6.12. Clustergram illustrating the gene expression of CDDP vs CDDP + BX0.05 (n=3).....	154
Figure 6.13. Hypothesised pathway of the renoprotective mechanism of BX.....	160
Figure 7.1. Graphical representation outlining the critical findings of this thesis.....	165
Figure A1. Renal perfusion setup with a graphical representation of the mouse.....	198
Figure A2. Illustration of the suture placement and tubing location to prepare the animal for renal perfusion.....	199

Figure A3. Real-time reading using MediDaq software to view the response of BX in the kidney. The figure above represents a real-time reading of infusion..... 200

List of tables

Table 1.1 Interventions assessed for renoprotective effects against CDDP-induced AKI in vivo, published in 2021-2022.	26
Table 2.1. Isometric tension analysis baseline stretching values.	36
Table 2.2. Rabbit antibodies: Antibodies used for CDDP-induced AKI model pilot study and BX pre-treated CDDP pilot study.	39
Table 3.1. Statistical significance and effect (Cohen's d) size values from pre-incubated thoracic aorta, interlobar arteries and mesenteric arteries of CD rabbits following a cumulative DRC to LKB1.	55
Table 3.2. LKB1 vs vehicle in the thoracic aorta and interlobar and mesenteric arteries and CD vs AD in the thoracic aorta and interlobar and mesenteric arteries p values and effect (Cohen's d) values.	56
Table 3.3. Log EC ₅₀ and AUC for CD and AD fed rabbit ILA and MA vessels (Denuded, ODQ, L-NAME or KPSS vs LKB1).	58
Table 3.4. Statistical significance and effect (Cohen's d) values from L-NAME pre-incubated thoracic aorta, interlobar and mesenteric arteries of CD and AD-fed rabbits following a cumulative DRC to LKB1.	60
Table 3.5. Statistical significance and effect (Cohen's d) values from the mechanically denuded thoracic aorta, interlobar arteries, and mesenteric arteries of CD and AD-fed rabbits.	62
Table 3.6. The effect of KPSS inhibited K ⁺ channels on LKB1 mediated relaxation in CD and AD thoracic aorta, interlobar, and mesenteric arteries.	65
Table 4.1. Drugs used to assess BX-induced vasodilation, with vessel type used, dosage and mechanism of action.	76
Table 4.2. Table of significance comparing relaxation responses of BX from doses (10 ⁻⁸ to 10 ⁻⁵ [M]) in CD thoracic aorta, interlobar arteries, and mesenteric arteries.	78
Table 4.3. BX vs. vehicle in the thoracic aorta and interlobar and mesenteric arteries and CD vs. AD in the thoracic aorta and interlobar and mesenteric arteries p values and Cohen's d values.	79
Table 4.4. Log EC ₅₀ and AUC for CD and AD-fed rabbit interlobar and mesenteric arteries (Denuded, ODQ, L-NAME or KPSS vs BX).	81
Table 4.5. The effect of KPSS inhibited K ⁺ channels on BX mediated relaxation in CD/AD of thoracic aorta, interlobar arteries and mesenteric arteries.	90
Table 4.6 Log EC ₅₀ and AUC for Inhibition of K ⁺ channels of CD-fed rabbit interlobar and mesenteric arteries (CTX, TEA, APA, and 4-AP) followed by a DRC to BX.	92
Table 5.1. Effect of CDDP (6.25 and 12.5) groups on vascular function, determined through cumulative dose-response curve to acetylcholine and sodium nitroprusside (10 ⁻⁸ to 10 ⁻⁵ [M]).	107
Table 5.2. LogEC ₅₀ and AUC of SHAM vs CDDP (6.25 and 12.5) treated mice.	110
Table 6.1. Effect of BX in vivo treatment on the prevention of cisplatin-induced vascular dysfunction.	135
Table 6.2. LogEC ₅₀ and AUC of CDDP and CDDP + BX (5, 0.5 and 0.05) treated mice.	136
Table 6.3. Effect of BX in vivo treatment on ANGII-induced vasoconstriction compared to CDDP alone.	138
Table 6.4. Effect of BX on expression of ICAM-1, VCAM-1 and E-Selectin in vascular layers of interlobar arteries.	148

List of abbreviations

4-AP	4-Aminopyridine
4-HNE	4-Hydroxynonenal
AA	Abdominal Aorta
ACH	Acetylcholine
AEC	Animal ethics committee
AKI	Acute Kidney Injury
ANGII	Angiotensin II
ANOVA	Analysis of variance
APA	Apamin
APN	Aminopeptidase N
ARBs	Angiotensin receptor blockers
ARC	Animal resource centre
AT1R	Angiotensin II receptor type 1
AT2R	Angiotensin II receptor type 2
ATF6	Activating transcription factor 6
ATN	Acute Tubular Necrosis
ATP7A	ATPase Copper Transporting Alpha
ATP7B	ATPase Copper Transporting Beta
AUC	Area under the curve
Bax	BCL-2-associated X protein
Bcl-2	B-cell lymphoma-2)
Bcl-xL	B-cell lymphoma-extra large
BHB	B-Hydroxybutyrate
BUN	Blood Urea Nitrogen
BX	BX-912
CAM	Calmodulin
CAT	Catalase
CDDP	Cisplatin
CHOP	C/EBP-homologous protein
CIAKI	Cisplatin induced Acute Kidney Injury
COX-2	Cyclooxygenase 1
COX-1	Cyclooxygenase 2
CTR1	Copper transport protein 1
CTX	charybdotoxin

CXCL1	C-X-C Motif chemokine ligand 1
CYP2e1	Cytochrome P450 2E1
DAB	3, 3'-diaminobenzidine
DAMP	Danger associated molecular pattern
ddH2O	Double distilled water
DEPTOR	DEP domain-containing mTOR-interacting protein
DMF	Dimethylformamide
DMSO	Dimethyl sulfoxide
DNA	Deoxyribonucleic Acid
DOCA	deoxycorticosterone acetate
DRC	Dose response curve
eNOS	endothelial nitric oxide synthase
ER	Endoplasmic Reticulum
EtOH	Ethanol
FDA	Food and drug administration
GFR	Glomerular Filtration Rate
GGT	Gamma-glutamyl transferase
GRP78	Glucose regulating protein 78
GSH	Glutathione
GST	Glutathione S-transferase
HCl	hydrochloric acid
HEK293	Human embryonic kidney 293 cells
HMDS	hexamethyldisilazane
HO	Heme oxygenase
HO-1	Heme oxygenase 1
HSK	homoserine kinase
HUVEC	Human umbilical vein endothelial cell
IA	Iliac Artery
ICAM-1	Intracellular adhesion molecule 1
IFN-γ	interferon-gamma
IHC	Immunohistochemistry
ILA	Interlobar Artery
IP	Intraperitoneal Injection
IRE1	Inositol-requiring enzyme 1
IV	Intravenous
JNK	c-Jun N-terminal kinases

KCL	Potassium chloride
KH₂PO₄	Potassium dihydrogen phosphate
KIM-1	Kidney Injury Molecule 1
KPSS	Potassium physiological salt solution
KREBS	Krebs–Henseleit solution
LDL	Low density lipoprotein
L-NAME	L-N ^G -Nitro arginine methyl ester
LPOS	Lipid Peroxidation
MA	Mesenteric Artery
MAP	Mean arterial pressure
MAPK	Mitogen-activated protein kinases
MAS	Mitochondrial assembly receptor
MATE1	multidrug and toxic compound extrusion transporter 1
MCID	Micro Computer Imaging Device 6.0 program
MCRP-1	Monocyte chemoattractant protein 1
MDA	Malondialdehyde
MgSO₄·7H₂O	Magnesium sulphate heptahydrate
MLKL	Mixed lineage kinase domain-like
MRI	Magnetic resonance imaging
MRP2	Multidrug resistance-associated protein 2
Na₂HPO₄	di-Sodium hydrogen phosphate anhydrous
NAC	N-acetylcysteine
NaCl	Sodium Chloride
NAD(P)H	Nicotinamide adenine dinucleotide phosphate
NaH₂PO₄·7H₂O	Sodium phosphate dibasic heptahydrate
NaHCO₃	Sodium Bicarbonate
NaOH	Sodium hydroxide
Nfκb	Nuclear factor kappa B
NGAL	Neutrophil gelatinase-associated lipocalin
NLRP3	NOD-, LRR- and pyrin domain-containing protein 3
NO	Nitric Oxide
NOX4	NADPH oxidase 4
Nrf2	nuclear factor erythroid 2–related factor 2
NRK-53E	Normal Rat Kidney-52E
OAT	Organic anion transporters
OCT	Organic cation transporter 2

ODQ	1H-(1,2,4) Oxadiazolo(4,3-a) quinoxalin-1-one
ONOO-	Peroxynitrite
PAMP	Pathogen-associated molecular patterns
PARP	Poly [ADP-ribose] polymerase
PARP-1	Poly [ADP-ribose] polymerase 1
PAS	Periodic Acid Schiff stain
PB	Phosphate buffer
PBS	Phosphate buffered saline
PCR	Polymerase chain reaction
PD	Panduratin A
PERK	Protein kinase RNA-like endoplasmic reticulum kinase
PFA	Paraformaldehyde
PFC	Perfluorocarbon
PI	Proportional intensity
PLGA	Poly (lactic-co-glycolic acid)
PRC2	Polycomb repressive complex 2
PTEC	Proximal Tubular Epithelial Cells
PUMA	The p53 upregulated modulator of apoptosis
RAS	Renin Angiotensin system
RFW	RNase free water
RIP1/RIP3	Receptor-interacting serine/threonine-protein kinase 1/Receptor-interacting serine/threonine-protein kinase 3
RLT	RNA lysis buffer
RNA	Ribonucleic acid
ROS	Reactive Oxygen Species
RPE	RNA Precipitating Elution Buffer
RPM	Revolutions per minute
RT-PCR	Real Time Polymerase chain reaction
RW1	RNA wash buffer
SA	Sinapic Acid
sCr	Serum Creatinine
SEM	Scanning electron microscopy
sGC	Soluble guanylyl cyclase
Sirt5	Sirtuin 5
SKF-86002	(6-(4-Fluorophenyl)-5-(4-pyridyl)-2,3-dihydroimidazo[2,1-b]-thiazole)

SNP	Sodium Nitroprusside
SOD	Superoxide dismutase
STING	Stimulator of interferon genes
TA	Thoracic Aorta
TEA	Tetraethylammonium
TIM-1	T-cell immunoglobulin and mucin domain 1
TLR	Toll-like receptor
TLS	Tumour Lysis Syndrome
TNFR1	Tumour Necrosis Factor receptor 1
TNF-α	Tumour Necrosis Factor Alpha
TUG891	[3-(4-((4-fluoro-4'-methyl-[1,1'-biphenyl]-2-yl) methoxy)phenyl)propanoic acid]
TUNEL	Terminal deoxynucleotidyl transferase dUTP nick end labelling
UPR	Unfolding protein response
VCAM-1	Vascular cellular adhesion molecule 1
VDR	Vitamin D receptor
VEH	Vehicle
VRAC	Volume-regulated anion channels
VSMC	Vascular Smooth Muscle Cell
VUAEEC	Victoria University Animal Experimental Ethics Committee
WCHRE	Western centre for health and research

List of symbols

μ l- microlitre

α - alpha

κ - Kappa

β - Beta

\geq - greater than/equal to

\uparrow - increased

\downarrow - decreased

Δ - delta

●- Cohen's d effect size

*- significance stars

†- 4x significance stars ($p < 0.0001$)

OFFICE FOR RESEARCH TRAINING, QUALITY AND INTEGRITY

DECLARATION OF CO-AUTHORSHIP AND CO-CONTRIBUTION: PAPERS INCORPORATED IN THESIS

This declaration is to be completed for each conjointly authored publication and placed at the beginning of the thesis chapter in which the publication appears.

1. PUBLICATION DETAILS (to be completed by the candidate)

Title of Paper/Journal/Book:	Mechanisms of Cisplatin-Induced Acute Kidney Injury: Pathological Mechanisms, Pharmacological Interventions, and Genetic Mitigations (Cancers 2021).		
Surname:	McSweeney	First name:	Kristen
Institute:	Institute for Health and Sport	Candidate's Co	
Status:		Date:	
Accepted and in press:	<input type="checkbox"/>	Date:	
Published:	<input checked="" type="checkbox"/>	Date:	29/03/2021

2. CANDIDATE DECLARATION

I declare that the publication above meets the requirements to be included in the thesis as outlined in the HDR Policy and related Procedures – policy.vu.edu.au.

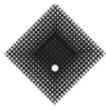
Kristen McSweeney	Digitally signed by Kristen McSweeney Date: 2023.02.19 13:10:07 +11'00'	19/02/2023
Signature		Date

3. CO-AUTHOR(S) DECLARATION

In the case of the above publication, the following authors contributed to the work as follows:

The undersigned certify that:

1. They meet criteria for authorship in that they have participated in the conception, execution or interpretation of at least that part of the publication in their field of expertise;
2. They take public responsibility for their part of the publication, except for the responsible author who accepts overall responsibility for the publication;



- 3. There are no other authors of the publication according to these criteria;
- 4. Potential conflicts of interest have been disclosed to a) granting bodies, b) the editor or publisher of journals or other publications, and c) the head of the responsible academic unit; and
- 5. The original data will be held for at least five years from the date indicated below and is stored at the following **location(s)**:

Name(s) of Co-Author(s)	Contribution (%)	Nature of Contribution	Signature	Date
Laura Gadanec	15	Manuscript preparation		20/03/23
Tawar Qaradakhi	2.5	Manuscript preparation		
Benazir Ashiana Ali	2.5	Manuscript preparation		21/03/2023

Updated: September 2019

Review

Mechanisms of Cisplatin-Induced Acute Kidney Injury: Pathological Mechanisms, Pharmacological Interventions, and Genetic Mitigations

Kristen Renee McSweeney , Laura Kate Gadanec , Tawar Qaradakhi, Benazir Ashiana Ali , Anthony Zulli ^{*,†} and Vasso Apostolopoulos ^{*,†} 

Institute for Health and Sport, Victoria University, Werribee, VIC 3030, Australia; kristen.mcsweeney@live.vu.edu.au (K.R.M.); laura.gadanec@live.vu.edu.au (L.K.G.); tawar.qaradakhi@live.vu.edu.au (T.Q.); benazir.ali@live.vu.edu.au (B.A.A.)

* Correspondence: anthony.zulli@vu.edu.au (A.Z.); vasso.apostolopoulos@vu.edu.au (V.A.)

† These authors contributed equally.

Simple Summary: Nephrotoxicity is the dose-limiting factor of cisplatin treatment. Nephrotoxicity is characterized by reduced kidney function. Although an often-reversible condition, effects are notably seen years after treatment with cisplatin has ceased. It has an extensive pathophysiological map. The purpose of this article is to consolidate cisplatin-induced acute kidney injury literature and present it in one collective paper. It explores each individual mechanism linked to the disease, the pharmacological options that have been tested to target each of them, and the results obtained by each study. The paper also describes genetic modification studies and their effectiveness in preventing disease development.



Citation: McSweeney, K.R.; Gadanec, L.K.; Qaradakhi, T.; Ali, B.A.; Zulli, A.; Apostolopoulos, V. Mechanisms of Cisplatin-Induced Acute Kidney Injury: Pathological Mechanisms, Pharmacological Interventions, and Genetic Mitigations. *Cancers* **2021**, *13*, 1572. <https://doi.org/10.3390/cancers13071572>

Academic Editor: Takeo Nakanishi

Received: 29 January 2021

Accepted: 25 March 2021

Published: 29 March 2021

Publisher's Note: MDPI stays neutral with regard to jurisdictional claims in published maps and institutional affiliations.



Copyright: © 2021 by the authors. Licensee MDPI, Basel, Switzerland. This article is an open access article distributed under the terms and conditions of the Creative Commons Attribution (CC BY) license (<https://creativecommons.org/licenses/by/4.0/>).

Abstract: Administration of the chemotherapeutic agent cisplatin leads to acute kidney injury (AKI). Cisplatin-induced AKI (CIAKI) has a complex pathophysiological map, which has been linked to cellular uptake and efflux, apoptosis, vascular injury, oxidative and endoplasmic reticulum stress, and inflammation. Despite research efforts, pharmaceutical interventions, and clinical trials spanning over several decades, a consistent and stable pharmacological treatment option to reduce AKI in patients receiving cisplatin remains unavailable. This has been predominately linked to the incomplete understanding of CIAKI pathophysiology and molecular mechanisms involved. Herein, we detail the extensively known pathophysiology of cisplatin-induced nephrotoxicity that manifests and the variety of pharmacological and genetic alteration studies that target them.

Keywords: cisplatin; acute kidney injury; AKI; cisplatin-induced acute kidney injury; nephrotoxicity

1. Introduction

1.1. Cisplatin

Cisplatin (cis-diamminedichloroplatinum II) is a platinum-containing antineoplastic drug first approved for clinical use in 1978 [1]. It is used extensively to treat a repertoire of malignancies per se or as a tailored combination in treatment [1]. Cisplatin is used to treat breast [2], cervical [2], oesophageal [3], bladder [4], small cell lung [5], and testicular cancers [6]. Cisplatin is also used as a combination therapy to treat high grade cancers such as osteosarcoma [7] and soft-tissue cancers including squamous cell carcinoma [8]. Cisplatin is one of the most potent and effective chemotherapies used to date [9], and its antitumor effects are well established [2,9,10]. However, the exact mechanism of cisplatin-induced cell death remains largely unknown. It is widely accepted that cisplatin causes 1–2 intrastrand or 1–3 interstrand crosslinks with purine bases on the deoxyribonucleic acid (DNA) strand [9,11]. This crosslinking impairs DNA repair mechanisms, inhibiting the production of a viable DNA replication template, stimulating cell-cycle arrest leading

to cell death [12]. Irrespective of its potent anticancer properties and efficacy, the clinical usage of cisplatin is limited due to the severity of adverse side effects including ototoxicity and neurotoxicity [13,14] and its dose-limiting factor nephrotoxicity [12,15–21].

1.2. Nephrotoxicity

Nephrotoxicity results from a rapid decline of excretory mechanisms within the kidney [22], enhancing the accretion of waste products produced by protein metabolism (including urea, nitrogen, and creatinine) [22–24]. Acute kidney injury (AKI) is commonly caused by nephrotoxic injury to kidney tissue, resulting in acute tubular necrosis [25]. It can also result from inadequate urinal drainage [26]. Decreased drainage causes an increase in intratubular pressure and decreases glomerular filtration rate (GFR). Decreased GFR can additionally be stimulated by afferent arteriole vasoconstriction [27]. Despite improved prognosis following the removal of diuretics to promote volume expansion and hydration, the prevalence of cisplatin-induced AKI (CIAKI) remains high [28]. Although cisplatin-induced nephrotoxicity can manifest in a variety of ways, acute tubular necrosis (ATN) is the most prevalent [29]. In the clinical setting, AKI frequently occurs despite low-dose cisplatin administration [30]. The uptake of cisplatin into proximal tubular epithelial cells (PTEC) is the initiator of the toxic effects of cisplatin [31]. To date, despite burgeoned research, there is no intervention that adequately treats or prevents CIAKI in cancer patients [32]. Therefore, further understanding the molecular pathways and their interactions is essential in finding or developing a suitable pharmacological treatment to be used in conjunction with cisplatin.

1.3. Pathophysiology of Cisplatin-Induced AKI

A variety of molecular pathways and mechanisms have been investigated to determine the unknown pathological events caused by CIAKI. The key molecular mechanisms involved in cisplatin-induced nephrotoxic adverse effects include cellular uptake and accumulation, inflammation, oxidative stress, vascular injury, endoplasmic reticulum (ER) stress, and necrosis and apoptosis (Figure 1). A plethora of pharmacological agents (Table 1) and genetic alterations (Table 2) have been investigated in experimental preclinical studies of CIAKI. Despite the prevalence of nephrotoxicity in cisplatin-treated patients, its clinical application must be accompanied by other treatments to counteract its harmful effects while allowing it to exert its potent anticancer properties. Cisplatin cellular uptake is the initiator of the nephrotoxic effects, with several studies investigating the various therapeutic options that promote renoprotection (Figure 2). The purpose of this review is to collectively present the magnitude of preclinical studies in addition to presenting the clinical studies recently completed and currently being conducted for the treatment of CIAKI. The data from these studies illustrates the broad pathophysiological mechanisms involved and the potential for their inter-relationships. This review sheds light on the current failure in preclinic to clinic translatability given the lack of studies currently moving from animal models to human clinical trials. Despite the frequent protective therapies evaluated in models of CIAKI, there is no evidence of treatment progression with almost all therapies evaluated, posing a highly concerning issue for cisplatin patients.

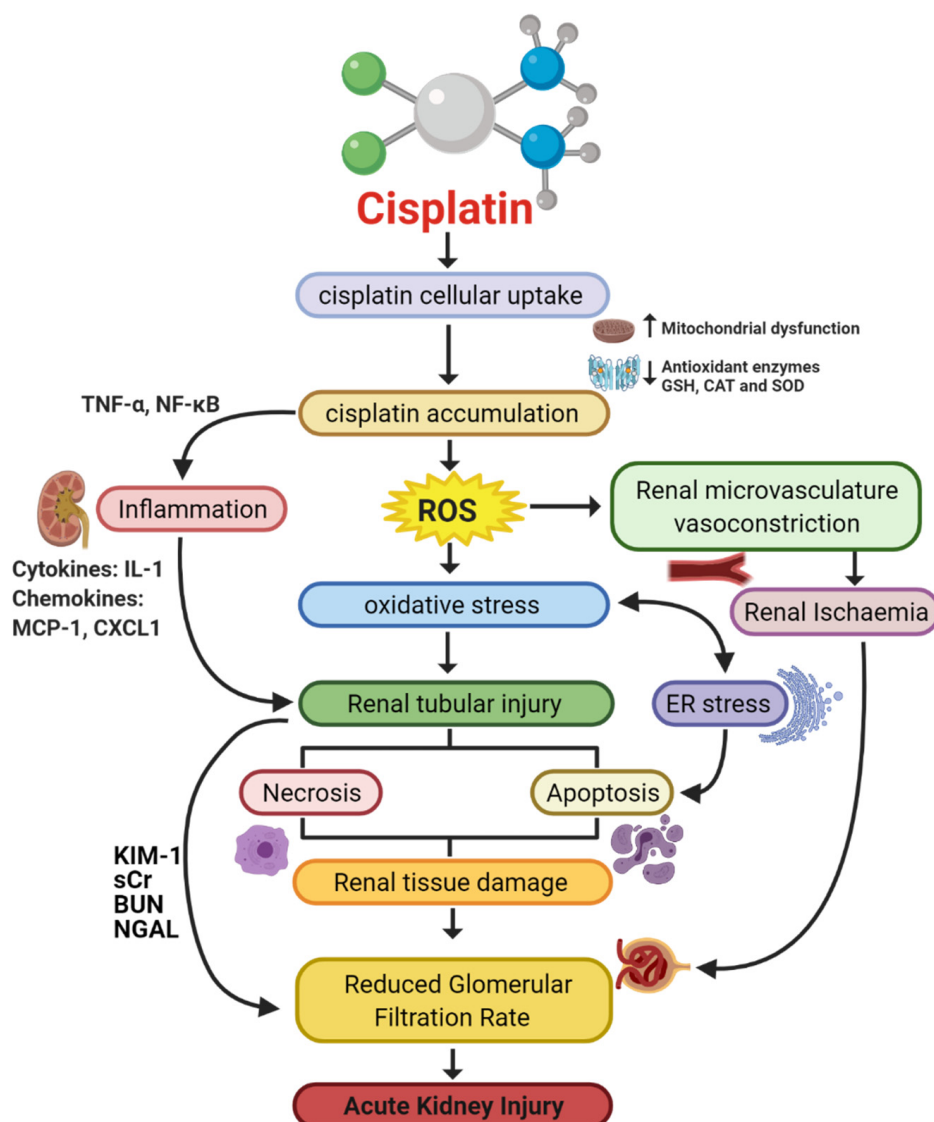


Figure 1. Pathophysiological map of the key molecular pathways demonstrated to play a role in the pathogenesis of cisplatin-induced acute kidney injury (AKI). The mechanisms associated with cisplatin-induced AKI (CIAKI) are complex, and the relationship between the key pathways remains unknown. However, it is believed that the detrimental nephrotoxic effect of cisplatin in renal tissue is due to platinum accumulation. Cisplatin accumulation triggers increased production of tumor necrosis factor alpha (TNF- α) [33,34] and reactive oxygen species (ROS), stimulating inflammation [35], oxidative stress [36], vascular injury [31], and apoptotic pathways [37]. The apoptotic mechanisms then promote renal tissue damage leading to the key clinical manifestation of nephrotoxicity (a reduction in glomerular filtration rate (GFR)) resulting in CIAKI. Abbreviations: GSH, glutathione; CAT, catalase; SOD, superoxide dismutase; TNF- α , tumor necrosis factor alpha; ROS, reactive oxygen species; ER stress, endoplasmic reticulum stress; and GFR, glomerular filtration rate. IL-1, Interleukin 1; MCP-1, monocyte chemoattractant protein 1; CXCL1, C-X-C Motif Chemokine Ligand 1; KIM-1, Kidney Injury Molecule 1; sCr, Serum Creatinine; BUN, Blood Urea Nitrogen; NGAL, Neutrophil gelatinase-associated lipocalin. Figure adapted from “Cisplatin nephrotoxicity: mechanisms and renoprotective strategies” by N. Pabla and Z. Dong, 2008, *Kidney International*, Volume 73, P994-1007, Copyright [2008] by the Elsevier.

Table 1. Pharmacological interventions assessed for renoprotective effects against cisplatin-induced AKI in vitro and in vivo, papers published in 2020.

Drug	Mechanism of Action	Findings	In Vitro	In Vivo	Reference
Aucubin	Anti-inflammatory	↓ Markers of oxidative stress (HO-1 and 4-HNE) ↓ Apoptosis (caspase-3, caspase-9 and PARP)	–	BALB/c mice	[38]
Curcumin	Anti-inflammatory, Antioxidative, oxygen-free radical scavenging, antifibrotic, and anticancer activities	↓ Tubular Injury ↓ BUN ↓ sCr (rats)	–	C57BL/6J mice/rats	[39,40]
Dexmedetomidine	Antiapoptotic via α 2AR/PI3K/AKT pathway	↑ Body weight and renal index ↓ Tubular epithelial cell apoptosis ↓ Expression of GRP78, CHOP and Caspase-12	–	Sprague Dawley Rats	[41]
Etoricoxib	Anti-inflammatory	↓ Inflammation (iNOS) ↓ Apoptosis (BAX) No changes to creatinine, BUN, GSH, and MDA	–	Rats	[40]
Eugenol	Antioxidant and anti-inflammatory properties	↓ sCr and BUN ↓ PAS tubular injury score ↓ cytoplasmic vacuolization of proximal tubular cells	–	BALB/c mice	[42]
Ferrostatin-1	Inhibits Ferroptotic cell death	↓ sCr and BUN ↓ apoptosis (TUNEL stain) ↓ Tubular injury score (H&E) ↓ Lipid peroxidation	–	C57BL/6J mice	[43]
Isoorientin	Anti-inflammatory, antioxidant	↓ ROS generation ↓ Apoptosis ↓ Inflammation	mTECs	Nrf2 ^{-/-}	[44]
Monotropein	Antioxidant, anti-inflammatory and antiapoptotic	↓ Tubular injury ↓ markers of oxidative stress ↓ markers of apoptosis ↓ BUN, no reduction in sCr	–	BALB/c mice	[45]
Paricalcitol	Synthetic vitamin D deficiency	↓ MDA (HK-2 cells) ↓ Cell death (HK-2 cells) ↓ sCr and BUN (WT mouse) ↓ Tissue Injury (WT mouse)	HK-2 cells	WT mice	[43]
Quercetin	Anti-inflammatory	↓ sCr and BUN ↓ mRNA expression of IL-1 β , IL-6, TNF- α ↓ reduced tubular necrosis score ↓ activity of Syk/NF- κ B	–	C57BL/6J mice	[46]

Abbreviations: sCr, SCr; BUN, blood urea nitrogen; PAS, periodic acid Schiff; KIM-1, kidney injury molecule-1; ROS, reactive oxygen species; mTECs, medullary thymic epithelial cells; iNOS, inducible nitric oxide synthase; BAX, BCL2-associated X protein; GSH, glutathione; MDA, malondialdehyde; TUNEL, Terminal deoxynucleotidyl transferase dUTP nick end labelling; H&E, haematoxylin and eosin; HK-2, human kidney 2; VDR, Vitamin D receptor; mRNA, messenger ribonucleic acid; ^{-/-}, knockout; IL-1 β , Interleukin-1 beta; IL-6, Interleukin-6; TNF- α , tumor necrosis factor-alpha; Syk, spleen tyrosine kinase; NF- κ B, nuclear factor kappa B; CHOP, CCAAT-enhancer-binding protein homologous protein; GRP78, glucose-regulated protein 78; HO-1, heme oxygenase-1; 4-HNE, 4-hydroxynonenal; and PARP, poly (ADP-ribose) polymerase, ↓; Decreased, ↑; Increased, –/–; genetic deletion, –/–.

2. Pharmacological Approaches Targeting Cisplatin Cellular Uptake

2.1. Cellular Uptake Transporters of Cisplatin

The cellular uptake of cisplatin has been implicated in the pathogenesis of CIAKI. Organic cation transporter 2 (OCT2), copper transporter 1 (CTR1), and the less explored volume-regulated anion channels (VRAC) are involved in cisplatin transportation into kidney cells [57] by enabling platinum accumulation, which has been linked to kidney dysfunction [28] (Figure 2). Kidney tissue following cisplatin treatment showed a five-fold increase in cisplatin concentration compared to serum, indicative of PTEC accumulation [9]. Organic cation transporter 2 is one of the transporters affiliated with cisplatin cellular uptake.

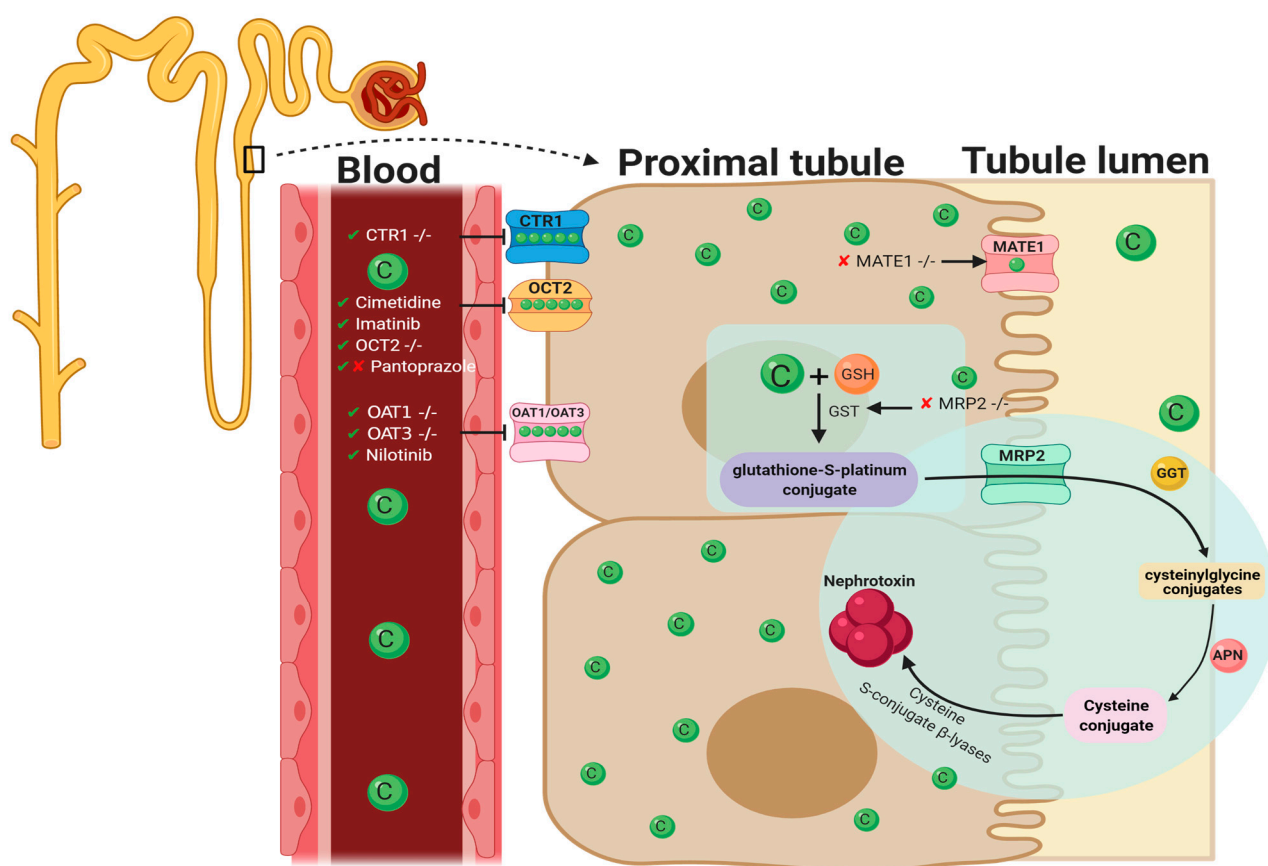


Figure 2. Graphical representation of key molecules and pathways involved in cisplatin transportation initiating nephrotoxic effects. Key transporters responsible for cellular uptake of cisplatin from the blood into PTECs resulting in a much greater platinum concentration compared to the blood. The key interventions trialed to date and their effectiveness in targeting CIAKI are also illustrated. Diagram details the cellular processes involved in the cellular uptake [57–64], efflux [65,66], and metabolism of cisplatin into a highly reactive thiol (nephrotoxin) [67] and the treatment targeted to prevent them.

2.2. Organic Cation Transporter 2 (OCT2)

OCT2 is expressed on the basolateral membrane of PTEC [57,59,60] and plays a central role in cisplatin uptake into tubular cells [57,59,60]. Amongst the transporters responsible for CIAKI, it has been shown that 30% of nephrotoxic effects caused by cisplatin is directly mediated by OCT2 uptake [68]. In *in vitro* studies investigating OCT2-mediated cisplatin cellular uptake, pharmacological inhibition was noted of OCT2 by cimetidine-inhibited cisplatin-induced apoptosis. In addition, nephrotoxicity stimulated by cisplatin transportation into renal tubular cells and subsequent platinum accumulation could be decreased with orally administered imatinib (a tyrosine kinase inhibitor) in rats. Histological investigations of kidney tissue confirmed that there was no evidence of severe renal damage

in mice co-treated with cisplatin and imatinib. However, tubular degeneration was observed in cisplatin-treated groups [61]. The results of blood analysis (plasma urea, nitrogen, creatinine, and creatinine clearance) were indicative of improved kidney function and platinum accumulation following imatinib adjunct therapy. In OCT2-expressed HEK293 cell studies, adjunct administration of cisplatin and imatinib showed decreased accumulation of platinum in PTECs and decreased cisplatin-induced cytotoxicity [61]. However, despite the renoprotective effects observed in preclinical animal models, imatinib has not provided positive toxicology results. According to the US Food and Drugs Administration adverse reporting system, 44 imatinib-treated cases cited renal-related toxicity. Of these 44 cases, 25 manifested as AKI [69]. As such, this may not be an adequate clinical treatment. Potentially irreversible acute kidney injury was also observed in a nonclinical trial in imatinib-treated chronic myeloid leukemia patients [70].

An experimental study using OCT2-deficient mice showed impairment of cisplatin uptake in renal cells, evident by reduced platinum accumulation [60]. Cairimboli et al. confirmed the importance of OCT2 in cisplatin uptake [58]. The authors associated the overexpression in HEK293 cells with increased cisplatin uptake causing cisplatin toxicity, because of increased cellular sensitivity [58]. To date, many pharmacological approaches targeting molecules responsible for cisplatin uptake or transportation into PTECs have been explored [57,61,71–74]. A murine model of CIAKI demonstrated downregulation of OCT2 expression by formononetin inhibited the development of AKI associated with cisplatin treatment through stimulation of renal tubular cell proliferation, survival, and apoptosis inhibition [71]. Despite the ameliorating effects of *in vivo* OCT2 inhibition in murine models of CIAKI, human studies failed to display the same renoprotective effects. Fox and colleagues used a randomized crossover experimental design to assess the prevention of cisplatin-induced nephrotoxicity using the OCT2 inhibitor pantoprazole, in young patients with osteosarcoma. To assess the effects, novel biomarkers were tested to investigate glomerular and tubular function. Measurement of serum cystatin c was used as an indirect indicator of GFR, and urinary biomarkers N-acetyl- β -glucosaminidase (NAG), kidney injury molecule-1 (KIM-1), and neutrophil gelatinase-associated lipocalin (NGAL) were used to quantify the degree of renal injury caused by cisplatin. The results of this study showed that concurrent administration of cisplatin with pantoprazole provided no protection against renal injury or function in young cancer patients [75]. Interestingly, a more recent study showed that pantoprazole can ameliorate CIAKI in mice [62]. Given the contradictory results of OCT2 inhibition on CIAKI in animal-versus-human studies further research needs to be conducted. It is important to note that OCT2 murine models were nontumor bearing, whilst the human studies were conducted in cancer patients, which could be a contributing factor to the failed clinical study.

2.3. Copper Transporter 1

CTR1 is located on the basolateral membrane of proximal tubules and is highly expressed in human kidneys [57,59]. The exact role of CTR1 in cellular uptake of cisplatin into renal proximal tubules resulting in nephrotoxicity is incompletely understood. However, studies have shown that CTR1 downregulation is protective against platinum accumulation [57]. The knockdown of CTR1 reduces cisplatin nephrotoxicity by up to 80% in both mouse embryonic fibroblasts and yeast [72,74]. *In vivo* studies indicated elevated levels of CTR1 expression was associated with increased cisplatin accumulation in tumors, a process also observed in PTEC [57,76]. Pabla and colleagues investigated the relationship between cisplatin and CTR1 expression to further define the role that CTR1 plays in nephrotoxicity. Interestingly, in mice, there were no significant differences in CTR1 expression 1–3 days following cisplatin treatment. They also demonstrated that incubation of HEK293 cells with copper generated both monomeric and trimeric CTR1 knockdown, resulting in approximately 50% diminution in cisplatin accumulation and a 30% reduction in apoptosis. Furthermore, CTR1 knockdown cells incubated with the OCT/MATE inhibitor cimetidine further inhibited both cellular uptake and apoptosis following treatment with

cisplatin [57,58]. The results of this study have shown that although both CTR1 inhibition and OCT2 inhibition alone are options to prevent nephrotoxicity, the combination of CTR1 and OCT2 inhibition together has better therapeutic potential. Interestingly, the majority of cellular uptake research regarding cisplatin into renal cells has focused on the two major cisplatin transporters OCT2 and CTR1. However, there have also been suggestions that there are other entry points for cisplatin into renal cells that are yet to be explored in models of CIAKI such as VRAC channels. Reduced VRAC channel activity is associated with cisplatin resistance [77], and the presence of VRAC channels in kidney cells [78] highlights a potential avenue for CIAKI research. Additionally, impaired cisplatin efflux has been shown to contribute to cisplatin accumulation and the nephrotoxic effects that follow [65,79].

2.4. OAT1/OAT3

In addition to OCT2 and CTR1, the organic anion transporter (OAT) family (OAT1 and OAT3) have also shown to transport cisplatin and potentially a nephrotoxic metabolite into PTEC resulting in nephrotoxic injury to renal cells [63]. OAT transporters are largely concentrated in the basolateral membrane of PTEC and facilitate transportation of hydrophilic anions into cells. This intake is via secondary/active transportation responsible for regulating anion balance in the body [80]. To investigate the influence of OAT transporters on cisplatin-induced nephrotoxicity, C57BL/6J mice with genetic deletion of OAT1 and OAT3 were injected with 30 mg/kg cisplatin. In cisplatin-treated wildtype mice, there were increases in biomarkers of CIAKI, in addition to histological indication of kidney damage such as tubule dilation and necrosis. There was no evidence of kidney dysfunction in OAT1- and OAT3-deficient mice treated with cisplatin. Further studies are needed to further understand the role of each individually and the interaction they have together on CIAKI nephrotoxicity. A different model was used to investigate OAT-stimulated CIAKI using nilotinib. Nilotinib is a tyrosine kinase inhibitor shown to noncompetitively inhibit OCT2 and both OAT1 and OAT3 [63]. Nilotinib was given to OCT1/2^{-/-} mice simultaneously with cisplatin, with results indicating no loss of kidney function in the adjuvant cisplatin- and nilotinib-treated group as confirmed by reduced BUN levels. This indicates that OAT1/inhibition by nilotinib provides some evidence of amelioration of CIAKI; however, as the paper elucidates, further investigations in the mechanisms of mitigation are required [63]. A separate study investigated the effects of nilotinib in a rodent model of CIAKI. Male Wistar albino rats were treated with 25 mg/kg Nilotinib 4 days prior to a single intraperitoneal injection of 6 mg/kg cisplatin and 6 days following the cisplatin injection. Results of their study showed that nilotinib improved creatinine clearance compared to cisplatin-treated rats; however, it had no influence on increased BUN [64]. It was also observed that nilotinib attenuated cisplatin increase in MDA, a biomarker of oxidative stress [81]. Morphological changes showed amelioration of CIAKI by nilotinib. Although this study did not look specifically at nilotinib influence on OAT1 and OAT3, it does confirm its ability to prevent CIAKI. Given this information, there is a clear correlation and link between the transporters, and therefore, further investigations need to be undertaken to understand their interactions and the influence that has on mediating cisplatin uptake. Given cisplatin uptake is the initial step mediating its nephrotoxic effects, potentially inhibiting all three synergistically may be an ideal strategy for CIAKI prevention.

3. Pharmacological Approaches Targeting Cisplatin Cellular Efflux

Apically localized efflux transporters P-type copper transporting ATPases (ATP7A and ATP7B), multi-antimicrobial extrusion protein transporter-1 (MATE 1), and multidrug-resistance-associated protein (MRPs) mediate excretion of cisplatin into the urine [57,59,65,82]. These transporters are highly expressed in the proximal and distal tubules [57]. Tubular injury is a key pathology associated with the nephrotoxic effects of cisplatin. Tubular injury promotes reduced GFR and therefore delayed urinary excretion of cisplatin, leading to

platinum accumulation within the tubules [83]. Given the pathogenesis linked to platinum accumulation in PTEC, increasing the expression of cisplatin efflux transporters has been a molecular target against CIAKI.

3.1. Apically Localized Efflux Transporters P-Type Copper Transporting ATPases7A/B

Although there is little research available determining the effects of ATP7A and ATP7B on cisplatin nephrotoxicity, they have both been extensively investigated in the setting of cisplatin drug resistance. Studies investigating overexpression of both ATP7A and ATP7B in cancer models have been shown to be independently linked to poor survival in ovarian cancer patients and cisplatin resistance in prostate carcinoma cells, respectively [84–86]. Therefore, overexpression of ATPases could prevent CIAKI; however, its therapeutic potential may not exceed the possible negative outcomes to cancer cells.

3.2. Multidrug-Resistance-Associated Protein 2

MRPs are associated with mediating the efflux of cisplatin and its nephrotoxic conjugates from kidney cells [87]. Previously, research investigating the role of MRP expression in cisplatin accumulation demonstrated that increased MRP expression resulted in reduced cisplatin accumulation and therefore has been suggested to play a critical role in cisplatin-induced nephrotoxicity [87]. Given its role in nephroprotection, you would expect its expression to be downregulated in response to cisplatin treatment, given that platinum accumulation is a well-established complication. However, acute renal failure induced in rats showed a significant upregulation of MRP2 72 h after cisplatin treatment; however, there were only minor increases in MRP4 expression compared to controls [88].

The glutathione-s-platinum conjugate, whose metabolism is responsible for the production of the reactive thiol nephrotoxin, is suggested to be eliminated by MRPs [89]. To determine the role of MRP2 on cisplatin efflux, MRP2-deficient mice were treated with 20 mg/kg of cisplatin, resulting in enhanced platinum accumulation and proximal tubular injury. MRP2-deficient mice showed increased mRNA expression of GST, the enzyme which catalyzes the formation of the cisplatin–glutathione conjugate. Platinum accumulation was reduced in transgenic knock-in MRP2-knockout mice, indicating that MRP2 plays a role in the accumulation of platinum [66]. However, the mechanisms involved in this accumulation and the effect they have on the production of the reactive thiol remain unclear. It is possible that an increase in MRP expression might be seen in models of nephrotoxicity; however, no studies are yet to present data investigating this. In addition to MRPs, multi-antimicrobial extrusion protein 1 (MATE1/SLC47A1) is suggested to be involved in platinum accumulation associated with cisplatin treatment [83].

3.3. Multi-Antimicrobial Extrusion Protein 1

MATE1 expression is largely concentrated in the brush-border membrane of PTECs and assists epithelial cell elimination of cationic molecules into urine [83]. Cisplatin has been identified as a substrate for MATE1 [90]. MATE1 has shown to mediate cisplatin efflux and prevent cisplatin accumulation in tubular cells preventing cisplatin nephrotoxic effects [65]. However, following cisplatin treatment, downregulation of MATE1 expression in human tubular epithelial cells is observed [83]. Given the ability for MATE1 to facilitate cisplatin urinary excretion, further investigations have been undertaken to isolate its role in cisplatin-induced AKI. A model of cisplatin-induced nephrotoxicity was undertaken in MATE1^{-/-} mice [65]. Blood urea nitrogen (BUN) and plasma creatinine concentration were significantly elevated in cisplatin-treated MATE1^{-/-} mice, compared with cisplatin-treated wildtype mice. It was observed that renal concentrations of platinum were at a 20-fold increase compared to plasma concentration in MATE1-deficient mice [65]. Increased serum creatinine (sCr) and BUN were also observed in MATE1 pharmacological inhibition studies [65,91]. Therefore, it has been concluded that MATE1 plays a key role in cisplatin accumulation and is thus a contributor to CIAKI [65]. A study investigating MATE1

upregulation in models of CIAKI may be a good therapeutic avenue in the prevention of nephrotoxicity.

4. Interventions Targeting Molecular Mechanisms CIAKI

4.1. Oxidative Stress

Despite the collection of research that has focused specifically on cisplatin transportation and accumulation, other models of CIAKI have targeted key molecules involved in ROS formation [92]. A balance occurs between ROS production and the antioxidant defense system to maintain homeostasis [2,3]. Cisplatin disrupts this equilibrium through overproduction of ROS and impaired antioxidant defense systems. This triggering reduced production of key antioxidants, including superoxide dismutase (SOD), glutathione (GSH) [2], and catalase (CAT) [93]. The reduction in the functionality of the antioxidant defense system leads to overexpression of key markers of oxidative stress following cisplatin treatment [36]. Elevated levels of cisplatin in PTEC also increase cisplatin accumulation in mitochondria, stimulating mitochondrial dysfunction, mitochondrial damage, and ROS production [94,95]. Following cisplatin infiltration into renal epithelial cells, it becomes a potent nephrotoxin via gamma-glutamyl transpeptidase (GGT)-dependent metabolic activation (Figure 2) [96]. Glutathione-S-transferase (GST) mediates the formation of glutathione-S-platinum conjugates, which passes through the kidneys [34]. It is cleaved into cysteine-glycine conjugate by Gama-glutamyl-transpeptidase [67]. Amino-dipeptidases further metabolizes this into cysteine conjugates, which are then transported into proximal tubules. Cysteine-S-conjugate β -lyase (CSC β L) is metabolized to form the cysteine conjugate into a highly reactive thiol, which is the initiator of cisplatin's cell toxicity [67,96]. Elevated levels of the highly reactive thiol molecule produced after cisplatin uptake is metabolized by CSC β L catalyze the enzymatic activation of glucose-6-phosphate dehydrogenase and hexokinase, increasing ROS [1].

Studies have determined the use of natural antioxidants including, vitamin C [97], vitamin E [98], and activation of the vitamin D receptor [43] to target ROS formation, which have all shown nephroprotective properties against renal toxicity [15]. The beneficial co-therapy of cisplatin and vitamin C in C57BL/6 mice has been previously demonstrated. Mice were inoculated with Lewis lung carcinoma followed by treatment with cisplatin. Levels of sBUN and sCr presented cisplatin-treated mice demonstrated higher levels of oxidative damage. Decreased levels of kidney dysfunction were also observed in adjunct vitamin C and cisplatin-treated mice, without compromising cisplatin cytotoxicity [97]. Furthermore, there have been extensive pharmaceutical interventions assessed for their antioxidant effects on CIAKI [94]. Oxidative stress, evident by reduced MDA/MPO expression, was observed in necrostatin-1- and cisplatin-treated mice [99]. This was also observed in hesperetin- and cisplatin-treated HK-2 cells. Both drugs, showed reduced levels of apoptosis [100], which could interfere with the cytotoxicity of cisplatin. Experimental and clinical studies have focused on cisplatin nephrotoxicity, specifically through targeting mechanisms and molecular pathways associated with pharmacological inhibition ROS production or stimulation of antioxidant pathways [36,44,49,92,93,97,101]. A pathway of interest recently targeted in CIAKI research is the nuclear factor erythroid 2-related factor 2/heme oxygenase-1 (Nrf2/HO-1) signaling pathway [100].

Monotropein (Nrf2/HO-1 Antioxidant Pathway)

Activation of Nrf2 has shown promise in multiple experimental models as a key modulator in the suppression of oxidative stress and inflammation to preserve kidney function [102,103]. Nrf2 is responsible for maintenance of the cellular redox balance, antioxidant response, and phase II detoxification process [104]. Nrf2 expression has shown to be downregulated in rats following cisplatin treatment [105]. Renal expression of Nrf2 and HO-1 was downregulated compared to control rats, however rats pretreated with Sinapic acid (SA) followed by cisplatin resulted in marked increase in Nrf2 and Ho-1 expression. Cisplatin treatment resulted in a significant downregulation of key

antioxidant enzymes SOD, CAT, and GSH. SA and cisplatin-treated rats showed elevation in these key antioxidants indicating an enhanced antioxidant defense system following SA treatment [103]. Pharmacologically, it has been demonstrated that activation of the Nrf2 signaling pathway by N,N-dimethylformamide (DMF) following cisplatin treatment attenuated AKI [102], as well as tubulointerstitial lesions [106]. Both ameliorating effects are associated with stimulation of antioxidants such as HO-1 and NAD(P)H quinone oxidoreductase 1 (NQO1) [102,106]. Stimulation of these two antioxidants was observed in mice treated with Isoorientin a flavone, suggested to activate the Nrf2 signaling cascade [44]. This was confirmed in Isoorientin-treated Nrf2-deficient mice, where renoprotection was abolished [44]. Taken together, these studies provide an insight to the promising effects of the Nrf2 pathway as a target for CIAKI. However, studies into the interaction between Nrf2 signaling activators and the apoptotic pathways that mediate cisplatin's cytotoxicity have yet to be determined.

4.2. Vascular Injury

Interestingly, a focus on anti-inflammatory and antioxidant pathways has been highlighted in most pharmaceutical and genetic modification studies published recently. Reduced GFR caused by reduced renal blood flow is a key pathology of CIAKI [107]. Little research specifically targeting the vasoconstriction properties of cisplatin to promote renal perfusion has been undertaken. Vasoconstriction stimulated through activation of adenosine A₁ receptors (AT₁s) by cisplatin is a suggested mechanism contributing to CIAKI. Additionally, CIAKI has been linked to vascular injury via endothelial dysfunction [31,107]. Reduced renal blood flow to kidney tissue through elevated vasoconstriction and impaired vascular autoregulation stimulated by damage to the endothelium is implicated in the pathogenesis of CIAKI [12]. Cisplatin has been suggested to cause damage to the vasculature within renal tubules [12]. It results in vascular resistance and constriction of vascular smooth muscle cells (VSMC) leading to reduced renal blood flow, decreased GFR, and hypoxia of renal tubular cells, leading to kidney damage [31,108]. Cisplatin has shown to alter the response of renal vascular endothelium to vasoactive substances [15]. Kidney vasculature and tubules are known to have extensive sympathetic nerve innervation, releasing catecholamines from their terminals, and triggering G-coupled adrenoceptors on the cell surface [109]. Adrenoceptors increase calcium and trigger contractions of vasculature muscle resulting in vasoconstriction of smooth muscle cells [110,111]. Vascular injury is linked to elevations in oxidative stress, resulting in a sequence of metabolic disturbances. Cisplatin treatment leads to oxidative stress induced by ROS and impaired function of the antioxidant defense system [79]. Excessively produced ROS include superoxide (O₂⁻), hydroxyl radical (HO•), hydrogen peroxide (H₂O₂), peroxynitrite (ONOO⁻), nitrogen oxide (NO•), and hypochlorous acid (HOCl). Increased oxidative stress leads to endothelial damage, resulting in impaired endothelial dependent vascular relaxation. Endothelial dependent VSMC relaxation is NO dependent and alterations in its production or bioavailability disrupt relaxation. Additionally, eNOS function is impaired when ROS production or function is not repressed [112]. Amino acids such as L-arginine synthesize the production of eNOS to produce NO [9]. Excess production of NO by inducible NO synthase is increased following cisplatin treatment [64]. NO reacts with the NO scavenger O₂⁻ to produce peroxynitrite (ONOO⁻) [4,10–12], resulting in reduced NO bioavailability and endothelial dysfunction [113].

Recently, levosimendan, a calcium sensitizing vasodilator, has been used in a model of CIAKI [114]. It attenuated renal damage, improved renal blood flow, and enhanced kidney morphology. Despite all those factors, there was only slight alleviation in biomarkers associated with kidney dysfunction (sCr and BUN), indicating only partial prevention of CIAKI. Levosimendan significantly reduced TNF- α expression in cisplatin-treated rats, indicating levosimendan also displays anti-inflammatory properties [114]. Interestingly, despite levosimendan renoprotective effects, earlier studies demonstrated it also plays a role in the prevention of H₂O₂-induced apoptosis of cardiomyocytes [115], indicating

antiapoptotic properties taken together with levosimendan may potentially interfere with the cytotoxic properties of cisplatin. The vasculature plays a role in the pathophysiology of CIAKI; to further elucidate these effects, research into the renin angiotensin system (RAS) has been studied.

The Renin Angiotensin System in Cisplatin-Induced Acute Kidney Injury

The RAS has been investigated in models of CIAKI for at least two decades to further identify the direct effects of cisplatin on the vasculature and renal hemodynamics [116]. The RAS is responsible for the homeostatic balance of blood pressure. Angiotensin I (Ang I) is converted to angiotensin II, which stimulates angiotensin II type I receptor (AT₁) and angiotensin II type 2 receptor (AT₂), stimulating vasoconstriction and vasodilation, respectively [117,118]. Stimulation of AT₁ has been associated with renal injury [119], whilst AT₂ activation has been correlated with renoprotection, through IL-10 stimulation and IL-6 downregulation [118,120–122]. Interestingly both receptors have been investigated in a CIAKI model to assess the role of both angiotensin II receptors in nephrotoxicity (Figure 3).

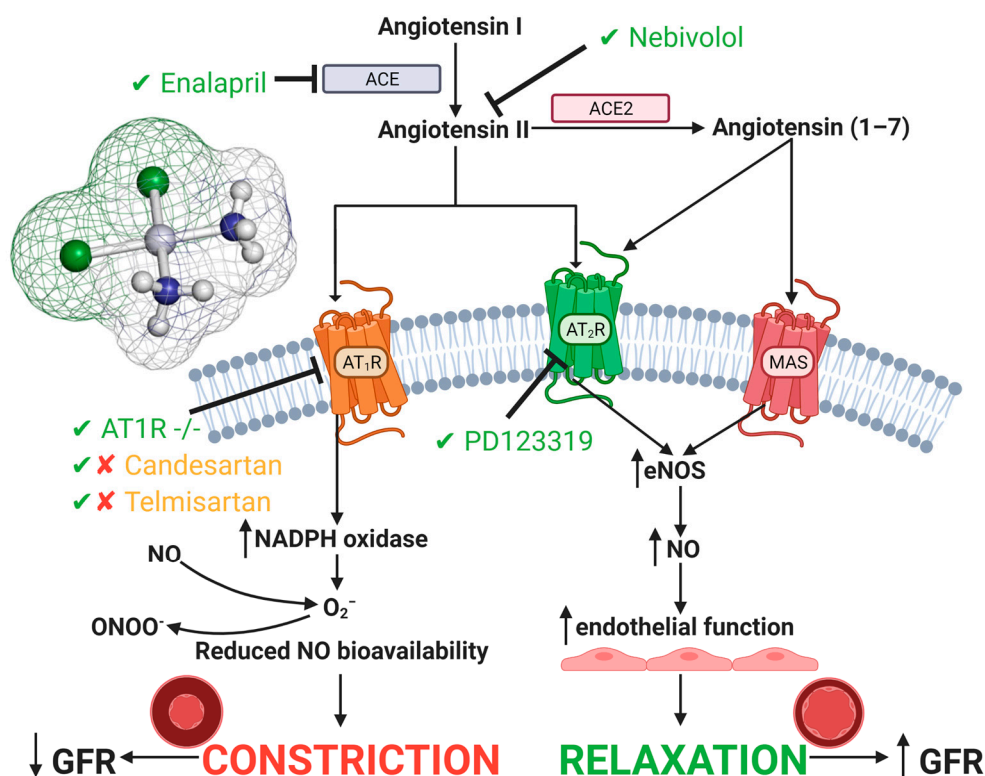


Figure 3. Cisplatin-induced acute kidney injury effects on the renin angiotensin system. A large focus has been on inhibition or genetic deletion of AT₁ and AT₂ receptors, both of which show amelioration in CIAKI [64,120,123–125]. Additionally, both ACE and Angiotensin II inhibition have also shown ameliorating qualities. Targeting the renin angiotensin system (RAS) system to prevent CIAKI is a promising pathway in potential treatments. Abbreviations: NO, nitric oxide; ONOO⁻, peroxynitrite; O₂⁻, superoxide; eNOS, endothelial nitric oxide synthase; ACE, angiotensin converting enzyme; GFR, glomerular filtration rate.

The role of the AT₁ receptor in response to nephrotoxicity is conflicting amongst the literature, with evidence linking it to renoprotection in AT₁ lymphocyte knockout models, whilst renal epithelial AT₁ knockout worsened AKI pathogenesis [126]. Interestingly, it has been reported that AT₁ stimulation worsened CIAKI through increased TNF-alpha [126]. Renal dysfunction and TNF-alpha expression was reduced in mice deficient in PTEC AT₁ receptor expression compared to WT, highlighting the protective effects of the AT₁

receptor in CIAKI [126]. Confirming these results, treatment of rats with the selective AT₁ antagonist telmisartan almost restored BUN and sCr back to control levels indicative of restored renal function [124]. Interestingly telmisartan has shown in a mouse model of CIAKI to exacerbates cisplatin-induced nephrotoxicity [123].

These results show that there is both ameliorating effects between AT₁ deficiency and stimulation in CIAKI. Additionally, this was supported by treatment with another AT₁ receptor antagonist candesartan [127], with one study reporting no impact on reduction in BUN and creatinine following cisplatin treatment [125], whilst another showed protection. Given this information, further understanding of the role of the AT₁ receptor in the pathogenesis of cisplatin-induced AKI is a critical component of understanding the pathophysiological map of the disease.

Administration of telmisartan could be causing off-target effects given the renoprotective effects were attributed to antioxidant and anti-inflammatory properties rather than its involvement in the RAS [124]. The protective effects of AT₁ inhibition in cisplatin-treated mice may be through increased activation of AT₂ or the mitochondrial assembly receptor (MAS) receptor, resulting in enhanced vascular relaxation and promoting medullary blood flow. However, antagonism of the AT₂ receptor by PD123319 improved renal function, indicated by reduced BUN and sCr when concurrently treated with cisplatin [125], suggesting that although stimulation of AT₂ is vasoprotective, it has exhibited both renoprotective and renotoxic properties [125]. Given this information, a cisplatin model using a potent and highly selective AT₂ receptor agonist may elucidate further as to its role in nephroprotection, specifically in CIAKI.

Vascular dysfunction is worsened by the overactivation of AngII production and the depletion of Angiotensin converting enzyme 2 (ACE2) [128–131]. Angiotensin converting enzyme 2 (ACE2) activation stimulates production of angiotensin (1-7) from AngII metabolism [132], increasing vascular relaxation through activation of the MAS receptor [133]. Morsi et al. (2015) confirmed AngII plays a role in cisplatin-induced nephrotoxicity; however, the direct effects it has on vascular relaxation remains unclear. In cisplatin-treated rats, there was increased protein expression of AngII, iNOS, TNF- α , and caspase-3 and decreased expression of eNOS. Nebivolol itself had no impact on protein expression; however, adjunct treatment of nebivolol with cisplatin improved eNOS expression and reduced expression of AngII, iNOS, TNF- α , and caspase-3 compared to cisplatin. Nebivolol is a selective β 1-adrenoreceptor antagonist, shown to have microvasculature vasodilatory [134], antioxidant [112,135], anti-inflammatory [136], and antiapoptotic properties. To determine the exact effects of nebivolol has on vascular function, further examinations into AT₁ and AT₂ with its use should be conducted. It is also unclear as to the exact mechanisms mediating the renoprotective effects of nebivolol, given that it may be having effects on the vasculature, inflammatory responses, and apoptotic pathways [64]. Further research specifically investigating the direct effects of vasodilation on cisplatin accumulation and resulting nephrotoxicity needs to be conducted. Cisplatin reduces expression of key molecules responsible for cisplatin efflux whilst increasing cellular uptake transporters. As such, specifically increasing blood flow without attenuating other pathologies such as inflammation and ROS production may in fact worsen CIAKI through increased platinum accumulation, potentiating worsened PTEC death.

4.3. Cell Death

There are two mechanisms whereby cisplatin induces cell death, necrosis, and apoptosis. Initial research showed necrosis to be the only mechanism responsible for renal damage caused by cisplatin. However, Lieberthalet et al. (1996) were some of the first to show that apoptosis also played a part in cisplatin-induced cell death. The study showed that high-dose cisplatin treatment induced cell death via necrosis, whilst a low dose stimulated apoptotic cell death. Clinically cisplatin is administered through frequent low-dose infusion in attempts to prevent nephrotoxic effects, which differs from the previous high-dose method [137]. However, studies investigating the relationship between necrosis and

apoptosis continues to be explored as death mechanisms caused by cisplatin-induced nephrotoxicity remain elusive [15].

4.3.1. Necrosis

Cisplatin induces cell death phenotypes in a concentration dependent manner. High concentrations of cisplatin cause a type of death independent of the classical features of apoptosis which resembles necrosis [138–140]. Necrotic damage is localized to the PTEC rather than the distal tubule as it reabsorbs filtered molecules including glucose, proteins, electrolytes, and drugs [141]. Sancho-Martinez et al. (2011) conducted a study in vitro using HK2 and Jurkat T cells, which showed activation of the apoptotic program with high necrotic concentrations of cisplatin [141]. The apoptotic program is further aborted at the level of effector caspases which emanates into necrotic-like death phenotype [141]. Necrosis is a passive mode of cell death which activates an inflammatory and immune response [141,142]. It is characterized by cell swelling, plasma membrane rupture, and loss of organelle structure [143]. Necrosis was considered as accidental cell death, which is unregulated [144] until genetic programmed necrosis was discovered in vivo [145,146]. A type of receptor-interacting protein kinase-based cell death that has similar signaling pathways with apoptosis and plays a major role in CI-AKI is namely necroptosis [142,147]. Xu et al. (2015) used RIP3-KO and mixed-lineage kinase domain-like protein (MLKL) knockout mice to investigate the role of necroptosis in CIAKI [142]. Necroptotic cell death induces inflammatory cytokines including, TNF- α , TNF-related weak inducer of apoptosis, and IFN- γ in cisplatin-treated kidneys [142]. Expression of these cytokines further contributes to the induction of receptor-interacting protein 1 (RIP1), RIP3, and MLKL expression in vivo that enhances the necroptotic signaling pathway by positive feedback [142]. Thus, necrotic cell death in renal tubules is dependent of the RIP1/RIP3 and MLKL which is stimulated by cisplatin [142]. Necrosis is caused by high-dose concentrations of cisplatin, whereas apoptosis is stimulated by lower doses [141]. There have been multiple signaling pathways linked to cisplatin-induced apoptosis. These pathways include the intrinsic (mitochondrial), extrinsic, and endoplasmic reticulum stress apoptosis pathways.

4.3.2. Apoptosis-Intrinsic/Mitochondrial Pathway

Cisplatin has been shown to induce the mitochondrial apoptotic pathway through a variety of physiological processes including ROS production and the release of cytochrome c through stimulation of proapoptotic proteins [89] (Figure 4). Mitochondrial dysfunction is associated with CIAKI [94,148]. A variety of pharmaceutical interventions that have targeted the mitochondrial apoptotic pathway have shown that nephroprotection is linked with a decrease in caspase-3 activity; however, cisplatin increases it [54,64,149]. The antiapoptotic protein Bcl-2 is established to prevent mitochondrial dysfunction-induced apoptosis [150]. Following cisplatin treatment, western blot analysis showed Bcl-2 expression is dose dependently downregulated in HK2 cells, leading to cytochrome c release, caspase-3 cleavage, and apoptosis. Cisplatin-treated cells showed a dose dependent reduction in Sirtuin 5 (Sirt5) expression. Sirt5 overexpression increased bcl-2 expression and reduced apoptosis as determined via Annexin V/PI staining. Results also showed that adjunct Sirt5 and cisplatin therapy reduced bcl-2 expression, a pathway known to induce apoptosis, indicating that Sirt5 exhibits its renoprotection in a bcl-2 independent manner, through activation of caspase-3. Interestingly resveratrol a Sirt5 activator in humans [151] attenuated CIAKI; however, there was no evaluation on Sirt5 expression [152]. It is possible that Sirt5 was activated by resveratrol and inhibited mitochondrial apoptosis by stimulating bcl-2 to inhibit mitochondrial dysfunction. Overexpression of bcl-2 is associated with reduced cisplatin cytotoxicity [153] and therefore may not be a suitable treatment option.

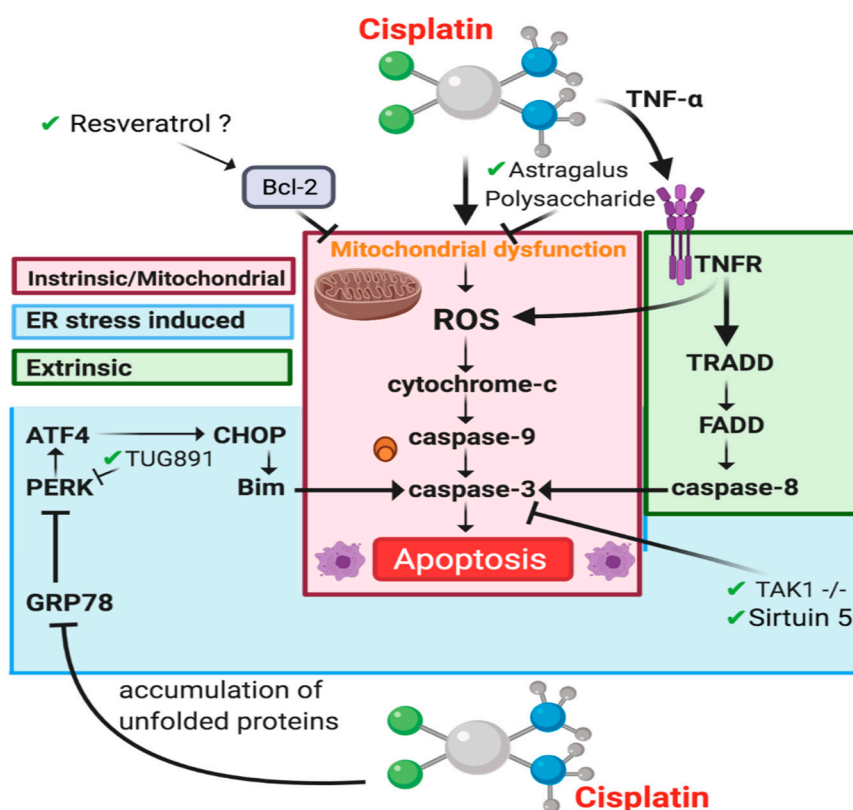


Figure 4. Apoptotic pathways involved in CIAKI. Cisplatin stimulation of ROS leads to cytochrome release and effector caspase activation in the Intrinsic/mitochondrial pathway (red) [54,94,154], ER stress is involved in two mechanisms, through stimulation of PERK to promote ER stress induced caspase-3 activation (blue) [155]. Extrinsic apoptosis is caused by TNFR1 signaling caspase-8 (green).

4.3.3. Apoptosis-Extrinsic Pathway

The extrinsic apoptotic pathway is triggered when a ligand binds to a death receptor located on the cytoplasmic membrane of cells (Figure 4). Activation of the extrinsic pathway contributes to the loss of tubular cells in AKI [156]. The extrinsic apoptotic pathway activates the caspase-8 molecules, which further activates the downstream effector caspase-3 [15,157]. Cisplatin induces the extrinsic pathway through an increase in proinflammatory cytokine TNF- α expression via its death receptor 1 (TNFR1). It is well established in the literature that TNFR1 is a major component of the TNF family, which plays an important role in the extrinsic apoptotic pathway as shown in studies where TNFR1 knockout mice have been suggested to be resistant to CIAKI [157–159]. The pathways of apoptosis are inter-related. There are three ways the extrinsic pathway is linked to the mitochondrial pathway that result in caspase-8 activation [160]. ROS generation in the mitochondria results in a direct link to the fas gene and Fas-ligand (Fas-1), which results in apoptosis [157]. In *in vitro* studies, using NRK-53E cells and α (E)-catenin knockdown cell line (C2) to identify the specific apoptotic pathway stimulated by downregulation of α (E)-catenin (linking protein) [157]. As a result, it was reported that a reduction in α (E)-catenin expression increased the susceptibility of AKI via the Fas-mediated apoptotic pathway, which confirms the role of Fas [157]. ROS generation also results in the phosphorylation of p38 and mitogen-activated protein kinase (MAPK) resulting in increased TNF- α production [161]. Ramesh and Reeves (2005) used a p38-MAPK inhibitor commonly known as SKF-86002 *in vivo* and reported that TNF- α levels were significantly decreased as well as the inhibition of p38 protected against CIAKI [162]. It was also suggested that a hydroxyl radical scavenger, dimethyl thiourea prevented the activation of the p38-MAPK pathway which completely ameliorated CIAKI [162]. Another study by Wang and colleagues (2018)

used DEP domain containing mTOR-interacting protein (DEPTOR) in vivo (in mice) and in vitro with CIAKI [163]. Evidently, DEPTOR expression increased significantly in the kidneys of mice after 3 days of cisplatin treatment [163]. DEPTOR deficiency in both in vivo and in vitro demonstrated protection of the proximal tubular cell apoptosis induced by AKI. This was achieved by inhibition of TNF- α production and p38 MAPK signaling pathway [163].

In addition to TNF- α mediated apoptosis, cisplatin activates the p53 pathway, which can be a result of elevated ROS or induced as a response to elevated ROS from the intrinsic pathway. Treatment with cisplatin results in an increased expression and activation of the p53 protein since it regulates apoptosis of proximal tubular cells via activation of repressions of genes that contain promoters p54-binding sites. Activation of p53 occurs because of alteration in the structure of DNA due to cisplatin treatment which causes activation of molecular DNA damage sensors including ataxia telangiectasia and Rad3-related proteins. These proteins further activate checkpoint kinase 2 which phosphorylate and activate p53 [154]. Herein, p53 allows an enhanced accumulation of p53-upregulated modulator of apoptosis (PUMA) in the mitochondria of tubular cells treated with cisplatin. An interaction between PUMA and B-cell lymphoma-extra-large (Bcl-xL) allows Bcl-2-associated X protein (Bax) to permeabilize the mitochondrial membrane, which then subsequently releases cytochrome C causing caspase activation and eventually causing apoptosis of tubular cells [154]. Jiang and colleagues conducted a study using p53-deficient animals and reported a reduction in the induction of PUMA, which protected against cisplatin-induced AKI [154].

4.3.4. Endoplasmic Reticulum Stress-Induced Apoptosis

Cisplatin induces cellular stress and via the mechanism can disrupt ER functions, as illustrated in Figure 1 [41]. It has been suggested the ER stress contributes to the disease manifestation of AKI [155,164]. Cisplatin increases the presence of glucose binding protein 78 (GRP78), an indicator of ER stress, in a variety of settings, [10] however, specifically in kidney tissue of both rats and mice [165,166]. GRP78 is a major ER chaperone protein. It is responsible for many processes including the translocation of newly formed polypeptides across the membrane of the ER. It also facilitates the formation of proteins (folding and assembly) and identification of faulty proteins for ER-associated degradation. GRP78 expresses antiapoptotic properties highlighting its function as an ER stress regulator [167]. GRP78 is responsible for keeping ER stress sensors (IRE1, PERK, and ATF6) inactive when a cell is not under stress. The ER stress response is initiated when the accumulation of unfolded proteins triggers dissociation of GRP78 from its receptor, ultimately resulting in the activation of the ER stress sensors [168]. The unfolded protein response reacts to the activation of stress sensors to restore proteostasis through a variety of complex mechanisms. Excessive stress or prolonged restoration of proteostasis triggers the unfolded protein responses apoptosis pathway to override cell survival [155,169]. The precise apoptotic mechanism has been linked to the activation of pro-caspase-12 in renal proximal tubular epithelial cells following cisplatin treatment [170]. Caspase-12 activation occurs in an independent manner of caspase-c function, through caspase-9 triggered effector caspase-3 activation [15]. Multiple pharmacological agents have been used to target ER stress stimulated by cisplatin treatment. Adjunct therapy with cisplatin and the G-protein-coupled receptor 120 receptor agonist TUG891 slightly reduced sCr compared to cisplatin; however, it was still greater than 2 times the concentration of both TUG891 sole treatment and control mice. Interestingly, following cisplatin treatment there was a significant increase in KIM-1 and NGAL gene expression, with TUG891 and cisplatin treatment restoring these levels almost back to control levels. TUG891 and cisplatin treatment also improved tubular injury score indicated by periodic acid Schiff staining. Investigating gene expression of key UPR and apoptotic genes PKR-like endoplasmic reticulum kinase (p-PERK), activating transcription factor 4 (ATF4) and X-box binding protein 1 (XBP1) showed that concurrent treatment with both cisplatin and TUG891 significantly reduced PERK and XBP1, whilst

minimally reducing ATF4 compared to cisplatin. The results of this study indicated that UG891 inhibited ER stress and consequently ER-stress-induced apoptosis demonstrated by reduced positive TUNEL staining and reduced caspase-3 expression [171]. This is one of many drugs published to date targeting ER-stress-induced apoptosis in models of CIAKI [41,172–176].

Pharmacological and genetic alterations that specifically target cell death and the various apoptotic pathways to stimulate cytoprotection, although highly effective in producing reno-protective effects, often reduce caspase activation and therefore disrupt or inhibit the cytotoxic pathways of cisplatin. This, although it protects against CIAKI, also diminishes the chemotherapeutic effects of cisplatin in cancer patients, therefore potentially reducing their prognosis. Previous research focused on the assessment of genetic deletion studies investigating the role of key molecules to unearth potential pathways involved in cisplatin-induced AKI. This then led to the magnitude of recent research published this year and the years preceding it, focusing largely on pharmaceutical interventions whereby inhibiting or stimulating key components of cisplatin's nephrotoxic inflammatory pathways.

5. Cisplatin-Induced Acute Kidney Injury: Role of the Immune System

Inflammatory pathways have been linked to major pathophysiological mechanisms resulting in CIAKI [45,46,52,124,177,178]. Models of AKI resulting from ischemia, sepsis, and nephrotoxicity all were presented with structural and functional changes to the vascular or tubular endothelium. These changes attract immune cells that infiltrate damaged kidney tissue. Extensive research has implicated a large array of cytokines and chemokines into the robust inflammatory response observed in models of CIAKI (Figure 5).

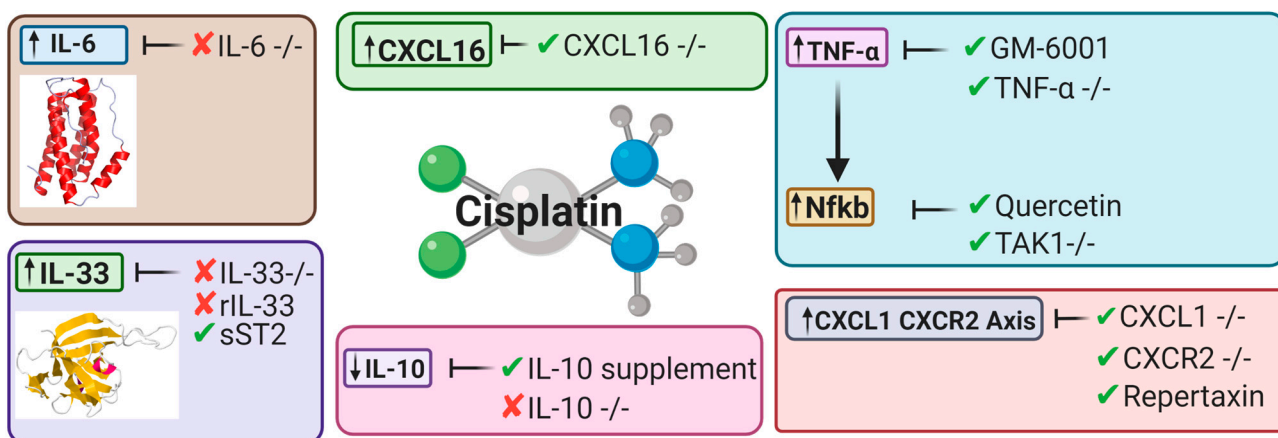


Figure 5. Key cytokines and chemokines upregulated or downregulated following cisplatin treatment. This diagram represents the therapeutic avenues published targeting inflammatory pathways and the targeted cytokines and chemokines involved [32,34,45,46,49,53,175–177].

Table 2. Genetic deletion studies investigating in vivo mechanisms associated with inflammatory processes involved in cisplatin-induced AKI pathogenesis. Key genetic deletion studies that have been targeted in both recent and hindsight applications targeting cisplatin-induced AKI with majority focusing on inflammatory pathways.

Genetic Deletion	Mechanism of Action	Results	Knockout Model	Reference
CXCL16	Antiapoptosis and anti-inflammatory	↓ Apoptosis of tubular cells ↓ Caspase-3 activation ↓ inhibition of macrophage and T cell infiltration	CXCL16 ^{-/-} mice C57BL/6J background WT	[47]
CYP2e1	Antioxidant	↓ ROS ↓ BUN ↓ sCr ↑ creatinine clearance	CYP2e1 ^{-/-} mice 129/sv background WT	[48]
IL-6	Antioxidant	↑ 4-HNE ↓ SOD1 ↓ SOD2 (no significance) ↑ ERK phosphorylation ↑ COX-2	IL-6 ^{-/-} mice C57BL/6J background WT	[49]
IL-33	Pro-inflammatory	↑ BUN ↑ sCr ↑ NGAL No attenuation in ATN and tubular apoptosis scores ↓ tumor weight, volume, and growth ↑ Cisplatin efficacy	IL-33 ^{-/-} mice C57BL/6J background WT	[50]
NLRP3	Unknown	No change to BUN, sCr, ATN score and tubular apoptosis score.	NLRP3 ^{-/-} mice C57BL/6J background WT	[51]
PARP-1	Anti-inflammatory, antioxidant and antinitrative	↓ BUN ↓ sCr ↓ PAS tubular injury score	PARP-1 ^{-/-} mice C57BL/6J background WT	[52]
T cell	Pro-inflammatory	↑ cisplatin administration survival rate ↓ sCr ↓ tubular injury score ↓ TNF-α	nu/nu mice	[53]
TAK1	Antiapoptotic, Anti-inflammatory	↓ Apoptosis of tubular cells ↓ Caspase-3 activation ↓ reduced mRNA expression of IL-6, TNF-α, MCP-1 and MIP-2 ↓ JNK phosphorylation	PT-TAK1 ^{-/-} mice	[54]
TLR-2	Inflammatory response	↑ BUN ↑ sCr ↑ tissue injury score	TLR2 ^{-/-}	[55]
TLR4	Anti-inflammatory response	↓ BUN ↓ sCr ↓ tissue injury index ↑ IL-4 and IL-10	TLR4 ^{-/-}	[55]
TLR-9	Pro-inflammatory	No significant change to either serum urea or tubular injury score.	TLR-9 ^{-/-}	[56]
TNF-α	Potentially anti-inflammatory	↓ BUN ↓ tubular necrosis score	TNF-α ^{-/-}	[33]

Abbreviations: BUN, blood urea nitrogen; sCr, sCr; PAS, periodic acid Schiff; PARP-1, Poly (ADP-ribose) polymerase-1; TLR, Toll-like receptors; TNF-α, tumor necrosis factor-alpha; 4-HNE, 4-hydroxy-2-nonenal; SOD, Superoxide dismutase; ERK, extracellular-signal-regulated kinase; COX-2, cyclooxygenase-2; NGAL, neutrophil gelatinase-associated lipocalin; CXCL16, CXC chemokine ligand 16; TAK1, transforming growth factor b-activated kinase 1; MCP-1, monocyte chemoattractant protein-1; MIP-2, macrophage inflammatory protein 2; JNK, c-Jun N-terminal kinases; CYP2e1, cytochrome P4502E1; ROS, reactive oxygen species; LRP3, LDL receptor-related protein 3; and ATN, acute tubular necrosis, ↓; Decreased, ↑; Increased, -/-; genetic deletion.

5.1. Toll-Like Receptors and Cisplatin-Induced Acute Kidney Injury

The innate immune system provides constituent primitive first-line defense mechanisms against an extensive repertoire of invading pathogens [179,180]. Integral to the

establishment of innate immunity is a distinct class of pattern recognition receptors, referred to as toll-like receptors (TLRs) [181,182]. TLRs are evolutionary-preserved transmembrane type I sentinel glycoproteins, responsible for facilitating host surveillance through the identification of molecular signatures present on pathogens and self/host cells [181,182]. TLRs contain three structural components: (i) an intracellular C-terminal toll/interleukin-1 receptor domain (TIR), (ii) a central helix spanning the plasma or organelle membrane, and (iii) an ectodomain that extends into the extracellular environment or the lumen of the intracellular organelle [183,184]. The cytoplasmic domain is responsible for mediating signal transduction upon association with activating ligands [183,184]. The leucine-rich ectodomain provides diversity and specificity between individual TLRs, as each TLR can respond to different pathogenic (Table 3) and endogenous activating ligands [184,185]. TLR expression is abundant in human non-immune and immune tissues, including cardiac; pulmonary; nervous; hepatic; gastrointestinal; lymphoid; reproductive; and renal [179]. Interestingly, the human genome contains codes for 11 TLRs [186]. However, only 10 functional TLRs are expressed [186]. It has been suggested that the absence of TLR11 may be responsible for human susceptibility to urinary tract infections, as in murine models TLR11 provides resistance against uropathogenic *Escherichia coli* [186]. Activating ligands of TLRs include pattern-associated molecular patterns (PAMP) [182] and danger-associated molecular patterns (DAMP) [187,188]. PAMPs are defined as highly conserved, invariant motifs present on pathogens, that promote microbial survivability [179,189]. DAMPs are host-derived endogenous cytoplasmic or nuclear immunogenic alarmins that are liberated by damaged, stressed, and necrotic cells in the presence or absence of pathogenic infection to restore homeostatic balance [187,188,190]. Independent of the origin of the activating ligand, the resulting end product of sterile inflammation, produced through the myeloid differentiation factor-88 (MyD88)-dependent pathway (TLR1, 2, 4–10) [191] or the TIR-containing adapter-inducing interferon- β (TRIF)-dependent pathway (TLR3 and 4) [192], is ubiquitous among TLRs [193]. Activation of TLRs results in the production of inflammatory modulators, including cytokines, chemokines, interferons, and adhesion molecules, promoting the inflammatory response [194].

Table 3. Summary of location and primary pathogens recognized by toll-like receptors.

Toll-Like Receptor	Location	Primary Pathogen (s)
1	Extracellular	Gram-positive bacterium Fungus Mycobacterium
2	Extracellular	Fungus Gram-positive bacterium Mycobacterium
3	Intracellular	Double-stranded virus
4	Extracellular	Gram-negative bacterium
5	Extracellular	Flagellum
6	Extracellular	Gram-positive bacterium Fungus
7	Intracellular	Single-stranded virus
8	Intracellular	Virus
9	Intracellular	Bacterium
10	Extracellular	Gram-positive bacterium

Receptor position influences pathogen specificity, dividing toll-like receptors (TLRs) into two subgroups [195]: (a) TLR1, 2, 4, 5, 6, and 10 are anchored to the plasma membrane and are predominantly responsible for detecting components expressed on the outer surface of flagella, fungi, and Gram-negative and -positive bacteria [181,182,196], and (b) TLR3, 7–9 reside on intracellular components (including endosomes, lysosomes, and endolysosomes) and are primarily responsible for recognizing nucleic acids derived from pathogens (bacteria and viruses) [181,182]. Internalization (trafficking of cell surface receptor into internal endosome) of TLR2 [197] and TLR4 [198] has also been reported.

TLR expression is abundant in non-diseased human renal tissue [179,199–213] (Figure 6). Thus, chronic unregulated and unresolving TLR activation may be responsible for immunopathological consequences, as augmented TLR-induced inflammation and increased expression have been reported in a plethora of non-infectious and autoimmune diseases that target the renal system, including nephrotoxicity [214]; renal disease [56,215,216]; lupus nephritis [202]; and diabetic nephropathy [217]. Furthermore, TLRs have also been implicated as potential drivers of cisplatin-induced pathologies and toxicities, including AKI [55,218,219]; renal injury [220–222]; allodynia [218]; and ototoxicity [223]. As demonstrated by TLR-deficient animal models [55,218,219] and polymorphisms in humans [224–227], the absence or improper function of TLRs may influence susceptibility and severity of pathologies affecting the renal system. Therefore, immunopathological consequences and renoprotective abilities originating from TLR activation in CIAKI are described.

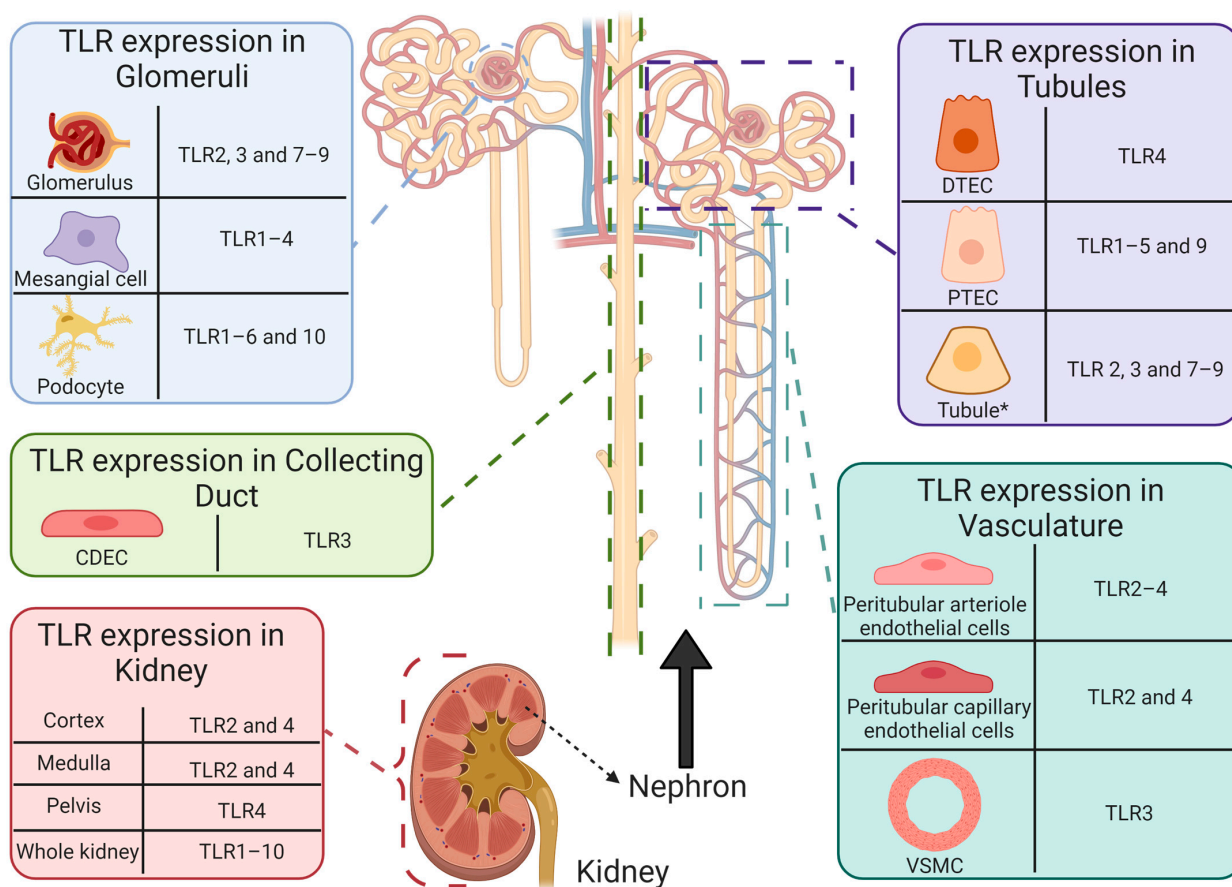


Figure 6. Functional expression of toll-like receptors in healthy human intrarenal cells and tissue. Basal expression of TLR1–10 has been reported in healthy human tissue [179]. However, determination of renal cell specific TLR expression remains limited. To date, TLR expression has been reported in intrarenal cells and structures, including: CDEC (TLR3 [199]), DTECs (TLR4 [200]), glomeruli (TLR2 [201]; TLR3 [199,202]; TLR7–9 [202,203]), mesangial cells (TLR1–4 [199,201]), peritubular arteriole (TLR2 [201] and TLR3 [199]) and capillary (TLR2 [201,204] and TLR4 [204]) endothelial cells, podocytes (TLR1–6 and 10 [205,206]), PTECs (TLR1–5 [204,207–210] and 9 [211]), tubules* (TLR2–4 [201–203,212] and TLR7–9 [203,213]), VSMCs (TLR3 [199]) and renal cortex (TLR2 [201] and TLR4 [212]), medulla (TLR2 [201] and TLR4 [212]), and pelvis (TLR4 [212]). * Tubules refers to literature that does not state the specific tubule on which TLR expression was reported. Abbreviations: collecting duct epithelial cell, CDEC; DTEC, distal tubule epithelial cell; PTEC, proximal tubule epithelial cell; toll-like receptor, TLR; vascular smooth muscle cell, VSMC.

5.1.1. Toll-Like Receptor 2 is Protective in Cisplatin-Induced Acute Kidney Injury

TLR2 is unique, as it requires recruitment of other TLRs to form heterodimers (TLR1 [228]; TLR6 [228]; and TLR10 [229]) to facilitate activation and subsequent signal transduction, promoting inflammation. While it has been postulated that TLR2 can form a homodimer, it has yet to be observed [230]. The ability of TLR2 to form heterodimer complexes with other TLRs enables it to recognize a broad spectrum of pathogens (e.g., bacterium; fungi; helminth; mycobacterium; protozoa; and virus) [231] and host-derived endogenous ligands [232]. Previous studies involving CIAKI have reported a beneficial role of TLR2 [55,233] in the progression of disease development through mediated autophagy, which has been shown to protect renal cells from the detrimental effects of cisplatin-mediated cell death [234]. Exacerbated CIAKI has been reported in mice with TLR2 deficiency, receiving daily intraperitoneal injections of cisplatin (20 mg/kg/day) [233]. Within 24 h of receiving cisplatin, TLR2-deficient mice displayed significantly increased levels of sCr and BUN, and severe morphological changes to renal tissue, including loss of brush-border cells, tubule dilation, and cast formation [233]. Furthermore, TLR2-deficient mice had reduced renal tubular epithelial cell autophagy, associated with increased protein levels of p62 (an autophagy substrate chaperone, involved in delivering of ubiquitinated peptides to autophagosomes for proteasomal degradation [235]), and decreased levels of microtubule-associated protein 1A/1B light chain 3 II (LC3 II) (a LC3-phosphatidylethanolamine conjugate that is integrated into lipid membranes of autophagosomes and phagophores, which interacts with p62 to select targets for degradation [236,237]) and phosphorylation of phosphoinositide 3-kinase and protein kinase B [233]. This study also reported significantly increased mRNA and protein expression of TLR2 in wild-type mice 24 h after cisplatin treatment, which continued to increase in a time-dependent manner [233]. A complimentary study also reported a protective role of TLR2 during CIAKI, as the absence of TLR2, in mice treated with cisplatin (20 mg/kg), resulted in renal dysfunction shown by increased levels of sCr, BUN, and urea [55]. Histological assessment determined that mice with TLR2 deficiency developed exacerbated renal injury and structural damage, including enlargement of glomerular cavity, renal tubular dilation, renal epithelial cell detachment, formation of renal casts, and infiltration of inflammatory cells (macrophages and neutrophils) into the renal medulla and presence of necrosis [55]. Additionally, lack of TLR2 reduced survivability and failed to protect mice from cisplatin-induced weigh loss [55]. This study also demonstrated a protective role in renal autophagy during CIAKI through induction of the TLR2 pathway, as autophagosome forming molecules may depend on the TLR2 signal [55]. Renal tubular cells isolated from TLR2-deficient mice had decreased levels of autophagy genes (LC3 and autophagy-related 5) and proteins (LC3II, autophagy-related protein-5 and CCAAT-enhancer-binding protein-homologous protein) after cisplatin treatment [55]. Taken together, these results suggest that TLR2 plays a beneficial role during CIAKI by regulating autophagy and reducing renal dysfunction and pathological changes.

5.1.2. Toll-Like Receptor 4 Has a Detrimental Role in Cisplatin-Induced Acute Kidney Injury

Since its discovery in 1997 [238], TLR4 has been extensively investigated in the literature, and its structure, function, and signal transduction remain the most characterised and established of the TLRs [239]. TLR4 plays an essential role in host Gram-negative immunity by identifying lipopolysaccharides, a lipid and polysaccharide conjugate that is a major component in the outer membrane of Gram-negative bacteria [240]. However, the ability of TLR4 to recognize a repertoire of pathogens has been reported, including enveloped viruses [241] and viral proteins (viral fusion proteins [242] and glycoproteins [243]), Gram-positive bacteria [244], and helminths [245]. Furthermore, TLR4 can respond to a broad range of DAMPs, including endoplasmic [239], high-mobility group-1 [246], and heat-shock protein 70 [247], which have been shown to be upregulated during cisplatin treatment. Interestingly, TLR4 has also been shown to participate in transition

metal sensing [248], and metals, including nickel, cobalt, and platinum [223,248] have been observed as TLR4-activating ligands. Due to the increase in circulating DAMPs and cisplatin (a platinum-based chemotherapy) acting as TLR4 ligands, TLR4 has been implemented as a major contributor in driving pathogenesis and development of CIAKI through upregulation of inflammation and proinflammatory and subsequent renal dysfunction, renal tissue injury, and nephrotoxicity [239]. A study involving TLR4-deficient mice administered a toxic dose of cisplatin (20 mg/kg) to induce acute renal failure within 72 h and reported significantly reduced markers of inflammation, nephrotoxicity, and renal function and decreased renal injury and histological abnormalities [239]. To determine the effect that TLR4 deficiency has on cisplatin-induced renal dysfunction and structural changes, BUN and sCr were used as indicators of function [239]. Severe renal failure (indicated by elevated levels of BUN and sCr) was observed between 48 and 72 h in WT after bolus dose of cisplatin and was accompanied by histological abnormalities including advanced tubular injury, cast formation, absence of brush-border membranes, shedding of tubular epithelial cells, necrosis of renal tubule cells, and dilation in renal tubules [239]. Mice with TLR4 deficiency has significantly preserved renal function 72 h after administration to cisplatin, as shown by reduced BUN and sCr concentrations and minimal histological changes. Thus, indicating that TLR4 contributes to structural and functional consequences during CIAKI [239]. Furthermore, immunopathological consequences, including reduced leukocyte infiltration, decreased concentrations of cytokine and chemokine in serum (i.e., TNF- α ; IL-1 β ; IL-2; IL-6; and IL-10), kidney (i.e., TNF- α ; IL-6; CCL5; MCP-10; and KC) urine (i.e., TNF- α ; IL-2; IL-6; CCL5; MCP-1; KC; and IP-10), and reduced activity of p38 MAPK and JNK phosphorylation was also observed in TLR4-deficient mice when compared to WT [239]. Thus, suggesting that the potent inflammatory response initiated by TLR4 may be responsible for initiating CIAKI [239]. Therefore, a tailored therapy encompassing a combination of cisplatin and a TLR4 inhibitor is an appealing approach to preserve renal structural integrity and preservation of function in CIAKI.

A potential TLR4 inhibitor to be used in conjunction with cisplatin, which has shown promising results in septic-induced AKI, is resatorvid (TAK242) [249,250]. TAK242 is a cyclohexene derivative [251], which exerts its inhibitory effect by binding to the intracellular domain of TLR4. Upon binding, TAK242 causes a conformational change in the cytoplasmic tail, which results in the inability of the bridging adaptor molecules TIR-containing adapter protein/myeloid differentiation factor-88 and translocating chain-associated membrane protein/TRIF to associate [252], thus preventing TLR4 signal transduction and subsequent production and release of proinflammatory mediators [252]. Administration of TAK242 to ovine models of Gram-negative bacteria resulted in enhanced renal function, demonstrated by abolishment of impaired Cr clearance in the urine, reduced BUN and sCr, prevention of renal hypoperfusion, and reduced swelling of endothelial cells in glomerular capillaries [249,250]. Additionally, a recent article has shown that TAK242 is able to enhance the cytotoxic effect of cisplatin in breast and ovarian cancer cells, while preventing its toxic effects on cells [253]. Thus, suggesting that dual treatment with TAK242 and cisplatin could enable a reduced dose of cisplatin given to patients. Taken together, TAK242 should be further investigated in CIAKI, as it represents a pharmaceutical that could (i) prevent detrimental chronic inflammation, (ii) retain structural integrity and renal function, and (c) intensify the effect of cisplatin in CIAKI.

5.1.3. Toll-Like Receptor 9 is Protective in Cisplatin-Induced Acute Kidney Injury

TLR9 is a cytosolic receptor bound to the membranes of intracellular organelles (e.g., endosomes, lysosomes, and endolysosomes) and is responsible for identification of unmethylated cytosine-phosphate-guanosine DNA present in bacteria and viruses [211,254,255]. Furthermore, TLR9 has been shown to directly contribute to cardiac, hepatic, and renal ischemic tissue injury [211] and lupus nephritis [256,257] through recognition of endogenous mitochondrial DNA products [258], chromatin IgG complex [259], GP96 [260], high-mobility group box-1 [261], and heat-shock protein 90 [262]. A study involving

CI-AKI determined a protective immunomodulating role of TLR9 in disease progression, as TLR9 absence resulted in accelerated and increased pathological development [56]. TLR9-deficient mice were administered cisplatin (20–25 mg/kg) via intraperitoneal injection and were then euthanised 24–72 h after treatment [56]. When compared to wild-type controls, TLR9-deficient mice had greater renal dysfunction and histological injury 24 h after cisplatin exposure, as shown by significant increases in serum urea, tubular injury score, neutrophil, and CD4+ cells and mRNA expression of CXCL1/2 [56]. Additionally, augmented disruption of renal tubular structure and integrity, tubular necrosis, cast formation, and accumulation of tubular cell debris was observed in kidneys derived from TLR9-deficient mice when compared to wild-type controls [56]. However, after 56 h of cisplatin exposure, no significance in renal function and histological injury was observed between TLR9-deficient mice and wild-type controls, suggesting that increased renal injury was not mediated by effector cell function in TLR9-deficient mice [56]. Previous *in vitro* studies involving human cells have postulated simultaneous activation of regulatory T cells (Tregs) and TLR9, suggesting the ability of TLR9 activation to regulate/suppress Treg activity [263]. Therefore, using this hypothesis, the authors determined if exacerbated renal injury and dysfunction was caused by Treg cell activity modulated by TLR9 [56]. The findings from this study showed that TLR9-deficient Tregs were not defective in functionally, abundance or apoptotic-inducing abilities but that the amount of adhesion molecules responsible for Treg recruitment into the kidneys was reduced in TLR9 absence [56]. This is supported by literature that shows that Tregs must be actively recruited into renal tissue to exert renoprotective abilities in AKI [56,264]. Therefore, taken together, this study suggests that TLR9 plays a beneficial role in CI-AKI by enabling recruitment of Tregs into inflamed renal tissue [56].

5.2. Cytokines

5.2.1. Tumor Necrosis Factor Alpha

Cisplatin-induced nephrotoxicity involves the activation of a proinflammatory response [265]. Cisplatin has been linked to the increased expression of TNF- α in both serum and urine concentrations of AKI [31]. TNF- α is a branch of the TNF family. These proteins are important cytokines responsible for cell signaling. They play an important role in immunity as well as the possession of proinflammatory properties [15,266]. TNF- α inhibitors have shown that in the absence of TNF- α .

α cisplatin-induced nephrotoxicity is attenuated, indicating that TNF- α plays a significant role in cisplatin's nephrotoxic effects. Treatment with the matrix metalloprotease inhibitor GM-6001, a TNF- α antagonist, reduced urea levels in GM-6001 mice compared to cisplatin, showing treatment with GM-6001 enhanced renal function. This improvement in renal function correlates with the improved renal histology [33]. Genetic modification of TNF- α also displayed renoprotective effects. Silencing of TNF-alpha showed amelioration of kidney dysfunction resulting from cisplatin treatment, with TNF-alpha $-/-$ mice protected against the nephrotoxic effects of cisplatin [33]. This highlights a crucial role of proinflammatory cytokines and chemokines in the pathogenesis of CI-AKI, particularly a central role for TNF-alpha [33]. Interestingly, TNF- α enhances the anticancer properties of cisplatin in breast cancer cells, both *in vitro* and *in vivo* [267]. It would be interesting to investigate the effects of TNF- α downregulation on the cytotoxicity of cisplatin in an *in vivo* model of CI-AK. In addition to upregulation by cisplatin, Nfkb is also activated by TNF- α [268] and in CI-AKI [33].

5.2.2. Nuclear Factor Kappa-Light-Chain Enhancer of Activated B Cells

Nuclear factor kappa-light-chain enhancer of activated B cells (NF- κ B) is a key pro-survival and inflammatory cell transcription factor and is induced by cisplatin treatment [269]. Expression of Nfkb was significantly upregulated in rats treated with cisplatin compared to control rats. SA pretreatment significantly downregulated NF- κ B expression compared to cisplatin [103]. Interleukin-6 (IL-6) and TNF- α levels were markedly reduced in the SA

and cisplatin compared to only cisplatin-treated rats; however, levels were not completely restored to control levels. Quercetin is a flavonoid that elicits anticancer, anti-inflammatory, and antioxidant properties. Results of this study showed quercetin restored kidney function indicated by reduced serum BUN and creatinine compared to cisplatin-treated mice. Quercetin also downregulated mRNA expression of key inflammatory markers IL-1 β , IL-6, and TNF- α compared to control, indicated by real-time PCR. Western blot analysis indicated Quercetin treatment decreased Syk/NF- κ B activity in kidney tissue following cisplatin-induced AKI. They concluded that inhibition of Mincle/Syk/NF- κ B signaling by quercetin exerts its renoprotective effects through reduced inflammation [46]. The progression would be to test quercetin in a tumor bearing model of cisplatin-induced AKI, and it is one of the first anticancer drugs to be used and could potentially exert its renoprotective effects whilst maintaining cisplatin's cytotoxicity. This is a promising therapeutic option for cancer patients. In addition to pharmacological inhibition of NF- κ B displaying renoprotective effects, transcriptional inhibition of NF- κ B also protects against cisplatin-induced AKI [269]. The literature has investigated the role of transforming growth factor- β -activated kinase-1 (TAK1) in cisplatin-induced acute kidney injury [54,270]. TAK-1 is a component of the NF- κ B pathway and protects cells from TNF- α -induced cell death through upregulation of antiapoptotic proteins [271]. TAK1 expression is known to be upregulated in response to cisplatin treatment [270]. TAK1 gene disruption was performed in order to generate a knockout in the proximal tubule to investigate the role of TAK1 following cisplatin treatment. Lower sCr and BUN and levels were observed in TAK1-deficient mice 72 h following injections of 20 mg/kg of cisplatin compared to controls. This is indicative of reduced renal dysfunction in the TAK-1-deficient group. H&E staining of kidney sections investigating tubular epithelial cell injury, proximal tubular dilation, and cast formation showed TAK-1 deficiency reduced histological evidence of kidney injury [54]. Following this knockout study, a pharmacological study of cisplatin-induced AKI was performed using a TAK1 inhibitor. Results of the study determined that TAK-1 inhibition increased sCr and BUN, suggesting TAK-1 plays a protective role against CIAKI. Interestingly, following the increased expression of TNF-alpha and consequently Nfkb observed in CIAKI, this is often correlated with a downregulation in Interleukin-10 (IL-10).

5.2.3. Interleukin-10

There is significant evidence implicating proinflammatory cytokines in the pathogenesis of cisplatin-induced renal dysfunction [272–274], stimulating the focus on anti-inflammatory cytokines as therapeutic targets against CIAKI. IL-10 is an anti-inflammatory cytokine produced by T helper cells, T cells, dendritic cells, and macrophages [31]. IL-10 inhibits many physiological processes including early-phase inflammation, cytokines, chemokines, neutrophil activation, and NO production [273]. Deng and colleagues conducted a study to investigate the effects of IL-10 on CIAKI in male BALB/c and C57BL/6 mice. A histological analysis was conducted 72 h after mice were treated with cisplatin. Results showed evidence of necrosis in the renal proximal tubule and the straight tubule. Cast formation and leukocyte accumulation was also shown, indicative of an inflammatory response. The results of the study showed that serum concentrations of IL-10 were downregulated in response to cisplatin treatment and maximal inhibition of renal injury was observed when cisplatin and 1g of IL-10 (determined via dose-dependent study) was administered concurrently. It was also determined that IL-10 administration one hour post cisplatin treatment also decreased renal damage [273]. A separate study in IL-10 KO mice showed enhanced CIAKI, further explicating its renoprotective effects [275]. Increased IL-10 expression has also been associated with the renoprotective effects of AT₂ receptor stimulation following TLR4-induced inflammation [118]. This shows that enhanced expression of IL-10 is renoprotective and finding a pharmaceutical activator of IL-10 to assess in a model of AKI may provide therapeutic benefit. Tumor cells are known to overexpress key cytokines, such as IL-10. IL-10 protected against chemotherapeutic agent effects, through upregulation of antiapoptotic proteins such as Bcl-2 and Bcl-xL [276]. As such,

further investigations into the effects of IL-10 attenuation of CIAKI in a tumor-bearing model should be completed. IL-33 another cytokine has been suggested to contribute to cisplatin's nephrotoxicity.

5.2.4. Interleukin-33

IL-33 is a proinflammatory cytokine. This cytokine contains a receptor ST2, which attracts immune cells such as CD4+ and T cells via chemotaxis [31]. Elevated kidney expression of IL-33 was observed in CIAKI and tubular injury, suggesting that IL-33 may contribute to the nephrotoxic effects detected following cisplatin treatment [50,277]. Akcay and colleagues conducted a study using a decoy receptor to identify the role IL-33 and CD4+ T cells play in cisplatin-induced acute tubular necrosis (ATN) and apoptosis. In the study, two experimental groups were used. The first group was administered sST2, a decoy receptor to inhibit IL-33 function. It was found that when this was administered, a reduction in the infiltration of CD4+ T cells was observed along with decreased ATN and apoptosis. In the second group, recombinant IL-33 was administered and was found to intensify CIAKI, whilst in CD4+-deficient mice administered with IL-33, kidney structure and function remained unaffected. The results of this inferred that CD4+ T cells were accountable for the damage caused by IL-33; in addition they concluded that IL-33 inhibition may have a therapeutic potential in CIAKI [277]. Ravichandran and colleagues conducted a study that investigated the protective role of IL-33 deficiency on cisplatin-induced AKI. The results showed that IL-33 deficiency was not protective against CIAKI in mice [50]. The interesting component of this study that differs from most CIAKI models is that it was a tumor-bearing model. This stimulated investigations regarding not only the nephroprotective effects of IL-33 deficiency but also the effects of the deficiency on cisplatin's anticancer activity. BUN and sCr were elevated in both IL-33 deficiency and WT mice treated with cisplatin in addition to increased expression of the AKI biomarker NGAL. ATN and tubular apoptosis observed in cisplatin-induced AKI were not alleviated in IL-33-deficient mice, furthering the evidence that IL-33 deficiency could not attenuate cisplatin's nephrotoxic effects. It has been demonstrated that IL-33 is upregulated in cisplatin treatment [277]. Although IL-33 may be involved and contribute to CIAKI, it is unlikely to be causative. To investigate IL-33 deficiency on the cytotoxicity of cisplatin, cleaved, caspase-3 expression was examined. In tumors of vehicle, WT-treated and IL-33-deficient mice, no significant differences in caspase-3 expression was observed; however, caspase-3 levels were elevated in tumors of cisplatin WT mice but not in IL-33-deficient mice. Although there was evidence of reduced apoptosis, tumor weight, tumor volume, and tumor growth were all reduced in IL-33-deficient mice, a beneficial outcome for cancer prognosis [50]. Recent publications have implicated tumors themselves in the pathogenesis of AKI potentially through tumor lysis syndrome (TLS). TLS is caused by cancer treatments; however, they can occur spontaneously themselves, discharging cancer contents into the bloodstream, clinically presenting as hyperuricemia, hyperkalemia, hyperphosphatemia, and hypocalcemia which can manifest and result in renal dysfunction [278]. Most publications to date use noncancer-bearing models to assess interventions for CIAKI. Healthy mice are injected with cisplatin either prior, concurrently, or following the intervention. This therefore investigates nephrotoxicity caused by cisplatin itself; however, it excludes the influence of cancer on kidney dysfunction. It has been suggested that TLS from cancer patients may contribute to the pathogenesis of CIAKI; therefore, Ravichandran and colleagues repeated the same experiments on IL-33 deficiency in cisplatin-treated mice without cancer. The results of this concluded that cancer did not influence the lack of renoprotection, elicited by IL-33 deficiency [50]. Knowing this, it highlights the importance of trialing therapies in both tumor-bearing and tumor-absent models of CIAKI.

5.2.5. Interleukin-6

IL-6 is a pleiotropic cytokine predominantly exerting proinflammatory functions but also exhibits anti-inflammatory properties [279]. It is a member of the interleukin

family of cytokines, a collective whose involvement has been extensively researched in the pathology of CIAKI for many years. Serum and urine levels of IL-6 are elevated following cisplatin treatment, and it has been used as an early serum and urine biomarker of AKI [280]. However, IL-6 stimulation has been proposed to play a protective role in models of cisplatin-induced AKI implied to be via upregulation of antioxidant markers [49]. IL-6 $-/-$ mice were administered 30 mg/kg of cisplatin via intraperitoneal injection. Twenty-four and 72 h post cisplatin administration blood and kidneys were harvested and analyzed for oxidative and antioxidative stress markers. Western blotting of IL-6 $-/-$ cisplatin-treated mice showed increased expression of 4-HNE compared to wild-type mice. Following this, gene expression of free radical scavengers SOD1 and SOD2 in cisplatin-treated kidneys was analyzed via RT-PCR assays. Kidneys excised 24 h after cisplatin treatment yielded no significant difference in SOD1 expression; however, SOD1 expression was reduced in wild-type and IL-6 $-/-$ mice 72 h after cisplatin treatment. In addition to investigating gene expression, enzymatic activity of SOD was analyzed indicating that SOD activity was significantly reduced in kidneys of IL-6 $-/-$ mice compared to wild type [49]. Previously, it was determined that although IL-6 deficiency did not accelerate the development of systemic injury, it did accelerate progression of cisplatin-induced acute renal failure [281]. This indicates that IL-6 may play a protective role in CIAKI, but to date, there is no pharmacological IL-6 antagonism studies investigating this. Cancer models have showed that increased expression of IL-6 enhances acquired cisplatin resistance and reduces cytotoxicity; therefore, direct stimulation of IL-6 over-expression may reduce the efficacy of cisplatin [282] and therefore may not be an appropriate therapeutic target for cancer patients to prevent CIAKI. Many cytokines have been explored in models of CIAKI; however, recent literature has elucidated the role of specific chemokines in the pathogenesis of the disease.

5.3. Chemokines

The development and progression of an inflammatory response has long been associated with kidney damage and nephrotoxicity stimulated by cisplatin treatment [283]. Evidence has presented a role for proinflammatory chemokines as potential mechanisms associated with CIAKI, which is suggested to be mediated via TNF- α [33]. Both CXC and CC chemokines have varying roles in cancer, with many members from both subfamilies recruited to tumor sites playing either a pro- or anti-tumor role. Multiple chemokines from the CXC family have been linked to the pathogenesis of cancer, particularly in the stimulation of angiogenesis [284]. Several chemokine family members have also been shown to contribute to the pathogenesis of CIAKI.

5.3.1. CXCL16

CXC chemokine ligand 16 (CXCL16) is a member of the CXC family of chemokines [47]. CXCL16 has been associated with proinflammatory properties in multiple diseases [285, 286]. Research suggests that CXCL16 may play a role in acute coronary syndrome most often associated with atherosclerosis [287]. Inhibition of CXCL16 has been linked to ameliorating effects in a variety of inflammatory related diseases such as liver inflammation and steatohepatitis [288], anti-GBM glomerulonephritis [289] and the regulation of CIAKI [47]. CXCL16 expression is upregulated in kidneys following cisplatin treatment [47]. To further understand the mechanisms stimulating this upregulation and the role CXCL16 plays in inflammation and apoptosis in renal tubular cells, wild-type and knockout mice were injected with 20 mg/kg of cisplatin. Seventy-two h after cisplatin treatment, the mice were culled. The results showed that kidney dysfunction was observed in wild-type mice, indicated by elevated levels of serum BUN. CXCL16 knockout mice were protected from cisplatin-induced renal dysfunction with reduced levels of serum BUN. Knockout mice also presented with reduced histological damage of renal tissue compared to WT mice. This study used RT-PCR to investigate mRNA expression of key proinflammatory cytokines associated with CIAKI. Results showed that following cisplatin injection expression of

TNF- α , IL-1 β , IL-6, and transforming growth factor β 1 were upregulated in wild-type mice compared to the vehicle. Inhibition of mRNA expression of these molecules was observed in CXCL16 knockout mice. Decreased caspase-3 activation was also seen in CXCL16 $-/-$ mice illustrating CXCL16's role in tubular epithelial cell apoptosis. [47]. A separate study also involving CXCL16 $-/-$ mice investigated renal injury associated with salt-sensitive hypertension. The study showed that DOCA-salt-treated $-/-$ mice showed reduced renal dysfunction, proteinuria, BUN, and fibrosis compared to wild-type mice [290]. The collection of these studies has highlighted a role for CXCL16 in the inflammatory response associated with renal injury. Given the information and results observed in these studies, the progression would be to assess concurrent treatment with cisplatin and the pharmacological inhibition of CXCL16 in the prevention of nephrotoxicity. Pharmacological treatment using a monoclonal, rat anti-mouse CXCL16 neutralising antibody has shown to reduce liver inflammation in chronic hepatic injury [291]. More relative to AKI, a study involving the pharmacological inhibition of CXCL16 using an antiserum generated against CXCL16 showed reduced progression of anti-GBM glomerulonephritis suggested to be through its role in leukocyte influx [289]. Despite the evidence linking CXCL16 to CIAKI, it is not the only CXC chemokine linked to the disease. The CXCL1-CXCR2 axis has also been shown to be involved in renal damage following cisplatin treatment.

5.3.2. CXCL1-CXCR2 Axis

The chemokine (C-X-C motif) ligand 1 (CXCL1) belongs to the CXC family of chemokines. The molecular structure of CXCL1 can be either a monomer or a dimer and is a highly potent CXCR2 receptor agonist [292]. The CXCL1-CXCR2 axis has been implicated in a variety of inflammatory diseases, specifically through its role in neutrophil recruitment and microbial death at sites of tissue injury [292,293]. A key component in the immune response triggered by AKI promoting renal injury is the accumulation of key leukocytes, such as neutrophils and monocyte/macrophages [294]. CXCL1 and its upregulation has been secondarily investigated in models of CIAKI specifically in IL-33-deficient mice [50]. A recent study published demonstrated the inhibition of the CXCL₁-CXCR₂ axis provided ameliorating effects against renal damage induced by CIAKI [35]. Following cisplatin treatment, a significant increase in kidney mRNA and protein expression for both CXCL1 and CXCR2 compared to control was observed, indicating that the CXCL₁-CXCR₂ axis plays a role in the nephrotoxic effects induced by cisplatin. Reduced sCr and BUN were observed in both CXCL1- and CXCR2-deficient mice, indicating axis silencing improves renal function and AKI induced by cisplatin. There was also evidence of reduced renal neutrophil infiltration, indicating the potential of a reduced immune response in both CXCL1- and CXCR2-deficient mice. Following the genetic deletion studies, pharmacological inhibition of CXCL1 and CXCR2 with repertaxin displayed ameliorating effects against CIAKI. The results of their study concluded that inhibition of the CXCL₁-CXCR₂ axis was renoprotective against CIAKI through inhibition of p38 and Nf κ b. [35]. Following this, the use of selective pharmacological antagonists of CXCL1 to and CXCR2 is needed to observe their isolated role in the disease pathogenesis of CIAKI.

6. Preclinic to Clinic Translation

Despite the magnitude of preclinical studies aimed at preventing CIAKI/nephrotoxicity, only a small number have progressed to preclinical stages. Interestingly, most models of CIAKI begin in a nontumor bearing model, with healthy mice that are treated with either a single high dose of cisplatin or multiple lower doses over an extended period. Mice present an important preclinical model in research, with a 99% similar genome to humans. Additionally, their small size provides a cost-effective alternative for large-scale studies. Many drugs have been validated in mice for efficacy and safe dosage, which have safely translated to humans [295]. However, there are also instances where this translatability has been questionable. In 2019, Leena and colleagues published a paper presenting an overview of the animal-to-human translational success rates, where they concluded that

translational success is unpredictable. They also pointed out that the data used were old and potentially biased and suggested that the data from newer papers were unreliable [296]. This was a paper published recently and it is interesting the lack of success rates published by newer studies. They do also suggest that suboptimal experimental design may be a contributing factor to translational failure in recent models. Reproducibility in both animal and human studies has also posed an issue regarding translatability [296]. In 2015, a paper was published specifically addressing five key improvement areas for preclinical models to improve drug development for CIAKI. Animal-based experiments are often the basis for clinical trial studies. A perfect example is the studies investigating the effects of *N*-acetylcysteine (NAC) in the prevention of contrast-induced AKI. In preclinical models, NAC data were supportive of its renoprotective effects warranting its use in clinical trials; however, there were key elements missing from the preclinical studies. Preclinically NAC was administered via IV, whilst in the clinical trial, it is was received orally, and there were no data obtained in the preclinical findings indicating half-life or duration of antioxidant effects and that could explain the failure in translation [297].

As mentioned earlier, cancer itself can cause renal damage through the biproducts released in cancer cell degradation stimulated by cancer itself or its treatment [298]. As such, it is critical that tumor-bearing models are tested following nontumor-bearing studies, given clinical trials will always be in patients with cancer. Majority of preclinical studies adapt a single high-dose injection with endpoint being 72 h after cisplatin, it may also be beneficial to complete a model in addition to this that closer replicates human cisplatin drug regimens before moving into clinical trials. It is also interesting that even despite all the preclinical drugs published that demonstrate amelioration of CIAKI, there is no evidence of the drug progressing further into a tumor-bearing model or clinical trials. A paper published in 2019 presented a drug that can prevent CIAKI whilst increasing cisplatin cytotoxicity as demonstrated in H1299 cancer cell lines [37]. This presents highly promising potential and hopefully a follow-up study by the same group in a tumor-bearing model will be a follow-up before its progression to clinical trials.

7. CIAKI Clinical Trials

There have only been a few clinical trials to date as described in Table 4. Not all clinical trials were completed or present results. Clinically Amifostine is the only FDA approved treatment in the prevention of CIAKI. It has undergone a variety of clinical trials in cancer patients treated with cisplatin, with result demonstrating its renoprotection and cytoprotection. However, its cytoprotection has yielded inconsistent results with toxicities still occurring despite the use of optimal Amifostine doses [299]. Another clinical study which is continuously disagreed upon throughout the literature is the safety and efficacy of mannitol as a therapeutic option for CIAKI [300,301]. Mannitol is an osmotic diuretic which has generated promising preclinical in vivo data in the prevention of cisplatin-induced acute kidney injury [302]. These preclinical data then provided the evidence required to progress the use of mannitol into clinical trials, leading it to FDA approval and the current standard of care for patients with CIAKI. However, there is evidence of increased hyponatremia in cisplatin-treated patients hydrated with saline and mannitol [303]. In addition to mannitol, another more recent clinical trial prevention strategy for CIAKI is magnesium preloading. Results of this study showed that although magnesium preloading prevented cisplatin-induced acute kidney disease, there was no statistical significance in the prevention of CIAKI. However, there was a reduction trend, and thus a larger-scale trial is required to further assess its amelioration of CIAKI [304]. Pretreatment with pantoprazole has provided an interesting therapy, providing ameliorating effects in preclinical findings [62]; however, in the clinical setting, results showed pantoprazole unprotective preventing cisplatin nephrotoxicity in osteosarcoma patients. This provided further evidence for cancer cell influence on nephrotoxicity and the importance of preclinical tumor-bearing models and publication of the findings of these studies. A universal issue that is observed throughout most clinical trials of CIAKI is a lack of statistical significance occurring due

to small sample size. This small sample size is largely attributed to the harsh exclusion criteria for this disease; generating a larger sample size would benefit clinical trials for CIAKI therapeutic studies.

Table 4. Cisplatin-induced acute kidney injury human clinical trials.

Name of Trial	Status	Year	Results	Clinical Trial Identifier/Reference
The Effect of Intravenous Mannitol Plus Saline on the Prevention of Cisplatin-induced Nephrotoxicity: A Randomized, Double-blind, Placebo Controlled Trial (MACIN)	Recruiting	2020	TBA	NCT04251689
The effect of melatonin on cisplatin-induced nephrotoxicity: A pilot, randomized, double-blinded, placebo-controlled clinical trial	Completed	2020	Reduced KIM-1/creatinine and NGAL/creatinine ratios indicative of reduced AKI. patients treated with melatonin showed reduced AKI episodes compared to the placebo group. This however was non-significant suggested to be due to the small sample size.	[305]
Mesenchymal Stem Cells in Cisplatin-Induced Acute Renal Failure in Patients with Solid Organ Cancers	Withdrawn	2011, updated 2018	Study withdraw as patients failed to develop acute renal failure (Key criterion for the study)	NCT01275612
Preloading Magnesium Attenuate Cisplatin-induced Nephrotoxicity	Completed	2015, updated 2019	—Beneficial in prevention of cisplatin-induced acute kidney disease No statistical significance in the prevention of CIAKI.	NCT02481518 [304]
Effects of DPP4 Inhibitor on Cisplatin-Induced Acute Kidney Injury	Unknown			NCT02250872 [306]
Preventing Nephrotoxicity and Ototoxicity from Osteosarcoma Therapy	Completed	2013, updated 2020	—serum creatinine/biomarkers of AKI (KIM-1/NGAL) were not improved by pantoprazole —The study concluded that pantoprazole was unable to ameliorate cisplatin-induced AKI.-	NCT01848457 [75]
Randomized phase II feasibility study of mannitol or furosemide hydration in moderate dose of cisplatin-based chemotherapy with short hydration for advanced non-small cell lung cancer	Completed	2014, updated 2021	No significant difference in renal toxicity compared to treatment without mannitol	UMIN000015293 [301]
Evaluation of the Effect of Acetazolamide, Mannitol and N-acetylcysteine on Cisplatin-Induced Nephrotoxicity	Completed	2016, updated 2017	TBA	NCT02760901 [307]
Effect of Silymarin Administration on Cisplatin Nephrotoxicity: Report from A Pilot, Randomized, Double-Blinded, Placebo-Controlled Clinical Trial	Completed	2013, updated 2015	NGAL/creatinine ratio was the same between silymarin and placebo groups Overall conclusion of the study is that silymarin was not effective against cisplatin-induced AKI.	[308]
Amifostine pretreatment for protection against cyclophosphamide-induced and cisplatin-induced toxicities: results of a randomized control trial in patients with advanced ovarian cancer	Completed	1996	Reduced number of patients requiring delaying or discontinue cisplatin treatment due to nephrotoxicity in Amifostine co treatment group compared to cisplatin alone. Amifostine reduced incidence of hypomagnesemia (key characteristic of cisplatin nephrotoxicity).	[309]

8. Potential Future Treatments

The current preventative treatments for cisplatin-induced nephrotoxicity are hyperhydration with intravenous saline, sodium loading (shown to have no influence on cisplatin-induced nephrotoxicity incidence [310]) and forced diuresis with mannitol [301,311]. Mannitol treatment has yielded conflicting results [312]. Mannitol has shown however, to cause over diuresis resulting in dehydration [95]. Physiologically cisplatin is known to reduce medullary blood flow and induce afferent arteriole vasoconstriction causing ischemic damage [31,313]. Normal autoregulatory renal vasodilation occurring in response to ischemia is instead replaced with enhanced vasoconstriction resulting in further hypoxic kidney injury [31]. We therefore hypothesize that in addition to hydration, treatment with a vasodilatory inducing or enhancing drug may work to flush cisplatin out of the kidney system. The use of drugs capable of stimulating vasodilation through other pathways that also promote cytotoxicity of cisplatin is another proposal. Currently a large proportion of successful preclinical therapies target antioxidant and anti-inflammatory pathways, which consequentially also result in antiapoptotic mechanisms. This poses an issue when cisplatin is given to promote cancer cell death to improve the prognosis for cancer patients. Stimulation of antiapoptotic mechanisms interfere with the anticancer pathway of cisplatin which makes giving a therapy to reduce cisplatin cytotoxicity to promote renoprotection counterproductive. Based on this, we propose the use of certain drugs capable of stimulating vascular relaxation to promote excretion of cisplatin using drugs that also enhance the cytotoxicity of cisplatin. TIC10, a chemotherapy currently in clinical trials as an anticancer agent is a TRAIL-inducing compound. TRAIL has been linked to potential of relaxation enhancement through increased eNOS shown in HUVECs. Our laboratory also published a paper showing the enhancement of vascular relaxation of healthy vessels by TIC10 [314]. Interestingly, given the anticancer properties of TIC10, more specifically its ability to selectively induce apoptosis in cancer cells whilst sparing healthy cells in addition to its relaxation properties, it presents a possible therapeutic option in the prevention of CIAKI.

9. Conclusions

Despite advances in oncology research and interventions, research is yet to yield a solid and universal solution to the detrimental nephrotoxic side effects experienced by patients treated with cisplatin [315]. To date, many pharmacological interventions have proven effective in the prevention of CIAKI. However, their nephroprotective effects directly interfere with the cytotoxic pathways of cisplatin and thus reduce its efficacy. Several potential therapies have been discovered that prove beneficial in the reduction of AKI in a preclinical research setting. However, the transference from animal to human clinical studies is disappointing [297]. This warrants the need for research into uncovering additional pharmacological interventions to develop a more translatable treatment. There is an extensive pathophysiological map identifying mechanisms involved to further develop understanding into this disease and how it manifests to create better prevention or treatment options. The purpose of this review is to present a large collective of recent studies as well as the most influential past studies to detail the extent of the complexity of this disease. It also elucidates the potential issues arising that are preventing preclinic to clinic translatability. Currently, despite the hundreds of preclinical promising models, there is a severe lack of progression of these therapies to tumor-bearing models and further progression to clinical trials. Many promising therapies also directly target cisplatin cytotoxic pathways and are therefore not feasible to progress with into clinic. Cellular uptake/efflux, oxidative stress, vascular injury, necrosis, apoptosis, and inflammation remain the focused therapeutic areas; however, perhaps this disease requires a broader treatment or a regimen of treatments to combat the array of mechanisms.

Author Contributions: K.R.M., L.K.G., T.Q., and B.A.A. wrote the paper and all authors (A.Z. and V.A.) reviewed and edited the article. All authors have read and agreed to the published version of the manuscript.

Funding: This review received no external funding.

Acknowledgments: All authors would like to thank the Institute for Health and Sport, Victoria University for their support. K.R.M., L.K.G. and T.Q. were supported by the Victoria University Postgraduate Scholarship. All figures presented in this article were created by the authors using biorender.com.

Conflicts of Interest: The authors declare no conflict of interest.

References

1. Gomez-Ruiz, S.; Maksimović-Ivanić, D.; Mijatović, S.; Kaluđerović, G.N. On the discovery, biological effects, and use of cisplatin and metallocenes in anticancer chemotherapy. *Bioinorg. Chem. Appl.* **2012**, *2012*, 140284. [[CrossRef](#)] [[PubMed](#)]
2. Wang, S.; Xie, J.; Li, J.; Liu, F.; Wu, X.; Wang, Z. Cisplatin suppresses the growth and proliferation of breast and cervical cancer cell lines by inhibiting integrin $\beta 5$ -mediated glycolysis. *Am. J. Cancer Res.* **2016**, *6*, 1108–1117.
3. Li, Z.; Zhang, P.; Ma, Q.; Wang, D.; Zhou, T. Cisplatin-based chemoradiotherapy with 5-fluorouracil or pemetrexed in patients with locally advanced, unresectable esophageal squamous cell carcinoma: A retrospective analysis. *Mol. Clin. Oncol.* **2017**, *6*, 743–747. [[CrossRef](#)] [[PubMed](#)]
4. Hussain, S.; Palmer, D.; Lloyd, B.; Collins, S.; Barton, D.; Ansari, J.; James, N. A study of split-dose cisplatin-based neo-adjuvant chemotherapy in muscle-invasive bladder cancer. *Oncol. Lett.* **2012**, *3*, 855–859. [[CrossRef](#)] [[PubMed](#)]
5. Chan, B.A.; Coward, J.I.G. Chemotherapy advances in small-cell lung cancer. *J. Thorac. Dis.* **2013**, *5* (Suppl. 5), S565–S578. [[CrossRef](#)]
6. Einhorn, L.H.; Donohue, J. Cis-Diamminedichloroplatinum, Vinblastine, and Bleomycin Combination Chemotherapy in Disseminated Testicular Cancer. *Ann. Intern. Med.* **1977**, *87*, 293–298. [[CrossRef](#)] [[PubMed](#)]
7. Wagner, M.J.; Livingston, J.A.; Patel, S.R.; Benjamin, R.S. Chemotherapy for Bone Sarcoma in Adults. *J. Oncol. Pract.* **2016**, *12*, 208–216. [[CrossRef](#)]
8. Le, X.; Hanna, E.Y. Optimal regimen of cisplatin in squamous cell carcinoma of head and neck yet to be determined. *Ann. Transl. Med.* **2018**, *6*, 229. [[CrossRef](#)]
9. Dasari, S.; Tchounwou, P.B. Cisplatin in cancer therapy: Molecular mechanisms of action. *Eur. J. Pharm.* **2014**, *740*, 364–378. [[CrossRef](#)]
10. Mandic, A.; Hansson, J.; Linder, S.; Shoshan, M.C. Cisplatin induces endoplasmic reticulum stress and nucleus-independent apoptotic signaling. *J. Biol. Chem.* **2003**, *278*, 9100–9106. [[CrossRef](#)] [[PubMed](#)]
11. Price, P.M.; Yu, F.; Kaldis, P.; Aleem, E.; Nowak, G.; Safirstein, R.L.; Megyesi, J. Dependence of cisplatin-induced cell death in vitro and in vivo on cyclin-dependent kinase 2. *J. Am. Soc. Nephrol.* **2006**, *17*, 2434–2442. [[CrossRef](#)]
12. Pabla, N.; Dong, Z. Cisplatin nephrotoxicity: Mechanisms and renoprotective strategies. *Kidney Int.* **2008**, *73*, 994–1007. [[CrossRef](#)]
13. Rybak, L.P.; Mukherjea, D.; Jajoo, S.; Ramkumar, V. Cisplatin ototoxicity and protection: Clinical and experimental studies. *Tohoku J. Exp. Med.* **2009**, *219*, 177–186. [[CrossRef](#)]
14. Rybak, L.P.; Whitworth, C.A.; Mukherjea, D.; Ramkumar, V. Mechanisms of cisplatin-induced ototoxicity and prevention. *Hear. Res.* **2007**, *226*, 157–167. [[CrossRef](#)] [[PubMed](#)]
15. Dos Santos, N.A.G.; Rodrigues, M.A.C.; Martins, N.M.; Dos Santos, A.C. Cisplatin-induced nephrotoxicity and targets of nephroprotection: An update. *Arch. Toxicol.* **2012**, *86*, 1233–1250. [[CrossRef](#)] [[PubMed](#)]
16. Xing, J.J.; Hou, J.G.; Ma, Z.N.; Wang, Z.; Ren, S.; Wang, Y.P.; Liu, W.C.; Chen, C.; Li, W. Ginsenoside Rb3 provides protective effects against cisplatin-induced nephrotoxicity via regulation of AMPK-/mTOR-mediated autophagy and inhibition of apoptosis in vitro and in vivo. *Cell Prolif.* **2019**, *52*, e12627. [[CrossRef](#)]
17. Hoek, J.; Bloemendal, K.M.; Van der Velden, L.A.A.; Van Diessen, J.N.; Van Werkhoven, E.; Klop, W.M.; Tesselaar, M.E. Nephrotoxicity as a Dose-Limiting Factor in a High-Dose Cisplatin-Based Chemoradiotherapy Regimen for Head and Neck Carcinomas. *Cancers* **2016**, *8*, 21. [[CrossRef](#)] [[PubMed](#)]
18. Mi, X.-J.; Hou, J.-G.; Wang, Z.; Han, Y.; Ren, S.; Hu, J.-N.; Chen, C.; Li, W. The protective effects of maltol on cisplatin-induced nephrotoxicity through the AMPK-mediated PI3K/Akt and p53 signaling pathways. *Sci. Rep.* **2018**, *8*, 15922. [[CrossRef](#)]
19. Ashrafi, F.; Haghshenas, S.; Nematbakhsh, M.; Nasri, H.; Talebi, A.; Eshraghi-Jazi, F.; Pezeshki, Z.; Safari, T. The Role of Magnesium Supplementation in Cisplatin-induced Nephrotoxicity in a Rat Model: No Nephroprotectant Effect. *Int. J. Prev. Med.* **2012**, *3*, 637–643.
20. Sastry, J.; Kellie, S.J. Severe neurotoxicity, ototoxicity and nephrotoxicity following high-dose cisplatin and amifostine. *Pediatric Hematol. Oncol.* **2005**, *22*, 441–445. [[CrossRef](#)]
21. Qin, Y.; Stokman, G.; Yan, K.; Ramaiahgari, S.; Verbeek, F.; De Graauw, M.; Van de Water, B.; Price, L.S. cAMP signalling protects proximal tubular epithelial cells from cisplatin-induced apoptosis via activation of Epac. *Br. J. Pharmacol.* **2012**, *165*, 1137–1150. [[CrossRef](#)]
22. Bellomo, R.; Kellum, J.A.; Ronco, C. Acute kidney injury. *Lancet* **2012**, *380*, 756–766. [[CrossRef](#)]
23. Kellum, J.A.; Unruh, M.L.; Murugan, R. Acute kidney injury. *BMJ Clin. Evid.* **2011**, *394*, 1949–1964. [[CrossRef](#)]
24. Lameire, N.; Van Biesen, W.; Vanholder, R. Acute kidney injury. *Lancet* **2008**, *372*, 1863–1865. [[CrossRef](#)]

25. Hanif, M.O.; Bali, A.; Ramphul, K. Acute renal tubular necrosis. In *StatPearls [Internet]*; StatPearls Publishing: Treasure Island, FL, USA, 2020.
26. Rahman, M.; Shad, F.; Smith, M.C. Acute kidney injury: A guide to diagnosis and management. *Am. Fam. Physician* **2012**, *86*, 631–639.
27. Dalal, R.; Bruss, Z.S.; Sehdev, J.S. Physiology, renal blood flow and filtration. In *StatPearls [Internet]*; StatPearls Publishing: Treasure Island, FL, USA, 2019.
28. Oh, G.-S.; Kim, H.-J.; Shen, A.; Lee, S.B.; Khadka, D.; Pandit, A.; So, H.-S. Cisplatin-induced kidney dysfunction and perspectives on improving treatment strategies. *Electrolytes Blood Press.* **2014**, *12*, 55–65. [[CrossRef](#)]
29. Miller, R.P.; Tadagavadi, R.K.; Ramesh, G.; Reeves, W.B. Mechanisms of Cisplatin Nephrotoxicity. *Toxins (Basel)* **2010**, *2*, 2490–2518. [[CrossRef](#)]
30. Bennis, Y.; Savry, A.; Rocca, M.; Gauthier-Villano, L.; Pisano, P.; Pourroy, B. Cisplatin dose adjustment in patients with renal impairment, which recommendations should we follow? *Int. J. Clin. Pharm.* **2014**, *36*, 420–429. [[CrossRef](#)] [[PubMed](#)]
31. Ozkok, A.; Edelstein, C.L. Pathophysiology of cisplatin-induced acute kidney injury. *Biomed. Res. Int.* **2014**, *2014*, 967826. [[CrossRef](#)]
32. Rosner, M.H.; Perazella, M.A. Acute kidney injury in the patient with cancer. *Kidney Res. Clin. Pract.* **2019**, *38*, 295. [[CrossRef](#)] [[PubMed](#)]
33. Ramesh, G.; Reeves, W.B. TNF- α mediates chemokine and cytokine expression and renal injury in cisplatin nephrotoxicity. *J. Clin. Investig.* **2002**, *110*, 835–842. [[CrossRef](#)] [[PubMed](#)]
34. Zhang, B.; Ramesh, G.; Norbury, C.; Reeves, W. Cisplatin-induced nephrotoxicity is mediated by tumor necrosis factor- α produced by renal parenchymal cells. *Kidney Int.* **2007**, *72*, 37–44. [[CrossRef](#)]
35. Liu, P.; Li, X.; Lv, W.; Xu, Z. Inhibition of CXCL1-CXCR2 axis ameliorates cisplatin-induced acute kidney injury by mediating inflammatory response. *Biomed. Pharmacother.* **2020**, *122*, 109693. [[CrossRef](#)]
36. Soni, H.; Kaminski, D.; Gangaraju, R.; Adebisi, A. Cisplatin-induced oxidative stress stimulates renal Fas ligand shedding. *Ren. Fail.* **2018**, *40*, 314–322. [[CrossRef](#)]
37. Ni, J.; Hou, X.; Wang, X.; Shi, Y.; Xu, L.; Zheng, X.; Liu, N.; Qiu, A.; Zhuang, S. 3-deazaneplanocin A protects against cisplatin-induced renal tubular cell apoptosis and acute kidney injury by restoration of E-cadherin expression. *Cell Death Dis.* **2019**, *10*, 355. [[CrossRef](#)] [[PubMed](#)]
38. Potočnjak, I.; Marinić, J.; Batičić, L.; Šimić, L.; Broznić, D.; Domitrović, R. Aucubin administered by either oral or parenteral route protects against cisplatin-induced acute kidney injury in mice. *Food Chem. Toxicol.* **2020**, *142*, 111472. [[CrossRef](#)]
39. Huang, S.-J.; Huang, J.; Yan, Y.-B.; Qiu, J.; Tan, R.-Q.; Liu, Y.; Tian, Q.; Guan, L.; Niu, S.-S.; Zhang, Y. The renoprotective effect of curcumin against cisplatin-induced acute kidney injury in mice: Involvement of miR-181a/PTEN axis. *Ren. Fail.* **2020**, *42*, 350–357. [[CrossRef](#)] [[PubMed](#)]
40. Abd El-Kader, M.; Taha, R.I. Comparative nephroprotective effects of curcumin and etoricoxib against cisplatin-induced acute kidney injury in rats. *Acta Histochem.* **2020**, *122*, 151534. [[CrossRef](#)] [[PubMed](#)]
41. Chai, Y.; Zhu, K.; Li, C.; Wang, X.; Shen, J.; Yong, F.; Jia, H. Dexmedetomidine alleviates cisplatin-induced acute kidney injury by attenuating endoplasmic reticulum stress-induced apoptosis via the α 2AR/PI3K/AKT pathway. *Mol. Med. Rep.* **2020**, *21*, 1597–1605. [[CrossRef](#)] [[PubMed](#)]
42. Kadir, A.; Sher, S.; Siddiqui, R.A.; Mirza, T. Nephroprotective role of eugenol against cisplatin-induced acute kidney injury in mice. *Pak. J. Pharm. Sci.* **2020**, *33*, 1281–1287.
43. Hu, Z.; Zhang, H.; Yi, B.; Yang, S.; Liu, J.; Hu, J.; Wang, J.; Cao, K.; Zhang, W. VDR activation attenuate cisplatin induced AKI by inhibiting ferroptosis. *Cell Death Dis.* **2020**, *11*, 1–11. [[CrossRef](#)] [[PubMed](#)]
44. Fan, X.; Wei, W.; Huang, J.; Liu, X.; Ci, X. Isoorientin attenuates cisplatin-induced nephrotoxicity through the inhibition of oxidative stress and apoptosis via activating the SIRT1/SIRT6/Nrf-2 pathway. *Front. Pharmacol.* **2020**, *11*, 264. [[CrossRef](#)]
45. Zhang, Y.; Chen, Y.; Li, B.; Ding, P.; Jin, D.; Hou, S.; Cai, X.; Sheng, X. The effect of monotropein on alleviating cisplatin-induced acute kidney injury by inhibiting oxidative damage, inflammation and apoptosis. *Biomed. Pharmacother.* **2020**, *129*, 110408. [[CrossRef](#)] [[PubMed](#)]
46. Tan, R.Z.; Wang, C.; Deng, C.; Zhong, X.; Yan, Y.; Luo, Y.; Lan, H.Y.; He, T.; Wang, L. Quercetin protects against cisplatin-induced acute kidney injury by inhibiting Mincle/Syk/NF- κ B signaling maintained macrophage inflammation. *Phytother. Res.* **2020**, *34*, 139–152. [[CrossRef](#)] [[PubMed](#)]
47. Liang, H.; Zhang, Z.; He, L.; Wang, Y. CXCL16 regulates cisplatin-induced acute kidney injury. *Oncotarget* **2016**, *7*, 31652. [[CrossRef](#)]
48. Liu, H.; Baliga, R. Cytochrome P450 2E1 null mice provide novel protection against cisplatin-induced nephrotoxicity and apoptosis. *Kidney Int.* **2003**, *63*, 1687–1696. [[CrossRef](#)] [[PubMed](#)]
49. Mitazaki, S.; Honma, S.; Suto, M.; Kato, N.; Hiraiwa, K.; Yoshida, M.; Abe, S. Interleukin-6 plays a protective role in development of cisplatin-induced acute renal failure through upregulation of anti-oxidative stress factors. *Life Sci.* **2011**, *88*, 1142–1148. [[CrossRef](#)]
50. Ravichandran, K.; Holditch, S.; Brown, C.N.; Wang, Q.; Ozkok, A.; Weiser-Evans, M.C.; Nemenoff, R.; Miyazaki, M.; Thiessen-Philbrook, H.; Parikh, C.R. IL-33 deficiency slows cancer growth but does not protect against cisplatin-induced AKI in mice with cancer. *Am. J. Physiol. Ren. Physiol.* **2018**, *314*, F356–F366. [[CrossRef](#)]

51. Kim, H.-J.; Lee, D.W.; Ravichandran, K.; Keys, D.O.; Akcay, A.; Nguyen, Q.; He, Z.; Jani, A.; Ljubanovic, D.; Edelstein, C.L. NLRP3 inflammasome knockout mice are protected against ischemic but not cisplatin-induced acute kidney injury. *J. Pharmacol. Exp. Ther.* **2013**, *346*, 465–472. [[CrossRef](#)] [[PubMed](#)]
52. Mukhopadhyay, P.; Horváth, B.; Kechrid, M.; Tanchian, G.; Rajesh, M.; Naura, A.S.; Boulares, A.H.; Pacher, P. Poly (ADP-ribose) polymerase-1 is a key mediator of cisplatin-induced kidney inflammation and injury. *Free Radic. Biol. Med.* **2011**, *51*, 1774–1788. [[CrossRef](#)]
53. Liu, M.; Chien, C.-C.; Burne-Taney, M.; Molls, R.R.; Racusen, L.C.; Colvin, R.B.; Rabb, H. A pathophysiologic role for T lymphocytes in murine acute cisplatin nephrotoxicity. *J. Am. Soc. Nephrol.* **2006**, *17*, 765–774. [[CrossRef](#)] [[PubMed](#)]
54. Zhou, J.; An, C.; Jin, X.; Hu, Z.; Safirstein, R.L.; Wang, Y. TAK1 deficiency attenuates cisplatin-induced acute kidney injury. *Am. J. Physiol. Ren. Physiol.* **2020**, *318*, F209–F215. [[CrossRef](#)] [[PubMed](#)]
55. Andrade-Silva, M.; Cenedeze, M.A.; Perandini, L.A.; Felizardo, R.J.F.; Watanabe, I.K.M.; Agudelo, J.S.H.; Castoldi, A.; Gonçalves, G.M.; Origassa, C.S.T.; Semedo, P. TLR2 and TLR4 play opposite role in autophagy associated with cisplatin-induced acute kidney injury. *Clin. Sci.* **2018**, *132*, 1725–1739. [[CrossRef](#)]
56. Alikhan, M.A.; Summers, S.A.; Gan, P.Y.; Chan, A.J.; Khouri, M.B.; Ooi, J.D.; Ghali, J.R.; Odobasic, D.; Hickey, M.J.; Kitching, A.R. Endogenous toll-like receptor 9 regulates AKI by promoting regulatory T cell recruitment. *J. Am. Soc. Nephrol.* **2016**, *27*, 706–714. [[CrossRef](#)]
57. Pabla, N.; Murphy, R.F.; Liu, K.; Dong, Z. The copper transporter Ctr1 contributes to cisplatin uptake by renal tubular cells during cisplatin nephrotoxicity. *Am. J. Physiol. Ren. Physiol.* **2009**, *296*, F505–F511. [[CrossRef](#)] [[PubMed](#)]
58. Ciarimboli, G.; Ludwig, T.; Lang, D.; Pavenstädt, H.; Koepsell, H.; Piechota, H.-J.; Haier, J.; Jaehde, U.; Zisowsky, J.; Schlatter, E. Cisplatin nephrotoxicity is critically mediated via the human organic cation transporter 2. *Am. J. Pathol.* **2005**, *167*, 1477–1484. [[CrossRef](#)]
59. Ciarimboli, G. Membrane transporters as mediators of cisplatin side-effects. *Anticancer Res.* **2014**, *34*, 547–550. [[CrossRef](#)] [[PubMed](#)]
60. Ciarimboli, G.; Deuster, D.; Knief, A.; Sperling, M.; Holtkamp, M.; Edemir, B.; Pavenstadt, H.; Lanvers-Kaminsky, C.; Am Zehnhoff-Dinnesen, A.; Schinkel, A.H.; et al. Organic cation transporter 2 mediates cisplatin-induced oto- and nephrotoxicity and is a target for protective interventions. *Am. J. Pathol.* **2010**, *176*, 1169–1180. [[CrossRef](#)]
61. Tanihara, Y.; Masuda, S.; Katsura, T.; Inui, K.-I. Protective effect of concomitant administration of imatinib on cisplatin-induced nephrotoxicity focusing on renal organic cation transporter OCT2. *Biochem. Pharmacol.* **2009**, *78*, 1263–1271. [[CrossRef](#)]
62. Ismail, R.S.; El-Awady, M.S.; Hassan, M.H. Pantoprazole abrogated cisplatin-induced nephrotoxicity in mice via suppression of inflammation, apoptosis, and oxidative stress. *Naunyn-Schmiedeberg's Arch. Pharmacol.* **2020**, *393*, 1–11. [[CrossRef](#)]
63. Hu, S.; Leblanc, A.; Gibson, A.; Hong, K.; Kim, J.; Janke, L.; Li, L.; Vasilyeva, A.; Finkelstein, D.; Sprowl, J. Identification of OAT1/OAT3 as contributors to cisplatin toxicity. *Clin. Transl. Sci.* **2017**, *10*, 412–420. [[CrossRef](#)] [[PubMed](#)]
64. Morsy, M.A.; Heeba, G.H. Nebivolol ameliorates cisplatin-induced nephrotoxicity in rats. *Basic Clin. Pharmacol. Toxicol.* **2016**, *118*, 449–455. [[CrossRef](#)]
65. Nakamura, T.; Yonezawa, A.; Hashimoto, S.; Katsura, T.; Inui, K. Disruption of multidrug and toxin extrusion MATE1 potentiates cisplatin-induced nephrotoxicity. *Biochem. Pharm.* **2010**, *80*, 1762–1767. [[CrossRef](#)] [[PubMed](#)]
66. Wen, X.; Buckley, B.; McCandlish, E.; Goedken, M.J.; Syed, S.; Pelis, R.; Manautou, J.E.; Aleksunes, L.M. Transgenic expression of the human MRP2 transporter reduces cisplatin accumulation and nephrotoxicity in Mrp2-null mice. *Am. J. Pathol.* **2014**, *184*, 1299–1308. [[CrossRef](#)] [[PubMed](#)]
67. Townsend, D.M.; Deng, M.; Zhang, L.; Lopus, M.G.; Hanigan, M.H. Metabolism of cisplatin to a nephrotoxin in proximal tubule cells. *J. Am. Soc. Nephrol.* **2003**, *14*, 1–10. [[CrossRef](#)]
68. Nieskens, T.T.; Peters, J.G.; Dabaghie, D.; Korte, D.; Jansen, K.; Van Asbeck, A.H.; Tavraz, N.N.; Friedrich, T.; Russel, F.G.; Masereeuw, R. Expression of organic anion transporter 1 or 3 in human kidney proximal tubule cells reduces cisplatin sensitivity. *Drug Metab. Dispos.* **2018**, *46*, 592–599. [[CrossRef](#)]
69. Jhaveri, K.D.; Wanchoo, R.; Sakhiya, V.; Ross, D.W.; Fishbane, S. Adverse renal effects of novel molecular oncologic targeted therapies: A narrative review. *Kidney Int. Rep.* **2017**, *2*, 108–123. [[CrossRef](#)] [[PubMed](#)]
70. Marcolino, M.; Boersma, E.; Clementino, N.; Macedo, A.; Marx-Neto, A.; Silva, M.; van Gelder, T.; Akkerhuis, K.; Ribeiro, A. Imatinib treatment duration is related to decreased estimated glomerular filtration rate in chronic myeloid leukemia patients. *Ann. Oncol.* **2011**, *22*, 2073–2079. [[CrossRef](#)]
71. Huang, D.; Wang, C.; Duan, Y.; Meng, Q.; Liu, Z.; Huo, X.; Sun, H.; Ma, X.; Liu, K. Targeting Oct2 and P53: Formononetin prevents cisplatin-induced acute kidney injury. *Toxicol. Appl. Pharmacol.* **2017**, *326*, 15–24. [[CrossRef](#)]
72. Ishida, S.; Lee, J.; Thiele, D.J.; Herskowitz, I. Uptake of the anticancer drug cisplatin mediated by the copper transporter Ctr1 in yeast and mammals. *Proc. Natl. Acad. Sci. USA* **2002**, *99*, 14298–14302. [[CrossRef](#)]
73. Bonventre, J.V.; Yang, L. Cellular pathophysiology of ischemic acute kidney injury. *J. Clin. Invest.* **2011**, *121*, 4210–4221. [[CrossRef](#)]
74. Lin, X.; Okuda, T.; Holzer, A.; Howell, S. The Copper Transporter CTR1 Regulates Cisplatin Uptake in *Saccharomyces cerevisiae*. *Mol. Pharmacol.* **2002**, *62*, 1154–1159. [[CrossRef](#)]
75. Fox, E.; Levin, K.; Zhu, Y.; Segers, B.; Balamuth, N.; Womer, R.; Bagatell, R.; Balis, F. Pantoprazole, an Inhibitor of the Organic Cation Transporter 2, Does Not Ameliorate Cisplatin-Related Ototoxicity or Nephrotoxicity in Children and Adolescents with Newly Diagnosed Osteosarcoma Treated with Methotrexate, Doxorubicin, and Cisplatin. *Oncologist* **2018**, *23*, 762. [[CrossRef](#)]

76. Kuo, M.T.; Chen, H.H.; Song, I.S.; Savaraj, N.; Ishikawa, T. The roles of copper transporters in cisplatin resistance. *Cancer Metastasis Rev.* **2007**, *26*, 71–83. [\[CrossRef\]](#)
77. Hoffmann, E.K.; Sørensen, B.H.; Sauter, D.P.; Lambert, I.H. Role of volume-regulated and calcium-activated anion channels in cell volume homeostasis, cancer and drug resistance. *Channels* **2015**, *9*, 380–396. [\[CrossRef\]](#)
78. Osei-Owusu, J.; Yang, J.; Del Carmen Vitery, M.; Qiu, Z. Molecular biology and physiology of volume-regulated anion channel (VRAC). In *Current Topics in Membranes*; Elsevier: Amsterdam, The Netherlands, 2018; Volume 81, pp. 177–203.
79. Holditch, S.J.; Brown, C.N.; Lombardi, A.M.; Nguyen, K.N.; Edelstein, C.L. Recent Advances in Models, Mechanisms, Biomarkers, and Interventions in Cisplatin-Induced Acute Kidney Injury. *Int. J. Mol. Sci.* **2019**, *20*, 3011. [\[CrossRef\]](#) [\[PubMed\]](#)
80. Lalan, M.; Bagchi, T.; Misra, A. The Cell. In *Challenges in Delivery of Therapeutic Genomics and Proteomics*; Elsevier: Amsterdam, The Netherlands, 2011; pp. 1–43.
81. Yonny, M.E.; García, E.M.; Lopez, A.; Arroquy, J.I.; Nazareno, M.A. Measurement of malondialdehyde as oxidative stress biomarker in goat plasma by HPLC-DAD. *Microchem. J.* **2016**, *129*, 281–285. [\[CrossRef\]](#)
82. Galgamuwa, R.; Hardy, K.; Dahlstrom, J.E.; Blackburn, A.C.; Wium, E.; Rooke, M.; Cappello, J.Y.; Tummala, P.; Patel, H.R.; Chuah, A. Dichloroacetate prevents cisplatin-induced nephrotoxicity without compromising cisplatin anticancer properties. *J. Am. Soc. Nephrol.* **2016**, *27*, 3331–3344. [\[CrossRef\]](#)
83. Mizuno, T.; Sato, W.; Ishikawa, K.; Terao, Y.; Takahashi, K.; Noda, Y.; Yuzawa, Y.; Nagamatsu, T. Significance of downregulation of renal organic cation transporter (SLC47A1) in cisplatin-induced proximal tubular injury. *Oncotargets Ther.* **2015**, *8*, 1701. [\[CrossRef\]](#) [\[PubMed\]](#)
84. Komatsu, M.; Sumizawa, T.; Mutoh, M.; Chen, Z.-S.; Terada, K.; Furukawa, T.; Yang, X.-L.; Gao, H.; Miura, N.; Sugiyama, T. Copper-transporting P-type adenosine triphosphatase (ATP7B) is associated with cisplatin resistance. *Cancer Res.* **2000**, *60*, 1312–1316. [\[PubMed\]](#)
85. Samimi, G.; Varki, N.M.; Wilczynski, S.; Safaei, R.; Alberts, D.S.; Howell, S.B. Increase in expression of the copper transporter ATP7A during platinum drug-based treatment is associated with poor survival in ovarian cancer patients. *Clin. Cancer Res.* **2003**, *9*, 5853–5859. [\[PubMed\]](#)
86. Kalayda, G.V.; Wagner, C.H.; Buß, I.; Reedijk, J.; Jaehde, U. Altered localisation of the copper efflux transporters ATP7A and ATP7B associated with cisplatin resistance in human ovarian carcinoma cells. *BMC Cancer* **2008**, *8*, 175. [\[CrossRef\]](#)
87. Harrach, S.; Ciarimboli, G. Role of transporters in the distribution of platinum-based drugs. *Front. Pharmacol.* **2015**, *6*, 85. [\[CrossRef\]](#)
88. Matsushima, A.; Oda, K.; Mori, N.; Murakami, T. Modulated function of multidrug resistance-associated proteins in cisplatin-induced acute renal failure rats. *Die Pharm. Int. J. Pharm. Sci.* **2017**, *72*, 209–213.
89. Hanigan, M.H.; Devarajan, P. Cisplatin nephrotoxicity: Molecular mechanisms. *Cancer Ther.* **2003**, *1*, 47. [\[PubMed\]](#)
90. Yonezawa, A.; Masuda, S.; Yokoo, S.; Katsura, T.; Inui, K.-I. Cisplatin and oxaliplatin, but not carboplatin and nedaplatin, are substrates for human organic cation transporters (SLC22A1–3 and multidrug and toxin extrusion family). *J. Pharmacol. Exp. Ther.* **2006**, *319*, 879–886. [\[CrossRef\]](#)
91. Li, Q.; Guo, D.; Dong, Z.; Zhang, W.; Zhang, L.; Huang, S.-M.; Polli, J.E.; Shu, Y. Ondansetron can enhance cisplatin-induced nephrotoxicity via inhibition of multiple toxin and extrusion proteins (MATEs). *Toxicol. Appl. Pharmacol.* **2013**, *273*, 100–109. [\[CrossRef\]](#) [\[PubMed\]](#)
92. Rubera, I.; Duranton, C.; Melis, N.; Cougnon, M.; Mograbi, B.; Tauc, M. Role of CFTR in oxidative stress and suicidal death of renal cells during cisplatin-induced nephrotoxicity. *Cell Death Dis.* **2013**, *4*, e817. [\[CrossRef\]](#) [\[PubMed\]](#)
93. Jesse, C.R.; Bortolatto, C.F.; Wilhelm, E.A.; Roman, S.S.; Prigol, M.; Nogueira, C.W. The peroxisome proliferator-activated receptor- γ agonist pioglitazone protects against cisplatin-induced renal damage in mice. *J. Appl. Toxicol.* **2014**, *34*, 25–32. [\[CrossRef\]](#)
94. Ma, Q.; Xu, Y.; Tang, L.; Yang, X.; Chen, Z.; Wei, Y.; Shao, X.; Shao, X.; Xin, Z.; Cai, B. Astragalus polysaccharide attenuates cisplatin-induced acute kidney injury by suppressing oxidative damage and mitochondrial dysfunction. *Biomed. Res. Int.* **2020**, *2020*, 2851349. [\[CrossRef\]](#)
95. Volarevic, V.; Djokovic, B.; Jankovic, M.G.; Harrell, C.R.; Fellabaum, C.; Djonov, V.; Arsenijevic, N. Molecular mechanisms of cisplatin-induced nephrotoxicity: A balance on the knife edge between renoprotection and tumor toxicity. *J. Biomed. Sci.* **2019**, *26*, 25. [\[CrossRef\]](#) [\[PubMed\]](#)
96. Townsend, D.M.; Tew, K.D.; He, L.; King, J.B.; Hanigan, M.H. Role of glutathione S-transferase Pi in cisplatin-induced nephrotoxicity. *Biomed. Pharmacother.* **2009**, *63*, 79–85. [\[CrossRef\]](#)
97. Chen, M.-F.; Yang, C.-M.; Su, C.-M.; Hu, M.-L. Vitamin C protects against cisplatin-induced nephrotoxicity and damage without reducing its effectiveness in C57BL/6 mice xenografted with Lewis lung carcinoma. *Nutr. Cancer* **2014**, *66*, 1085–1091. [\[CrossRef\]](#) [\[PubMed\]](#)
98. Darwish, M.A.; Abo-Youssef, A.M.; Khalaf, M.M.; Abo-Saif, A.A.; Saleh, I.G.; Abdelghany, T.M. Vitamin E mitigates cisplatin-induced nephrotoxicity due to reversal of oxidative/nitrosative stress, suppression of inflammation and reduction of total renal platinum accumulation. *J. Biochem. Mol. Toxicol.* **2017**, *31*, 1–9. [\[CrossRef\]](#)
99. Ning, Y.; Shi, Y.; Chen, J.; Song, N.; Cai, J.; Fang, Y.; Yu, X.; Ji, J.; Ding, X. Necrostatin-1 attenuates cisplatin-induced nephrotoxicity through suppression of apoptosis and oxidative stress and retains klotho expression. *Front. Pharmacol.* **2018**, *9*, 384. [\[CrossRef\]](#)

100. Chen, X.; Wei, W.; Li, Y.; Huang, J.; Ci, X. Hesperetin relieves cisplatin-induced acute kidney injury by mitigating oxidative stress, inflammation and apoptosis. *Chem. Biol. Interact.* **2019**, *308*, 269–278. [[CrossRef](#)]
101. Cha, J.J.; Min, H.S.; Kim, K.T.; Kim, J.E.; Ghee, J.Y.; Kim, H.W.; Lee, J.E.; Han, J.Y.; Lee, G.; Ha, H.J.; et al. APX-115, a first-in-class pan-NADPH oxidase (Nox) inhibitor, protects db/db mice from renal injury. *Lab. Investig.* **2017**, *97*, 419–431. [[CrossRef](#)]
102. Zhao, K.; Wen, L. DMF attenuates cisplatin-induced kidney injury via activating Nrf2 signaling pathway and inhibiting NF- κ B signaling pathway. *Eur. Rev. Med. Pharm. Sci.* **2018**, *22*, 8924–8931.
103. Ansari, M.A. Sinapic acid modulates Nrf2/HO-1 signaling pathway in cisplatin-induced nephrotoxicity in rats. *Biomed. Pharmacother.* **2017**, *93*, 646–653. [[CrossRef](#)] [[PubMed](#)]
104. Ben-Yehuda Greenwald, M.; Ben-Sasson, S.; Bianco-Peled, H.; Kohen, R. Skin redox balance maintenance: The need for an Nrf2-activator delivery system. *Cosmetics* **2016**, *3*, 1. [[CrossRef](#)]
105. Liu, Q.; Hu, S.; He, Y.; Zhang, J.; Zeng, X.; Gong, F.; Liang, L.N. The protective effects of Zhen-Wu-Tang against cisplatin-induced acute kidney injury in rats. *PLoS ONE* **2017**, *12*, e0179137. [[CrossRef](#)] [[PubMed](#)]
106. Sasaki, A.; Koike, N.; Murakami, T.; Suzuki, K. Dimethyl fumarate ameliorates cisplatin-induced renal tubulointerstitial lesions. *J. Toxicol. Pathol.* **2019**, *32*, 79–89. [[CrossRef](#)]
107. Winston, J.A.; Safirstein, R. Reduced renal blood flow in early cisplatin-induced acute renal failure in the rat. *Am. J. Physiol.* **1985**, *249*, F490–F496. [[CrossRef](#)] [[PubMed](#)]
108. Guo, Y.; Wang, M.; Mou, J.; Zhao, Z.; Yang, J.; Zhu, F.; Pei, G.; Zhu, H.; Wang, Y.; Xu, G. Pretreatment of Huaqiqi Huang extractum protects against cisplatin-induced nephrotoxicity. *Sci. Rep.* **2018**, *8*, 1–10.
109. Dibona, G.F.; Kopp, U.C. Neural control of renal function. *Physiol. Rev.* **1997**, *77*, 75–197. [[CrossRef](#)]
110. Walsh, M.P. Regulation of vascular smooth muscle tone. *Can. J. Physiol. Pharmacol.* **1994**, *72*, 919–936. [[CrossRef](#)]
111. Salomonsson, M.; Arendshorst, W.J. Calcium recruitment in renal vasculature: NE effects on blood flow and cytosolic calcium concentration. *Am. J. Physiol. Ren. Physiol.* **1999**, *276*, F700–F710. [[CrossRef](#)] [[PubMed](#)]
112. Coats, A.; Jain, S. Protective effects of nebivolol from oxidative stress to prevent hypertension-related target organ damage. *J. Hum. Hypertens.* **2017**, *31*, 376–381. [[CrossRef](#)]
113. Guzik, T.J.; West, N.E.; Pillai, R.; Taggart, D.P.; Channon, K.M. Nitric oxide modulates superoxide release and peroxynitrite formation in human blood vessels. *Hypertension* **2002**, *39*, 1088–1094. [[CrossRef](#)]
114. Abdelrahman, A.M.; Al Suleimani, Y.; Shalaby, A.; Ashique, M.; Manoj, P.; Al-Saadi, H.; Ali, B.H. Effect of levosimendan, a calcium sensitizer, on cisplatin-induced nephrotoxicity in rats. *Toxicol. Rep.* **2019**, *6*, 232–238. [[CrossRef](#)]
115. Parissis, J.T.; Andreadou, I.; Bistola, V.; Paraskevaidis, I.; Filippatos, G.; Kremastinos, D.T. Novel biologic mechanisms of levosimendan and its effect on the failing heart. *Expert Opin. Investig. Drugs* **2008**, *17*, 1143–1150. [[CrossRef](#)] [[PubMed](#)]
116. Deegan, P.M.; Nolan, C.; Ryan, M.P.; Basinger, M.A.; Jones, M.M.; Hande, K.R. The role of the renin-angiotensin system in cisplatin nephrotoxicity. *Ren. Fail.* **1995**, *17*, 665–674. [[CrossRef](#)]
117. Fountain, J.H.; Lappin, S.L. Physiology, Renin Angiotensin System. In *StatPearls [Internet]*; StatPearls Publishing: Treasure Island, FL, USA, 2017.
118. Dhande, I.; Ma, W.; Hussain, T. Angiotensin AT2 receptor stimulation is anti-inflammatory in lipopolysaccharide-activated THP-1 macrophages via increased interleukin-10 production. *Hypertens. Res.* **2015**, *38*, 21–29. [[CrossRef](#)] [[PubMed](#)]
119. Kobori, H.; Mori, H.; Masaki, T.; Nishiyama, A. Angiotensin II blockade and renal protection. *Curr. Pharm. Des.* **2013**, *19*, 3033–3042. [[CrossRef](#)]
120. Zhang, C.; Hein, T.W.; Wang, W.; Kuo, L. Divergent roles of angiotensin II AT1 and AT2 receptors in modulating coronary microvascular function. *Circ. Res.* **2003**, *92*, 322–329. [[CrossRef](#)]
121. Cao, Z.; Bonnet, F.; Candido, R.; Nesteroff, S.P.; Burns, W.C.; Kawachi, H.; Shimizu, F.; Carey, R.M.; De Gasparo, M.; Cooper, M.E. Angiotensin type 2 receptor antagonism confers renal protection in a rat model of progressive renal injury. *J. Am. Soc. Nephrol.* **2002**, *13*, 1773–1787. [[CrossRef](#)] [[PubMed](#)]
122. Dhande, I.; Ali, Q.; Hussain, T. Proximal tubule angiotensin AT2 receptors mediate an anti-inflammatory response via interleukin-10: Role in renoprotection in obese rats. *Hypertension* **2013**, *61*, 1218–1226. [[CrossRef](#)]
123. Hosoda, A.; Matsumoto, Y.; Toriyama, Y.; Tsuji, T.; Yoshida, Y.; Masamichi, S.; Kohno, T. Telmisartan Exacerbates Cisplatin-Induced Nephrotoxicity in a Mouse Model. *Biol. Pharm. Bull.* **2020**, *43*, 1331–1337. [[CrossRef](#)] [[PubMed](#)]
124. Malik, S.; Suchal, K.; Gamad, N.; Dinda, A.K.; Arya, D.S.; Bhatia, J. Telmisartan ameliorates cisplatin-induced nephrotoxicity by inhibiting MAPK mediated inflammation and apoptosis. *Eur. J. Pharm.* **2015**, *748*, 54–60. [[CrossRef](#)]
125. Okui, S.; Yamamoto, H.; Li, W.; Gamachi, N.; Fujita, Y.; Kashiwamura, S.-I.; Miura, D.; Takai, S.; Miyazaki, M.; Urade, M. Cisplatin-induced acute renal failure in mice is mediated by chymase-activated angiotensin-aldosterone system and interleukin-18. *Eur. J. Pharm.* **2012**, *685*, 149–155. [[CrossRef](#)] [[PubMed](#)]
126. Zhang, J.; Rudemiller, N.P.; Patel, M.B.; Wei, Q.; Karlovich, N.S.; Jeffs, A.D.; Wu, M.; Sparks, M.A.; Privratsky, J.R.; Herrera, M. Competing actions of type 1 angiotensin II receptors expressed on T lymphocytes and kidney epithelium during cisplatin-induced AKI. *J. Am. Soc. Nephrol.* **2016**, *27*, 2257–2264. [[CrossRef](#)]
127. Sherif, I.O.; Al-Mutabagani, L.A.; Alnakhli, A.M.; Sobh, M.A.; Mohammed, H.E. Renoprotective effects of angiotensin receptor blocker and stem cells in acute kidney injury: Involvement of inflammatory and apoptotic markers. *Exp. Biol. Med.* **2015**, *240*, 1572–1579. [[CrossRef](#)] [[PubMed](#)]

128. Dharmashankar, K.; Widlansky, M.E. Vascular Endothelial Function and Hypertension: Insights and Directions. *Curr. Hypertens. Rep.* **2010**, *12*, 448–455. [[CrossRef](#)] [[PubMed](#)]
129. Qaradakhi, T.; Apostolopoulos, V.; Zulli, A. Angiotensin (1-7) and Alamandine: Similarities and differences. *Pharmacol. Res.* **2016**, *111*, 820–826. [[CrossRef](#)]
130. Velkoska, E.; Patel, S.K.; Burrell, L.M. Angiotensin converting enzyme 2 and diminazene: Role in cardiovascular and blood pressure regulation. *Curr. Opin. Nephrol. Hypertens.* **2016**, *25*, 384–395. [[CrossRef](#)]
131. Rabelo, L.A.; Todiras, M.; Nunes-Souza, V.; Qadri, F.; Szijarto, I.A.; Gollasch, M.; Penninger, J.M.; Bader, M.; Santos, R.A.; Alenina, N. Genetic Deletion of ACE2 Induces Vascular Dysfunction in C57BL/6 Mice: Role of Nitric Oxide Imbalance and Oxidative Stress. *PLoS ONE* **2016**, *11*, e0150255. [[CrossRef](#)] [[PubMed](#)]
132. Shenoy, V.; Gjymishka, A.; Jarajapu, Y.P.; Qi, Y.; Afzal, A.; Rigatto, K.; Ferreira, A.J.; Fraga-Silva, R.A.; Kearns, P.; Douglas, J.Y.; et al. Diminazene attenuates pulmonary hypertension and improves angiogenic progenitor cell functions in experimental models. *Am. J. Respir. Crit. Care Med.* **2013**, *187*, 648–657. [[CrossRef](#)]
133. Sampaio, W.O.; Souza dos Santos, R.A.; Faria-Silva, R.; Da Mata Machado, L.T.; Schiffrin, E.L.; Touyz, R.M. Angiotensin-(1-7) through receptor Mas mediates endothelial nitric oxide synthase activation via Akt-dependent pathways. *Hypertension* **2007**, *49*, 185–192. [[CrossRef](#)] [[PubMed](#)]
134. Gupta, S.; Wright, H.M. Nebivolol: A highly selective β 1-adrenergic receptor blocker that causes vasodilation by increasing nitric oxide. *Cardiovasc. Ther.* **2008**, *26*, 189–202. [[CrossRef](#)] [[PubMed](#)]
135. Varagic, J.; Ahmad, S.; Voncannon, J.L.; Moniwa, N.; Simington, S.W., Jr.; Brosnihan, B.K.; Gallagher, P.E.; Habibi, J.; Sowers, J.R.; Ferrario, C.M. Nebivolol reduces cardiac angiotensin II, associated oxidative stress and fibrosis but not arterial pressure in salt-loaded spontaneously hypertensive rats. *J. Hypertens.* **2012**, *30*, 1766. [[CrossRef](#)] [[PubMed](#)]
136. Wolf, S.; Sauter, G.; Preyer, M.; Poerner, T.; Kempf, V.; Risler, T.; Brehm, B. Influence of nebivolol and metoprolol on inflammatory mediators in human coronary endothelial or smooth muscle cells. Effects on neointima formation after balloon denudation in carotid arteries of rats treated with nebivolol. *Cell. Physiol. Biochem.* **2007**, *19*, 129–136. [[CrossRef](#)]
137. Szturz, P.; Wouters, K.; Kiyota, N.; Tahara, M.; Prabhash, K.; Noronha, V.; Adelstein, D.; Van Gestel, D.; Vermorken, J.B. Low-dose vs. high-dose cisplatin: Lessons learned from 59 chemoradiotherapy trials in head and neck cancer. *Front. Oncol.* **2019**, *9*, 86. [[CrossRef](#)] [[PubMed](#)]
138. Edinger, A.L.; Thompson, C.B. Death by design: Apoptosis, necrosis and autophagy. *Curr. Opin Cell Biol.* **2004**, *16*, 663–669. [[CrossRef](#)]
139. Gillespie, S.K.; Zhang, X.D.; Hersey, P. Ingenol 3-angelate induces dual modes of cell death and differentially regulates tumor necrosis factor-related apoptosis-inducing ligand-induced apoptosis in melanoma cells. *Mol. Cancer* **2004**, *3*, 1651–1658.
140. Saito, Y.; Nishio, K.; Ogawa, Y.; Kimata, J.; Kinumi, T.; Yoshida, Y.; Noguchi, N.; Niki, E. Turning point in apoptosis/necrosis induced by hydrogen peroxide. *Free Radic. Res.* **2006**, *40*, 619–630. [[CrossRef](#)] [[PubMed](#)]
141. Sancho-Martínez, S.M.; Piedrafita, F.J.; Cannata-Andía, J.B.; López-Novoa, J.M.; López-Hernández, F.J. Necrotic concentrations of cisplatin activate the apoptotic machinery but inhibit effector caspases and interfere with the execution of apoptosis. *Toxicol. Sci.* **2011**, *122*, 73–85. [[CrossRef](#)] [[PubMed](#)]
142. Xu, Y.; Ma, H.; Shao, J.; Wu, J.; Zhou, L.; Zhang, Z.; Wang, Y.; Huang, Z.; Ren, J.; Liu, S.; et al. A Role for Tubular Necroptosis in Cisplatin-Induced AKI. *J. Am. Soc. Nephrol. JASN* **2015**, *26*, 2647–2658. [[CrossRef](#)]
143. Green, D.R.; Llambi, F. Cell Death Signaling. *Cold Spring Harb Perspect Biol.* **2015**, *7*, a006080. [[CrossRef](#)] [[PubMed](#)]
144. Kroemer, G.; El-Deiry, W.S.; Golstein, P.; Peter, M.E.; Vaux, D.; Vandenabeele, P.; Zhivotovskiy, B.; Blagosklonny, M.V.; Malorni, W.; Knight, R.A.; et al. Classification of cell death: Recommendations of the Nomenclature Committee on Cell Death. *Cell Death Differ.* **2005**, *12*, 1463–1467. [[CrossRef](#)]
145. Zhang, D.-W.; Shao, J.; Lin, J.; Zhang, N.; Lu, B.-J.; Lin, S.-C.; Dong, M.-Q.; Han, J. RIP3, an Energy Metabolism Regulator That Switches TNF-Induced Cell Death from Apoptosis to Necrosis. *Science* **2009**, *325*, 332. [[CrossRef](#)]
146. Vandenabeele, P.; Galluzzi, L.; Vanden Berghe, T.; Kroemer, G. Molecular mechanisms of necroptosis: An ordered cellular explosion. *Nat. Rev. Mol. Cell Biol.* **2010**, *11*, 700–714. [[CrossRef](#)] [[PubMed](#)]
147. Galluzzi, L.; Vitale, I.; Abrams, J.M.; Alnemri, E.S.; Baehrecke, E.H.; Blagosklonny, M.V.; Dawson, T.M.; Dawson, V.L.; El-Deiry, W.S.; Fulda, S.; et al. Molecular definitions of cell death subroutines: Recommendations of the Nomenclature Committee on Cell Death 2012. *Cell Death Differ.* **2012**, *19*, 107–120. [[CrossRef](#)] [[PubMed](#)]
148. Yang, Y.; Liu, S.; Gao, H.; Wang, P.; Zhang, Y.; Zhang, A.; Jia, Z.; Huang, S. Ursodeoxycholic acid protects against cisplatin-induced acute kidney injury and mitochondrial dysfunction through acting on ALDH1L2. *Free Radic. Biol. Med.* **2020**, *152*, 821–837. [[CrossRef](#)] [[PubMed](#)]
149. Cao, W.; Yuan, Y.; Liu, X.; Li, Q.; An, X.; Huang, Z.; Wu, L.; Zhang, B.; Zhang, A.; Xing, C. Adenosine kinase inhibition protects against cisplatin-induced nephrotoxicity. *Am. J. Physiol. Ren. Physiol.* **2019**, *317*, F107–F115. [[CrossRef](#)]
150. Shimizu, S.; Eguchi, Y.; Kamiike, W.; Funahashi, Y.; Mignon, A.; Lacronique, V.; Matsuda, H.; Tsujimoto, Y. Bcl-2 prevents apoptotic mitochondrial dysfunction by regulating proton flux. *Proc. Natl. Acad. Sci. USA* **1998**, *95*, 1455–1459. [[CrossRef](#)]
151. Gertz, M.; Nguyen, G.T.T.; Fischer, F.; Suenkel, B.; Schlicker, C.; Fränzel, B.; Tomaschewski, J.; Aladini, F.; Becker, C.; Wolters, D. A molecular mechanism for direct sirtuin activation by resveratrol. *PLoS ONE* **2012**, *7*, e49761. [[CrossRef](#)]
152. Hao, Q.; Xiao, X.; Zhen, J.; Feng, J.; Song, C.; Jiang, B.; Hu, Z. Resveratrol attenuates acute kidney injury by inhibiting death receptor-mediated apoptotic pathways in a cisplatin-induced rat model. *Mol. Med. Rep.* **2016**, *14*, 3683–3689. [[CrossRef](#)] [[PubMed](#)]

153. Xu, L.; Xie, Q.; Qi, L.; Wang, C.; Xu, N.; Liu, W.; Yu, Y.; Li, S.; Xu, Y. Bcl-2 overexpression reduces cisplatin cytotoxicity by decreasing ER-mitochondrial Ca²⁺ signaling in SKOV3 cells. *Oncol. Rep.* **2018**, *39*, 985–992. [[CrossRef](#)]
154. Jiang, M.; Wei, Q.; Wang, J.; Du, Q.; Yu, J.; Zhang, L.; Dong, Z. Regulation of PUMA- α by p53 in cisplatin-induced renal cell apoptosis. *Oncogene* **2006**, *25*, 4056–4066. [[CrossRef](#)] [[PubMed](#)]
155. Yan, M.; Shu, S.; Guo, C.; Tang, C.; Dong, Z. Endoplasmic reticulum stress in ischemic and nephrotoxic acute kidney injury. *Ann. Med.* **2018**, *50*, 381–390. [[CrossRef](#)] [[PubMed](#)]
156. Linkermann, A.; Chen, G.; Dong, G.; Kunzendorf, U.; Krautwald, S.; Dong, Z. Regulated cell death in AKI. *J. Am. Soc. Nephrol. JASN* **2014**, *25*, 2689–2701. [[CrossRef](#)]
157. Wang, X.; Parrish, A.R. Loss of α (E)-catenin promotes Fas mediated apoptosis in tubular epithelial cells. *Apoptosis* **2015**, *20*, 921–929. [[CrossRef](#)] [[PubMed](#)]
158. Scaffidi, C.; Fulda, S.; Srinivasan, A.; Friesen, C.; Li, F.; Tomaselli, K.J.; Debatin, K.M.; Kramer, P.H.; Peter, M.E. Two CD95 (APO-1/Fas) signaling pathways. *Embo J.* **1998**, *17*, 1675–1687. [[CrossRef](#)]
159. Tsuruya, K.; Ninomiya, T.; Tokumoto, M.; Hirakawa, M.; Masutani, K.; Taniguchi, M.; Fukuda, K.; Kanai, H.; Kishihara, K.; Hirakata, H.; et al. Direct involvement of the receptor-mediated apoptotic pathways in cisplatin-induced renal tubular cell death. *Kidney Int.* **2003**, *63*, 72–82. [[CrossRef](#)] [[PubMed](#)]
160. García-Berrocal, J.; Nevado, J.; Ramírez-Camacho, R.; Sanz, R.; González-García, J.; Sánchez-Rodríguez, C.; Cantos, B.; España, P.; Verdguer, J.; Trinidad Cabezas, A. The anticancer drug cisplatin induces an intrinsic apoptotic pathway inside the inner ear. *Br. J. Pharmacol.* **2007**, *152*, 1012–1020. [[CrossRef](#)]
161. Chirino, Y.L.; Pedraza-Chaverri, J. Role of oxidative and nitrosative stress in cisplatin-induced nephrotoxicity. *Exp. Toxicol. Pathol.* **2009**, *61*, 223–242. [[CrossRef](#)]
162. Ramesh, G.; Reeves, W.B. p38 MAP kinase inhibition ameliorates cisplatin nephrotoxicity in mice. *Am. J. Physiol. Ren. Physiol.* **2005**, *289*, F166–F174. [[CrossRef](#)]
163. Wang, C.; Dai, H.; Xiong, Z.; Song, Q.; Zou, Z.; Li, M.; Nie, J.; Bai, X.; Chen, Z. Loss of DEPTOR in renal tubules protects against cisplatin-induced acute kidney injury. *Cell Death Dis.* **2018**, *9*, 441. [[CrossRef](#)] [[PubMed](#)]
164. Inagi, R. Endoplasmic reticulum stress as a progression factor for kidney injury. *Curr. Opin. Pharmacol.* **2010**, *10*, 156–165. [[CrossRef](#)] [[PubMed](#)]
165. Peyrou, M.; Hanna, P.E.; Cribb, A.E. Cisplatin, gentamicin, and p-aminophenol induce markers of endoplasmic reticulum stress in the rat kidneys. *Toxicol. Sci.* **2007**, *99*, 346–353. [[CrossRef](#)]
166. Long, Y.; Zhen, X.; Zhu, F.; Hu, Z.; Lei, W.; Li, S.; Zha, Y.; Nie, J. Hyperhomocysteinemia exacerbates cisplatin-induced acute kidney injury. *Int. J. Biol. Sci.* **2017**, *13*, 219. [[CrossRef](#)]
167. Wang, M.; Wey, S.; Zhang, Y.; Ye, R.; Lee, A.S. Role of the unfolded protein response regulator GRP78/BiP in development, cancer, and neurological disorders. *Antioxid Redox Signal.* **2009**, *11*, 2307–2316. [[CrossRef](#)]
168. Nishitoh, H. CHOP is a multifunctional transcription factor in the ER stress response. *J. Biochem.* **2012**, *151*, 217–219. [[CrossRef](#)]
169. Zhang, K.; Kaufman, R.J. Chapter Twenty Identification and Characterization of Endoplasmic Reticulum Stress-Induced Apoptosis In Vivo. *Methods Enzymol.* **2008**, *442*, 395–419. [[PubMed](#)]
170. Liu, H.; Baliga, R. Endoplasmic reticulum stress-associated caspase 12 mediates cisplatin-induced LLC-PK1 cell apoptosis. *J. Am. Soc. Nephrol.* **2005**, *16*, 1985–1992. [[CrossRef](#)]
171. Huang, Z.; Guo, F.; Xia, Z.; Liang, Y.; Lei, S.; Tan, Z.; Ma, L.; Fu, P. Activation of GPR120 by TUG891 ameliorated cisplatin-induced acute kidney injury via repressing ER stress and apoptosis. *Biomed. Pharmacother.* **2020**, *126*, 110056. [[CrossRef](#)] [[PubMed](#)]
172. Chen, B.; Liu, G.; Zou, P.; Li, X.; Hao, Q.; Jiang, B.; Yang, X.; Hu, Z. Epigallocatechin-3-gallate protects against cisplatin-induced nephrotoxicity by inhibiting endoplasmic reticulum stress-induced apoptosis. *Exp. Biol. Med.* **2015**, *240*, 1513–1519. [[CrossRef](#)] [[PubMed](#)]
173. Hao, Y.; Guo, F.; Huang, Z.; Feng, Y.; Xia, Z.; Liu, J.; Li, L.; Huang, R.; Lin, L.; Ma, L. 2-Methylquinazoline derivative 23BB as a highly selective histone deacetylase 6 inhibitor alleviated cisplatin-induced acute kidney injury. *Biosci. Rep.* **2020**, *40*, BSR20191538. [[CrossRef](#)]
174. Kong, D.; Zhuo, L.; Gao, C.; Shi, S.; Wang, N.; Huang, Z.; Li, W.; Hao, L. Erythropoietin protects against cisplatin-induced nephrotoxicity by attenuating endoplasmic reticulum stress-induced apoptosis. *J. Nephrol.* **2013**, *26*, 219–227. [[CrossRef](#)] [[PubMed](#)]
175. Gao, Z.; Liu, G.; Hu, Z.; Li, X.; Yang, X.; Jiang, B.; Li, X. Grape seed proanthocyanidin extract protects from cisplatin-induced nephrotoxicity by inhibiting endoplasmic reticulum stress-induced apoptosis. *Mol. Med. Rep.* **2014**, *9*, 801–807. [[CrossRef](#)]
176. Tan, Z.; Guo, F.; Huang, Z.; Xia, Z.; Liu, J.; Tao, S.; Li, L.; Feng, Y.; Du, X.; Ma, L. Pharmacological and genetic inhibition of fatty acid-binding protein 4 alleviated cisplatin-induced acute kidney injury. *J. Cell. Mol. Med.* **2019**, *23*, 6260–6270. [[CrossRef](#)] [[PubMed](#)]
177. Furuichi, K.; Kaneko, S.; Wada, T. Chemokine/chemokine receptor-mediated inflammation regulates pathologic changes from acute kidney injury to chronic kidney disease. *Clin. Exp. Nephrol.* **2009**, *13*, 9–14. [[CrossRef](#)]
178. Liu, X.-Q.; Jin, J.; Li, Z.; Jiang, L.; Dong, Y.-H.; Cai, Y.-T.; Wu, M.-F.; Wang, J.-N.; Ma, T.-T.; Wen, J.-G. Rutaecarpine Derivative Cpd-6c Alleviates Acute Kidney Injury by Targeting PDE4B, a Key Enzyme Mediating inflammation in Cisplatin Nephropathy. *Biochem. Pharmacol.* **2020**, *180*, 114132. [[CrossRef](#)]
179. Zarembek, K.A.; Godowski, P.J. Tissue expression of human Toll-like receptors and differential regulation of Toll-like receptor mRNAs in leukocytes in response to microbes, their products, and cytokines. *J. Immunol.* **2002**, *168*, 554–561. [[CrossRef](#)] [[PubMed](#)]

180. Kimbrell, D.A.; Beutler, B. The evolution and genetics of innate immunity. *Nat. Rev. Genet.* **2001**, *2*, 256–267. [[CrossRef](#)]
181. Aderem, A.; Ulevitch, R.J. Toll-like receptors in the induction of the innate immune response. *Nature* **2000**, *406*, 782–787. [[CrossRef](#)]
182. Akira, S.; Uematsu, S.; Takeuchi, O. Pathogen recognition and innate immunity. *Cell* **2006**, *124*, 783–801. [[CrossRef](#)]
183. Godfroy, J.I., III; Roostan, M.; Moroz, Y.S.; Korendovych, I.V.; Yin, H. Isolated Toll-like receptor transmembrane domains are capable of oligomerization. *PLoS ONE* **2012**, *7*, e48875. [[CrossRef](#)] [[PubMed](#)]
184. Bell, J.K.; Mullen, G.E.; Leifer, C.A.; Mazzoni, A.; Davies, D.R.; Segal, D.M. Leucine-rich repeats and pathogen recognition in Toll-like receptors. *Trends Immunol.* **2003**, *24*, 528–533. [[CrossRef](#)]
185. Butcher, S.K.; O’Carroll, C.E.; Wells, C.A.; Carmody, R.J. Toll-like receptors drive specific patterns of tolerance and training on restimulation of macrophages. *Front. Immunol.* **2018**, *9*, 933. [[CrossRef](#)]
186. Zhang, D.; Zhang, G.; Hayden, M.S.; Greenblatt, M.B.; Bussey, C.; Flavell, R.A.; Ghosh, S. A toll-like receptor that prevents infection by uropathogenic bacteria. *Science* **2004**, *303*, 1522–1526. [[CrossRef](#)] [[PubMed](#)]
187. Sharma, S.; Zou, W.; Sun, Q.; Grandvaux, N.; Julkunen, I.; Hemmi, H.; Yamamoto, M.; Akira, S.; Yeh, W.-C.; Lin, R. Activation of TBK1 and IKK ϵ kinases by vesicular stomatitis virus infection and the role of viral ribonucleoprotein in the development of interferon antiviral immunity. *J. Virol.* **2004**, *78*, 10636–10649.
188. Patel, S. Danger-associated molecular patterns (DAMPs): The derivatives and triggers of inflammation. *Curr. Allergy Asthma Rep.* **2018**, *18*, 63. [[CrossRef](#)] [[PubMed](#)]
189. Kurup, S.P.; Tarleton, R.L. Perpetual expression of PAMPs necessary for optimal immune control and clearance of a persistent pathogen. *Nat. Commun.* **2013**, *4*, 2616. [[CrossRef](#)]
190. Piccinini, A.; Midwood, K. DAMPening inflammation by modulating TLR signalling. *Mediat. Inflamm.* **2010**, *2010*, 672395. [[CrossRef](#)]
191. Bagchi, A.; Herrup, E.A.; Warren, H.S.; Trigilio, J.; Shin, H.-S.; Valentine, C.; Hellman, J. MyD88-dependent and MyD88-independent pathways in synergy, priming, and tolerance between TLR agonists. *J. Immunol.* **2007**, *178*, 1164–1171. [[CrossRef](#)] [[PubMed](#)]
192. Yamamoto, M.; Sato, S.; Hemmi, H.; Hoshino, K.; Kaisho, T.; Sanjo, H.; Takeuchi, O.; Sugiyama, M.; Okabe, M.; Takeda, K. Role of adaptor TRIF in the MyD88-independent toll-like receptor signaling pathway. *Science* **2003**, *301*, 640–643. [[CrossRef](#)]
193. Mäkelä, S.M.; Strengell, M.; Pietilä, T.E.; Österlund, P.; Julkunen, I. Multiple signaling pathways contribute to synergistic TLR ligand-dependent cytokine gene expression in human monocyte-derived macrophages and dendritic cells. *J. Leukoc. Biol.* **2009**, *85*, 664–672. [[CrossRef](#)]
194. Grassin-Delyle, S.; Abrial, C.; Salvator, H.; Brollo, M.; Naline, E.; Devillier, P. The role of toll-like receptors in the production of cytokines by human lung macrophages. *J. Innate Immun.* **2020**, *12*, 63–73. [[CrossRef](#)]
195. Zhang, Y.; He, X.; Yu, F.; Xiang, Z.; Li, J.; Thorpe, K.L.; Yu, Z. Characteristic and functional analysis of toll-like receptors (TLRs) in the lophotrocozoan, *Crassostrea gigas*, reveals ancient origin of TLR-mediated innate immunity. *PLoS ONE* **2013**, *8*, e76464.
196. Mulla, M.J.; Myrtolli, K.; Tadesse, S.; Stanwood, N.L.; Garipey, A.; Guller, S.; Norwitz, E.R.; Abrahams, V.M. Cutting-Edge Report: TLR 10 Plays a Role in Mediating Bacterial Peptidoglycan-Induced Trophoblast Apoptosis. *Am. J. Reprod. Immunol.* **2013**, *69*, 449–453. [[CrossRef](#)]
197. Shamsul, H.M.; Hasebe, A.; Iyori, M.; Ohtani, M.; Kiura, K.; Zhang, D.; Totsuka, Y.; Shibata, K. The Toll-like receptor 2 (TLR2) ligand FSL-1 is internalized via the clathrin-dependent endocytic pathway triggered by CD14 and CD36 but not by TLR2. *Immunology* **2010**, *130*, 262–272. [[CrossRef](#)] [[PubMed](#)]
198. Tan, Y.; Zanoni, I.; Cullen, T.W.; Goodman, A.L.; Kagan, J.C. Mechanisms of Toll-like receptor 4 endocytosis reveal a common immune-evasion strategy used by pathogenic and commensal bacteria. *Immunity* **2015**, *43*, 909–922. [[CrossRef](#)]
199. Wörnle, M.; Schmid, H.; Banas, B.; Merkle, M.; Henger, A.; Roeder, M.; Blattner, S.; Bock, E.; Kretzler, M.; Gröne, H.-J. Novel role of toll-like receptor 3 in hepatitis C-associated glomerulonephritis. *Am. J. Pathol.* **2006**, *168*, 370–385. [[CrossRef](#)]
200. Kropf, P.; Freudenberg, M.A.; Modolell, M.; Price, H.P.; Herath, S.; Antoniazzi, S.; Galanos, C.; Smith, D.F.; Müller, I. Toll-like receptor 4 contributes to efficient control of infection with the protozoan parasite *Leishmania major*. *Infect. Immun.* **2004**, *72*, 1920–1928. [[CrossRef](#)] [[PubMed](#)]
201. Shigeoka, A.A.; Holscher, T.D.; King, A.J.; Hall, F.W.; Kiesses, W.B.; Tobias, P.S.; Mackman, N.; McKay, D.B. TLR2 is constitutively expressed within the kidney and participates in ischemic renal injury through both MyD88-dependent and-independent pathways. *J. Immunol.* **2007**, *178*, 6252–6258. [[CrossRef](#)]
202. Conti, F.; Spinelli, F.R.; Truglia, S.; Miranda, F.; Alessandri, C.; Ceccarelli, F.; Bombardieri, M.; Giannakakis, K.; Valesini, G. Kidney expression of toll like receptors in lupus nephritis: Quantification and clinicopathological correlations. *Mediat. Inflamm.* **2016**, *2016*. [[CrossRef](#)]
203. Ciferska, H.; Horak, P.; Kontinen, Y.T.; Krejci, K.; Tichy, T.; Hermanova, Z.; Zadrazil, J. Expression of nucleic acid binding Toll-like receptors in control, lupus and transplanted kidneys—a preliminary pilot study. *Lupus* **2008**, *17*, 580–585. [[CrossRef](#)]
204. Lin, M.; Yiu, W.H.; Wu, H.J.; Chan, L.Y.; Leung, J.C.; Au, W.S.; Chan, K.W.; Lai, K.N.; Tang, S.C. Toll-like receptor 4 promotes tubular inflammation in diabetic nephropathy. *J. Am. Soc. Nephrol.* **2012**, *23*, 86–102. [[CrossRef](#)]
205. Srivastava, T.; Sharma, M.; Yew, K.-H.; Sharma, R.; Duncan, R.S.; Saleem, M.A.; McCarthy, E.T.; Kats, A.; Cudmore, P.A.; Alon, U.S. LPS and PAN-induced podocyte injury in an in vitro model of minimal change disease: Changes in TLR profile. *J. Cell Commun. Signal.* **2013**, *7*, 49–60. [[CrossRef](#)] [[PubMed](#)]

206. Shimada, M.; Ishimoto, T.; Lee, P.Y.; Lanaspá, M.A.; Rivard, C.J.; Roncal-Jimenez, C.A.; Wymer, D.T.; Yamabe, H.; Mathieson, P.W.; Saleem, M.A. Toll-like receptor 3 ligands induce CD80 expression in human podocytes via an NF- κ B-dependent pathway. *Nephrol. Dial. Transplant.* **2012**, *27*, 81–89. [[CrossRef](#)]
207. Li, D.; Zou, L.; Feng, Y.; Xu, G.; Gong, Y.; Zhao, G.; Ouyang, W.; Thurman, J.M.; Chao, W. Complement factor B production in renal tubular cells and its role in sodium transporter expression during polymicrobial sepsis. *Crit. Care Med.* **2016**, *44*, e289. [[CrossRef](#)]
208. Bäckhed, F.; Söderhäll, M.; Ekman, P.; Normark, S.; Richter-Dahlfors, A. Induction of innate immune responses by *Escherichia coli* and purified lipopolysaccharide correlate with organ- and cell-specific expression of Toll-like receptors within the human urinary tract. *Cell. Microbiol.* **2001**, *3*, 153–158. [[CrossRef](#)]
209. Jonassen, J.A.; Kohjimoto, Y.; Scheid, C.R.; Schmidt, M. Oxalate toxicity in renal cells. *Urol. Res.* **2005**, *33*, 329–339. [[CrossRef](#)]
210. Yang, W.S.; Kim, J.-S.; Han, N.J.; Lee, M.J.; Park, S.-K. Toll-like receptor 4/spleen tyrosine kinase complex in high glucose signal transduction of proximal tubular epithelial cells. *Cell. Physiol. Biochem.* **2015**, *35*, 2309–2319. [[CrossRef](#)]
211. Han, S.J.; Li, H.; Kim, M.; Shlomchik, M.J.; Lee, H.T. Kidney proximal tubular TLR9 exacerbates ischemic acute kidney injury. *J. Immunol.* **2018**, *201*, 1073–1085. [[CrossRef](#)] [[PubMed](#)]
212. Samuelsson, P.; Hang, L.; Wullt, B.; Irjala, H.; Svanborg, C. Toll-like receptor 4 expression and cytokine responses in the human urinary tract mucosa. *Infect. Immun.* **2004**, *72*, 3179–3186. [[CrossRef](#)] [[PubMed](#)]
213. Papadimitraki, E.; Tzardi, M.; Bertsiás, G.; Sotsiou, E.; Boumpas, D.T. Glomerular expression of toll-like receptor-9 in lupus nephritis but not in normal kidneys: Implications for the amplification of the inflammatory response. *Lupus* **2009**, *18*, 831–835. [[CrossRef](#)]
214. González-Guerrero, C.; Cannata-Ortiz, P.; Guerri, C.; Egido, J.; Ortiz, A.; Ramos, A.M. TLR4-mediated inflammation is a key pathogenic event leading to kidney damage and fibrosis in cyclosporine nephrotoxicity. *Arch. Toxicol.* **2017**, *91*, 1925–1939. [[CrossRef](#)] [[PubMed](#)]
215. Lepenies, J.; Eardley, K.S.; Kienitz, T.; Hewison, M.; Ihl, T.; Stewart, P.M.; Cockwell, P.; Quinkler, M. Renal TLR4 mRNA expression correlates with inflammatory marker MCP-1 and profibrotic molecule TGF- β 1 in patients with chronic kidney disease. *Nephron Clin. Pract.* **2011**, *119*, c97–c104. [[CrossRef](#)] [[PubMed](#)]
216. Leemans, J.C.; Stokman, G.; Claessen, N.; Rouschop, K.M.; Teske, G.J.; Kirschning, C.J.; Akira, S.; Van der Poll, T.; Weening, J.J.; Florquin, S. Renal-associated TLR2 mediates ischemia/reperfusion injury in the kidney. *J. Clin. Investig.* **2005**, *115*, 2894–2903. [[CrossRef](#)]
217. Verzola, D.; Cappuccino, L.; D’amato, E.; Villaggio, B.; Gianiorio, F.; Mij, M.; Simonato, A.; Viazzi, F.; Salvidio, G.; Garibotto, G. Enhanced glomerular Toll-like receptor 4 expression and signaling in patients with type 2 diabetic nephropathy and microalbuminuria. *Kidney Int.* **2014**, *86*, 1229–1243. [[CrossRef](#)]
218. Park, H.J.; Stokes, J.A.; Corr, M.; Yaksh, T.L. Toll-like receptor signaling regulates cisplatin-induced mechanical allodynia in mice. *Cancer Chemother. Pharmacol.* **2014**, *73*, 25–34. [[CrossRef](#)] [[PubMed](#)]
219. Volarevic, V.; Markovic, B.S.; Jankovic, M.G.; Djokovic, B.; Jovicic, N.; Harrell, C.R.; Fellabaum, C.; Djonov, V.; Arsenijevic, N.; Lukic, M.L. Galectin 3 protects from cisplatin-induced acute kidney injury by promoting TLR-2-dependent activation of IDO1/Kynurenine pathway in renal DCs. *Theranostics* **2019**, *9*, 5976. [[CrossRef](#)] [[PubMed](#)]
220. Ma, X.; Yan, L.; Zhu, Q.; Shao, F. Puerarin attenuates cisplatin-induced rat nephrotoxicity: The involvement of TLR4/NF- κ B signaling pathway. *PLoS ONE* **2017**, *12*, e0171612. [[CrossRef](#)] [[PubMed](#)]
221. Cenedeze, M.; Goncalves, G.; Feitoza, C.; Wang, P.; Damiao, M.; Bertocchi, A.; Pacheco-Silva, A.; Camara, N. The role of toll-like receptor 4 in cisplatin-induced renal injury. *Transplant. Proc.* **2007**, *39*, 409–411. [[CrossRef](#)]
222. Ramesh, G.; Zhang, B.; Uematsu, S.; Akira, S.; Reeves, W.B. Endotoxin and cisplatin synergistically induce renal dysfunction and cytokine production in mice. *Am. J. Physiol. Ren. Physiol.* **2007**, *293*, F325–F332. [[CrossRef](#)] [[PubMed](#)]
223. Babolmorad, G.; Latif, A.; Pollock, N.M.; Domingo, I.K.; Delyea, C.; Rieger, A.M.; Allison, W.T.; Bhavsar, A.P. Toll-like receptor 4 is activated by platinum and contributes to cisplatin-induced ototoxicity. *bioRxiv* **2020**, e51280. [[CrossRef](#)]
224. Dessing, M.C.; Kers, J.; Damman, J.; Leuvenink, H.G.; Van Goor, H.; Hillebrands, J.-L.; Hepkema, B.G.; Snieder, H.; Van den Born, J.; De Borst, M.H. Toll-like receptor family polymorphisms are associated with primary renal diseases but not with renal outcomes following kidney transplantation. *PLoS ONE* **2015**, *10*, e0139769. [[CrossRef](#)]
225. Elloumi, N.; Fakhfakh, R.; Abida, O.; Ayadi, L.; Marzouk, S.; Hachicha, H.; Fourati, M.; Bahloul, Z.; Mhiri, M.; Kammoun, K. Relevant genetic polymorphisms and kidney expression of Toll-like receptor (TLR)-5 and TLR-9 in lupus nephritis. *Clin. Exp. Immunol.* **2017**, *190*, 328–339. [[CrossRef](#)]
226. Ducloux, D.; Deschamps, M.; Yannaraki, M.; Ferrand, C.; Bamoulid, J.; Saas, P.; Kazory, A.; Chalopin, J.-M.; Tiberghien, P. Relevance of Toll-like receptor-4 polymorphisms in renal transplantation. *Kidney Int.* **2005**, *67*, 2454–2461. [[CrossRef](#)] [[PubMed](#)]
227. Santos-Martins, M.; Sameiro-Faria, M.; Ribeiro, S.; Rocha-Pereira, P.; Nascimento, H.; Reis, F.; Miranda, V.; Quintanilha, A.; Belo, L.; Beirão, I. TLR4 and TLR9 polymorphisms effect on inflammatory response in end-stage renal disease patients. *Eur. J. Inflamm.* **2014**, *12*, 521–529. [[CrossRef](#)]
228. Farhat, K.; Riekenberg, S.; Heine, H.; Debarry, J.; Lang, R.; Mages, J.; Buwitt-Beckmann, U.; Röschmann, K.; Jung, G.; Wiesmüller, K.H. Heterodimerization of TLR2 with TLR1 or TLR6 expands the ligand spectrum but does not lead to differential signaling. *J. Leukoc. Biol.* **2008**, *83*, 692–701. [[CrossRef](#)]

229. Guan, Y.; Ranoa, D.R.E.; Jiang, S.; Mutha, S.K.; Li, X.; Baudry, J.; Tapping, R.I. Human TLRs 10 and 1 share common mechanisms of innate immune sensing but not signaling. *J. Immunol.* **2010**, *184*, 5094–5103. [[CrossRef](#)]
230. Matsushima, N.; Tanaka, T.; Enkhbayar, P.; Mikami, T.; Taga, M.; Yamada, K.; Kuroki, Y. Comparative sequence analysis of leucine-rich repeats (LRRs) within vertebrate toll-like receptors. *Bmc Genom.* **2007**, *8*, 124. [[CrossRef](#)]
231. De Oliveira Nascimento, L.; Massari, P.; Wetzler, L.M. The role of TLR2 in infection and immunity. *Front. Immunol.* **2012**, *3*, 79. [[CrossRef](#)]
232. Raby, A.-C.; González-Mateo, G.T.; Williams, A.; Topley, N.; Fraser, D.; López-Cabrera, M.; Labéta, M.O. Targeting Toll-like receptors with soluble Toll-like receptor 2 prevents peritoneal dialysis solution-induced fibrosis. *Kidney Int.* **2018**, *94*, 346–362. [[CrossRef](#)]
233. Shen, Q.; Zhang, X.; Li, Q.; Zhang, J.; Lai, H.; Gan, H.; Du, X.; Li, M. TLR2 protects cisplatin-induced acute kidney injury associated with autophagy via PI3K/Akt signaling pathway. *J. Cell. Biochem.* **2019**, *120*, 4366–4374. [[CrossRef](#)]
234. Takahashi, A.; Kimura, T.; Takabatake, Y.; Namba, T.; Kaimori, J.; Kitamura, H.; Matsui, I.; Niimura, F.; Matsusaka, T.; Fujita, N. Autophagy guards against cisplatin-induced acute kidney injury. *Am. J. Pathol.* **2012**, *180*, 517–525. [[CrossRef](#)]
235. Myeku, N.; Figueiredo-Pereira, M.E. Dynamics of the degradation of ubiquitinated proteins by proteasomes and autophagy association With sequestosome 1/p62. *J. Biol. Chem.* **2011**, *286*, 22426–22440. [[CrossRef](#)] [[PubMed](#)]
236. Cherra III, S.J.; Kulich, S.M.; Uechi, G.; Balasubramani, M.; Mountzouris, J.; Day, B.W.; Chu, C.T. Regulation of the autophagy protein LC3 by phosphorylation. *J. Cell Biol.* **2010**, *190*, 533–539. [[CrossRef](#)]
237. Barth, S.; Glick, D.; Macleod, K.F. Autophagy: Assays and artifacts. *J. Pathol.* **2010**, *221*, 117–124. [[CrossRef](#)]
238. Xu, Y.; Chen, S.; Cao, Y.; Zhou, P.; Chen, Z.; Cheng, K. Discovery of novel small molecule TLR4 inhibitors as potent anti-inflammatory agents. *Eur. J. Med. Chem.* **2018**, *154*, 253–266. [[CrossRef](#)] [[PubMed](#)]
239. Zhang, B.; Ramesh, G.; Uematsu, S.; Akira, S.; Reeves, W.B. TLR4 signaling mediates inflammation and tissue injury in nephrotoxicity. *J. Am. Soc. Nephrol.* **2008**, *19*, 923–932. [[CrossRef](#)] [[PubMed](#)]
240. Park, B.S.; Lee, J.-O. Recognition of lipopolysaccharide pattern by TLR4 complexes. *Exp. Mol. Med.* **2013**, *45*, e66. [[CrossRef](#)] [[PubMed](#)]
241. Haynes, L.M.; Moore, D.D.; Kurt-Jones, E.A.; Finberg, R.W.; Anderson, L.J.; Tripp, R.A. Involvement of toll-like receptor 4 in innate immunity to respiratory syncytial virus. *J. Virol.* **2001**, *75*, 10730–10737. [[CrossRef](#)] [[PubMed](#)]
242. Kurt-Jones, E.A.; Popova, L.; Kwinn, L.; Haynes, L.M.; Jones, L.P.; Tripp, R.A.; Walsh, E.E.; Freeman, M.W.; Golenbock, D.T.; Anderson, L.J. Pattern recognition receptors TLR4 and CD14 mediate response to respiratory syncytial virus. *Nat. Immunol.* **2000**, *1*, 398–401. [[CrossRef](#)] [[PubMed](#)]
243. Lai, C.-Y.; Strange, D.P.; Wong, T.A.S.; Lehrer, A.T.; Verma, S. Ebola virus glycoprotein induces an innate immune response in vivo via TLR4. *Front. Microbiol.* **2017**, *8*, 1571. [[CrossRef](#)] [[PubMed](#)]
244. Rashidi, N.; Mirahmadian, M.; Jeddi-Tehrani, M.; Rezania, S.; Ghasemi, J.; Kazemnejad, S.; Mirzadegan, E.; Vafaei, S.; Kashanian, M.; Rasoulzadeh, Z. Lipopolysaccharide-and lipoteichoic acid-mediated pro-inflammatory cytokine production and modulation of TLR2, TLR4 and MyD88 expression in human endometrial cells. *J. Reprod. Infertil.* **2015**, *16*, 72.
245. Thomas, P.G.; Carter, M.R.; Atochina, O.; Da'Dara, A.A.; Piskorska, D.; McGuire, E.; Harn, D.A. Maturation of dendritic cell 2 phenotype by a helminth glycan uses a Toll-like receptor 4-dependent mechanism. *J. Immunol.* **2003**, *171*, 5837–5841. [[CrossRef](#)] [[PubMed](#)]
246. Oh, S.-M.; Park, G.; Lee, S.H.; Seo, C.-S.; Shin, H.-K.; Oh, D.-S. Assessing the recovery from prerenal and renal acute kidney injury after treatment with single herbal medicine via activity of the biomarkers HMGB1, NGAL and KIM-1 in kidney proximal tubular cells treated by cisplatin with different doses and exposure times. *BMC Complementary Altern. Med.* **2017**, *17*, 544.
247. Ullah, M.; Liu, D.D.; Rai, S.; Concepcion, W.; Thakor, A.S. HSP70-Mediated NLRP3 Inflammasome Suppression Underlies Reversal of Acute Kidney Injury Following Extracellular Vesicle and Focused Ultrasound Combination Therapy. *Int. J. Mol. Sci.* **2020**, *21*, 4085. [[CrossRef](#)] [[PubMed](#)]
248. Rachmawati, D.; Bontkes, H.J.; Verstege, M.I.; Muris, J.; Von Blomberg, B.M.E.; Schepers, R.J.; Van Hoogstraten, I.M. Transition metal sensing by Toll-like receptor-4: Next to nickel, cobalt and palladium are potent human dendritic cell stimulators. *Contact Dermat.* **2013**, *68*, 331–338. [[CrossRef](#)] [[PubMed](#)]
249. Fenhammar, J.; Rundgren, M.; Hultenby, K.; Forestier, J.; Taavo, M.; Kenne, E.; Weitzberg, E.; Eriksson, S.; Ozenci, V.; Wernerson, A. Renal effects of treatment with a TLR4 inhibitor in conscious septic sheep. *Crit. Care* **2014**, *18*, 488.
250. Fenhammar, J.; Rundgren, M.; Forestier, J.; Kalman, S.; Eriksson, S.; Frithiof, R. Toll-like receptor 4 inhibitor TAK-242 attenuates acute kidney injury in endotoxemic sheep. *Anesthesiol. J. Am. Soc. Anesthesiol.* **2011**, *114*, 1130–1137. [[CrossRef](#)]
251. Yamada, M.; Ichikawa, T.; Ii, M.; Sunamoto, M.; Itoh, K.; Tamura, N.; Kitazaki, T. Discovery of novel and potent small-molecule inhibitors of NO and cytokine production as antiseptic agents: Synthesis and biological activity of alkyl 6-(N-substituted sulfamoyl) cyclohex-1-ene-1-carboxylate. *J. Med. Chem.* **2005**, *48*, 7457–7467. [[CrossRef](#)] [[PubMed](#)]
252. Takashima, K.; Matsunaga, N.; Yoshimatsu, M.; Hazeki, K.; Kaisho, T.; Uekata, M.; Hazeki, O.; Akira, S.; Iizawa, Y.; Ii, M. Analysis of binding site for the novel small-molecule TLR4 signal transduction inhibitor TAK-242 and its therapeutic effect on mouse sepsis model. *Br. J. Pharmacol.* **2009**, *157*, 1250–1262. [[CrossRef](#)] [[PubMed](#)]
253. Kashani, B.; Zandi, Z.; Karimzadeh, M.R.; Bashash, D.; Nasrollahzadeh, A.; Ghaffari, S.H. Blockade of TLR4 using TAK-242 (resatorvid) enhances anti-cancer effects of chemotherapeutic agents: A novel synergistic approach for breast and ovarian cancers. *Immunol. Res.* **2019**, *67*, 505–516. [[CrossRef](#)]

254. Pedersen, G.; Andresen, L.; Matthiessen, M.; Rask-Madsen, J.; Brynskov, J. Expression of Toll-like receptor 9 and response to bacterial CpG oligodeoxynucleotides in human intestinal epithelium. *Clin. Exp. Immunol.* **2005**, *141*, 298–306. [[CrossRef](#)] [[PubMed](#)]
255. Wang, Y.; Abel, K.; Lantz, K.; Krieg, A.M.; McChesney, M.B.; Miller, C.J. The Toll-like receptor 7 (TLR7) agonist, imiquimod, and the TLR9 agonist, CpG ODN, induce antiviral cytokines and chemokines but do not prevent vaginal transmission of simian immunodeficiency virus when applied intravaginally to rhesus macaques. *J. Virol.* **2005**, *79*, 14355–14370. [[CrossRef](#)] [[PubMed](#)]
256. Wu, X.; Peng, S.L. Toll-like receptor 9 signaling protects against murine lupus. *Arthritis Rheum. Off. J. Am. Coll. Rheumatol.* **2006**, *54*, 336–342. [[CrossRef](#)]
257. Machida, H.; Ito, S.; Hirose, T.; Takeshita, F.; Oshiro, H.; Nakamura, T.; Mori, M.; Inayama, Y.; Yan, K.; Kobayashi, N. Expression of Toll-like receptor 9 in renal podocytes in childhood-onset active and inactive lupus nephritis. *Nephrol. Dial. Transplant.* **2010**, *25*, 2430–2537. [[CrossRef](#)] [[PubMed](#)]
258. Mallavia, B.; Liu, F.; Lefrançois, E.; Cleary, S.J.; Kwaan, N.; Tian, J.J.; Magnen, M.; Sayah, D.M.; Soong, A.; Chen, J. Mitochondrial DNA stimulates TLR9-dependent neutrophil extracellular trap formation in primary graft dysfunction. *Am. J. Respir. Cell Mol. Biol.* **2020**, *62*, 364–372. [[CrossRef](#)]
259. Busconi, L.; Bauer, J.W.; Tumang, J.R.; Laws, A.; Perkins-Mesires, K.; Tabor, A.S.; Lau, C.; Corley, R.B.; Rothstein, T.L.; Lund, F.E. Functional outcome of B cell activation by chromatin immune complex engagement of the B cell receptor and TLR9. *J. Immunol.* **2007**, *179*, 7397–7405. [[CrossRef](#)] [[PubMed](#)]
260. Brooks, J.; Sun, W.; Chiosis, G.; Leifer, C.A. Heat shock protein gp96 regulates Toll-like receptor 9 proteolytic processing and conformational stability. *Biochem. Biophys. Res. Commun.* **2012**, *421*, 780–784. [[CrossRef](#)] [[PubMed](#)]
261. Jiang, S.; Chen, X. Expression of high-mobility group box 1 protein (HMGB1) and toll-like receptor 9 (TLR9) in retinas of diabetic rats. *Med. Sci. Monit. Int. Med. J. Exp. Clin. Res.* **2017**, *23*, 3115. [[CrossRef](#)]
262. Saito, K.; Kukita, K.; Kutomi, G.; Okuya, K.; Asanuma, H.; Tabeya, T.; Naishiro, Y.; Yamamoto, M.; Takahashi, H.; Torigoe, T. Heat shock protein 90 associates with Toll-like receptors 7/9 and mediates self-nucleic acid recognition in SLE. *Eur. J. Immunol.* **2015**, *45*, 2028–2041. [[CrossRef](#)] [[PubMed](#)]
263. Urry, Z.; Xystrakis, E.; Richards, D.F.; McDonald, J.; Sattar, Z.; Cousins, D.J.; Corrigan, C.J.; Hickman, E.; Brown, Z.; Hawrylowicz, C.M. Ligation of TLR9 induced on human IL-10-secreting Tregs by 1 α , 25-dihydroxyvitamin D3 abrogates regulatory function. *J. Clin. Investig.* **2009**, *119*, 387–398. [[CrossRef](#)]
264. Lai, L.-W.; Yong, K.-C.; Lien, Y.-H.H. Pharmacologic recruitment of regulatory T cells as a therapy for ischemic acute kidney injury. *Kidney Int.* **2012**, *81*, 983–992. [[CrossRef](#)] [[PubMed](#)]
265. Humanes, B.; Camaño, S.; Lara, J.M.; Sabbiseti, V.; González-Nicolás, M.Á.; Bonventre, J.V.; Tejedor, A.; Lázaro, A. Cisplatin-induced renal inflammation is ameliorated by cilastatin nephroprotection. *Nephrol. Dial. Transplant.* **2017**, *32*, 1645–1655. [[CrossRef](#)] [[PubMed](#)]
266. Szlosarek, P.W.; Balkwill, F.R. Tumour necrosis factor α : A potential target for the therapy of solid tumours. *Lancet Oncol.* **2003**, *4*, 565–573. [[CrossRef](#)]
267. Wu, X.; Wu, M.-Y.; Jiang, M.; Zhi, Q.; Bian, X.; Xu, M.-D.; Gong, F.-R.; Hou, J.; Tao, M.; Shou, L.-M. TNF- α sensitizes chemotherapy and radiotherapy against breast cancer cells. *Cancer Cell Int.* **2017**, *17*, 13. [[CrossRef](#)]
268. Wang, X.; Lin, Y. Tumor necrosis factor and cancer, buddies or foes? 1. *Acta Pharmacol. Sin.* **2008**, *29*, 1275–1288. [[CrossRef](#)]
269. Ozkok, A.; Ravichandran, K.; Wang, Q.; Ljubanovic, D.; Edelstein, C.L. NF- κ B transcriptional inhibition ameliorates cisplatin-induced acute kidney injury (AKI). *Toxicol. Lett.* **2016**, *240*, 105–113. [[CrossRef](#)]
270. Zhou, J.; Fan, Y.; Zhong, J.; Huang, Z.; Huang, T.; Lin, S.; Chen, H. TAK1 mediates excessive autophagy via p38 and ERK in cisplatin-induced acute kidney injury. *J. Cell. Mol. Med.* **2018**, *22*, 2908–2921. [[CrossRef](#)]
271. Mihaly, S.; Ninomiya-Tsuji, J.; Morioka, S. TAK1 control of cell death. *Cell Death Differ.* **2014**, *21*, 1667–1676. [[CrossRef](#)] [[PubMed](#)]
272. Faubel, S.; Lewis, E.C.; Reznikov, L.; Ljubanovic, D.; Hoke, T.S.; Somers, H.; Oh, D.-J.; Lu, L.; Klein, C.L.; Dinarello, C.A. Cisplatin-induced acute renal failure is associated with an increase in the cytokines interleukin (IL)-1 β , IL-18, IL-6, and neutrophil infiltration in the kidney. *J. Pharmacol. Exp. Ther.* **2007**, *322*, 8–15. [[CrossRef](#)] [[PubMed](#)]
273. Deng, J.; Kohda, Y.; Chiao, H.; Wang, Y.; Hu, X.; Hewitt, S.M.; Miyaji, T.; Mcleroy, P.; Nibhanupudy, B.; Li, S. Interleukin-10 inhibits ischemic and cisplatin-induced acute renal injury. *Kidney Int.* **2001**, *60*, 2118–2128. [[CrossRef](#)] [[PubMed](#)]
274. Lu, L.H.; Oh, D.-J.; Dursun, B.; He, Z.; Hoke, T.S.; Faubel, S.; Edelstein, C.L. Increased macrophage infiltration and fractalkine expression in cisplatin-induced acute renal failure in mice. *J. Pharmacol. Exp. Ther.* **2008**, *324*, 111–117. [[CrossRef](#)]
275. Tadagavadi, R.K.; Reeves, W.B. Endogenous IL-10 attenuates cisplatin nephrotoxicity: Role of dendritic cells. *J. Immunol.* **2010**, *185*, 4904–4911. [[CrossRef](#)]
276. Jones, V.S.; Huang, R.-Y.; Chen, L.-P.; Chen, Z.-S.; Fu, L.; Huang, R.-P. Cytokines in cancer drug resistance: Cues to new therapeutic strategies. *Biochim. Biophys. Acta Rev. Cancer* **2016**, *1865*, 255–265. [[CrossRef](#)]
277. Akcay, A.; Nguyen, Q.; He, Z.; Turkmen, K.; Lee, D.W.; Hernandez, A.A.; Altmann, C.; Toker, A.; Pacic, A.; Ljubanovic, D.G. IL-33 exacerbates acute kidney injury. *J. Am. Soc. Nephrol.* **2011**, *22*, 2057–2067. [[CrossRef](#)]
278. Scott, H.; Jones, D.; Pui, C. The tumor lysis syndrome. *N. Engl. J. Med.* **2011**, *364*, 1844–1854.
279. Scheller, J.; Chalaris, A.; Schmidt-Arras, D.; Rose-John, S. The pro- and anti-inflammatory properties of the cytokine interleukin-6. *Biochim. Biophys. Acta Mol. Cell Res.* **2011**, *1813*, 878–888. [[CrossRef](#)] [[PubMed](#)]

280. Dennen, P.; Altmann, C.; Kaufman, J.; Klein, C.L.; Andres-Hernando, A.; Ahuja, N.H.; Edelstein, C.L.; Cadnapaphornchai, M.A.; Keniston, A.; Faubel, S. Urine interleukin-6 is an early biomarker of acute kidney injury in children undergoing cardiac surgery. *Crit. Care* **2010**, *14*, 1–13. [[CrossRef](#)]
281. Mitazaki, S.; Kato, N.; Suto, M.; Hiraiwa, K.; Abe, S. Interleukin-6 deficiency accelerates cisplatin-induced acute renal failure but not systemic injury. *Toxicology* **2009**, *265*, 115–121. [[CrossRef](#)]
282. Suchi, K.; Fujiwara, H.; Okamura, S.; Okamura, H.; Umehara, S.; Todo, M.; Furutani, A.; Yoneda, M.; Shiozaki, A.; Kubota, T. Overexpression of Interleukin-6 suppresses cisplatin-induced cytotoxicity in esophageal squamous cell carcinoma cells. *Anticancer Res.* **2011**, *31*, 67–75. [[PubMed](#)]
283. Reeves, W.B. Innate Immunity in Nephrotoxic Acute Kidney Injury. *Trans. Am. Clin. Climatol. Assoc.* **2019**, *130*, 33. [[PubMed](#)]
284. Mollica Poeta, V.; Massara, M.; Capucetti, A.; Bonecchi, R. Chemokines and chemokine receptors: New targets for cancer immunotherapy. *Front. Immunol.* **2019**, *10*, 379. [[CrossRef](#)] [[PubMed](#)]
285. Hu, Z.B.; Chen, Y.; Gong, Y.X.; Gao, M.; Zhang, Y.; Wang, G.H.; Tang, R.N.; Liu, H.; Liu, B.C.; Ma, K.L. Activation of the CXCL16/CXCR6 pathway by inflammation contributes to atherosclerosis in patients with end-stage renal disease. *Int. J. Med. Sci.* **2016**, *13*, 858. [[CrossRef](#)] [[PubMed](#)]
286. Wehr, A.; Tacke, F. The roles of CXCL16 and CXCR6 in liver inflammation and fibrosis. *Curr. Pathobiol. Rep.* **2015**, *3*, 283–290. [[CrossRef](#)]
287. Lehrke, M.; Millington, S.C.; Lefterova, M.; Cumarantunge, R.G.; Szapary, P.; Wilensky, R.; Rader, D.J.; Lazar, M.A.; Reilly, M.P. CXCL16 is a marker of inflammation, atherosclerosis, and acute coronary syndromes in humans. *J. Am. Coll. Cardiol.* **2007**, *49*, 442–449. [[CrossRef](#)] [[PubMed](#)]
288. Baeck, C.; Wehr, A.; Karlmark, K.R.; Heymann, F.; Vucur, M.; Gassler, N.; Huss, S.; Klussmann, S.; Eulberg, D.; Luedde, T. Pharmacological inhibition of the chemokine CCL2 (MCP-1) diminishes liver macrophage infiltration and steatohepatitis in chronic hepatic injury. *Gut* **2012**, *61*, 416–426. [[CrossRef](#)]
289. Garcia, G.E.; Truong, L.D.; Li, P.; Zhang, P.; Johnson, R.J.; Wilson, C.B.; Feng, L. Inhibition of CXCL16 attenuates inflammatory and progressive phases of anti-glomerular basement membrane antibody-associated glomerulonephritis. *Am. J. Pathol.* **2007**, *170*, 1485–1496. [[CrossRef](#)]
290. Liang, H.; Ma, Z.; Peng, H.; He, L.; Hu, Z.; Wang, Y. CXCL16 deficiency attenuates renal injury and fibrosis in salt-sensitive hypertension. *Sci. Rep.* **2016**, *6*, 28715. [[CrossRef](#)] [[PubMed](#)]
291. Wehr, A.; Baeck, C.; Ulmer, F.; Gassler, N.; Hittatiya, K.; Luedde, T.; Neumann, U.P.; Trautwein, C.; Tacke, F. Pharmacological inhibition of the chemokine CXCL16 diminishes liver macrophage infiltration and steatohepatitis in chronic hepatic injury. *PLoS ONE* **2014**, *9*, e112327. [[CrossRef](#)] [[PubMed](#)]
292. Sawant, K.V.; Poluri, K.M.; Dutta, A.K.; Sepuru, K.M.; Troshkina, A.; Garofalo, R.P.; Rajarathnam, K. Chemokine CXCL1 mediated neutrophil recruitment: Role of glycosaminoglycan interactions. *Sci. Rep.* **2016**, *6*, 33123. [[CrossRef](#)]
293. Ravindran, A.; Sawant, K.V.; Sarmiento, J.; Navarro, J.; Rajarathnam, K. Chemokine CXCL1 dimer is a potent agonist for the CXCR2 receptor. *J. Biol. Chem.* **2013**, *288*, 12244–12252. [[CrossRef](#)]
294. Kinsey, G.R.; Okusa, M.D. Role of leukocytes in the pathogenesis of acute kidney injury. *Crit. Care* **2012**, *16*, 1–5. [[CrossRef](#)]
295. Vandamme, T.F. Use of rodents as models of human diseases. *J. Pharm. Bioallied Sci.* **2014**, *6*, 2. [[CrossRef](#)] [[PubMed](#)]
296. Leenaars, C.H.; Kouwenaar, C.; Stafleu, F.R.; Bleich, A.; Ritskes-Hoitinga, M.; De Vries, R.B.; Meijboom, F.L. Animal to human translation: A systematic scoping review of reported concordance rates. *J. Transl. Med.* **2019**, *17*, 1–22. [[CrossRef](#)]
297. Skrypnik, N.I.; Siskind, L.J.; Faubel, S.; De Caestecker, M.P. Bridging translation for acute kidney injury with better preclinical modeling of human disease. *Am. J. Physiol. Ren. Physiol.* **2016**, *310*, F972–F984. [[CrossRef](#)] [[PubMed](#)]
298. Mirrakhimov, A.E.; Ali, A.M.; Khan, M.; Barbaryan, A. Tumor lysis syndrome in solid tumors: An up to date review of the literature. *Rare Tumors* **2014**, *6*, 68–76. [[CrossRef](#)] [[PubMed](#)]
299. Manohar, S.; Leung, N. Cisplatin nephrotoxicity: A review of the literature. *J. Nephrol.* **2018**, *31*, 15–25. [[CrossRef](#)] [[PubMed](#)]
300. Bégin, A.-M.; Monfette, M.-L.; Boudrias-Dalle, É.; Lavallée, E.; Samouelian, V.; Soulières, D.; Chagnon, M.; Fournier, M.-A.; Letarte, N.; Adam, J.-P. Effect of mannitol on acute kidney injury induced by cisplatin. *Supportive Care Cancer* **2021**, *29*, 2083–2091. [[CrossRef](#)] [[PubMed](#)]
301. Makimoto, G.; Hotta, K.; Oze, I.; Ninomiya, K.; Ninomiya, T.; Kubo, T.; Ohashi, K.; Ichihara, E.; Rai, K.; Tabata, M. Randomized phase II study comparing mannitol with furosemide for the prevention of cisplatin-induced renal toxicity in advanced non-small cell lung cancer. *OLCSG1406 Trial* **2019**, *72*, 319–323. [[CrossRef](#)]
302. Cvitkovic, E.; Spaulding, J.; Bethune, V.; Martin, J.; Whitmore, W.F. Improvement of Cis-dichlorodiammineplatinum (NSC 119875): Therapeutic index in an animal model. *Cancer* **1977**, *39*, 1357–1361. [[CrossRef](#)]
303. McKibbin, T.; Cheng, L.L.; Kim, S.; Steuer, C.E.; Owonikoko, T.K.; Khuri, F.R.; Shin, D.M.; Saba, N.F. Mannitol to prevent cisplatin-induced nephrotoxicity in patients with squamous cell cancer of the head and neck (SCCHN) receiving concurrent therapy. *Supportive Care Cancer* **2016**, *24*, 1789–1793. [[CrossRef](#)]
304. Phitakwatchara, W.; Reungweteattana, T.; Kananuraks, S.; Pathumarak, A.; Assanatham, M.; Nongnuch, A. Preloading Magnesium Attenuate Cisplatin-Induced Nephrotoxicity: SP241. *Nephrol. Dial. Transplant.* **2017**, *32*.
305. Ghadrddan, E.; Sadighi, S.; Ebrahimpour, S.; Abdollahi, A.; Hadjibabaei, M.; Gholami, K.; Jahangard-Rafsanjani, Z. The effect of melatonin on cisplatin-induced nephrotoxicity: A pilot, randomized, double-blinded, placebo-controlled clinical trial. *Eur. J. Integr. Med.* **2020**, *34*, 101065. [[CrossRef](#)]

306. Baek, S.H.; Kim, S.H.; Kim, J.W.; Kim, Y.J.; Lee, K.-W.; Na, K.Y. Effects of a DPP4 inhibitor on cisplatin-induced acute kidney injury: Study protocol for a randomized controlled trial. *Trials* **2015**, *16*, 1–7. [[CrossRef](#)] [[PubMed](#)]
307. El Hamamsy, M.; Kamal, N.; Bazan, N.S.; El Haddad, M. Evaluation of the effect of acetazolamide versus mannitol on cisplatin-induced nephrotoxicity, a pilot study. *Int. J. Clin. Pharm.* **2018**, *40*, 1539–1547. [[CrossRef](#)] [[PubMed](#)]
308. Shahbazi, F.; Sadighi, S.; Dashti-Khavidaki, S.; Shahi, F.; Mirzania, M.; Abdollahi, A.; Ghahremani, M.H. Effect of silymarin administration on cisplatin nephrotoxicity: Report from a pilot, randomized, double-blinded, placebo-controlled clinical trial. *Phytother. Res.* **2015**, *29*, 1046–1053. [[CrossRef](#)]
309. Kemp, G.; Rose, P.; Lurain, J.; Berman, M.; Manetta, A.; Rouillet, B.; Homesley, H.; Belpomme, D.; Glick, J. Amifostine pretreatment for protection against cyclophosphamide-induced and cisplatin-induced toxicities: Results of a randomized control trial in patients with advanced ovarian cancer. *J. Clin. Oncol.* **1996**, *14*, 2101–2112. [[CrossRef](#)] [[PubMed](#)]
310. Nematbakhsh, M.; Pezeshki, Z.; Jazi, F.E.; Mazaheri, B.; Moeini, M.; Safari, T.; Azarkish, F.; Moslemi, F.; Maleki, M.; Rezaei, A. Cisplatin-induced nephrotoxicity; protective supplements and gender differences. *Asian Pac. J. Cancer Prev. APJCP* **2017**, *18*, 295.
311. Beeler, B.; Delacruz, W.P.; Flynt, F.L.; Terrazzino, S.; Hullinger, N.; Aden, J.; Byrd, T.; King, M.M.; Nelson, D.A. Saline alone vs saline plus mannitol hydration for the prevention of acute cisplatin nephrotoxicity: A randomized trial. *J. Clin. Oncol.* **2018**, *36*, 242. [[CrossRef](#)]
312. Ruggiero, A.; Rizzo, D.; Trombatore, G.; Maurizi, P.; Riccardi, R. The ability of mannitol to decrease cisplatin-induced nephrotoxicity in children: Real or not? *Cancer Chemother. Pharmacol.* **2016**, *77*, 19–26. [[CrossRef](#)]
313. Komaki, K.; Kusaba, T.; Tanaka, M.; Kado, H.; Shiotsu, Y.; Matsui, M.; Shiozaki, A.; Nakano, H.; Ishikawa, T.; Fujiwara, H. Lower blood pressure and risk of cisplatin nephrotoxicity: A retrospective cohort study. *BMC Cancer* **2017**, *17*, 1–8. [[CrossRef](#)]
314. McSweeney, K.R.; Gadanec, L.K.; Qaradakhi, T.; Gammune, T.M.; Kubatka, P.; Caprnda, M.; Fedotova, J.; Radonak, J.; Kruzliak, P.; Zulli, A. Imipridone enhances vascular relaxation via FOXO1 pathway. *Clin. Exp. Pharmacol. Physiol.* **2020**, *47*, 1816–1823. [[CrossRef](#)]
315. Mercantepe, F.; Mercantepe, T.; Topcu, A.; Yilmaz, A.; Tumkaya, L. Protective effects of amifostine, curcumin, and melatonin against cisplatin-induced acute kidney injury. *Naunyn-Schmiedeberg's Arch. Pharmacol.* **2018**, *391*, 915–931. [[CrossRef](#)] [[PubMed](#)]

Chapter 1: Cisplatin-induced acute kidney injury: Up to date.

** Superscript values beside abbreviations represent footnotes*

1.1 Introduction

Cisplatin-induced Acute Kidney Injury (CIAKI)¹ remains a critical research area linked to the prevalence and incidence of disease development and its association with high mortality rates. In March 2021, a literature review was published by our laboratory titled "Mechanisms of Cisplatin-Induced Acute Kidney Injury: Pathological Mechanisms, Pharmacological Interventions, and Genetic Mitigations" [1]. This publication outlined the fundamental pathophysiological mechanisms associated with CIAKI and the current preclinical and clinical interventions (pharmaceutical and genetic) aimed at treating or preventing CIAKI. The publication primarily focused on studies from 2018-2020. Since March 2021, numerous publications have emerged, contributing to the broader understanding of CIAKI pathophysiology and presenting many potential therapies for clinical trials. To demonstrate the significance governing CIAKI research, implying its importance, a literature search using the keywords "cisplatin-induced acute kidney injury" and setting the range to "since 2021" produced 17,700 results, primarily original article publications. This appendix will examine a small subsection of preclinical research released since 2021 detailing the novel molecular targets and additional well-established pathways, (figure 1.1). For a detailed summary of each treatment discussed; please refer to table 1A.1.

1.2 Targeted drug delivery

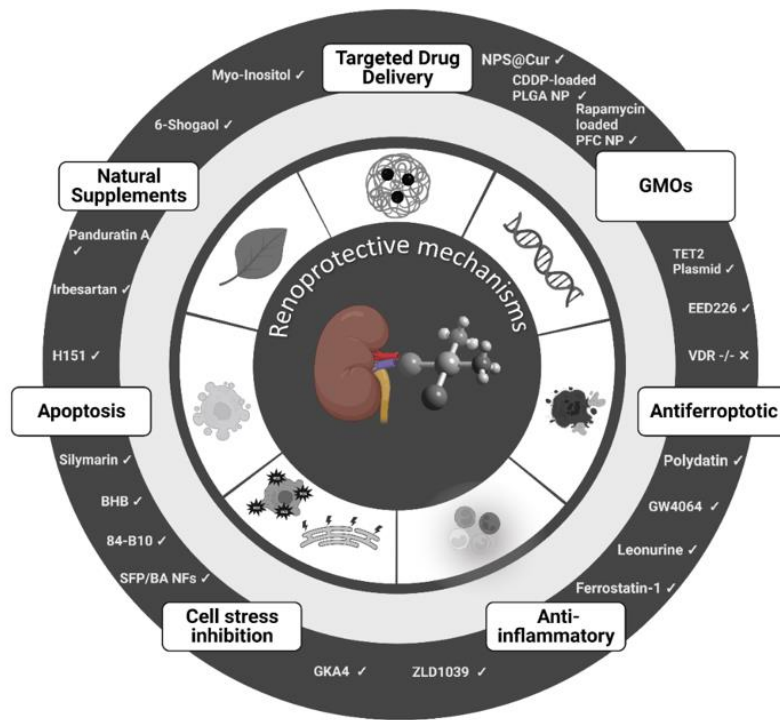
Interestingly, one of the most exciting and novel therapeutic options has only become a target for CIAKI research in the past year. It is not a preventative drug, but a new method of drug delivery aimed at enhancing the therapeutic specificity and overall potential of pharmaceutical agents. Its use has been documented to show mitigating effects against CIAKI [2, 3]. Drug delivery through loaded nanoparticles is a promising new avenue to overcome challenges related to therapeutics, including off-target effects enabling the potential for personalised and non-personalised nanoparticle drug delivery pathways and increasing the efficacy of therapies in patients [4].

The development of nanoparticles is a highly complex process. There are three main classes of nanoparticles which are then further classified into subcategories. The three

¹ CIAKI, cisplatin-induced acute kidney injury

main categories are polymeric, inorganic, and lipid-based, and they target various medical conditions and diseases. However, its initial and most targeted disease is cancer [4]. The use of nanoparticles is relatively new in its engineering and application process, with food and drug administration approval limited, however ever evolving. It provides a novel approach for individualised therapies, particularly in nephrotoxicity and acute kidney injury (AKI). Currently, publications involving nanoparticles in CIAKI research are minimal; however, a study investigated curcumin, the active ingredient in turmeric, to prevent CIAKI through nanoparticle drug delivery. Curcumin, a known anti-oxidant and anti-inflammatory drug, has already exhibited renoprotective effects as a free therapeutic against CIAKI in mice [3]. For this, curcumin-loaded nanoparticles were injected intraperitoneally into either healthy or CIAKI mice. The study concluded that curcumin-loaded nanoparticles alleviated mitochondrial injury associated with CIAKI, reduced oxidative and endoplasmic reticulum (ER) stress, increased autophagy, and reduced apoptosis [5]. A study investigating the effects of rapamycin on CIAKI showed it was ineffective in preventing damage in proximal tubular epithelial cell (PTEC) lines [6]. However, these results do not support an earlier publication that reported that rapamycin protects proximal tubules against CIAKI through the induction of autophagy [7]. The conflict in the literature does not provide a clear delineation of the effects of rapamycin against CIAKI. A recent publication has emerged using nanoparticle drug delivery to administer rapamycin. Their publication supported a previous study demonstrating that free rapamycin does provide a minor protective effect; however, that effect was significantly increased when administered as a rapamycin perfluorocarbon nanoparticle [8]. This generates the idea that targeted drug delivery may contribute substantially to the efficacy of previously identified drugs that show any degree of

renoprotection against CIAKI. It provides evidence for nanoparticle drug delivery in renal diseases, including nephrotoxicity. Another promising characteristic of nanoparticle drug delivery in CIAKI research is the potential elimination of adjunct



treatment. The fundamental concern with chemotherapies is the inability to distinguish healthy from diseased cells. The administration of CDDP in nanoparticle delivery could be a valuable strategy to combat systemic toxicities associated with its use, including nephrotoxicity. Developing this technology for CDDP delivery has already commenced. A 2016 study showed reduced side effects, the preservation of cytotoxicity and maintained CDDP efficacy in mice administered CDDP-loaded poly (lactic-co-glycolic acid) nanoparticles [9]. Although a highly promising strategy, it was reported that these nanoparticles delivered more significant amounts of CDDP, which were still absorbed by the liver and spleen, which could result in severe tissue damage. This scientific advancement is an essential step in the safety and efficacy of drug delivery and provides a clear path for systemic toxicity research.

Figure 1.1 Renoprotective mechanisms associated with CIAKI mitigation. Figure 1.1 demonstrates some of the current renoprotective mechanisms identified in 2021-2022, targeting critical well-established molecular mechanisms and novel avenues in the prevention of CIAKI. Abbreviations: BHB, β -hydroxybutyric acid; GMOs, genetically modified animals; SFP/BA NFs, baicalein-loaded silk fibroin peptide nanofiber; VDR -/-, vitamin D receptor-deficient. Figure created with BioRender.com.

1.3 Ferroptosis

Ferroptosis is a non-apoptotic or oxidative damage-induced form of programmed cell death [10] that is stimulated by iron-dependent lipid peroxidation [11]. It is involved in the pathogenesis of various diseases and has recently become a therapeutic target in studies of CIAKI. Multiple well-established cell death pathways are involved in the

pathogenesis of CIAKI, including apoptosis (intrinsic/extrinsic/ER), necrosis, and autophagy. However, inhibition of ferroptosis has become a recently targeted form of cell death in the prevention of CIAKI [12-14]. Lipid peroxidation is a critical ferroptosis regulator, and expression of 4-hydroxynonenal (4-HNE) and malondialdehyde (MDA) as biomarkers of lipid peroxidation [10] are often used as biomarkers for the development of ferroptosis. To identify the ferroptosis inhibitory potential of polydatin in the attenuation of CIAKI, mice were administered with polydatin or the ferroptosis inhibitor ferrostatin-1 (fer-1) one day before and 24 hours following a 20mg/kg injection of CDDP. Mice were humanely euthanised 48 hours post CDDP injection, with blood and organs harvested for pathological analysis.

Concomitant administration of CDDP with polydatin showed reduced renal damage. The histological evaluation also demonstrated that polydatin reduced the histological score of kidney injuries and terminal deoxynucleotidyl transferase dUTP nick end labelling (TUNEL)-positive staining in polydatin and CDDP-treated kidneys compared to CDDP alone [13]. Ferroptosis is an iron-dependent oxidative cell death method associated with increased lipid peroxidation and poor lipid peroxide elimination [15]. Given this, to determine the protective effects of polydatin against ferroptosis, an evaluation of lipid peroxidation biomarkers, including 4HNE and MDA, was performed. CDDP significantly elevated these biomarkers, a result that was markedly suppressed by treatment with polydatin, suggesting that it can diminish CIAKI-associated lipid peroxidation and ferroptosis as a method of or a contributing factor to CIAKI mitigation [13]. Additionally, other methods of ferroptosis inhibition have also proven ameliorative to CIAKI, including fer-1 [12, 13], the Farnesoid X receptor (FXR) agonist GW4064 [16], and Leonurine [14].

1.4 Genetics/Epigenetics

The use of genetically modified animals has become a widespread target of many publications in the late 2010s. It involved the use of knockout (KO) mice, genetic silencing, or genetic overexpression to further the understanding of the genes involved in the development and potential prevention of CIAKI. Recent literature has focused significantly on CIAKI mitigation through the inhibition of ferroptosis. However, some studies still target genetics and, more specifically, epigenetics. Results of a study in translocation methylcytosine dioxygenase 1 (TET2) KO mice showed that TET2 deletion significantly exacerbated CIAKI. This effect was mitigated when TET2 KO mice were intravenously administered a TET2 plasmid prior to CDDP treatment [17].

Inhibition of histone methylation through *Polycomb repressive complex 2* antagonisms by EED226 demonstrated renoprotective qualities against CDDP treatment [8]. This

study showed that pre-treatment with EED226 improved renal function while simultaneously reducing the expression of tumour protein 53, Forkhead box O3a (FOXO3a), and pro-apoptotic cleaved caspase 3. Interestingly, vitamin D receptor deficiency resulted in exacerbated CIAKI, evidenced by increased sBUN², sCr, 4-HNE, and reduced glutathione peroxidase 4 (GPX4), indicating the presence of ferroptosis, highlighting its role in CIAKI pathogenesis [12]. Understanding the genetics involved in CIAKI manifestation may increase the likelihood of drug identification for preventative strategies and remains a critical component of CIAKI research.

² sBUN, serum blood urea nitrogen

Table 1.1 Interventions assessed for renoprotective effects against CDDP-induced AKI in vivo, published in 2021-2022.

Intervention	CDDP Dose	Mechanism of action	Findings vs. CDDP	<i>In vivo</i> Model	Reference
EZH2 inhibitor (ZLD1039)	20 mg/kg	EZH2 inhibitor (anti-inflammatory)	↓sBUN and sCr ↑RKIP ↓transcriptional activity of Nfκb and tubular injury score	<i>Mice</i>	[18]
Silymarin	50 mg/kg	Anti-oxidant	↓TNF-α and NF-κB ↑IL-10	<i>Rats</i>	[19]
Curcumin-loaded nanoparticles (NPS@Cur)	20 mg/kg	Anti-oxidant/ anti-inflammatory	↓sBUN, sCr, TNF-α and IL-6	<i>Mice</i>	[5]
Rapamycin PFC nanoparticles	10 mg/kg	Autophagy inducer	↓sBUN, p62, p65 and Bax	<i>Mice</i>	[8]
Polydatin	20 mg/kg	Ferroptosis inhibition	↓sBUN, sCr, HSK, TUNEL, MDA and 4-HNE		[13]
Ferrostatin-1	20 mg/kg	Ferroptosis inhibition	↓sBUN, sCr, TUNEL and 4-HNE		[12]
Leonurine	20 mg/kg	Anti-oxidant/ ferroptosis inhibition	↑Nrf2 ↓ iron accumulation, renal damage, sBUN, sCr, KIM-1, and NGAL	<i>Mice</i>	[14]
GW4064	20 mg/kg	(FXR agonist) anti-inflammatory/ anti-oxidant/ferroptosis inhibition	↓ sBUN, sCr, NGAL, MDA and ROS	<i>Mice</i>	[16]
Baicalein-loaded silk fibroin peptide nanofibers (SFP/BA NFs)	20 mg/kg	Anti-oxidant	↓ sBUN and sCr ↑ SOD and GSH	<i>Mice</i>	[20]
<i>P. acidilactici</i> GKA4 (GKA4)	20 mg/kg	Anti-inflammatory/ anti-oxidant	↓ sBUN, sCr, renal function, TNF-α, and IL-6	<i>Mice</i>	[21]
Tet-2 Overexpression plasmids	22 mg/kg	Anti-inflammatory	↓ sBUN, sCr, tubular injury, and IL-6	<i>Mice</i>	[17]

H151	25 mg/kg	(STING antagonist) anti-inflammatory/anti-apoptotic	↓ sBUN, sCr, tubular injury, and TUNEL positive staining	<i>Mice</i>	[22]
EED226	25 mg/kg	(PRC2 antagonist) histone methylation inhibition	↑ renal function ↓ P53, FOXO3a and cleaved caspase-3	<i>Mice</i>	[8]
6-Shogaol	20 mg/kg	Anti-oxidant/ anti-inflammatory	↓ sBUN, sCr, tubular injury, NGAL, KIM-1	<i>Mice</i>	[23]
B-Hydroxybutyrate	20 mg/kg	Anti-inflammatory/ anti-oxidant	↓ sBUN, sCr, tubular injury, NLRP3, KIM-1	<i>Mice</i>	[24]
84-B10	25 mg/kg	Anti-oxidant	↓ sBUN, sCr, and 4-HNE ↑ Nrf2, SLC7A11, GSH and GPX4		[25]
Myo-Inositol	25 mg/kg	Anti-oxidant/ferroptosis inhibition	↓ sBUN, sCr, hyaline casts, NOX4, KIM-1, and NGAL	<i>Mice</i>	[26]
VDR -/-	20 mg/kg	Ferroptosis inhibition	↑ sBUN, sCr and 4-HNE ↓ GPX4		[12]
Irbesartan	7.5 mg/kg	Anti-apoptotic	↓ sBUN, sCr, caspase-3, TNF- α , Bax ↑ Bcl-2	<i>Rats</i>	[27]
Panduratin A	20 mg/kg	Anti-apoptotic	↓ sCr, NGAL and caspase 3		[28]

Abbreviations: 4-HNE, 4-Hydroxynonenal; Bax, Bcl-2 associated X protein; sBUN, Blood urea nitrogen; CDDP, Cisplatin; sCr, Creatinine; EZH2, Enhancer of zeste homolog 2; FOXO3a, Forkhead box class O 3a; FXR, Farnesoid X Receptor; GPX4, Glutathione peroxidase 4; GSH, glutathione; HSK, Histological score of kidney injuries; IL-10, Interleukin 10; IL-6, Interleukin 6; KIM-1, Kidney Injury Molecule 1; MDA, Malondialdehyde; Nfkb, Nuclear factor Kappa B; NGAL, Neutrophil gelatinase-associated lipocalin; NLRP3, NLR family pyrin domain containing 3; NOX4, NADPH oxidase 4; Nrf2, The nuclear factor erythroid-2-related factor 2; PRC2, Polycomb repressive complex 2; RKIP, Raf-1 kinase inhibitor protein; ROS, Reactive oxygen species; SLC7A11, Solute carrier family 7 member 11; SOD, Superoxide dismutase; STING, Stimulator of interferon genes; Tumour necrosis factor alpha; TUNEL, Terminal deoxynucleotidyl transferase dUTP nick end labelling and VDR, Vitamin D-receptor.

1.5 Inflammation

The highly complex pathway of the immune system remains one of the focal physiological targets for CIAKI treatments. Therefore, it is unsurprising that prospective anti-inflammatory drugs identified in preclinical evaluation have demonstrated such promise in preventing the condition. However, no current discovery replaces the current standards of care. Targeting pro-inflammatory cytokines and chemokines has proven beneficial in preventing CIAKI and remains a well-studied area. Co-treatment with the enhancer of zeste homolog 2 inhibitor ZLD1039 and 20mg/kg of CDDP reduced sBUN and sCr compared to CDDP alone. Nfkb protein expression was downregulated following treatment with ZLD1039 compared to CDDP alone. Histological examination showed a reduction in tubular injury score following ZLD1039 treatment [18]. Pre-treatment with *Lactobacillus acidophilus* GKA4 displayed positive pathological alterations in many areas, including inflammation, oxidative stress, renal function, lipid peroxidation, and oxidative stress suggesting a non-specific mechanistic effect. Although inflammation and its targeting are a therapeutic avenue for CIAKI studies, it is often rare to observe studies that potently and specifically target inflammatory molecules without producing off-target effects. This is especially important in an *in vivo* systemic environment, with the most concerning complication being the potential effects on the cytotoxicity of CDDP.

1.6 Cell stress

Multiple drugs have been identified in recent years as treatments against CIAKI. Many of these studies address key pathologies associated with cell stress. Research is ongoing to understand the molecular mechanisms of these drugs. An interesting publication by Altindag et al. used the anti-oxidant silymarin, which provided strong evidence that in male rats, silymarin does exert renoprotective properties against CIAKI. However, immunohistochemical analysis of kidney tissues showed that tumour necrosis factor α (TNF- α) and nuclear factor kappa b (NF- κ B) expression was reduced, and the anti-inflammatory cytokine interleukin 10 (IL-10) was increased compared to CDDP when co-administered with silymarin [19]. Surprisingly, in 2015 a randomised, double-blinded, placebo-controlled clinical trial was performed to investigate the effects of the anti-oxidant silymarin against CIAKI. It was concluded that silymarin could not prevent urine electrolyte wasting or improve renal function following CDDP treatment. This suggested that despite its theoretical potential, silymarin is not a promising target for CIAKI prevention. [29].

Intriguingly, one of the significant concerns regarding human dosing that could be a contributing factor in preclinical translatability is the "one size fits all" approach to drug delivery. In the human study of silymarin, all patients received 5.25 mg/kg of the therapeutic drug, while rats received 50 mg/kg. It is possible that the dose used in humans (10x) less than the dose used in rats may contribute to the less than therapeutic effects observed in clinic. It is possible that increasing the dose to the equivalent observed in rats, may be more beneficial than the 5.25 mg/kg dose used.

In addition to silymarin, two key oxidant targets in CIAKI have been reported to demonstrate renoprotective effects, the NACHT, leucine-rich repeat, and pyrin domain-containing protein 3 (NLRP3) inflammasome inhibitor β -hydroxybutyrate and 84-B10, a derivative of 3-phenylglutaric acid derivative. Both drugs were evaluated in high-dose CDDP models of AKI in mice and demonstrated reduced biomarkers of kidney dysfunction (sBUN and sCr). β -hydroxybutyric acid also showed reduced tubular injury, reduced kidney injury molecule 1 (KIM-1) expression, and reduced NLRP3, all signifying mitigating effects [24]. Decreased presence of lipid peroxidation was observed following treatment with 84-B10, evidenced by decreased 4-HNE and increased GPX4. Increased expression of anti-oxidant molecules nuclear factor erythroid 2-related factor 2, solute carrier family 7 member 11, and glutathione following treatment with 84-B10 compared to CDDP highlights its ameliorative effects [25]. Similar results were confirmed using an alternative anti-oxidant baicalein-loaded silk fibroin peptide nanofiber (SFP/BA NFs). In mice treated with CDDP and SFP/BA NFs, sBUN, sCr and reactive oxygen species were reduced compared to CDDP alone, whilst anti-oxidative proteins SOD and GSH [20] were increased, demonstrating further the renoprotective mechanism of anti-oxidant therapy in the prevention of CIAKI.

1.7 Apoptosis

Apoptosis is one of the most effective signalling cascades stimulating renoprotection against CIAKI. However, reducing apoptosis, although beneficial to kidney protection, often reduces CDDP cytotoxicity, which is not helpful for the anticancer efficacy of CDDP. CDDP has been shown to enhance the Stimulator of interferon genes (STING) [22], a known promotor of cytokine production [30]. In mice treated with 25 mg/kg of CDDP in addition to 7 mg/kg of the STING antagonist H151, a reduction in sBUN, sCr, tubular injury, and positive TUNEL staining was observed. This suggests that H151 may exert its renoprotection directly through apoptosis inhibition, inhibiting the inflammatory cascade independently or enhancing STING-inhibited inflammation.

Irbesartan is an antihypertensive agent used as an angiotensin receptor blocker (ARB) that has been a beneficial therapy for reducing blood pressure [31]. Interestingly, opinions regarding ARBs in combination with CDDP are somewhat conflicting throughout the literature, with preclinical evaluations demonstrating both protective and harmful effects. In mice treated with CDDP and irbesartan, reductions in sBUN and sCr were only mildly reduced compared to CDDP. However, marked reductions in caspase-3, TNF- α , and Bax revealed both antiapoptotic and anti-inflammatory effects. Additionally, irbesartan also increased CDDP-suppressed Bcl-2 expression [27]. Another study also showed reduced caspase-3 in mice co-treated with CDDP and the phytochemical Panduratin-a, which demonstrated reduced sCr, neutrophil gelatinase-associated lipocalin (NGAL), and the pro-apoptotic protein caspase-3 demonstrating its antiapoptotic properties. Investigations into its potential antihypertensive effects and the direct influence of that on kidney function could be helpful in future studies, given the suggestive importance of blood vessel function in the pathogenesis of CIAKI.

1.8 Natural Supplements

Despite the magnitude of pharmacological and genetic interventions for CIAKI identified to date, some of the most promising treatment strategies are from natural ingredients. Many classifications have shown promise as interventions, including flavonoids, saponins, alkaloids, polysaccharides, phenylpropanoids, and others [32]. In mice treated with 6-shogaol, the main bioactive ingredient in dried ginger, and then adjunctly treated with 20 mg/kg, CDDP showed reduced sBUN, sCr, tubular injury, NGAL, and KIM-1 compared to CDDP alone. These characteristics correlate positively with renoprotection, highlighting 6-Shogaol as a promising therapy for CIAKI. Furthermore, a different natural supplement also showed mitigating effects against CIAKI. Myo-inositol is a carbocyclic sugar produced in the body and sourced from food, with the kidney being considered one of its major catabolic sites. In mice treated with myo-inositol and 25 mg/kg of CDDP, periodic acid Schiff (PAS)-positive hyaline cast formation was significantly reduced, a critical morphological characteristic associated with CIAKI.

Reduced sBUN and sCr, in addition to increased anti-oxidant and ferroptosis inhibition was observed indicated by reduced NADPH oxidase 4 (NOX4). Myo-inositol also reduced key biomarkers of AKI, including KIM-1 and NGAL, compared to CDDP alone [26]. This highlights the vital role of natural products in the prevention of CIAKI and provides patients with potential alternatives to pharmacological approaches.

1.9 Conclusion

In a short period, the studies evolving in CIAKI research have increased rapidly which highlights the desperate need for therapeutic options. Previously, targeting inflammation, oxidative stress, apoptosis, and more recently ferroptosis have demonstrated to be clear renoprotective targets against CIAKI. However, the systemic nature of drug delivery in conjunction with the mechanism of action of each drug does not account for the cytotoxicity mechanism of CDDP. Most of these therapeutic molecular mechanisms interfere with the efficacy of CDDP by inhibiting its direct apoptotic pathways. Which although may be suitable for the renal preservation of patients, it does not portend well for their cancer prognosis. However, the novel targeted drug delivery method may enable more PTEC-targeted therapies that will protect kidneys without causing excessive interference with the cytotoxicity of CDDP. This unique development may provide an innovative engineering application in CIAKI mitigation.

Chapter 2: General Methods

2.1 Animals / experimental regimens

All experimental procedures involving the use of animals were carried out according to the Victoria University Animal Experimental Ethics Committee (VUAEEC) approved projects, 17/013 and 20/003 and per the Australian code for the care and use of animals for scientific purposes. All experiments and procedures were conducted at Victoria University, Werribee campus animal facility.

2.1.1 *Healthy and atherogenic rabbit model (AEC project 12/013)*

New Zealand male white rabbits aged between 8 and 16 weeks were obtained from the Animal Resource Centre (ARC) and were fed *ad libitum*, either a control diet (CD) or an atherogenic diet (AD) (heart disease-inducing) containing (0.5% cholesterol + 1% methionine + 5% peanut oil) purchased from (Cat#: SF00-218; Specialty Feeds, Victoria, Australia) for four weeks before culling (detailed below). This model is established in our laboratory to induce endothelial dysfunction, the initiating phase of atherosclerosis [33-35].

2.1.2 *Cisplatin-induced AKI (5-day model) (AEC Project 20/003)*

Male, C57BL/6J mice obtained from the ARC, Murdoch, Western Australia, were acclimatised for one week. Mice aged between 10 and 12 weeks were subjected to a four-day treatment schedule and culled on day five. Two variations of this model were used in this thesis. (Figure 2.1A) shows the experimental protocol for the CDDP dose finding cisplatin-induced acute kidney injury (CIAKI)³ study. In the mornings of days zero to three, mice received a single intraperitoneal (IP) injection per animal (AEC SOP 016 (2021) Mouse/Rat intraperitoneal (IP) injections) of 0.9% saline. On day one, four hours following the saline injection, mice received an IP injection of either 6.25 or 12.5 mg/kg of cisplatin (CDDP)⁴ dissolved in 0.9% saline. These mice were euthanised for *ex vivo* experiments 72 hours following the CDDP injection (day 4). (Figure 2.1B) describes the experimental protocol used for assessing BX-912 (BX) in the prevention of CIAKI. On days zero to three, mice received a morning IP injection of either BX (5, 0.5 or 0.05 mg/kg) or a vehicle of 1:9 dimethylformamide (DMF): phosphate buffered saline (PBS) pH 7.3. On day one, four hours following the morning injection, mice received a dose of 12.5 mg/kg of CDDP dissolved in 0.9% saline via IP injection. On day 4, 72 hours after CDDP injection, mice were euthanised and tissues harvested for

³ CIAKI, cisplatin induced acute kidney injury.

⁴ CDDP, cisplatin

further experiments. This 72-hour end-point protocol is a commonly used experimental model for CIAKI studies throughout the literature [36-39].

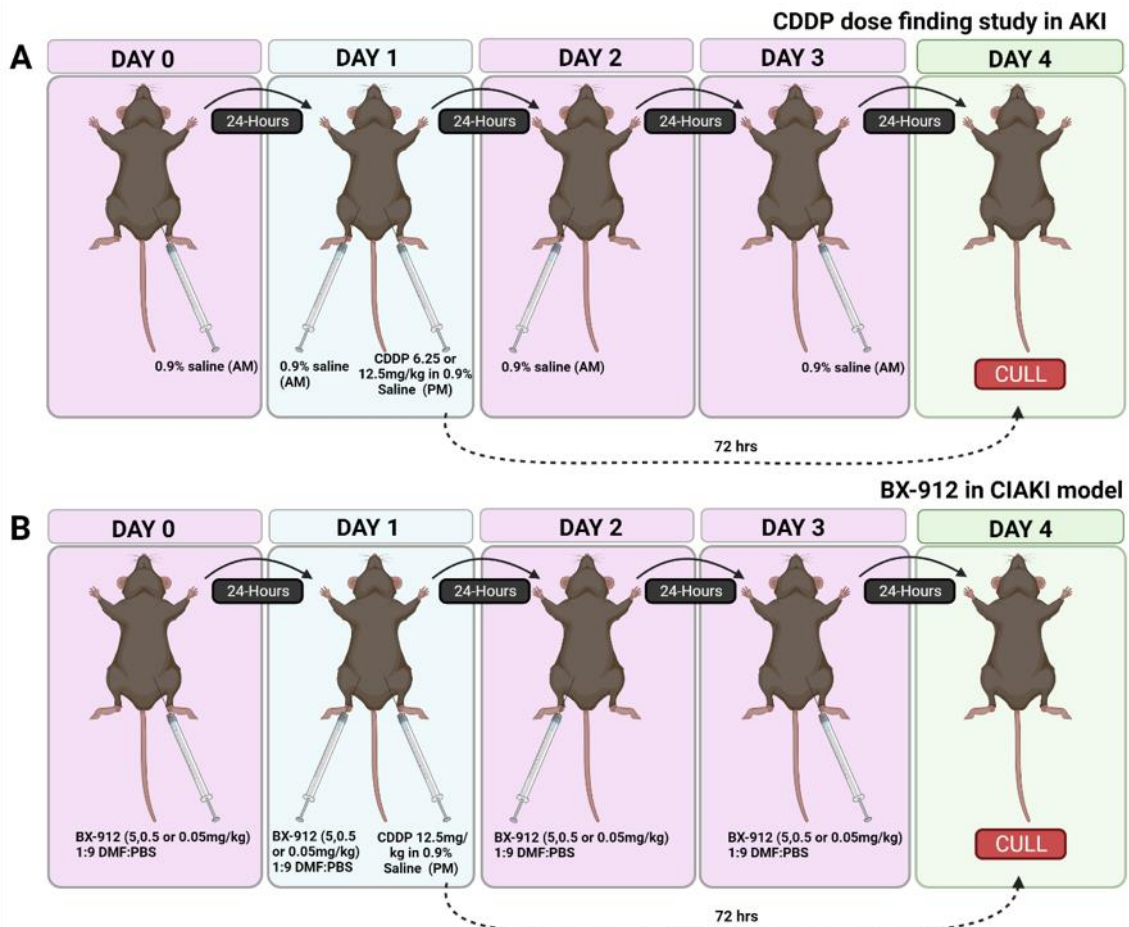


Figure 2.1. Treatment timeline for the CIAKI mouse model. This diagram represents the model performed in **A. Chapter 5: establishment of CIAKI model** and **B. Chapter 6. BX in the prevention of CDDP-induced AKI.** Figure created with BioRender.com

2.2 Monitoring

2.2.1 Mice monitoring

To uphold the Australian code for the care and use of animals for scientific purposes, after injections, mice were monitored three times daily (7AM, 12PM, and 5PM) to ensure animals were recovering after the drug treatment. Specialty monitoring was undertaken on day one following the CDDP injection. Due to the high dose of CDDP used in this project, it was critical that close monitoring was performed as sickness of the mice was a highly probable occurrence. Following the CDDP injection, mice were observed continuously for the initial 30 minutes and every 30 minutes after for two hours (a total of two and a half hours). This monitoring is in addition to the regular morning, midday, and evening monitoring.

2.3 Anesthesia and culling

2.3.1 Rabbit

Rabbits were swaddled with a towel in accordance with (AEC SOP 036 (2021) Rabbit Handling and Restraint) and injected subcutaneously with 0.25 mg/kg of medetomidine to sedate the rabbit. Once sedated (about 10 minutes, per AEC SOP 026 (2019) General Anesthesia of Rabbits and Guinea pigs), the rabbit was placed into an induction chamber with 4% isoflurane and an oxygen flow rate of 1.5 L for 10 minutes. Once no righting reflexes were present, the rabbit was transferred to a nose cone containing 4% isoflurane and an oxygen flow rate of 1.5 L for 5 minutes. A toe pinch was used to assess the paw withdrawal reflex, and corneal reflexes were tested to ensure the depth of anesthesia. Once reflexes were absent, a scalpel was used to open the thoracic cavity, and a slit was made in the vena cava to exsanguinate the rabbit. After three minutes, the rabbit's skin colour and eye dilation were checked, and once a loss of colour and pupil dilation occurred, the rabbit's thoracic cavity was opened completely. The diaphragm was cut entirely from the rib cage to confirm death.

2.3.2 2.3.2 Mouse

In accordance with (AEC SOP 004 (2021) General Anesthesia for Rats and Mice), mice were placed into an induction box containing 4% isoflurane and an oxygen flow rate of 1.5 L until no righting reflex was observed. Mice were then transferred to a nose cone containing 2-2.5% isoflurane and an oxygen flow rate of 0.8 L. A toe pinch test was used to assess the anaesthetic depth and autonomic response. Following confirmation of an absent autonomic response, the thoracic cavity of the mouse was opened to expose the heart. A heparin-coated syringe was used to perform a cardiac bleed for centrifugation and blood analysis. Cold, oxygenated KREBS pH 7.4 was syringed into the thoracic and abdominal cavities of the animal to ensure organ preservation.

2.4 Dissection

2.4.1 Rabbit dissection

A t-tube was inserted into the uppermost section of the thoracic aorta. The iliac arteries were severed, and three 50 ml syringes filled with cold Krebs-Henseleit buffer solution (KREBS)⁵ pH 7.4 were syringed through the vessels to clear the system of any remaining blood. The abdominal aorta was inspected to confirm the absence of clot formation and gently massaged to dislodge any clots that formed. Blood vessel sections of the rabbit required for isometric tension analysis were removed from the rabbit and immediately placed into cold KREBS pH 7.4 in preparation for further processing.

⁵ KREBS, *Krebs-Henseleit buffer* solution

Aortic, kidney and mesenteric tissue were harvested and immediately placed into cold KREBS solution pH 7.4. Thoracic aorta, interlobar and mesenteric arteries were identified, cleaned of fat and connective tissue, cut into 2mm sections, and placed into organ baths.

2.4.2 Mouse dissection

Following death by cardiac bleed, mice were carefully dissected while simultaneously being kept cold through syringing with cold KREBS pH 7.4. The thoracic cavity was opened, and organs were harvested for pathological analysis. The right kidneys were cut in half using a scalpel, placed into 4% paraformaldehyde (PFA), pH 7.4 overnight, and the other fixed for scanning electron microscopy (SEM) analysis (for information on SEM fixation protocol, please refer to General Methods, section 2.10). The left kidney was snap-frozen in liquid nitrogen and frozen at -80 °C in preparation for ribonucleic acid (RNA) purification for polymerase chain reaction (PCR) experiments. Following organ harvesting, fat and connective tissue was removed, exposing the thoracic aorta. A tube was placed inside and secured with sutures, and the abdominal aorta and iliac arteries were flushed to remove any remaining blood from the vasculature. The abdominal aorta and iliac artery sections were cut into 2-3mm rings and placed into organ baths for isometric tension analysis.

2.5 2.5 EchoMRI

Firstly, mice were subjected to an EchoMRI (EchoMRI 700), as per (AEC SOP 037 (2021) Use of EchoMRI 700 with Mice and Rats), one day prior to the commencement of the experimental period. This was to determine baseline body composition. Mice underwent a secondary EchoMRI on day four prior to being euthanised.

2.6 Isometric tension analysis

Thoracic aorta, interlobar and mesenteric arteries extracted from rabbits and abdominal aorta and iliac arteries obtained from mice were cut into 2mm rings and assessed for vascular function. Rings were placed into organ baths containing KREBS solution pH 7.4 (5 mL) and bubbled with carbogen (95% O₂ /5% CO₂), maintained at 37 °C for 30 minutes to acclimatise. The vessels were then mounted to two metal hooks connected to force displacement transducers (OB8, Zultek Engineering, Australia). It is critical to ensure that scraping of the endothelium does not occur during the mounting process. Arteries were stretched according to table 2.1.

Table 2.1. Isometric tension analysis baseline stretching values. Upon completion of the acclimatisation period, vessels were stretched according to the values below. The stretch of vessels varied amongst animals and depended on the size of the vascular lumen.

	Animal	Vessel type	Stretch
	Rabbit	TA	2 g
		ILA	0.5 g
		MA	0.25-0.5 g
	Mouse	AA	0.3-0.5g
IA		0.2 g	

Abbreviations: AA, abdominal aorta; IA, iliac arteries; ILA, interlobar arteries; MA, mesenteric arteries; TA, thoracic aorta.

Once mounted, the KREBS pH 7.4 solution was refreshed, and vessels were allowed to stabilise for 30 minutes. Rings were then re-stretched to their respective tensions, refreshed, and rested for 30 minutes. Then, after those 30 minutes and a final refreshment, vessels were pre-constricted. Once the vessels reached a plateau, drugs were added as blocking agents (if required), followed by a dose-response curve (DRC). For a graphical representation of the isometric tension process, please refer to (figure 2.2). For drugs and doses used, please refer to General Methods section 2.6, subsections 2.6.1 and 2.6.2. For angiotensin II (ANGII)-induced vasoconstriction curves in mice, vessels were not pre-constricted. Instead, a vasoconstriction DRC was performed using cumulative doses of ANGI (10⁻⁸ to 10⁻⁵ [M]) at 2-minute intervals between doses. After the DRC, vessels were washed out by replacing the contents of the organ bath well with fresh KREBS pH 7.4. After vessels returned to baseline, a bolus dose of U46619 2x10⁻⁵ [M] was added to each well to determine maximum vasoconstriction.

2.6.1 Rabbit drug stimulations

2.6.1.1 Vasoconstrictors

Thoracic aorta/ interlobar artery (Phenylephrine 6x10⁻⁷ [M], potassium physiological salt solution (KPSS 40 [mM])

Mesenteric artery (Cirazoline, 2x10⁻⁶ [M], KPSS 40 [mM])

2.6.1.1 Drug incubations

1. Inhibition of nitric oxide stimulated soluble guanylyl cyclase activity: 1H-[1,2,4] oxadiazolo [4,3-a] quinoxaline-1-one (ODQ) 10^{-5.0} [M] (thoracic aorta, interlobar and mesenteric arteries).

2. Inhibition of endothelial nitric oxide synthase: N(ω)-nitro-L-arginine methyl ester (L-NAME) $10^{-3.0}$ [M], (thoracic aorta, interlobar and mesenteric arteries).
3. Inhibition of cyclooxygenase (COX) 1 and 2 activities: Indomethacin $10^{-6.0}$ [M] (interlobar and mesenteric arteries)
4. Potassium (K^+) channel blockers, ILA/MA (interlobar and mesenteric arteries)
 - a. Inhibition of calcium (Ca^{2+}) activated K^+ channels (KCa): Charybdotoxin (CTX) $10^{-8.0}$ [M], Apamin (APA) $10^{-8.0}$ [M].
 - b. Inhibition of non-selective K^+ channels: Tetraethylammonium (TEA) $10^{-8.0}$ [M]
 - c. Inhibition of voltage-gated K^+ channels: 4-Aminopyridine (4-AP) $10^{-6.0}$ [M]

2.6.1.2 Vasodilators

1. BX (10^{-8} to 10^{-5} [M]) at 5-minute intervals).
2. LKB1 (10^{-8} to 10^{-5} [M]) at 5-minute intervals).
3. Dimethyl sulfoxide (DMSO) (10^{-8} to 10^{-5} [M]) at 5-minute intervals).

2.6.2 Mouse drug stimulations

2.6.2.1 Vasoconstrictors

Abdominal aorta: U46619 (thromboxane/prostaglandin agonist) at concentration 10^{-4} [M]

Iliac arteries: Angiotensin II (10^{-8} to 10^{-5} [M]) at 2-minute intervals).

2.6.2.2 Vasodilators

1. Acetylcholine (10^{-8} to 10^{-5} [M]) at 2-minute intervals).
2. Sodium Nitroprusside (10^{-8} to 10^{-5} [M]) at 2-minute intervals).

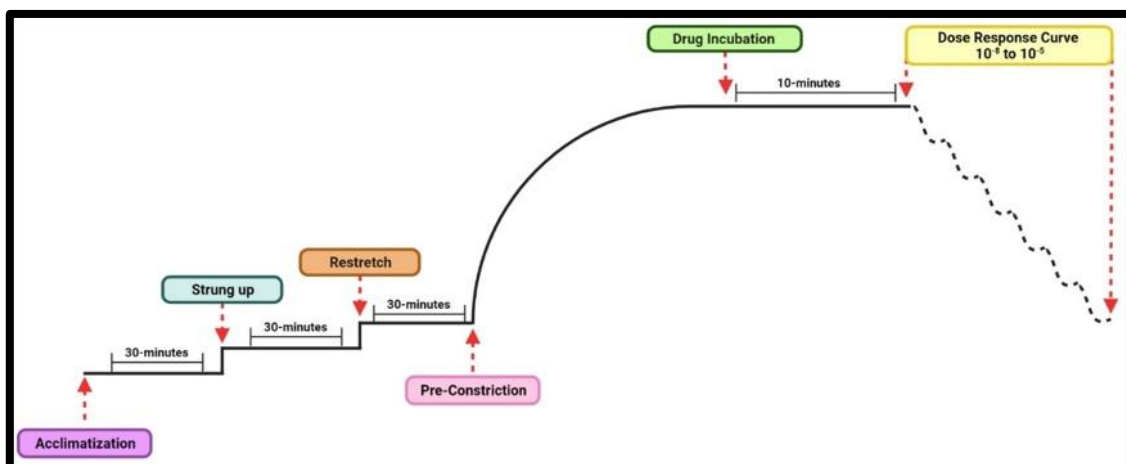


Figure 2.2. Schematic diagram of the isometric tension process to assess vascular relaxation. Created with BioRender.com

2.7 Tissue processing

Vessels and organs were fixed in 4% PFA, pH 7.4 for 24 hours, placed into cassettes (purchased from Sapphire Bioscience Cat#: 14708) in 1xPBS, pH 7.3, and then processed at Western Centre for Health and Research (WCHRE) for paraffin tissue processing using the (Thermo Scientific Spin Tissue Processor Microm STP, 120). Tissues were placed into a series of buckets for 1 hour per bucket (70% ethanol (EtOH), 80% EtOH, 90% EtOH, 3x 100% EtOH, 2x xylene, and 2x liquid paraffin). Tissues were then removed for embedment. Mouse kidneys were halved transversely and embedded coronally in paraffin. Paraffin ribbons were cut using the manually operated rotary microtome instrument (MicroTec, CUT 5060) at 5 μ M thicknesses. Ribbons were placed into a gelatin-containing water bath (45 °C) and enabled to return to their original sizing before being placed onto microscope slides and incubated to dry for a minimum of 4 days at 37 °C.

2.8 Histology

2.8.1 Immunohistochemistry

Immunohistochemical staining was performed using the Vector ImmPRESS™ Anti-Rabbit Ig Reagent, made in goat, 50 mL, (MP-7451) (purchased from ABACUS DX, Queensland, Australia). Slides were then deparaffinised and rehydrated using xylene to ethanol gradient. Slides were placed in xylene (10 mins), xylene (10 mins), 100% EtOH (20 dips), 100% EtOH (20 dips), 90% EtOH (20 dips), ddH₂O (20 dips), 10 [mM] tromethamine TRIS pH7.4 (20 dips) then left for 5 mins. 1% goat serum was added to each slide for 30 minutes to block non-specific binding. Slides were incubated overnight with a primary antibody; please refer to table 2.2 for details on the antibodies used. After incubation with the primary antibody, tissues were placed in TRIS pH7.4 solution for 5 minutes before incubating for 1 hour with the rabbit IgG secondary antibody. Slides were then placed in TRIS pH7.4 for 5 minutes before being incubated for 2 minutes with 3,3'-diaminobenzidine (DAB) from the DAB Substrate Kit: Purchased from BD Pharmingen, Cat#: 550880. Excess DAB was removed with double distilled water (ddH₂O), slides incubated with hematoxylin for 1.5 minutes, washed off with double distilled water (ddH₂O), and placed in Scott's tap reagent to gently blue the hematoxylin. Slides were then dehydrated using ethanol to xylene gradient 90% EtOH (20 dips), 100% EtOH (20 dips), 100% EtOH (20 dips), xylene (20 dips), xylene (20 dips), xylene (20 dips then left for 5 mins). A small amount of dibutyl phthalate polystyrene xylene (DPX) mountant was placed in the centre of the slide, followed by a cover slip.

Table 2.2. Rabbit antibodies: Antibodies used for CDDP-induced AKI model pilot study and BX pre-treated CDDP pilot study. Provided are details on the host, clonality, supplier, and catalogue numbers for each antibody used, in addition to the dilution concentrations of antibodies for the CDDP and BX pilot studies.

Antibody	Clonality	Supplier	Antibody Cat#:	CDDP-induced AKI pilot study			BX in CDDP induce AKI		
				Tubules	Glomeruli	Interlobar	Tubules	Glomeruli	Interlobar
ICAM	Monoclonal	Abcam	ab179707	1:3000	1:3000	1:3000	1:3000	1:3000	1:3000
VCAM	Monoclonal	Abcam	ab134047	1:400	1:200	1:200	1:400	1:100	1:100
E-Selectin	Polyclonal	ThermoFisher Scientific	PA596091	1:200	1:200	1:200	1:1000	1:100	1:100
TNF- α	Polyclonal	GeneTex	GTX110520	1:200	-	-	-	-	-
TIM-1/KIM-1	Polyclonal	Abcam	ab47635	1:400	-	-	1:400	1:100	1:100
GRP78	Polyclonal	GeneTex	GTX127934	1:1000	-	-	1:1000	1:500	1:500

Abbreviations: CDDP, Cisplatin; ICAM-1, Intercellular adhesion molecule 1; VCAM-1, Vascular cell adhesion molecule 1; TNF- α , Tumour Necrosis Factor-alpha; TIM-1/KIM-1, T cell immunoglobulin mucin domain-1/Kidney Injury Molecule-1; GRP78, Glucose-regulating protein 78.

To identify the concentration of antibodies used above each antibody in each section underwent a lengthy optimisation process using tissues from the CIAKI pilot study to isolate the specific concentrations required for each antibody. This process is completed to avoid overstaining or under-staining sections. Slides were sectioned off using a wax pen and serially diluted from 1:100-1:500 concentrations. If slides were overstained, this was repeated for 1:600-1:1000 concentrations. Furthermore, if overstaining was still observed at 1:1000, the dilution factor was increased to evaluate positive-background staining at concentrations, 1:1000 to 1:5000. This gave a range of concentrations, and the best was chosen. All antibodies were incubated overnight for a minimum of 12 hours.

2.8.2 PAS stain

Slides were deparaffinised and rehydrated as described in the immunohistochemistry protocol above. PAS stain was performed using Periodic Acid-Schiff's (PAS) Staining system (395B-1KT), (purchased from Sigma-Aldrich). Slides were incubated with Periodic acid for 5 minutes, followed by 20 dips in fresh ddH₂O, then set in Schiff's reagent for 15 minutes. Following washing in fresh ddH₂O, slides were incubated for

1.5 minutes in hematoxylin and rinsed again in fresh ddH₂O. Slides were then placed in SCOTT'S tap water for 2 minutes until blue. Tissues were dehydrated, and a coverslip was placed on top.

2.9 Semi-Quantification of immunohistochemistry slides

Images were taken of slides using Leica acquisition software (Leica DFC 450F, Leica Germany). Tubular images were taken at 40x magnification, and glomeruli/interlobar arteries were imaged at 100x magnification under oil immersion. For tubules, the circle tool was used to eliminate glomeruli from quantification then the line tool was used to quantify the remaining area of the image (figure 2.3). The circular tool was used to quantify the glomeruli (figure 2.4). The size of the circular tool remained consistent for the entire analysis of the slide. For interlobar arteries, each layer was traced individually. The endothelium was traced using the ribbon tool, and the media and adventitial layers were traced using the outline tool, (figure 2.5). (MCID, Interfocus UK software Micro Computer Imaging Device 6.0) The software detects colour intensity and proportional area for each picture taken. These values were used in the formula $\left(\frac{1}{\text{Colour Intensity}}\right) \times \text{Proportional area}$ to generate data. A minimum of ten kidney images were taken, and the values were averaged. These values were then normalised to control, and GraphPad Prism was used for analysis.

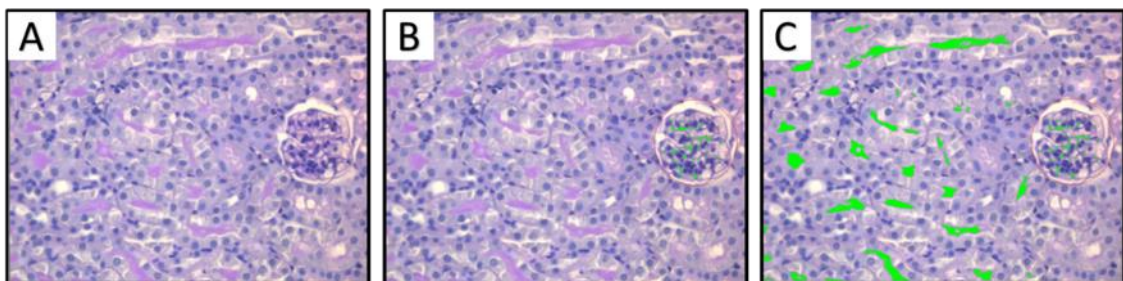


Figure 2.3. Tubule Analysis method using MCID. A. Image to be traced, B. Glomeruli blocked out of the tubular analysis, and C. Positive PAS staining indicated by green colour.

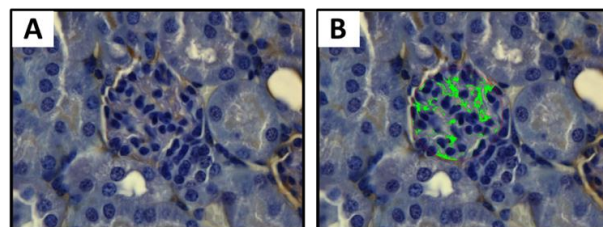


Figure 2.4. Immunohistochemical analysis using MCID analysis of DAB-stained Glomeruli. A. 100x magnified image of DAB-stained Glomeruli, B. Circular tool used to measure the colour intensity and proportional area indicated by green scanning displayed by MCID software.

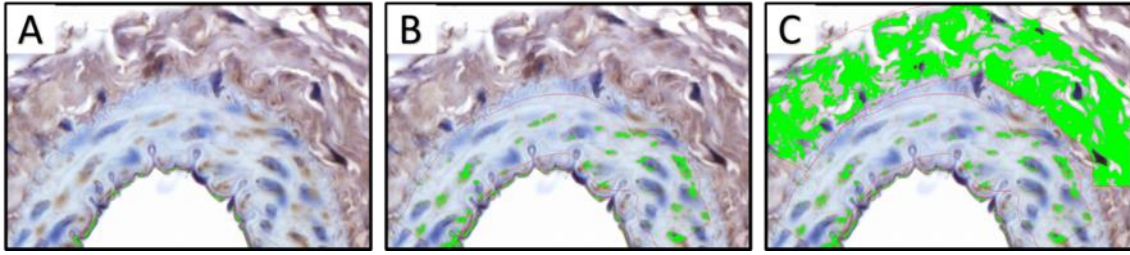


Figure 2.5. MCID Analysis of Interlobar arteries. The green colour represents software detection of DAB stain. A. Endothelium tracing B. Media tracing C. Adventitia Tracing.

2.10 SEM metal composition analysis

The protocol for SEM was adapted from published literature [40, 41]. Briefly, the mouse kidney was sliced into 1 mm sections and placed into McDowell and Trump fixative (please refer to section 2.13.2 General chemicals for McDowell and Trump fixative formulation.) at room temperature for 2 hours. Tissues were thoroughly washed with fresh phosphate buffer (PB) pH 7.4, then post-fixed in 1% osmium tetroxide for 90 minutes. Samples were then rinsed twice for 5-minutes in fresh ddH₂O, then dehydrated in an ethanol gradient: 35% EtOH for 15-minutes, 50% EtOH for 15-minutes, 75% EtOH for 15-minutes, twice in 95% EtOH for 15-minutes, three times in 100% EtOH for 20-minutes. Following dehydration, samples were immersed in hexamethyldisilazane (HMDS) twice for 10 minutes. HMDS was decanted from vials, and the sample was placed in a desiccator to air dry at room temperature overnight. Samples were then mounted on an SEM stamp, sputter coated twice using the (Mini Sputter Coater: SC760), then placed inside the instrument (ThermoScientific Phenom XL G2 Desktop) SEM for analysis.

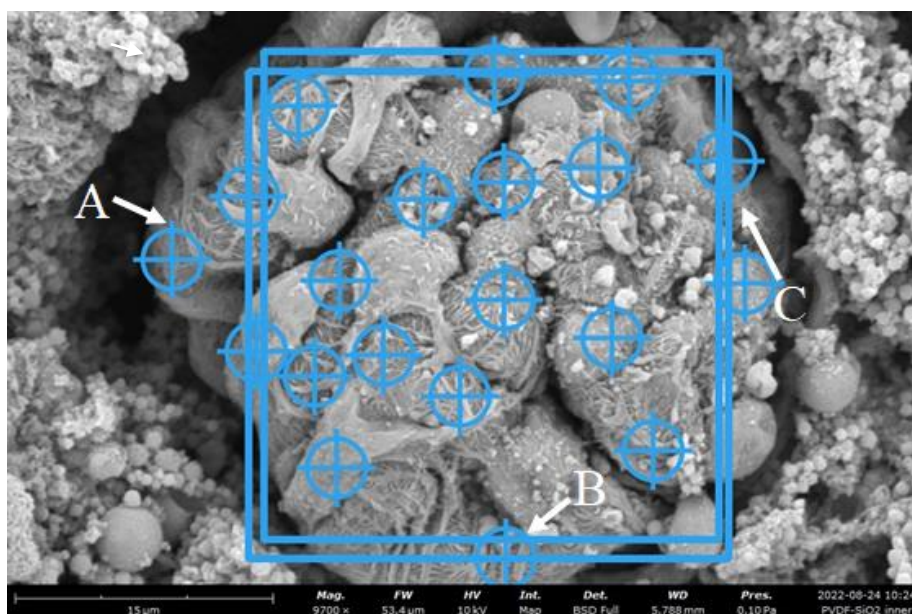


Figure 2.6. Pt analysis area of glomeruli. Spot areas (Circles, A.), Pt Content area (Blue square B), Pt Mapped area (Blue square C). Glomeruli were analysed for Platinum (Pt) content. Twenty spot areas were taken of each glomerulus, and ten glomeruli were analysed per sample. A total content Pt analysis and a Pt mapping of the same area were performed, as shown in (figure 2.6).

2.11 Nephrotoxicity real-time (RT²) profiler PCR.

PCR analysis was performed using the (Qiagen RT² Profiler PCR Array Mouse Nephrotoxicity, Gene globe ID-PAMM-094Z), and all experiments were completed per the manufacturer's protocol.

2.11.1 RNA isolation protocol

Kidneys from CDDP and BX + CDDP treated mice were harvested and snap-frozen in liquid nitrogen. RNA purification was performed using the (Qiagen, RNeasy Mini Kit) (50) (Cat#: 74104). Kidneys were cut into 30 mg sections, placed into a 2ml collection tube containing 1 g of 1.0 mm diameter Zirconia/Silica beads, (purchased from BioSpec Cat#: 110791102), and immediately placed on dry ice to ensure tissue remained frozen. RNA lysis buffer was added (600 μ l) to each tube, and sample containing tubes were homogenised at 10-second intervals until lysate was produced using the (savant bio 101 fast prep fp120 cell disruption system). Tubes were centrifuged at 10,000 revolutions per minute (RPM) for 4 minutes using the (Sigma 3-30KS high-speed centrifuge). The supernatant was pipetted and added to a tube containing an equal 75% molecular-grade ethanol volume. 700 μ l was added to an RNeasy spin column. The column was spun down at 10,000 RPM for 15 seconds, and the flow through was discarded. RNA wash buffer (700 μ l) was added to the spin column and centrifuges for 15 seconds at 10,000 RPM, and the flow through was discarded. RNA precipitating elution buffer (500 μ l) was added to the spin column and spun at 10,000 RPM for 15 seconds, and the flow through was discarded. This was repeated and the centrifugation time was increased to 2 minutes. Finally, 20 μ l of RNase-free water was added to the spin column and centrifuged for 1 minute at 10,000 RPM to elute the RNA sample. The RNA concentration was measured (Thermo Scientific™ NanoDrop™ 2,000/2,000c Spectrophotometer) and standardised.

2.11.2 cDNA synthesis protocol

RNA samples were converted to complementary deoxyribonucleic acid (cDNA) using the (Qiagen RT² First Strand Kit (12)) (Cat#: 330401). RNA was then standardised to the lowest RNA concentration. RNA stock, GE2 buffer and RNase-free water (RFW) were combined and briefly centrifuged to create the genomic deoxyribonucleic acid (DNA) elimination mix. This mix was then incubated for 5 minutes at 42 °C using the (Bio-Rad MyCycler thermal cycler) and immediately placed on ice. The reverse-transcription mixture was prepared, containing BC3 buffer, Control P2, RE3 Reverse Transcriptase Mix, and RFW. The Reverse Transcriptase Mix was added to the genomic DNA elimination mix and returned to

the thermocycler. Samples were incubated at 42 °C for 15 minutes and then immediately incubated at 95 °C for 5 minutes to stop the reaction. The concentrations of cDNA were measured using the NanoDrop standardised and immediately placed at -80 °C in preparation for PCR arrays.

2.11.3 RT² profiler PCR arrays protocol

The concentration of cDNA samples was standardised to 29.64 µg (The lowest concentration of cDNA obtained from the samples) To make the cDNA synthesis reaction 19 µl of cDNA was added to 91 µl of RFW for a final volume of 110 µl. In an RNase-free tube, 500 µl of SYBR Green Master mix, 398 µl of RFW, and 102 µl of cDNA synthesis reaction were combined. This mix was centrifuged briefly before 10 µl of the sample was added to each well of the RT² profiler PCR Array plate (Cat#: PAMM-094ZA-6). Optical thin-wall 8-cap strips were placed on the plate and centrifuged for 1 minute at 1,000 RPM at room temperature before being placed into the Eppendorf Master cycler realplex². The PCR program used is described in (figure 2.7).

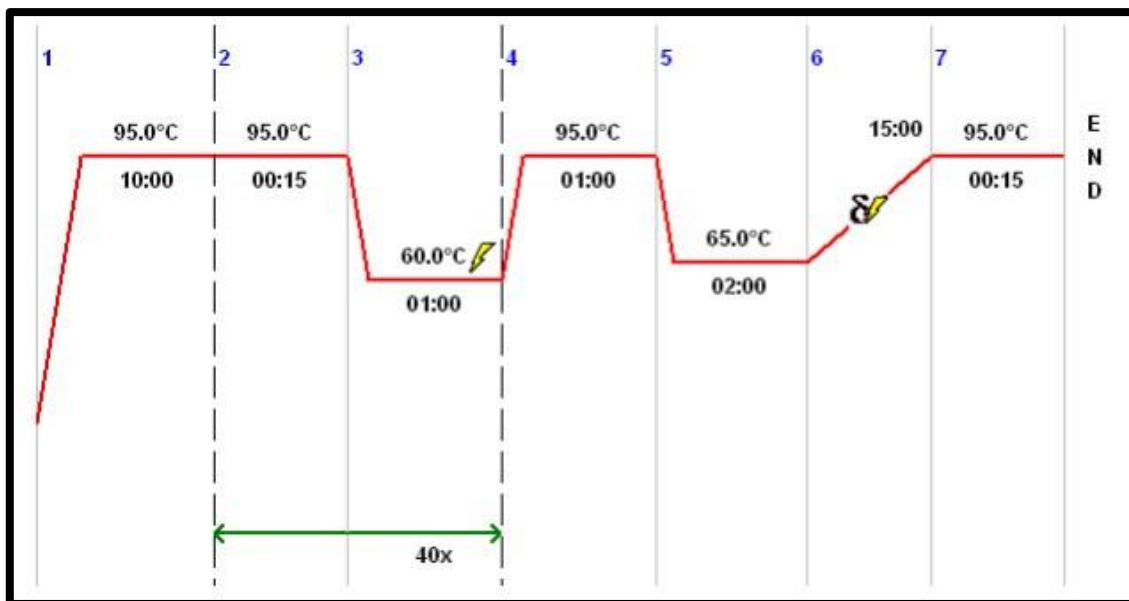


Figure 2.7. Mouse Nephrotoxicity RT² profiler PCR Array Program. The manufacturer provided a specific program illustrated above for use with their kits.

2.12 Statistical analysis

2.12.1 ANOVA

A two-way analysis of variance (ANOVA) was used to analyse isometric tension studies for rabbits and mice, followed by a post hoc test. A one-way ANOVA followed by a post hoc test was used for histology and area under the curve. Analyses were performed using the multiple comparisons of Dunnett's (when comparing data to its respective control), students t-test (for comparison of 2 groups) and Sidaks (for multiple

comparisons) as a post hoc test in their specific ANOVAs. Statistical significance is taken at ($p < 0.05$).

2.12.2 Cohen's *d*

Additionally, a *Cohen's d* test was performed to identify effect size where statistical significance was lacking. The formula used to calculate *Cohen's d* was $d = \frac{(\text{Mean}_1 - \text{Mean}_2)}{SD_{\text{pooled}}}$. To calculate the pooled standard deviation (SD), a formula specific for

use with unequal sample size was used, $SD_{\text{pooled}} = \sqrt{\frac{(n_1 - 1)S_1^2 + (n_2 - 1)S_2^2}{n_1 + n_2 - 2}}$. *Cohen's d* calculates effect size, where • $d = 0.2 - 0.5$ (small effect), •• $d = 0.5 - 0.8$ (medium effect), and ••• $d \geq 0.8$ (large effect).

2.13 Solutions

2.13.1 Drug formulations

2.13.1.1 Rabbit

- **BX-912:** purchased from Sigma Aldrich Cat#: 702674-56-4 was dissolved in DMSO, stored as a 10^{-2} M stock solution, and serially diluted in ddH₂O to make 10^{-3} , 10^{-4} , and 10^{-5} [M] doses.
- **LKB-1** purchased from APEX BIO, Cat#: A3556 (Dissolved in DMSO, formulated as a 10^{-2} [M] stock solution and serially diluted in ddH₂O to make 10^{-3} , 10^{-4} , and 10^{-5} [M] doses.
- **Dimethyl Sulfoxide (DMSO)** was purchased from Sigma Aldrich Cat#: 67-68-5 and was used as the solvent for the LKB1 and BX DRC stock concentrations. (DMSO was used as 10^{-2} [M], then serially diluted in ddH₂O to make 10^{-3} , 10^{-4} , and 10^{-5} [M], which was used as a control group.
- **Phenylephrine:** was purchased from Sigma Aldrich Cat#: 59-42-7 (selective α_1 -adrenergic receptor agonist used at 3×10^{-7} [M]).
- **Cirazoline (Ciraz) hydrochloride** Cat#: 4600-13-3 (α_1 A-adrenergic receptor agonist, partial α_1 B/ α_1 D-adrenergic receptor agonist and non-selective α_2 -adrenergic receptor): 2×10^{-6} [M].
- **1H-(1,2,4) oxadiazolo (4,3-a) quinoxalin-1-one (ODQ):** was purchased from Cayman Chemical (MI, USA), Cat#: 41443281, soluble guanylyl cyclase inhibitor.
- **L-N^G-nitro arginine methyl ester (L-NAME):** was purchased from Sigma Aldrich, Cat#: 51298-62-5, NO production inhibitor.

- **4-Aminopyridine (4-AP):** was purchased from Cayman Chemical, Cat#: 504245 and formulated as a [$10^{-6.0}$ M] stock solution.
- **Apamin (APA):** was purchased from Sigma Aldrich, Cat#: 24345-16-2 and formulated as a [$10^{-8.0}$ M] stock solution.
- **Charybdotoxin (CTX):** was purchased from Sigma Aldrich, Cat#: 95751-30-7 and formulated as a [$10^{-8.0}$ M] stock solution.
- **Indomethacin (INDO):** was purchased from Sigma Aldrich, Cat#: 53861 and was formulated as a [$10^{-6.0}$ M] stock solution.
- **Tetraethylammonium (TEA):** was purchased from Sigma Aldrich, Cat#:56348 and formulated as a [$10^{-8.0}$ M] stock solution.

2.13.1.2 *Mouse*

- **Heparin:** Purchased from Abcam Cat#: ab270804. Heparin salt (50 mg) was dissolved in 1 mL of 0.9% saline.
- **Cisplatin:** Purchased from Sigma Aldrich Cat#: PHR1624, formulated in a 1 mg/ml solution in 0.9% saline.
- **BX-912:** 9:1 PBS: Dimethylformamide (DMF). BX powder was dissolved in DMF to a concentration of 26.519 [mM] and further diluted into PBS for the desired dose.
- **Human Angiotensin II:** Cat#: 51480, was purchased from Mimitopes (VIC, Australia). A 10^{-2} [M]. stock solution. The stock was then serially diluted to produce vials of 10^{-3} , 10^{-4} , and 10^{-5} [M] for pharmacological studies.
- **9,11-Dideoxy-11 α ,9 α -epoxymethanoprostaglandin F_{2a} (U46619) (Thromboxane receptor agonist):** was purchased from MERK Cat#: D8174 and 1 μ L of 10 mg/ml were added to 270 μ L ddH₂O to produce a stock concentration. 1 μ L of stock concentration was added to each organ bath well, resulting in a bath concentration of 10^{-4} [M].
- **Acetylcholine Chloride (ACH),** Purchased from MERK Cat#: A6625: A 10^{-2} [M]. stock solution. The stock was then serially diluted to produce vials of 10^{-3} , 10^{-4} , and 10^{-5} [M] for pharmacological studies.
- **Sodium Nitroprusside (SNP),** Purchased from MERK Cat#: 13755-38-9: A 10^{-2} [M] stock solution. Then serial dilutions were formulated for 10^{-3} , 10^{-4} , and 10^{-5} [M].

2.14 General chemicals

- **Phosphate Buffered Saline (PBS) pH 7.4:** The following was dissolved in 800mL ddH₂O: NaCl (80 g), KCL (2.0 g), Na₂HPO₄ (14.4 g), KH₂PO₄ (2.4 g). following this, the pH was adjusted to 7.4 and the volume to 1L. For 1xPBS, 10% of 10xPBS was added to 90% ddH₂O of the total volume.
- **Phosphate Buffer (PB):** 3.4 g of NaH₂PO₄·7H₂O and 9.1 g of Na₂HPO₄ dissolved in 1 L of ddH₂O, pH 7.4.
- **Krebs-Henseleit buffer solution (KREBS):** NaCl (27.3 g), KCL (1.4 g), MgSO₄·7H₂O (1.2 g), KH₂PO₄ (0.65 g), NaHCO₃ (8.4 g), Glucose (7.5 g) mixed with 4L of ddH₂O. The solution was mixed using a magnetic flea until dissolved, then bubbled with carbogen for 30 mins; then 10 ml of 1[M] CaCl₂ was added, and pH adjusted to 7.4.
- **Paraformaldehyde (PFA)** was Purchased from Sigma Aldrich Cat#: 30525-89-4: 50 ml ddH₂O and 10 drops 1 [M] NaOH was added to 4 g of PFA powder and heated to 55 °C. 10ml of 10x PBS and 30ml ddH₂O was added. HCl was then added to achieve a pH of 7.4. Finally, ddH₂O was added to reach a final volume of 100 ml.
- **KPSS (40 mM):** KCL (1.5 g), MgSO₄·7H₂O (0.2 g), KH₂PO₄ (0.1 g), NaHCO₃ (1.1 g), and Glucose (0.9 g) dissolved in 500 ml ddH₂O. Before use, 50 ml of KPSS at 37 °C was carbogenated for 10 minutes, and 125 µL of 1[M] CaCl₂ was added immediately before use.
- **TRIS HCL:**
 - **1 M:** 32 g TRIS HCL into 200 ml ddH₂O
 - **10 mM:** 10 ml of 1 [M] TRIS HCL in 1L ddH₂O
- **SCOTTS TAP water:** MgSO₄ (30 g) and NaHCO₃ (2 g) added to 3 L ddH₂O
- **Calcium Chloride (CaCl₂)** was purchased from Sigma Aldrich Cat#: 10043-52-4 in powdered form and dissolved in ddH₂O to make a 1 [M] solution.
- **McDowell and Trump Fixative:** The following was added to a constantly stirred 86mls of ddH₂O: 10 ml of 37-40% formaldehyde, 4 ml of 25 per cent glutaraldehyde (biological grade), 1.16 g NaH₂PO₄ ·H₂O, 0.27 g NaOH. pH checked when complete (pH should be 7.2-7.4)
- **Osmium Tetroxide** was purchased from Sigma Aldrich Cat#: 20816-12-0: 1% solution made in fresh phosphate buffer (100 mg in 10 ml PB pH 7.4)

- **Hexamethyldisilazane (HMDS)** was purchased from Sigma Aldrich Cat#: 213-668-5.

Chapter 3: LKB1, identification as a novel vasodilator

3.1 Abstract

Background: Cisplatin (CDDP)⁶ is a potent platinum based-anticancer agent whose use is often limited by its dose-limiting factor nephrotoxicity, resulting from altered renal hemodynamics, namely afferent arteriole vasoconstriction, which quickly progresses and manifests as acute kidney injury, defined by a sudden reduction in glomerular filtration rate (GFR)⁷. Therefore, we hypothesise that increased vasodilation will inhibit renal pathologies. The inhibition of the proviral integration site for Moloney murine leukemia virus-1 (PIM1) kinase by LKB1 could prevent afferent arteriole vasoconstriction and therefore reduce nephrotoxicity and the vascular pathologies resulting in reduced GFR associated with cisplatin-induced acute kidney injury (CIAKI)⁸. **Methods:** To determine the vasodilatory potential of LKB1 thoracic aorta, interlobar and mesenteric arteries were harvested from male New Zealand White rabbits and processed for isometric tension analysis. Vessels were subjected to a dose-response curve (DRC) of LKB1 from doses (10^{-8} to 10^{-5} [M]). Additionally, a mechanistic study was performed to isolate the specific mechanism of action of LKB1. Analysis of (*Cohen's d*) was performed to determine effect size. **Results:** LKB1 dilated arteries, both interlobar and mesenteric arteries, had increased relaxation compared to thoracic aorta, ($p < 0.0001$), and mesenteric arteries had increased relaxation compared to the interlobar arteries, ($p < 0.0001$). Mechanical denudation and pre-treatment with the NO synthase inhibitor L-N^G-nitro arginine methyl ester (L-NAME) increased relaxation in thoracic aorta ($p < 0.01$ and $d = 0.41$); however, decreased relaxation in the mesenteric arteries ($p < 0.01$ and $p < 0.01$), respectively. Non-selective K⁺ channel inhibition via 40mM KPSS pH 7.4 pre-constriction significantly reduced LKB1-induced relaxation in mesenteric arteries, ($p < 0.0001$); however, this was not observed in thoracic aorta or interlobar arteries. A cumulative DRC to a non-selective pan-PIM kinase inhibitor did not affect vasorelaxation in thoracic aorta, interlobar or mesenteric arteries. **Discussion:** Results of this study demonstrated that LKB1-induced vasodilation occurred in smaller arteries, including mesenteric arteries and interlobar arteries but not in the larger thoracic aorta. It is unclear why this occurred and is beyond the scope of the study; however, it justifies its continual use in diseases associated with microvascular

⁶ CDDP, cisplatin

⁷ GFR, glomerular filtration rate

⁸ CIAKI, cisplatin-induced acute kidney injury

vasoconstriction, such as CIAKI. In addition to eNOS-dependent vasodilation, LKB1-induced vasodilation is mediated partially by potassium (K^+) channels, suggesting that LKB1-induced vasodilation is partly a result of vascular smooth muscle cell (VSMC) hyperpolarisation. Although some mechanistic discoveries have been made, further studies are required to understand how LKB1 stimulates these pathways and whether any crosstalk occurs between mechanisms that could explain these results. **Conclusion:** The results obtained in this study demonstrate that LKB1 is a vasodilator and could prove helpful in treating vascular disorders.

3.2 Introduction

CDDP is a highly potent and effective chemotherapy used to treat a variety of malignancies, including those of the breast [42], cervical [42], oesophageal [43], bladder [44], small cell lung [45], testicular [46] soft tissue and blood cancers [47]. Although the anticancer mechanism of CDDP is incompletely understood, it is generally accepted that CDDP-induced deoxyribonucleic acid (DNA) damage results in a variety of cellular processes, including cell replication arrest, transcriptional inhibition, cell cycle arrest and apoptosis [48]. Although CDDP results in a broad array of systemic toxicities [49-56], its clinical use is restricted due to the severity, incidence and potentially fatal outcomes of its dose-limiting side effect, nephrotoxicity [52, 57-63].

Although CIAKI is considered a reversible condition, increased risk of mortality [64, 65] and chronic kidney disease [64, 66] are associated with recurrent episodes. CDDP-induced vasculature damage resulting in impaired renal blood flow caused by afferent arteriole vasoconstriction is reported to occur within as little as three hours post-CDDP infusion, which precedes the clinical reduction in GFR used as the diagnostic factor for CIAKI manifestation [67, 68]. Endothelial dysfunction and vascular injury are two key pathologies associated with the long-term effects of CDDP-based chemotherapy in testicular cancer survivors. These comorbidities may contribute to developing other severe and potentially fatal complications, including cardiovascular disease (CVD) and atherosclerosis [8, 69]. Although research targeting vascular function in pre-clinical models of CIAKI is limited, some studies have demonstrated that reduced renal blood flow and increased vascular resistance are associated with CDDP treatment and contribute to CIAKI development [70-72]. Reduced GFR is stimulated by reduced renal blood flow due to afferent arteriole vasoconstriction and increased vascular resistance caused by endothelial dysfunction [73] and is the diagnostic factor for CIAKI in

patients. Increasing renal blood flow and decreasing vascular resistance through enhanced vasodilation [74] is a theoretically beneficial strategy to mitigate CIAKI.

The proviral insertion in murine (PIM) family of enzymes function as oncogenes and plays a regulatory role in cell survival, proliferation, differentiation and apoptosis [75, 76]. The PIM family comprises three isoforms, PIM1, PIM2 and PIM3, which although display a similar homolog, expression is cancer specific. Overexpression of PIM1 and PIM2 is associated with haematological cancers and some solid tumours, whilst PIM3 overexpression is mainly linked to solid tumours of the gastrointestinal system [75].

Proviral insertion in murine 1 (PIM1) is a proto-oncogene enzyme encoded by the PIM1 gene whose expression is low in healthy cells [77]. It has multiple roles in disease [78], including tumorigenesis [79], inflammation [80] and cardioprotection [81]. PIM1 kinase inhibition has been used to treat various conditions, including cancer [82], pulmonary arterial hypertension (PAH)⁹ [83] and lupus nephritis [84]. LKB1 is a novel selective PIM1 kinase inhibitor that has yet to be evaluated as a treatment for disease.

The role of PIM1 kinase inhibition in the vasculature, particularly in vascular function models, is limited. However, some studies have provided mechanistic insight to infer the role of PIM1 in vasculature. In patients with PAH, the circulating levels of PIM1 are higher than those without PAH, highlighting it as a useful PAH biomarker [77]. It has been shown that PIM1 knockout (KO) mice are resistant to the development of PAH [85]. Dehydroepiandrosterone has also been shown to prevent PAH, mediated through Src/signal transducer and activator of transcription 3 inhibition and subsequent PIM1 downregulation [86]. These studies highlight a clear role for PIM1 kinase in regulating pulmonary smooth muscle cell activity, leading us to hypothesise that LKB1, through PIM1 kinase inhibition, could be a novel vasodilator.

This study aimed to understand the vasodilative qualities of an LKB1 inhibitor in different vascular beds, which will aid in the clinical understanding of its adverse effects. Furthermore, considering that humans with cancer might also have heart disease, two animal models will be used in this study. If it is also shown that the LKB1 inhibitor targets resistance arteries, then this could be used in a future CIAKI model. Various approaches were used to investigate the vasodilatory pathway(s) involved in LKB1-induced vasodilation. To determine endothelial-dependent vasodilation, vessels were mechanically denuded prior to a cumulative DRC to LKB1. Potassium physiological salt solution (40 mM KPSS) constricted vessels were used to non-

⁹ PAH, pulmonary arterial hypertension

selectively inhibit K⁺ channels. Inhibition of nitric oxide (NO) synthase by L-NAME and soluble guanylyl cyclase (sGC) induced vasodilation by 1H-(1,2,4) oxadiazolo (4,3-a) quinoxalin-1-one (ODQ) were used to determine endothelium and VSMC dependent NO stimulated vasodilation. This study identifies PIM1 kinase inhibitor LKB1 as a vasodilator; it highlights its potential to promote afferent arteriole vasodilation, justifying the use of LKB1 as a potential treatment for the prevention of CIAKI.

3.3 Methods

3.3.1 Materials

KREBS pH 7.4 and 40mM KPSS (for instructions on formulation, please refer to Chapter 2, section 2.14 General chemicals. For purchasing information on LKB1, dimethyl sulfoxide (DMSO), ODQ and L-NAME, please refer to Chapter 2, section 2.13.1 subsection 2.13.1.1 Rabbit drug formulations.

3.3.2 Animals

For detailed experimental design, refer to Chapter 2, section 2.1 Animals/experimental regimens, subsection 2.1.1 Healthy and atherogenic rabbit model (AEC) project 17/013.

3.3.2.1 Anaesthetisation

For Anaesthetization protocol, refer to Chapter 2, section 2.3 Anaesthesia and culling, subsection 2.3.1 Rabbit.

3.3.2.2 Dissection

Refer to Chapter 2, section 2.4 Dissection, subsection 2.4.1 Rabbit dissection.

3.4 Isometric tension

For Isometric tension, refer to Chapter 2, section 2.6 Isometric tension. The following variations have been applied to the general method. The only drug incubations relevant to this chapter specified from chapter 2, section 2.6, subsection 2.6.1 Rabbit drug incubations are 1. ODQ 10^{-5.0} [M] and 2. L-NAME 10^{-3.0} [M]. The vasodilators used in this chapter for DRC are 2. LKB1 (10⁻⁸ to 10⁻⁵ [M]) at 5-minute intervals and serially diluted DMSO (10⁻⁸ to 10⁻⁵ [M]) at 5-minute intervals.

3.5 Data/Statistical Analysis

Statistical analyses are detailed in Chapter 2: General methods section 2.12. For analysis of variance (ANOVA) details, to section 2.12.1 and for information on *Cohen's d* analysis, please refer to section 2.12.2. For *Cohen's d* analysis of effect size, values are compared to LKB1 CD (control diet group). Positive *d* values indicate a reduction compared to CDDP, and negative values represent an increase compared to CDDP.

3.6 Results

3.6.1 *LKB1 induces vasodilation in a vessel-specific manner.*

To determine the vasodilatory response of LKB1, thoracic aorta, interlobar and mesenteric arteries were assessed for vascular function to cumulative doses of LKB1 (10^{-8} to 10^{-5} [M]). Vasodilation in interlobar and mesenteric arteries was significantly increased compared to thoracic aorta at multiple doses, as shown in (figure 3.1). Relaxation in interlobar arteries was increased compared to thoracic aorta at LKB1 doses 10^{-6} , $10^{-5.5}$ and 10^{-5} [M] (figure 3.1A). These same results were observed in mesenteric arteries, demonstrating that vasodilation was enhanced compared to thoracic aorta at doses 10^{-6} , $10^{-5.5}$ and 10^{-5} [M] (figure 3.1B). Surprisingly, a significant difference was observed between interlobar and mesenteric arteries, (figure 3.1C). Increased relaxation was observed in mesenteric arteries compared to interlobar arteries at LKB1 doses, $10^{-5.5}$ and 10^{-5} [M]. For statistically significant p values and effect size (*Cohen's d*) values obtained for each dose, please refer to table 3.1. Results obtained by area under the curve (AUC) analysis confirm results obtained in the DRC, (figure 3.1), although interlobar arteries had no significant difference in AUC compared to thoracic aorta. AUC of mesenteric arteries showed an increase compared to thoracic aorta (72.6 ± 8.0 vs 40.3 ± 10.4 ; $p < 0.05$) and had a small effect (*Cohen's d*) compared to interlobar arteries AUC (72.6 ± 8.02 vs 44.3 ± 10.9 ; $p = \text{ns}$, $d = -0.2$).

Vessel specificity

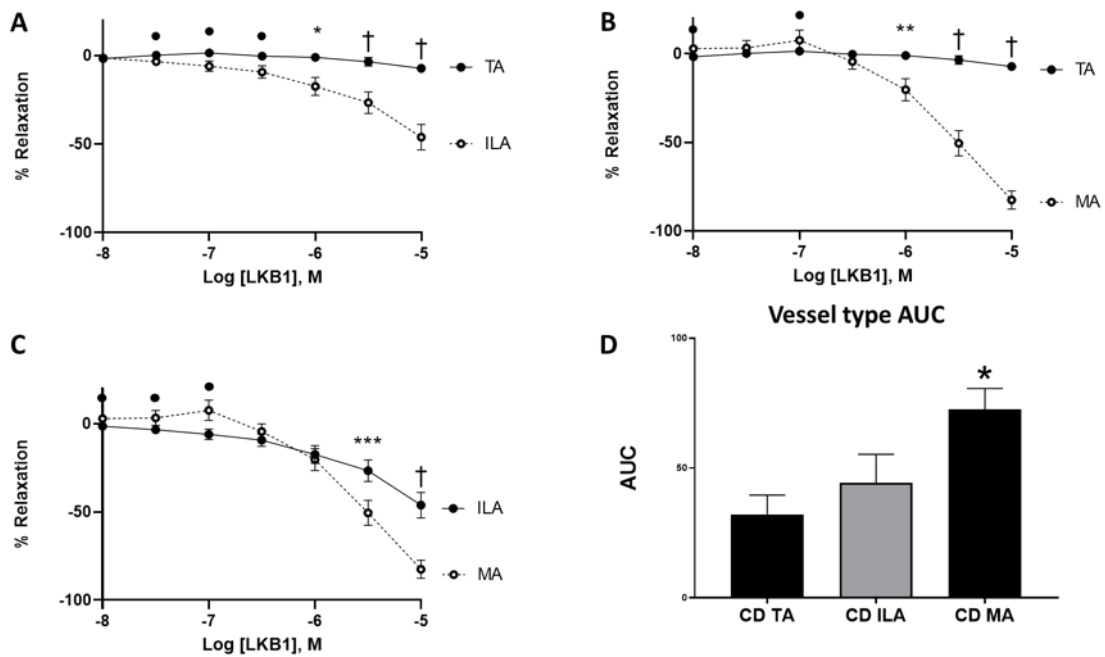


Figure 3.1. LKB1-induced vasodilation is vessel-specific, (n=4-13). Vessels were pre-constricted and exposed to cumulative doses of LKB1 (10^{-8} to 10^{-5} [M]) and represented as % vasodilation. **A.** TA vs. ILA, **B.** TA vs. MA, **C.** ILA vs. MA, and **D.** AUC of the three vessel types used in the study. All data is represented as Mean \pm SEM, and statistical analysis was performed using a one-way ANOVA followed by a Dunnett's post hoc test. * ($p < 0.05$), ** ($p < 0.01$), *** ($p < 0.001$), \dagger ($p < 0.0001$). Effect size (d) and Cohen's d values are taken as $\bullet d = 0.2-0.5$ (small effect), $\bullet\bullet d = 0.5-0.8$ (medium effect), and $\bullet\bullet\bullet d \geq 0.8$ (large effect). **Abbreviations:** AUC, area under the curve; CD, control diet; ILA, interlobar artery; MA, mesenteric artery; [M], Molar; n, sample size; TA, thoracic aorta.

Table 3.1. Statistical significance and effect (Cohen's *d*) size values from pre-incubated thoracic aorta, interlobar arteries and mesenteric arteries of CD rabbits following a cumulative DRC to LKB1.

LKB1 [M]	TA vs. ILA	TA vs. MA	ILA vs. MA
10^{-8}	p=ns	$d= -0.33$	$d= -0.28$
$10^{-7.5}$	$d= 0.25$	p=ns	$d= -0.24$
10^{-7}	$d= 0.40$	$d=-0.26$	$d= -0.34$
$10^{-6.5}$	$d= 0.36$	p=ns	p=ns
10^{-6}	p= 0.02	p= 0.01	p=ns
$10^{-5.5}$	p=0.0004	p<0.0001	p=0.0003
10^{-5}	p <0.0001	p<0.0001	p<0.0001

Statistical significance is taken at ($p < 0.05$), and effect size (*d*) and Cohen's *d* values are taken as $d = 0.2 - < 0.5$ (small effect), $d = 0.5 - < 0.8$ (medium effect), and $d = \geq 0.8$ (large effect). **Abbreviations:** CD, control diet; *d*, Cohen's *d*; TA, thoracic aorta; MA, mesenteric artery; ILA, interlobar artery; p= ns, non-significant; Conc, concentration; [M], Molar.

3.6.2 Effects of vehicle and Atherogenesis on LKB1-induced vasodilation.

To confirm that the vasodilatory effects were a direct result of LKB1 stimulation, control diet (CD) vessels were subjected to a DRC of serially diluted DMSO (vehicle) compared to LKB1 consisting of LKB1 dissolved in the vehicle in each vessel type. This demonstrated that the LKB1 of all three vessels increased vasodilation compared to the vehicle. LKB1 thoracic aorta increased relaxation compared to vehicle at dose 10^{-5} [M], (figure 3.2A). LKB1-induced relaxation was increased in LKB1 interlobar arteries compared to the vehicle group at doses $10^{-5.5}$ and 10^{-5} [M], (figure 3.2C). Interestingly, interlobar arteries had a small effect (Cohen's *d*) size of $d = 0.36$ in shifting the LogEC₅₀ compared to the vehicle group. A small effect (Cohen's *d*) size was observed for AUC in the vehicle compared to the LKB1 group $d = 0.2$. In mesenteric arteries, LKB1-induced vasodilation was increased compared to the vehicle group at doses $10^{-5.5}$ and 10^{-5} [M], (figure 3.2E). Results showed that AUC was increased in the LKB1 group in mesenteric arteries, (figure 3.2K) compared to the vehicle group; however, no shift in LogEC₅₀ was observed in the LKB1 vs the vehicle group, table 3.3. After establishing that the LKB1 group induced vasodilation by comparing it to the vehicle group, LKB1-induced vasodilation was assessed in a diseased setting, more specifically in atherosclerosis, to determine if this affected LKB1-mediated relaxation.

Results showed that LKB1-induced vasodilation in thoracic aorta, interlobar and mesenteric arteries, (figures 3.2B, D and F) remained unaffected despite the induction of an atherogenic diet (AD). For statistically significant p values and effect size (Cohen's d) values obtained for each dose, refer to table 3.2.

Table 3.2. LKB1 vs vehicle in the thoracic aorta and interlobar and mesenteric arteries and CD vs AD in the thoracic aorta and interlobar and mesenteric arteries p values and effect (Cohen's d) values.

LKB1 Conc [M]	TA LKB1 vs vehicle	ILA LKB1 vs vehicle	MA LKB1 vs vehicle	TA CD vs AD	ILA CD vs AD	MA CD vs AD
10^{-8}	d=0.39	p=ns	p=ns	p=ns	p=ns	p=ns
$10^{-7.5}$	d=0.34	d=0.21	p=ns	d=0.24	p=ns	p=ns
10^{-7}	d=0.28	d=0.30	p=ns	d=0.24	p=ns	d=0.27
$10^{-6.5}$	d=0.41	d=0.33	d=0.23	p=ns	p=ns	d=0.27
10^{-6}	d=0.40	d=0.50	d=0.38	p=ns	p=ns	p=ns
$10^{-5.5}$	d=0.54	p= 0.03	p= 0.001	p=ns	p=ns	p=ns
10^{-5}	p= 0.01	p<0.0001	p<0.0001	p=ns	p=ns	p=ns

Statistical significance is taken at ($p<0.05$), and effect size (d) and Cohen's d values are taken as $d=0.2-<0.5$ (small effect), $d=0.5-<0.8$ (medium effect), and $d=\geq 0.8$ (large effect).

Abbreviations: AD, atherogenic diet; Conc, concentration; CD, control diet; d , Cohen's d ; ILA, interlobar artery; MA, mesenteric artery; [M], Molar; n , sample size; $p= ns$, non-significant; TA, thoracic aorta

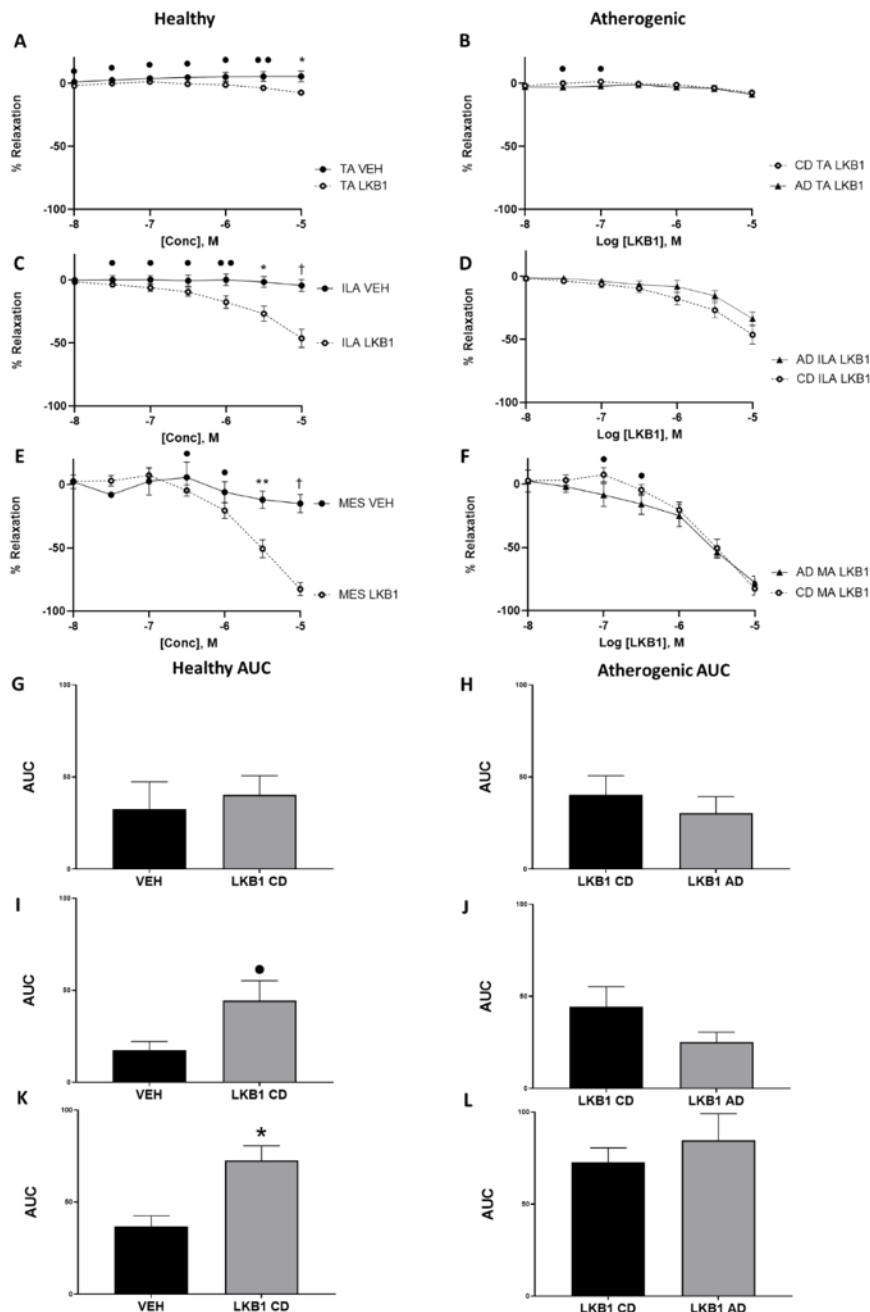


Figure 3.2. *LKB1 Dose-response curves and AUC graphs of vehicle vs LKB1 and LKB1 vs AD in TA, ILA, and MA isolated from Male, white New Zealand rabbits (n=4-13). Comparative graphs of DRC to either LKB1 (10^{-8} to 10^{-5}) or its vehicle (DMSO 10^{-8} to 10^{-5}) in various vessel types are shown in CD vs vehicle DRC, **A**. TA, **C**. ILA, and **E**. MA. The effect of LKB1 on vasodilation was further assessed in an AD: CD vs AD DRC; **B**. TA, **D**. ILA, and **F**. MA. AUC graphs that correlate with either CD vs vehicle are shown in **G**. TA, **I**. ILA, and **K**. MA, or CD vs AD, **H**. TA, **J**. ILA, and **L**. MA. All data is represented as Mean \pm SEM, and statistical analysis was performed using a one-way ANOVA followed by a Dunnett's post hoc test. * ($p < 0.05$), ** ($p < 0.01$), *** ($p < 0.001$), † ($p < 0.0001$). Effect size (d) and Cohen's d values are taken as • $d = 0.2-0.5$ (small effect), •• $d = 0.5-0.8$ (medium effect), and ••• $d \geq 0.8$ (large effect). **Abbreviations:** AD, atherogenic diet; AUC, area under the curve; CD, control diet; ILA, interlobar artery; MA, mesenteric artery; [M], Molar; n, sample size; TA, thoracic aorta; VEH, vehicle.*

Table 3.3. Log EC₅₀ and AUC for CD and AD fed rabbit ILA and MA vessels (Denuded, ODQ, L-NAME or KPSS vs LKBI).

<i>ILA – LKBI DRC</i>	<i>n</i>	<i>Log EC₅₀ ± SEM</i>	<i>p vs LKBI</i>	<i>d vs LKBI</i>	<i>AUC ± SEM</i>	<i>p vs LKBI</i>	<i>d vs LKBI</i>
<i>(CD) LKBI</i>	13	-5.81 ± 0.1			44.33 ± 10.9		
<i>(CD) vehicle</i>	4	-6.48 ± 0.2	p=ns	<i>d=0.364</i>	17.45 ± 4.8	p=ns	<i>d=-0.20</i>
<i>(CD) Denuded</i>	7	-5.96 ± 0.5	p=ns	-	73.39 ± 23.6	p=ns	<i>d=-0.20</i>
<i>(CD) ODQ</i>	8	-5.80 ± 0.1	p=ns	-	41.11 ± 11.0	p=ns	-
<i>(CD) L-NAME</i>	9	-6.05 ± 0.2	p=ns	-	80.39 ± 25.3	p=ns	<i>d=-0.24</i>
<i>(CD) KPSS</i>	8	-5.84 ± 0.1	p=ns	-	59.89 ± 8.9	p=ns	-
<i>(AD) LKBI</i>	8	-5.83 ± 0.2			25.13 ± 5.5		
<i>(AD) Denuded</i>	4	-6.03 ± 0.1	p=ns	-	62.38 ± 12.8	p=ns	<i>d=-0.85</i>
<i>(AD) ODQ</i>	8	-5.53 ± 0.04	p=ns	-	21.46 ± 4.1	p=ns	-
<i>(AD) L-NAME</i>	7	-5.67 ± 0.1	p=ns	-	24.69 ± 6.6	p=ns	-
<i>(AD) KPSS</i>	7	-5.54 ± 0.1	p=ns	-	55.81 ± 15.3	p=ns	<i>d=-0.57</i>
<i>MA – LKBI DRC</i>	<i>n</i>	<i>Log EC₅₀ ± SEM</i>	<i>p vs LKBI</i>	<i>d vs LKBI</i>	<i>AUC ± SEM</i>	<i>p vs LKBI</i>	<i>d vs LKBI</i>
<i>(CD) LKBI</i>	10	-6.0 ± 0.1			72.56 ± 8.0		
<i>(CD) vehicle</i>	3	-6.00 ± 0.5	p=ns	-	36.67 ± 5.8	p= 0.04	<i>d=0.47</i>
<i>(CD) Denuded</i>	10	-5.90 ± 0.1	p=ns	-	62.40 ± 10.7	p=ns	<i>d=0.24</i>
<i>(CD) ODQ</i>	10	-5.95 ± 0.2	p=ns	-	75.09 ± 23.5	p=ns	-
<i>(CD) L-NAME</i>	9	-5.78 ± 0.1	p=ns	-	52.49 ± 11.5	p=ns	-
<i>(CD) KPSS</i>	9	-5.73 ± 0.2	p=ns	-	37.28 ± 6.8	p=ns	<i>d=0.45</i>
<i>(AD) LKBI</i>	9	-6.14 ± 0.2			84.65 ± 14.5		
<i>(AD) Denuded</i>	9	-5.94 ± 0.1	p=ns	-	86.19 ± 12.4	p=ns	-
<i>(AD) ODQ</i>	10	-5.78 ± 0.13	p=ns	-	49.58 ± 8.2	p=ns	-
<i>(AD) L-NAME</i>	10	-5.70 ± 0.55	p=ns	-	108.7 ± 14.2	p=ns	<i>d=0.28</i>
<i>(AD) KPSS</i>	8	-5.67 ± 0.09	p=ns	-	54.50 ± 11.5	p=ns	<i>d=0.24</i>

All data is represented as Mean ± SEM, and statistical analysis was performed using a one-way ANOVA followed by a Dunnett's post hoc test. Statistical significance is taken at ($p < 0.05$), and effect size (d) and Cohen's d values are taken as $d = 0.2 - < 0.5$ (small effect), $d = 0.5 - < 0.8$ (medium effect), and $d = \geq 0.8$ (large effect). **Abbreviations:** AUC, Area Under the Curve; CD, Control Diet; AD, Atherogenic Diet; ILA, Interlobar Artery; MA, Mesenteric Artery; DEN, Denuded; ODQ; L-NAME, L-N^G-Nitroarginine Methyl Ester and KPSS, Potassium physiological salt solution.

3.6.3 Mechanistic evaluation of the vasodilatory effects of LKB1.

Once LKB1 was identified as a vasodilator in a healthy and diseased atherogenic environment, a preliminary mechanistic evaluation was performed to identify the specific pathway(s) LKB1 uses to induce its relaxation effects. Drug incubations preceding LKB1 DRC were completed to determine endothelial-dependent relaxation, the involvement of the eNOS/NO/sGC signalling cascade and K⁺ channel-dependent relaxation.

3.6.3.1 Effect of L-NAME to assess eNOS dependency on LKB1-induced vasodilation.

To determine whether LKB1 was inducing vasodilation through endothelial mechanisms, vessels were either mechanically denuded or incubated with the NO synthesis inhibitor L-NAME. Pre-treatment with L-NAME was used to inhibit the eNOS/NO signalling cascade. Interestingly, in the CD, L-NAME inhibition enhanced LKB1-induced relaxation in thoracic aorta compared to the LKB1 group at doses (10^{-7} - 10^{-5} [M]), (figure 3.3A). This enhancement was abolished in AD vessels. A small or medium effect was observed, showing that interlobar arteries enhanced relaxation in the CD of the L-NAME group compared to the LKB1 group at doses (10^{-8} - $10^{-6.5}$ [M]), (figure 3.3C). In the CD of interlobar arteries, in the L-NAME group, AUC was increased, showing a small effect (*Cohen's d*) compared to the LKB1 group (80.4 ± 25.3 vs 44.3 ± 10.9 ; $p=ns$, $d=-0.24$). In the L-NAME group, pre-incubation significantly reduced relaxation in CD mesenteric arteries compared to the LKB1 group at dose 10^{-5} [M], (figure 3.3E). In the AD group, L-NAME incubation did not affect relaxation compared to the LKB1 group in mesenteric arteries at any LKB1 doses. No effect was observed in the AD of the L-NAME-treated interlobar arteries compared to the LKB1 group at any doses, (figures 3.3B, D and F). Interestingly, LogEC₅₀ remained unchanged in the L-NAME group of interlobar, and mesenteric arteries compared to the LKB1 group in both a CD and an AD. Vessels pre-incubated with L-NAME had no effect in AUC analysis for mesenteric arteries in a CD and interlobar arteries in an AD compared to the LKB1 group, table 3.3. For statistically significant *p* values and effect size (*Cohen's d*) values obtained for each dose, please refer to table 3.4.

Table 3.4. Statistical significance and effect (Cohen's d) values from L-NAME pre-incubated thoracic aorta, interlobar and mesenteric arteries of CD and AD-fed rabbits following a cumulative DRC to LKB1.

LKB1 Conc [M]	CD (LKB1 vs L-NAME)			AD (LKB1 vs L-NAME)		
	TA	ILA	MA	TA	ILA	MA
10^{-8}	p=ns	d= 0.52	d= 0.33	p=ns	p=ns	p=ns
$10^{-7.5}$	d= 0.30	d= 0.32	p=ns	d= -0.22	p=ns	p=ns
10^{-7}	p= 0.03	d= 0.29	d= 0.22	p=ns	p=ns	d= -0.23
$10^{-6.5}$	p= 0.01	d= 0.22	p=ns	p=ns	p=ns	p=ns
10^{-6}	p= 0.03	p=ns	p=ns	d= -0.22	p=ns	p=ns
$10^{-5.5}$	p= 0.05	p=ns	d= -0.29	p=ns	p=ns	p=ns
10^{-5}	p= 0.01	p=ns	p= 0.003	d= 0.40	p=ns	p=ns

Statistical significance is taken at ($p < 0.05$), and effect size (d) and Cohen's d values are taken as $d = 0.2 - < 0.5$ (small effect), $d = 0.5 - < 0.8$ (medium effect), and $d = \geq 0.8$ (large effect).

Abbreviations: AD, atherogenic diet; Conc, concentration; CD, control diet; d , Cohen's d ; ILA, interlobar artery; L-NAME, $N(\omega)$ -nitro-L-arginine methyl ester; MA, mesenteric artery; [M], Molar; n , sample size; $p = ns$, non-significant; TA, thoracic aorta.

LKB1 vs. L-NAME

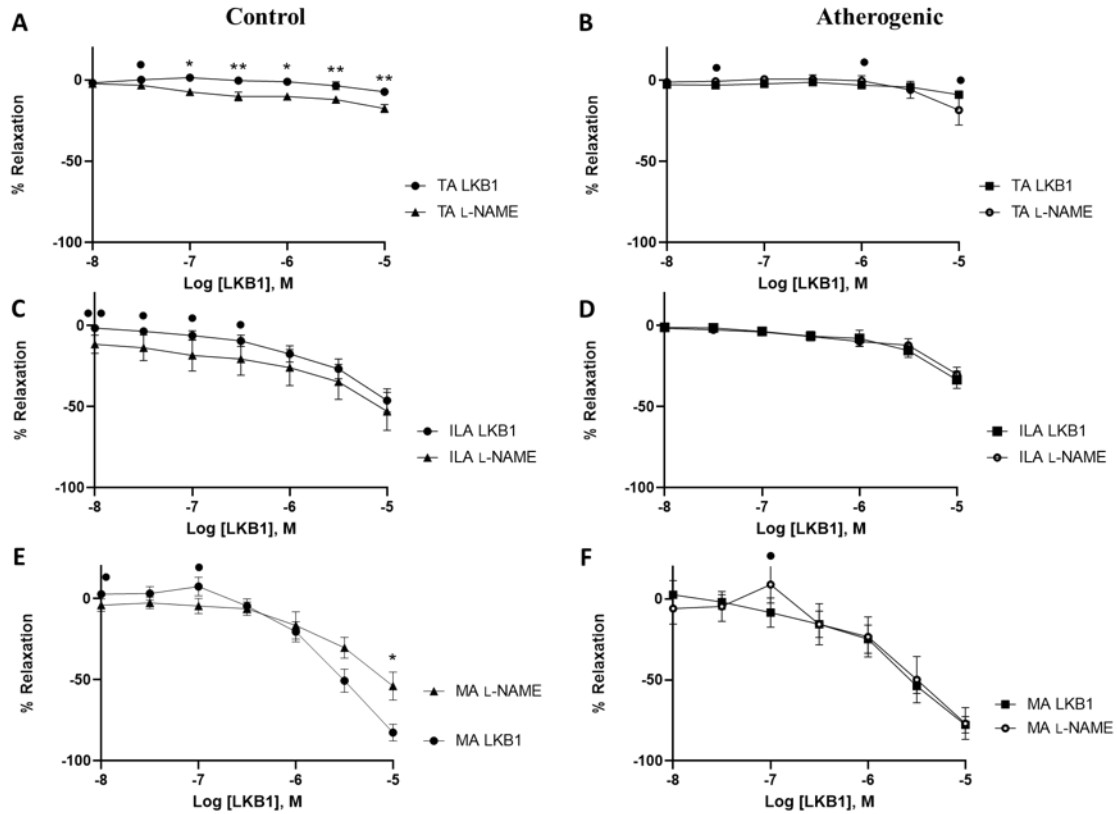


Figure 3.3. Mechanistic evaluation of eNOS inhibition by L-NAME on LKB1 induced relaxation ($n=7-13$). A. TA, C. ILA, and E. MA represent L-NAME inhibition prior to a cumulative DRC to LKB1 in CD and B. TA, D. ILA, and F. MA represent the response to L-NAME vs LKB1 in an AD. All data is represented as Mean \pm SEM, and statistical analysis was performed using a one-way ANOVA followed by a Dunnett's post hoc test. * ($p<0.05$), **($p<0.01$), *** ($p<0.001$), \dagger ($p<0.0001$). Effect size (d) and Cohen's d values are taken as • $d=0.2-0.5$ (small effect), •• $d=0.5-0.8$ (medium effect), and ••• $d\geq 0.8$ (large effect). **Abbreviations:** AD, atherogenic diet; CD, control diet; ILA, interlobar artery; MA, mesenteric artery; L-NAME, L-N^G-Nitroarginine Methyl Ester; [M], Molar; n , sample size; TA, thoracic aorta.

3.6.3.2 Effects of mechanical denudation on LKB1-induced relaxation.

To determine endothelial-dependent relaxation, the endothelium was removed from vessels through mechanical denudation¹⁰ prior to the beginning of any experimental incubations. For both CD and AD, this method was performed in all three vessel types (thoracic aorta, interlobar and mesenteric arteries). A small effect (Cohen's d) in the CD thoracic aorta showed that relaxation in the mechanical denudation (DEN) group was enhanced compared to the LKB1 group at doses 10^{-7} , $10^{-6.5}$, 10^{-6} , $10^{-5.5}$ and 10^{-5} [M], (figure 3.4A). In an AD, the DEN group showed increased relaxation compared to the LKB1 group at dose 10^{-5} [M], (figure 3.4B). Analysis of effect (Cohen's d) in interlobar

¹⁰ Mechanical denudation, elimination of endothelium to remove endothelial vasodilatory mechanisms

arteries showed that the DEN group increased AUC compared to the LKB1 group in both a CD, $d=-0.20$ and an AD, $d=-0.85$. Surprisingly, mechanical denudation did not affect CD and AD LogEC₅₀ in interlobar or mesenteric arteries compared to the LKB1 group. In interlobar arteries, an increase in relaxation in the DEN group compared to the LKB1 group showed a small effect (*Cohen's d*) in CD at doses 10⁻⁷ and 10^{-6.5} [M], (figure 3.4C) and had an effect (*Cohen's d*) in an AD at doses 10⁻⁸, 10^{-7.5}, 10⁻⁷, 10^{-6.5}, 10^{-5.5} and 10⁻⁵ [M], (figure 3.4D). In mesenteric arteries, the DEN group significantly reduced relaxation compared to the LKB1 group in a CD at dose 10⁻⁵ [M], (figure 3.4E) but had no significant effect or (*Cohen's d*) effect size in an AD, (figure 3.4F). AUC in CD of mesenteric arteries showed that mechanical denudation had a small effect (*Cohen's d*) on reducing LKB1-induced vasodilation compared to the LKB1 group, $d=0.24$ however, it had no effect in an AD. For statistically significant *p* values and effect size (*Cohen's d*) values obtained for each dose, please refer to table 3.5.

Table 3.5. Statistical significance and effect (*Cohen's d*) values from the mechanically denudated thoracic aorta, interlobar arteries, and mesenteric arteries of CD and AD-fed rabbits.

LKB1 Conc [M]	Control Diet (CD) (LKB1 vs DEN)			Atherogenic diet (AD) (LKB1 vs DEN)		
	TA	ILA	MA	TA	ILA	MA
10 ⁻⁸	p=ns	p=ns	d= 0.25	d= -0.28	d= 0.98	p=ns
10 ^{-7.5}	p=ns	p=ns	d= 0.31	d= -0.33	d= 0.31	p=ns
10 ⁻⁷	d= 0.42	d= 0.26	d= 0.22	d= -0.35	d= -0.38	p=ns
10 ^{-6.5}	d= 0.28	d= 0.30	p=ns	d= -0.37	d= -0.43	p=ns
10 ⁻⁶	d= 0.28	p=ns	p=ns	d= -0.37	p=ns	p=ns
10 ^{-5.5}	d= 0.30	p=ns	d= -0.28	p=ns	d= 0.30	p=ns
10 ⁻⁵	d= 0.41	p=ns	p= 0.005	p= 0.031	d= 0.21	p=ns

Statistical significance is taken at ($p<0.05$), and effect size (*d*) and *Cohen's d* values are taken as $d=0.2-<0.5$ (small effect), $d=0.5-<0.8$ (medium effect), and $d=\geq 0.8$ (large effect). **Abbreviations:** AD, atherogenic diet; Conc, concentration; CD, control diet; *d*, *Cohen's d*; DEN, denuded; ILA, interlobar artery; MA, mesenteric artery; [M], Molar; *n*, sample size; *p*=ns, non-significant; TA, thoracic aorta.

LKB1 vs. MECHANICAL DENUDATION

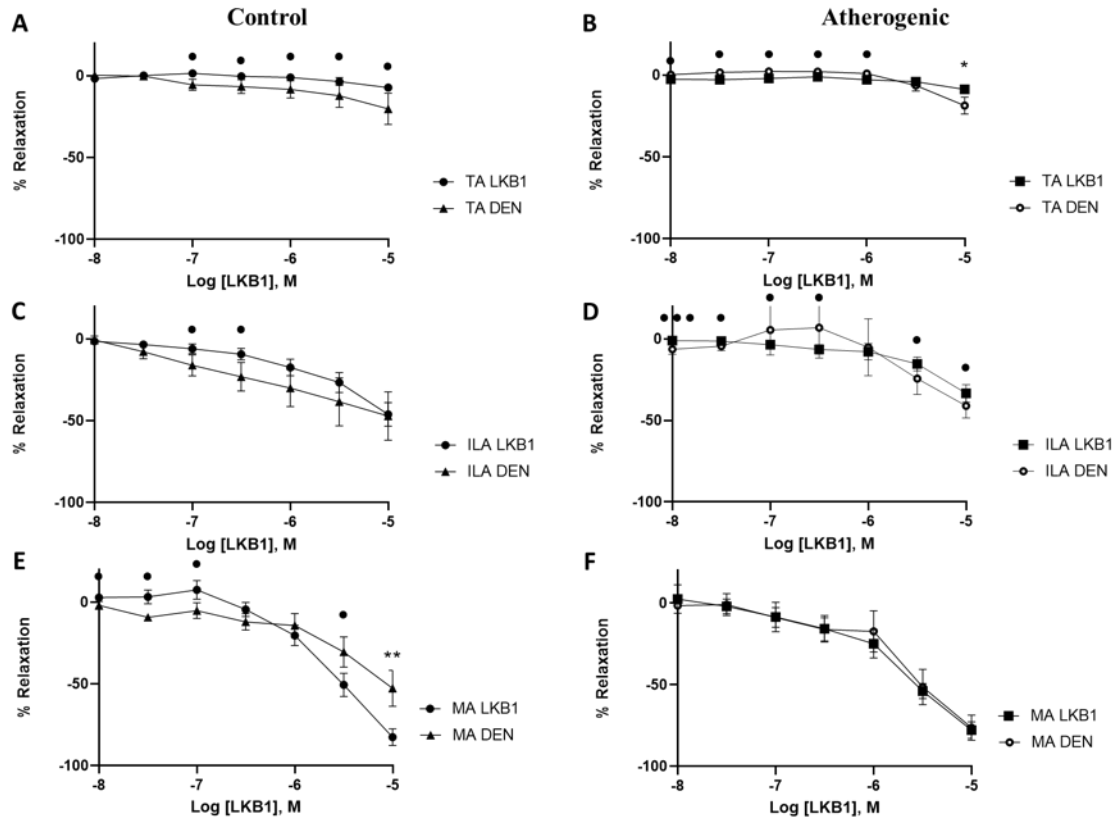


Figure 3.4. Effect of mechanical denudation of vessels on LKB1 induced relaxation (n=4-13). A. TA, C. ILA, and E. MA represent mechanical denudation prior to a cumulative DRC to LKB1 in CD and B. TA, D. ILA, and F. MA represent the response to DEN vs LKB1 in an AD. All data is represented as mean \pm standard error of the mean (SEM), and statistical analysis was performed using a one-way ANOVA followed by a Dunnett's post hoc test. * ($p < 0.05$), ** ($p < 0.01$), *** ($p < 0.001$), \dagger ($p < 0.0001$). Effect size (d) and Cohen's d values are taken as $\bullet d = 0.2-0.5$ (small effect), $\bullet\bullet d = 0.5-0.8$ (medium effect), and $\bullet\bullet\bullet d \geq 0.8$ (large effect). **Abbreviations:** AD, atherogenic diet; CD, control diet; DEN, denuded; ILA, interlobar artery; MA, mesenteric artery; [M], Molar; n, sample size; TA, thoracic aorta.

3.6.3.3 LKB1-induced vasodilation is unaffected by ODQ pre-incubation.

To identify NO donor-stimulated sGC-specific relaxation, vessels from either a CD or AD were incubated with the sGC inhibitor ODQ prior to a cumulative DRC of LKB1. Results demonstrated that the LogEC₅₀ and AUC provided no difference in ODQ-treated vessels compared to the LKB1 group in interlobar or mesenteric arteries for either a CD or an AD. Pre-treatment with ODQ to inhibit sGC had no significant effect on reducing or enhancing LKB1-induced relaxation in the thoracic aorta (figures 3.5 A and B), interlobar arteries (figures 3.5 C and D), or mesenteric arteries (figure 3.5 E and F). Analysis of effect size showed that at some doses, an effect (Cohen's d) was obtained for some vessel types.

LKB1 vs. ODQ

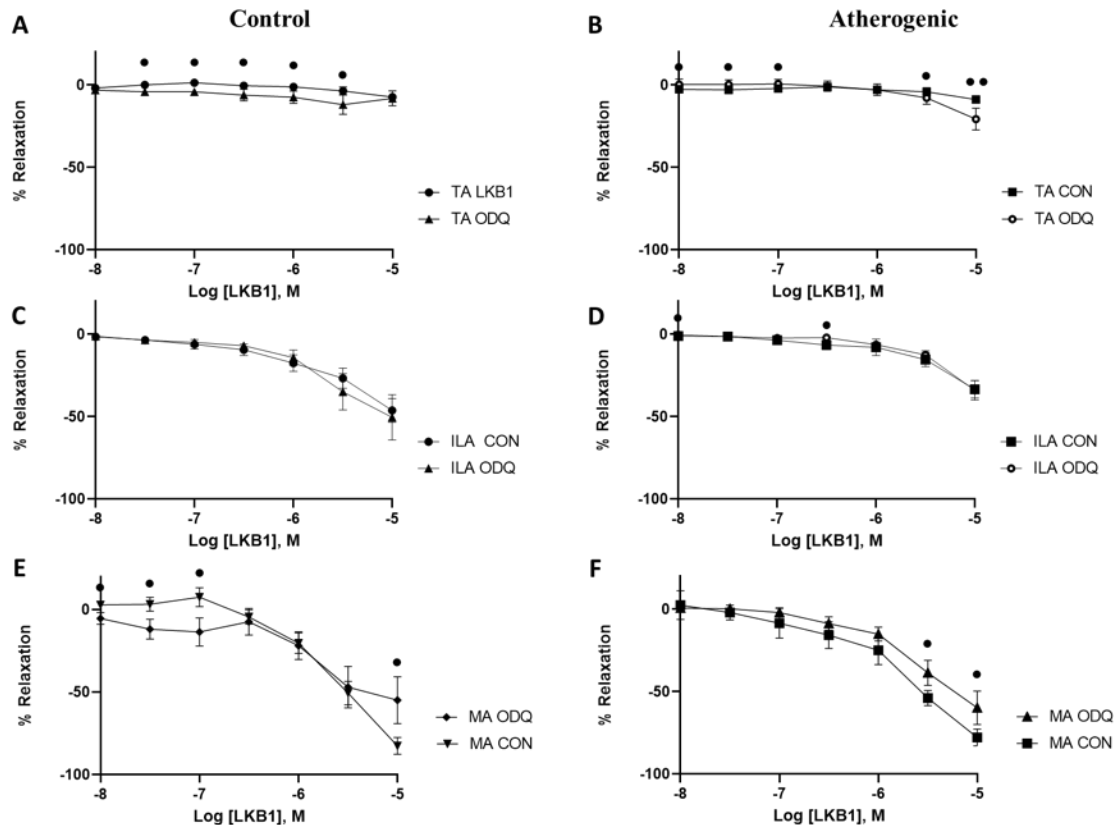


Figure 3.5. LKB1 induced relaxation DRC graphs of CD and AD in TA, ILA, and MA pre-incubated with the sGC inhibitor ODQ ($n=8-13$). A. TA, C. ILA, and E. MA represent ODQ inhibition prior to a cumulative DRC to LKB1 in CD and B. TA, D. ILA, and F. MA represent the response to ODQ vs LKB1 in an AD. All data is represented as Mean \pm SEM, and statistical analysis was performed using a one-way ANOVA followed by a Dunnett's post hoc test. * ($p<0.05$), ** ($p<0.01$), *** ($p<0.001$), \dagger ($p<0.0001$). Effect size (d) and Cohen's d values are taken as $\bullet d=0.2-0.5$ (small effect), $\bullet\bullet d=0.5-0.8$ (medium effect), and $\bullet\bullet\bullet d\geq 0.8$ (large effect). **Abbreviations:** AD, atherogenic diet; CD, control diet; ILA, interlobar artery; MA, mesenteric artery; [M], Molar; n , sample size; ODQ, 1H- [1,2,4] oxadiazolo [4,3-a] quinoxaline-1-one; TA, thoracic aorta.

3.6.3.4 Inhibition of K^+ channels by KPSS mildly reduced LKB1-induced vasorelaxation in mesenteric arteries.

To determine the involvement of the K^+ channels in the vasodilatory response of LKB1, vessels were pre-constricted with 40mM KPSS to inhibit all K^+ channels. In thoracic aorta, the KPSS group only yielded a small effect (Cohen's d) compared to the LKB1 group at dose 10^{-5} [M], $d=-0.27$ in a CD, (figure 3.6A). However, in an AD, either a small or medium effect (Cohen's d) was produced for each dose in the LKB1 group, (figure 3.6B). In a CD of interlobar arteries, a small effect (Cohen's d) was observed at

doses 10^{-8} and $10^{-7.5}$ [M], $d=0.41$ and $d=0.24$, (figure 3.6C); however, in an AD, relaxation in the KPSS group was enhanced compared to the LKB1 group, (figure 3.6D) at dose 10^{-5} [M]. In CD of mesenteric arteries, relaxation was significantly reduced in the KPSS group compared to the LKB1 group at doses $10^{-5.5}$ and 10^{-5} [M], (figure 3.6E). Additionally, a small-medium effect (*Cohen's d*) showed that LKB1 stimulated vasodilation was reduced in the KPSS group compared to the LKB1 group in the AD at almost all doses ($10^{-7.5}$ to 10^{-5} [M]) (figure 3.6F). Table 3.3 illustrates a medium effect size (*Cohen's d*) was observed showing increased AUC of AD interlobar arteries in KPSS-treated vessels compared to the LKB1 group, $d=-0.57$. A small effect (*Cohen's d*) was observed in mesenteric arteries compared to the LKB1 group, showing that the KPSS group reduced AUC compared to the LKB1 group in CD, $d=0.45$ and AD, $d=0.24$. Following KPSS pre-constriction, there was no effect on EC_{50} in interlobar arteries or mesenteric arteries compared to the LKB1 group for CD or AD. Interlobar arteries showed no significant difference in the AUC in CD of the KPSS group compared to the LKB1 group. For statistically significant *p* values and effect size (*Cohen's d*) values obtained for each dose, please refer to table 3.6.

Table 3.6. The effect of KPSS inhibited K^+ channels on LKB1 mediated relaxation in CD and AD thoracic aorta, interlobar, and mesenteric arteries.

LKB1 Conc [M]	CD (LKB1 vs 40 [mM] KPSS)			AD (LKB1 vs 40 [mM] KPSS)		
	TA	ILA	MA	TA	ILA	MA
10^{-8}	d= -0.27	d= 0.41	p=ns	d= -0.34	d= -0.41	p=ns
$10^{-7.5}$	p=ns	d= 0.24	p=ns	d= -0.40	d= -0.43	d= -0.28
10^{-7}	p=ns	p=ns	p=ns	d= -0.48	d= -0.51	d= -0.32
$10^{-6.5}$	p=ns	p=ns	d= -0.27	d= -0.52	d= -0.42	d= -0.46
10^{-6}	p=ns	p=ns	d= -0.39	d= -0.61	d= -0.29	d= -0.44
$10^{-5.5}$	p=ns	p=ns	p= <0.0001	d= -0.56	p=ns	d= -0.54
10^{-5}	p=ns	p=ns	p= <0.0001	d= -0.69	p= 0.02	d= -0.38

Statistical significance is taken at ($p<0.05$), and effect size (*d*) and *Cohen's d* values are taken as $d=0.2-<0.5$ (small effect), $d=0.5-<0.8$ (medium effect), and $d=\geq 0.8$ (large effect).

Abbreviations: AD, atherogenic diet; Conc, concentration; CD, control diet; *d*, *Cohen's d*; KPSS, potassium physiological salt solution; ILA, interlobar artery; MA, mesenteric artery; [M], Molar; *n*, sample size; *p*= ns, non-significant; TA, thoracic aorta.

LKB1 vs. 40mM KPSS

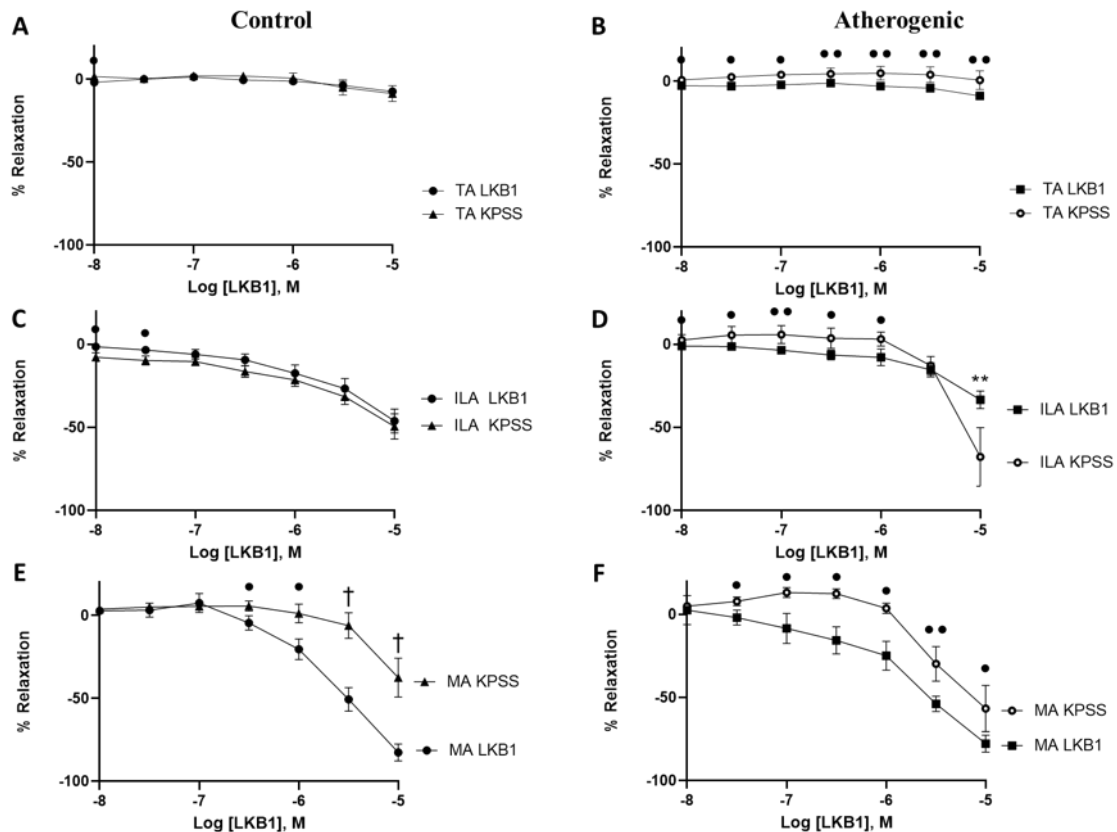


Figure 3.6. LKB1 DRC graphs of CD and AD in TA, ILA, and MA pre-constricted with 40mM KPSS to non-selectively inhibit potassium channels ($n=7-13$). A, TA, C, ILA, and E. MA represent 40mM pre-constricted vessels prior to a cumulative DRC to LKB1 in CD and B. TA, D, ILA, and F. MA represent the response to 40mM KPSS vs LKB1 in an AD. All data is represented as Mean \pm SEM, and statistical analysis was performed using a one-way ANOVA followed by a Dunnett's post hoc test. * ($p<0.05$), ** ($p<0.01$), *** ($p<0.001$), † ($p<0.0001$). Effect size (d) and Cohen's d values are taken as * $d=0.2-0.5$ (small effect), ** $d=0.5-0.8$ (medium effect), and *** $d\geq 0.8$ (large effect). **Abbreviations:** AD, atherogenic diet; CD, control diet; ILA, interlobar artery; KPSS, potassium physiological salt solution; MA, mesenteric artery; [M], Molar; n , sample size; TA, thoracic aorta.

3.6.3.5 Effects of a non-selective PIM1 kinase inhibitor on vasodilation

Given the results obtained in Chapter 3, which investigated the vasodilatory capacity of LKB1, a highly selective PIM1 kinase inhibitor, we decided to investigate if the non-selective PIM kinase inhibitor AZD1208 would also generate a vasorelaxation response to rule out the involvement of all three PIM kinase isoforms. Inhibition of all PIM kinase isoforms did not affect vasodilation in any vessel type. No difference occurred between the AZD1208 group and the vehicle group.

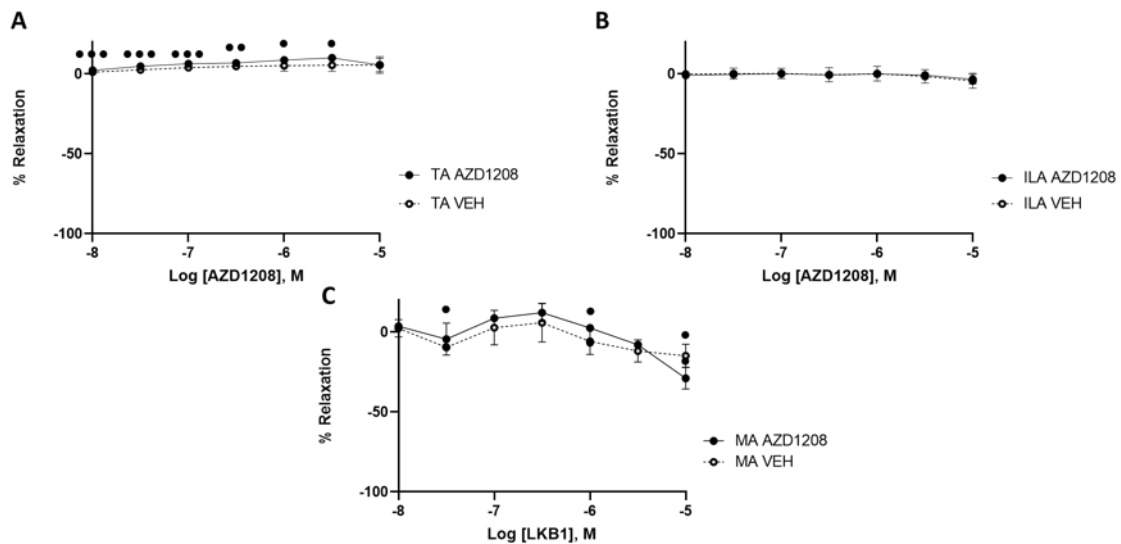


Figure 3.7. Vasorelaxation response to cumulative doses of AZD1208 in TA, ILA, and MA of white New Zealand (male) rabbits ($n=2-4$). A. TA, B. ILA, and C. MA. All data is represented as Mean \pm SEM, and statistical analysis was performed using a one-way ANOVA followed by a Dunnett's post hoc test. Effect size (d) and Cohen's d values are taken as $\bullet d=0.2-0.5$ (small effect), $\bullet\bullet d=0.5-0.8$ (medium effect), and $\bullet\bullet\bullet d\geq 0.8$ (large effect). **Abbreviations:** AZD, AZD1208; CD, control diet; ILA, interlobar artery; MA, mesenteric artery; [M], Molar; n , sample size; TA, thoracic aorta; VEH, vehicle.

3.7 Discussion

Interlobar arteries were investigated as our principal vessel as the disease being targeted is associated with renal microvascular vasoconstriction. Thoracic aorta and mesenteric arteries were used to determine vessel specificity. The significant findings of this study show that a) LKB1 is a novel vasodilator and induces vasodilation in a vessel-specific manner. A mechanistic evaluation demonstrated that b) endothelial denudation and L-NAME increased relaxation in thoracic aorta but decreased relaxation in mesenteric arteries. As well, c) LKB1-induced vasodilation is K⁺ channel-dependent in mesenteric arteries. Interestingly, d) Atherogenic diet did not affect relaxation compared to Control diet, e) a similar result occurred in ODQ-treated rings. Surprisingly, f) a DRC with an alternative but non-selective pan-PIM kinase inhibitor did not induce relaxation in thoracic aorta, interlobar, or mesenteric arteries.

a) LKB1-induced vasodilation

Understanding which blood vessels dilate is critical in vulnerable patients, including those with cancer, given the risk of hypotension associated with increased systemic vasodilation [87]. The results of this study showed that vasodilation occurred in smaller arteries, including mesenteric arteries and interlobar arteries but not in the larger thoracic aorta segments. This suggests that LKB1 might be a small artery-specific vasodilator, which can prove beneficial in conditions involving vasoconstriction of small vessels such as CIAKI [88]. Increasing vasodilation of afferent arterioles will reduce adverse vascular effects, increase renal perfusion, and promote the excretion of accumulated waste products associated with reduced GFR [68]. Variations in vascular responses are likely attributed to differences in cellular protein expressions and potential genetic differences; however, further investigations are required to confirm this hypothesis.

b) PIM1 kinase as a target for CIAKI treatment

The results of this study demonstrated that LKB1-induced relaxation occurred in an endothelial and eNOS-dependent manner in mesenteric arteries. Although the signalling cascade initiated by LKB1 leading to vascular relaxation is unknown, using another PIM1 kinase inhibitor, resveratrol, could provide a potential insight into the function of LKB1. Resveratrol is a plant compound suggested to act as an anti-oxidant, which could confound any mechanistic insights. Additionally, resveratrol has also shown to inactivate PIM1 kinase activity [50] directly. Pre-treatment with resveratrol has exhibited acute endothelium-dependent renal vasodilation through increased eNOS expression and activity, consequently stimulating elevated NO levels [89].

Additionally, treatment with resveratrol has shown to increase renal blood flow [90], which could be via a PIM1 kinase-dependent manner. Interestingly, quercetin, identified as another PIM1 kinase inhibitor [91], has exhibited vasodilatory effects through increased eNOS phosphorylation in an Akt-independent and protein kinase A-dependent manner [92]. Given the results observed in this study suggesting a partly endothelial and eNOS/NO-dependent vasodilatory response of LKB1 and confirmation by a similar mechanism of two alternative PIM1 kinase inhibitors, it could be a valuable treatment for endothelial dysfunction associated with CIAKI. PIM1 kinase activation has shown in models of angiogenesis to phosphorylate eNOS at Ser-633 in diabetic mice, a crucial process for NO production [93]. This suggests that PIM1 activation may be a potential vasodilatory mechanism (due to its effects on eNOS phosphorylation) in addition to PIM1 inhibition elucidated by this study. This highlights inconsistencies in understanding the role of PIM1 in vasodilation, and further studies could help understand the results obtained by this study. It may also help to determine if a mechanistic shift occurs or a direct effect of the pharmacokinetics in a systemic environment. Previously, resveratrol has also been shown to mitigate CIAKI, suggested to be a result of restored sirtuin 1 expression, a protein downregulated by CDDP [94].

Additionally, quercetin has also showed protective effects against CIAKI. Results from their study showed that quercetin significantly downregulated the expression of pro-inflammatory proteins IL-1 β , IL-6 and TNF- α . Additionally, the downregulation of NF- κ B was observed in western blot analysis of kidney macrophages from CIAKI mice. They concluded that the renoprotective effects of quercetin are mediated by the inhibition of Mincle/Syk/NF- κ B signalling [39]. This highlights the potential of pharmacological inhibition of PIM1 kinase as a renoprotective strategy against CIAKI. Given the vasodilatory effects of resveratrol and quercetin and the amelioration they both display against CIAKI, LKB1 as a PIM1 kinase inhibitor with vasodilatory effects may also display renoprotective qualities.

c) Mechanisms of action: KPSS reduced vasodilation in mesenteric arteries.

This study demonstrated that vasoconstriction and subsequent K⁺ channel inhibition by the KPSS group reduced LKB1-mediated vasodilation in mesenteric arteries and at 10⁻⁵ [M] in AD, a response not observed in interlobar arteries from CD rabbits. This suggests that LKB1-induced vasodilation is partly a result of VSMC hyperpolarisation. Following the identification that KPSS is partly responsible for mediating the relaxation response of LKB1, further investigations are required to elucidate this further. The use

of specific pharmacological inhibitors will enable the determination of which specific K^+ channels are involved in the relaxation effects. This will provide a better understanding of the molecular signalling cascade of LKB1 in the vasculature.

d) An AD did not affect LKB1-induced relaxation

Considering that heart disease will be present in a subpopulation of cancer patients, it is essential to determine if risk factors for heart disease would affect LKB1 vasodilation.

This study concludes that heart disease risk factors hypercholesterolemia and hyperhomocysteinemia do not affect LKB1-mediated vasodilation, at least at a four-week time. Notably, a small effect was observed after mechanical denudation or incubation with L-NAME, which reduces eNOS; it was surprising that the vessels remained unaffected. Therefore, it is possible that although the AD may have suppressed the eNOS/NO pathway, there may be compensation for this reduced eNOS by other endothelial or K^+ channel mechanisms.

Interestingly, this study suggests that two different pathways mediate LKB1-induced vasodilation. This could be beneficial, particularly in the prevention of CIAKI. It is established that CDDP induces endothelial dysfunction and subsequently reduces eNOS and NO, resulting in increased vasoconstriction of renal arteries and increased afferent arteriolar vascular resistance [95].

e) ODQ does not affect LKB1-induced vasorelaxation.

Results suggest that LKB1-induced relaxation is eNOS and endothelial-dependent and is not sGC dependent. This could largely be attributed to the involvement in K^+ channels and the induction of relaxation through stimulation of K^+ channels [96]. The stimulation of these K^+ channels ultimately induces relaxation through VSMC hyperpolarisation, a well-documented vasodilatory mechanism [97].

f) Pan-PIM kinase inhibitor AZD1208 did not induce relaxation.

To confirm the results observed in this study, the pan-PIM kinase inhibitor AZD1208 was used. LKB1 specifically inhibits PIM1, whilst comparatively, AZD1208 inhibits all three PIM kinase isoforms (PIM1, PIM2 and PIM3). Remarkably, the results from our study indicated that it did not induce vasodilation, suggesting that PIM1 may be the only homolog involved in vasodilation. Additionally, inhibition of all three PIM kinases may result in counteractive effects resulting in reduced vasodilation exhibited in this study (figure 3.7).

3.8 Future directions

These results suggest that LKB1 in mesenteric arteries is partly mediated through mechanisms mediated via the endothelium, in addition to the involvement of K⁺ channels. This study could benefit from further mechanistic evaluations to determine the involvement of specific K⁺ channels through pre-incubation with K⁺ channel blockers prior to cumulative DRC with LKB1. Further investigations are required to determine the vasodilatory mechanisms of LKB1 in interlobar arteries. Interestingly, vasodilatory roles of the endothelium partly mediate the relaxation properties of mesenteric arteries; however, the mechanism responsible for LKB1-induced relaxation in interlobar arteries was not elucidated by this study. This could be due to variations in protein expression; however, further investigations are required to confirm this.

This study has generated essential data to promote the progression to further understanding the effects of direct PIM1 kinase inhibition on vascular function. To date, the literature provides little clarity on the involvement of PIM1 on a molecular level, and it is a signalling cascade either in the endothelium or in VSMC. From the results obtained in this study, we have concluded that LKB1 is a novel small-vessel *in vitro* vasodilator that could be used as a treatment for diseases associated with vasoconstriction. Therefore, we suggest it as a potential option for preventing afferent arteriole vasoconstriction associated with CIAKI. However, prior to using LKB1 in any *in vivo* models, additional *in vitro* work is required to justify its use; furthermore, blood pressure testing through cannulated infusion into the ear vein of rabbits to determine the effect of each dose on blood pressure is essential.

3.9 Conclusion

This study concluded that LKB1 directly induced vasodilation, and these effects were partially mediated via endothelial mechanisms and K⁺ channels. Results suggest it could be used to further the pharmacological repurposing of LKB1 and highlight its potential in treating vascular diseases associated with chronic vasoconstriction.

Chapter 4: BX-912: a potential treatment for reduced renal blood flow and vascular resistance in cisplatin-induced acute kidney injury through its function as a vasodilator.

4.1 Abstract

Background: Cisplatin (CDDP) is a highly potent chemotherapeutic agent; however, despite its efficacy, the clinical use of CDDP is limited due to nephrotoxicity, often manifesting as acute kidney injury (AKI). AKI can be caused by intrarenal vasoconstriction of afferent arterioles. We hypothesise that BX-912 (BX) inhibits phosphoinositide-dependent kinase-1 (PDK1), which will induce vascular relaxation of afferent arterioles and prevent the pathologies associated with cisplatin-induced acute kidney injury (CIAKI). **Methods:** To investigate the vasodilatory capacity of BX and its mechanism of action, thoracic aorta, interlobar and mesenteric arteries harvested from male white New Zealand rabbits were pre-incubated with mechanistic pathway inhibitory drugs and subjected to a cumulative dose-response curve of BX (10^{-8} to 10^{-5} [M]). **Results:** This study showed that BX-induced-vascular relaxation in a vessel-specific manner, an atherogenic diet (AD)-increased BX-induced-relaxation in mesenteric arteries, and BX-induced-vasodilation is endothelial and eNOS independent. Additionally, it was shown that potassium physiological salt solution (KPSS) inhibited BX-induced-relaxation in control diet (CD)/AD) of interlobar arteries ($p < 0.0001$) and mesenteric arteries ($p < 0.0001$). Interestingly, calcium-activated potassium (KCa) channel blocker charybdotoxin (CTX) reduced BX relaxation in interlobar arteries of CD rabbits ($p < 0.01$). Pre-treatment with the non-selective cyclooxygenase inhibitor indomethacin enhanced BX-induced relaxation in interlobar arteries ($p < 0.001$) but not in mesenteric arteries. **Discussion:** This study elucidates the potential mechanism of BX-induced relaxation. BX acts independently of the endothelium and endothelial nitric oxide synthase (eNOS)/ nitric oxide (NO) pathway suggesting a practical approach to endothelial dysfunction associated with reduced renal blood flow stimulated by CDDP. BX also acts via potassium channels, providing a direction for future investigations. Cyclooxygenase (COX) inhibition with indomethacin enhanced the relaxation of interlobar vessels compared to BX alone, suggesting the potential for COX/PDK1 signalling crosstalk. **Conclusion:** BX-induced relaxation is at least partially mediated by potassium channels in small arteries whilst having no effect on

larger arteries and presents a promising treatment to mitigate reduced renal blood flow and subsequent reduced glomerular filtration rate associated with CIAKI.

4.2 Introduction

CDDP is a highly potent and effective anticancer agent used to treat many cancers, including solid, soft tissue and blood [47]. CDDP induces cell death by forming 1–2 intrastrand or 1–3 interstrand crosslinks with purine bases on the deoxyribonucleic acid (DNA) strand [56, 98]. This crosslinking impairs DNA repair mechanisms, preventing the production of a viable DNA replication template and triggering cell-cycle arrest [57]. Its clinical use is limited due to patient development of systemic toxicities [49-56] and increased and rapid CDDP resistance. However, its dose-limiting side effect is nephrotoxicity [52, 57-63], resulting in reversible AKI. However, recurrent AKI episodes significantly increase the risk of chronic kidney disease development [64, 66] and mortality rates [64, 65]. A study involving testicular cancer survivors who received a CDDP-based chemotherapy regimen showed evidence of increased endothelial dysfunction and vascular injury after the cessation of treatment. This increases their risk of added long-term comorbidities, including cardiovascular disease and atherosclerosis [8, 69]. The use of an atherogenic diet has been well documented in our laboratory to induce endothelial dysfunction [33, 34]. Endothelial dysfunction is a recognised pathophysiological vascular complication associated with CIAKI [99] and is implicated in reduced renal blood flow and impaired kidney function [100].

CIAKI damages intrarenal vessels, decreasing renal perfusion and subsequently diminishing glomerular filtration rate (GFR) [67]. Multiple pre-clinical animal models investigating the involvement of the vascular network in CIAKI have demonstrated that CDDP reduces renal blood flow and increases vascular resistance [70-72]. Reduced renal blood flow and GFR are often affected causally. Denoting that impairment to renal blood flow consequently stimulates a reduction in GFR [73], the diagnostic factor for AKI. Enhancing vasodilation is a critical mechanism that promotes blood flow and decreases systemic vascular resistance [74]. Therefore, identifying a novel vasodilator to stimulate renal blood flow to improve or prevent reductions in GFR could be a valuable target in the prevention of CIAKI. This method of enhanced relaxation has been used in previous studies of CIAKI in the form of angiotensin receptor blockers (ARBs) and angiotensin-converting enzyme inhibitors (ACEIs). However, pre-clinical studies have provided conflicting results on their beneficial effects [1]. ARBs and ACEIs have also been identified as independent risk factors for CIAKI development in

the elderly [101]. Alternative therapy is required to improve patient prognosis and prevent CIAKI development.

BX is a potent and selective adenosine triphosphate (ATP) competitive inhibitor of PDK1. X-ray diffraction methods confirmed that BX binds to the ATP binding site on PDK1. It was initially identified as an anticancer drug due to its inhibition of the phosphoinositide 3-kinases (PI3K)/Akt/mammalian target of rapamycin (mTORC) survival pathway [102]. However, it has shown beneficial effects in the treatment of cancer [103, 104] and a wide variety of molecular mechanisms, including the inhibition of osteoblast differentiation [105], decreased chemotaxis in response to vascular injury [106] and mediation of eosinophil inhibition [107]. BX-92 has not been used in functional studies of the vasculature; however, previous literature, in addition to the mechanisms associated with PDK1 inhibition, provides evidence in cell culture studies highlighting its theoretical potential as a relaxation-inducing drug [108-110].

Furthermore, inhibition of other members of the PI3K/Akt/mTORC pathway has shown renoprotective effects against CIAKI. Rapamycin, an mTORC inhibitor, has been shown to reduce blood urea nitrogen and apoptosis biomarkers [8]. Indirect Akt and mTORC inhibition through the blockade of protein kinase c have also demonstrated mitigative effects against CIAKI [111]. Further to its indirect protective effects on kidney tissue, PDK1 inhibition has also provided cardioprotective effects. PDK1 silencing has been shown to prevent hypoxia-induced pulmonary arterial hypertension [108], and PDK1 inhibition has also been shown to reduce blood pressure in mice subjected to intermittent hypoxia [112].

Given the recent focus on vascular involvement and the suggestion that vascular preservation could be a useful preventative option to mitigate CIAKI [113], this study aimed to identify a novel small vessel vasodilator that can enhance renal blood flow and subsequently GFR and further elucidate the mechanism of action of BX. In the thoracic aorta, interlobar and mesenteric arteries, multiple mechanisms were investigated to identify the potential vasodilatory pathway(s) exhibited by BX. Some of the pathways investigated are illustrated in (figure 4.3). They include nitric oxide synthase (NOS) dependent, endothelial-dependent, soluble guanylyl cyclase (sGC) dependent, potassium channel (K^+) dependent and cyclooxygenase (COX) dependent relaxation. This was performed in a CD and an endothelial dysfunction-inducing AD to determine variations in relaxation responses between healthy vs diseased states. Promising results will provide relevant evidence to support its future use in a mouse model of CIAKI.

4.3 Methods

4.3.1 Materials

KREBS pH 7.4 and 40mM KPSS (for instructions on formulation, please refer to Chapter 2, section 14.0, subsection 14.2 general chemicals. For purchasing information on BX, dimethyl sulfoxide (DMSO), ODQ, 1H- [1,2,4] oxadiazolo [4,3-a] quinoxaline-1-one; L-NAME, N(ω)-nitro-L-arginine methyl ester, apamin, CTX, indomethacin (INDO), Tetraethylammonium (TEA), 4-AP, 4-Aminopyridine (4-AP) please refer to Chapter 2, sections 2.13 Drug formulations and 2.14, General chemicals.

4.3.2 Animals

For detailed experimental design, please refer to Chapter 2, section 2.1 Animals/experimental regimens, subsection 2.1.1 Healthy and atherogenic rabbit model (AEC) project 17/013.

4.3.2.1 Anaesthetisation

For Anaesthetization protocol, please refer to Chapter 2, section 2.3 Anaesthesia and culling, subsection 2.3.1 Rabbit.

4.3.2.2 Dissection

Refer to Chapter 2, section 2.4 Dissection, subsection 2.4.1 Rabbit dissection.

4.3.3 Isometric tension

For Isometric tension, refer to Chapter 2, section 2.6 Isometric tension. The following variations have been applied to the general method. The only drug incubations relevant to this chapter specified from chapter 2, section 2.6, subsection 2.6.1 Rabbit drug incubations are 1. BX (10^{-8} to 10^{-5} [M]) at 5-minute intervals) and 2. Vehicle (serially diluted DMSO) (10^{-8} to 10^{-5} [M]) at 5-minute intervals). For specific drugs used and their concentrations, please refer to table 4.1.

Table 4.1. Drugs used to assess BX-induced vasodilation, with vessel type used, dosage and mechanism of action.

Vessel Type	Drug	Final Conc	Mechanism
TA/ILA/MA	ODQ	10 ^{-5.0} [M]	NO stimulated sGC inhibitor
	L-NAME	10 ^{-3.0} [M]	eNOS activation inhibitor
ILA/MA	CTX	10 ^{-8.0} [M]	KCa channel inhibitor
	TEA	10 ^{-8.0} [M]	Non-selective K ⁺ channel inhibitor
	Apamin	10 ^{-8.0} [M]	KCa channel inhibitor
	4-AP	10 ^{-6.0} [M]	Voltage-gated K ⁺ channels inhibitor
	Indomethacin	10 ^{-6.0} [M]	COX 1 and 2 Inhibitor

Abbreviations: 4-AP, 4-Aminopyridine; Ca²⁺, Calcium; CTX, Charybdotoxin; COX, cyclooxygenase; Conc, concentration; L-NAME, N(ω)-nitro-L-arginine methyl ester; [M], Molar; ODQ, 1H- [1,2,4] oxadiazolo [4,3-a] quinoxaline-1-one; K⁺, Potassium; TEA, Tetraethylammonium.

4.3.4 Data/Statistical Analysis

Statistical analyses are detailed in Chapter 2: General methods section 2.12. For analysis of variance (ANOVA) details, to section 2.12.1 and for information on effect (*Cohen's d*) analysis, please refer to section 2.12.2. For effect (*Cohen's d*), values are compared to BX CD (control diet group). Positive *d* values indicate a reduction compared to BX, and negative values represent an increase compared to BX.

4.4 Results

4.4.1 BX-induced vasodilation is vessel specific.

Various vessels were excised from CD or AD-fed white New Zealand rabbits to determine the vasodilatory potential of BX. To identify vessel specificity, thoracic aorta, interlobar arteries, and mesenteric arteries were assessed through DRC analysis using isometric tension to cumulative doses of BX (10⁻⁸ to 10⁻⁵ [M]). Results demonstrated that CD, interlobar, and mesenteric arteries had increased relaxation compared to thoracic aorta vessels; however, they had no significant difference from each other (figure 4.1C). The BX group enhanced interlobar arteries relaxation compared to thoracic aorta at doses 10^{-6.5}, 10⁻⁶, 10^{-5.5} and 10⁻⁵ [M]. Additionally, the BX group increased mesenteric artery relaxation compared to thoracic aorta at doses 10^{-5.5} and 10⁻⁵ [M]. Area under the curve (AUC) analysis (figure 4.1D) supports the results obtained in (figure 4.1A) that demonstrated interlobar arteries had an increased relaxation compared

to thoracic aorta (55.0 ± 11.1 vs 16.7 ± 4.2 %; $p < 0.05$) and mesenteric arteries (78.5 ± 13.9 vs 16.7 ± 4.2 %; $p < 0.001$), (figure 4.1B). Interlobar and mesenteric arteries had no significant difference from each other in AUC. For statistically significant p values and effect size (*Cohen's d*) values obtained for each dose, please refer to table 4.2.

Vessel specificity

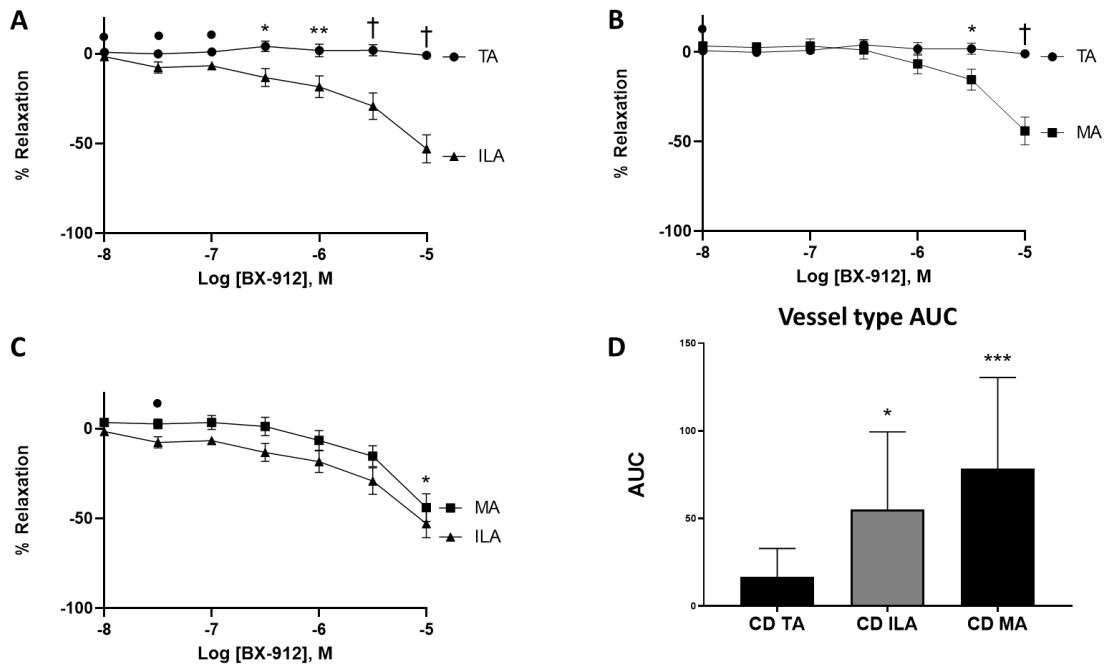


Figure 4.1. BX directly induces vascular relaxation in mesenteric and interlobar arteries but not in thoracic aorta ($n=15$). **A.** TA vs. ILA, **B.** TA vs. MA, **C.** ILA vs. MA, and **D.** AUC of the three vessel types used in the study. All data is represented as Mean \pm SEM, and statistical analysis was performed using a one-way ANOVA followed by a Dunnett's post hoc test. * ($p < 0.05$), ** ($p < 0.01$), *** ($p < 0.001$), † ($p < 0.0001$). Effect size (d) and Cohen's d values are taken as * $d=0.2-0.5$ (small effect), ** $d=0.5-0.8$ (medium effect), and *** $d \geq 0.8$ (large effect). **Abbreviations:** AUC, area under the curve; CD, control diet; DRC, dose-response curve; ILA, interlobar artery; MA, mesenteric artery; [M], Molar; n , sample size; TA, thoracic aorta.

Table 4.2. Table of significance comparing relaxation responses of BX from doses (10^{-8} to 10^{-5} [M]) in CD thoracic aorta, interlobar arteries, and mesenteric arteries.

BX Conc [M]	TA vs. ILA	TA vs. MA	ILA vs. MA
10^{-8}	d= 0.24	d= -0.32	p=ns
$10^{-7.5}$	d= 0.35	p=ns	d= -0.24
10^{-7}	d= 0.33	p=ns	d= -0.31
$10^{-6.5}$	p= 0.02	p=ns	d= -0.21
10^{-6}	p= 0.01	p=ns	p=ns
$10^{-5.5}$	p<0.0001	p= 0.02	p=ns
10^{-5}	P<0.0001	p<0.0001	p=ns

Statistical significance is taken at ($p<0.05$), and effect size (d) and Cohen's d values are taken as $d=0.2-<0.5$ (small effect), $d=0.5-<0.8$ (medium effect), and $d=\geq 0.8$ (large effect). **Abbreviations:** Conc, concentration; CD, control diet; d , Cohen's d ; ILA, interlobar artery; MA, mesenteric artery; [M], Molar; n , sample size; $p=ns$, non-significant; TA, thoracic aorta.

4.4.2 An AD does not reduce BX-induced relaxation.

BX has been pre-clinically evaluated in the treatment of a variety of conditions and diseases. However, its relaxation of vascular smooth muscle cells (VSMC) as a target for asthma treatment led us to elucidate its vasodilatory capabilities further and, additionally, its vessel specificity. Thoracic aorta, interlobar arteries, and mesenteric arteries obtained from white New Zealand male rabbits were isolated and subjected to cumulative dose-response curves of BX (10^{-8} to 10^{-5} [M]) dissolved in DMSO. Firstly, vessels were compared to their vehicle (cumulative doses of serially diluted DMSO). Results showed that the BX group had a small effect (Cohen's d) in thoracic aorta $d=0.32$ compared to the vehicle group at 10^{-5} [M], (figure 4.2A). The BX group had a significant effect on vasodilation compared to the vehicle group in interlobar arteries at dose 10^{-5} [M] (-53.0 ± 7.8 vs -4.3 ± 4.7 %; $p<0.0001$), (figure 4.2C) and mesenteric arteries at dose 10^{-5} [M] (-43.9 ± 7.8 vs -14.8 ± 7.2 %; $p<0.05$), (figure 4.2E). A small effect (Cohen's d) in AUC was observed in thoracic aorta and interlobar arteries, $d=0.24$ $d=-0.43$, (figure 4.2G and I) however, no effect (Cohen's d) was observed in mesenteric arteries, (figure 4.2K). After establishing the effect of the BX group compared to the vehicle group in healthy vessels, the relaxation effects were assessed in vessels from the AD group to determine its impact in a diseased setting. Vessels were extracted from rabbits given a 4-week atherogenic diet to induce vascular dysfunction

[114]. This showed that an atherogenic environment did not affect BX-induced relaxation or AUC analysis in thoracic aorta, (figures 4.2B and H) or interlobar arteries, (figures 4.2D and J). However, the BX group enhanced relaxation in AD compared to a CD in mesenteric arteries at doses 10^{-7} , $10^{-6.5}$, 10^{-6} , $10^{-5.5}$ and 10^{-5} [M]. This was supported by (figure 4.2I), which showed that the BX group enhanced AUC in an AD compared to CD in mesenteric arteries (-249.2 ± 51.7 vs 78.5 ± 13.9 %; $p < 0.01$). For statistically significant p values and effect size (*Cohen's d*) values obtained for each dose, please refer to table 4.3.

Table 4.3. BX vs. vehicle in the thoracic aorta and interlobar and mesenteric arteries and CD vs. AD in the thoracic aorta and interlobar and mesenteric arteries p values and Cohen's d values.

BX Conc [M]	BX vs Vehicle			CD vs AD		
	TA	IL	MA	TA	IL	MA
10^{-8}	p=ns	p=ns	p=ns	d=0.48	p=ns	d=0.42
$10^{-7.5}$	d=0.24	d=0.33	d=-0.66	p=ns	p=ns	d=0.61
10^{-7}	d=0.23	d=0.37	p=ns	p=ns	p=ns	p=0.02
$10^{-6.5}$	p=ns	d=0.35	p=ns	p=ns	p=ns	p=0.0004
10^{-6}	p=ns	d=0.42	p=ns	p=ns	p=ns	p=0.0002
$10^{-5.5}$	p=ns	d=0.49	p=ns	p=ns	p=ns	p<0.0001
10^{-5}	d=0.32	p<0.0001	p=0.04	p=ns	p=ns	p=0.0005

Statistical significance is taken at ($p < 0.05$), and effect size (d) and Cohen's d values are taken as $d = 0.2 - < 0.5$ (small effect), $d = 0.5 - < 0.8$ (medium effect), and $d = \geq 0.8$ (large effect).

Abbreviations: AD, atherogenic diet; Conc, concentration; CD, control diet; d , Cohen's d ; ILA, interlobar artery; MA, mesenteric artery; [M], Molar; n , sample size; $p = ns$, non-significant; TA, thoracic aorta.

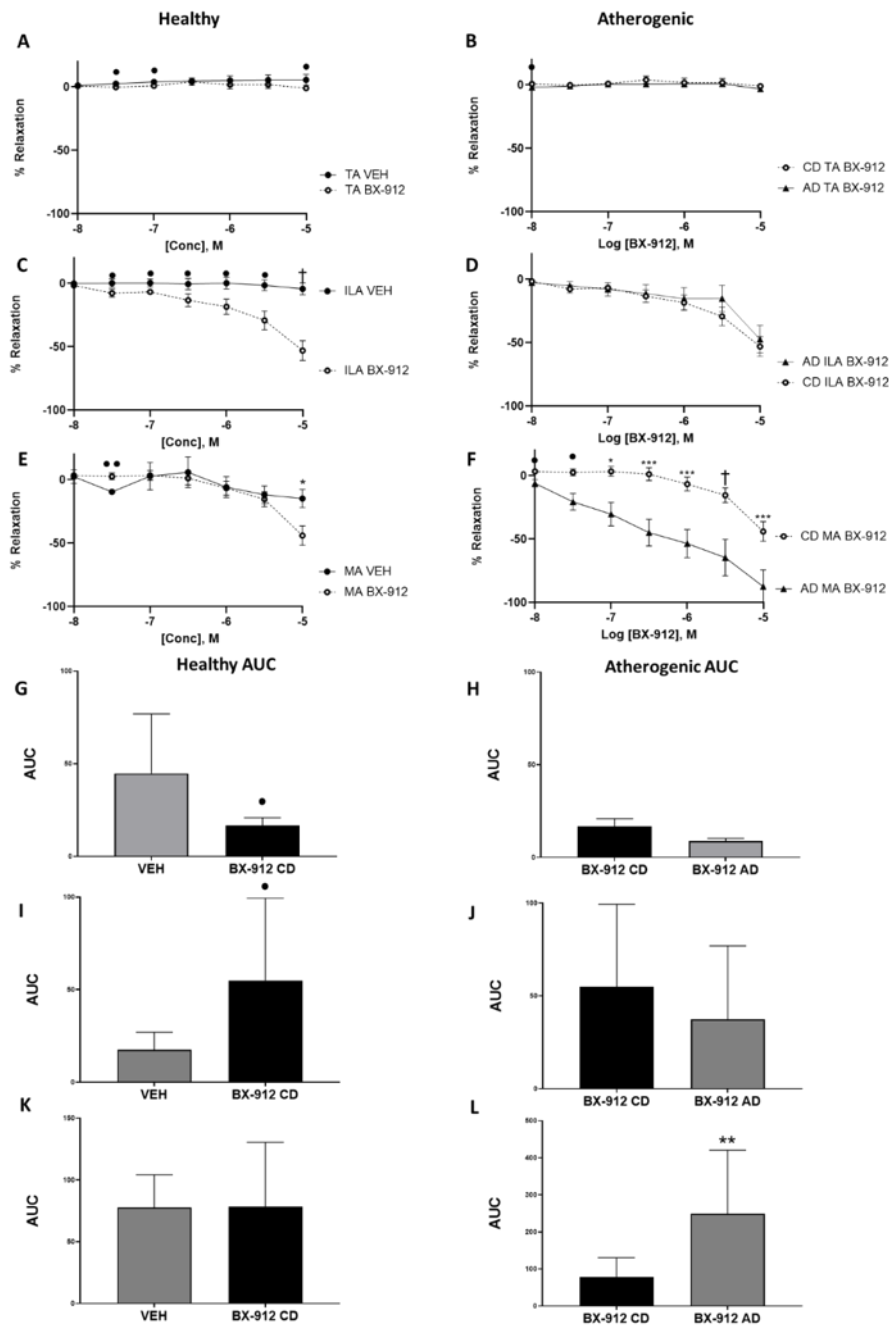


Figure 4.2. BX dose-response curves and AUC graphs of vehicle vs BX and BX CD vs AD in thoracic aorta, interlobar and mesenteric arteries isolated from male, white New Zealand rabbits ($n=4-15$). Comparative graphs of dose-response curves to either BX (10^{-8} to 10^{-5} [M]) or its vehicle (DMSO 10^{-8} to 10^{-5} [M]) in various vessel types are shown in images A, E, and I: CD vs vehicle DRC; A. TA, C. ILA, and E. MA. The effect of BX on vasodilation was further assessed in an AD: CD vs AD DRC; B. TA, D. ILA, and F. MA. AUC graphs that correlate with either CD vs vehicle; G. TA, I. ILA, and K. MA, or CD vs AD; H. TA, J. ILA, and L. MA. All data is represented as mean \pm standard error of the mean (SEM), and statistical analysis was performed using a one-way ANOVA followed by a Dunnett's post hoc test. * ($p < 0.05$), ** ($p < 0.01$), *** ($p < 0.001$), † ($p < 0.0001$). Effect size (d) and Cohen's d values are taken as • $d=0.2-0.5$ (small effect), ** $d=0.5-0.8$ (medium effect), and *** $d \geq 0.8$ (large effect). **Abbreviations:** AD, atherogenic diet; AUC, area under the curve; CD, control diet; ILA, interlobar artery; MA, mesenteric artery; [M], Molar; n , sample size; TA, thoracic aorta; VEH, vehicle.

Table 4.4. Log EC₅₀ and AUC for CD and AD-fed rabbit interlobar and mesenteric arteries (Denuded, ODQ, L-NAME or KPSS vs BX).

<i>ILA – BX DRC</i>	<i>n</i>	<i>Log EC₅₀ ± SEM</i>	<i>p vs BX</i>	<i>d vs BX</i>	<i>AUC ± SEM</i>	<i>p vs BX</i>	<i>d vs BX</i>
(CD) BX	15	-5.9 ± 0.1			55.0 ± 11.1		
(CD) Denuded	8	-5.9 ± 0.1	p=ns	-	44.4 ± 8.2	p=ns	-
(CD) ODQ	10	-6.1 ± 0.2	p=ns	-	54.9 ± 16.3	p=ns	-
(CD) L-NAME	7	-6.0 ± 0.2	p=ns	-	67.1 ± 25.9	p=ns	-
(CD) KPSS	13	-6.2 ± 0.1	p=ns	-	27.2 ± 5.0	p= 0.04	-
(AD) BX	5	-5.6 ± 0.2			37.4 ± 16.2		
(AD) Denuded	5	-5.9 ± 0.1	p=ns	-	35.3 ± 5.1	p=ns	-
(AD) ODQ	5	-5.6 ± 0.1	p=ns	-	11.6 ± 3.6	p=ns	<i>d= 0.29</i>
(AD) L-NAME	5	-5.6 ± 0.1	p=ns	-	37.2 ± 13.2	p=ns	-
(AD) KPSS	4	-6.3 ± 0.1	p= 0.002	-	27.3 ± 5.0	p=ns	-
<i>MA – BX DRC</i>	<i>n</i>	<i>Log EC₅₀ ± SEM</i>	<i>p vs BX</i>	<i>d vs BX</i>	<i>AUC ± SEM</i>	<i>p vs BX</i>	<i>d vs BX</i>
(CD) BX	14	-5.7 ± 0.1			78.5 ± 13.9		
(CD) Denuded	8	-5.6 ± 0.1	p=ns	-	101.3 ± 17.4	p=ns	-
(CD) ODQ	14	-5.7 ± 0.2	p=ns	-	96.6 ± 22.6	p=ns	-
(CD) L-NAME	13	-5.8 ± 0.1	p=ns	-	112.9 ± 17.0	p=ns	-
(CD) KPSS	10	-6.1 ± 0.3	p=ns	-	60.7 ± 8.9	p=ns	-
(AD) BX	10	-6.2 ± 0.2			249.2 ± 51.7		
(AD) Denuded	6	-6.1 ± 0.2	p=ns	-	191.0 ± 40.7	p=ns	-
(AD) ODQ	7	-5.8 ± 0.1	p=ns	-	139.1 ± 36.07	n/s	<i>d= 0.20</i>
(AD) L-NAME	8	-5.9 ± 0.2	p=ns	-	147.6 ± 38.48	p=ns	-
(AD) KPSS	9	-5.6 ± 0.1	p= 0.0099	<i>d= -0.20</i>	66.57 ± 12.61	p= 0.0051	<i>d= 0.34</i>

All data is represented as Mean ± standard error of the mean (SEM), and statistical analysis was performed using a Two-way ANOVA followed by a Dunnett's post hoc test. Statistical significance is taken at ($p < 0.05$), and effect size (d) and Cohen's d values are taken as $d = 0.2 - < 0.5$ (small effect), $d = 0.5 - < 0.8$ (medium effect), and $d = \geq 0.8$ (large effect). Abbreviations: AUC, area under the curve; CD, control diet; AD, atherogenic diet; ILA, interlobar artery; MA, mesenteric artery; DEN, denuded; ODQ; L-NAME, L-NG-Nitroarginine methyl ester and KPSS, potassium physiological salt solution.

4.4.3 BX Mechanistic Analysis

Given that BX has, as far as our knowledge, not been used in the context of vascular function in published literature, it was essential to investigate the molecular mechanism of action. Several pathways were assessed to identify the mechanism of action of BX, including endothelial-dependent relaxation, determined by mechanical denudation of vascular endothelial cells. Additional endothelial mechanisms evaluated were through inhibition of eNOS induced by incubation with L-NAME. ODQ was used to inhibit sGC in VSMC. KPSS was used to pre-constrict vessels to non-selectively inhibit K⁺ channels.

Further, specific K⁺ channel inhibitors were used to identify if BX-induced vasodilation is actioned via a specific channel. CTX and APA were used to inhibit Ca²⁺ activated K⁺ channels (KCa) inhibitor, TEA was used to non-selectively inhibit K⁺ channels, and 4-AP was used to inhibit voltage-gated K⁺ channels inhibitor. Finally, INDO was used to inhibit COX-2; (figure 4.3) is a schematic representation of the pathways each drug inhibits.

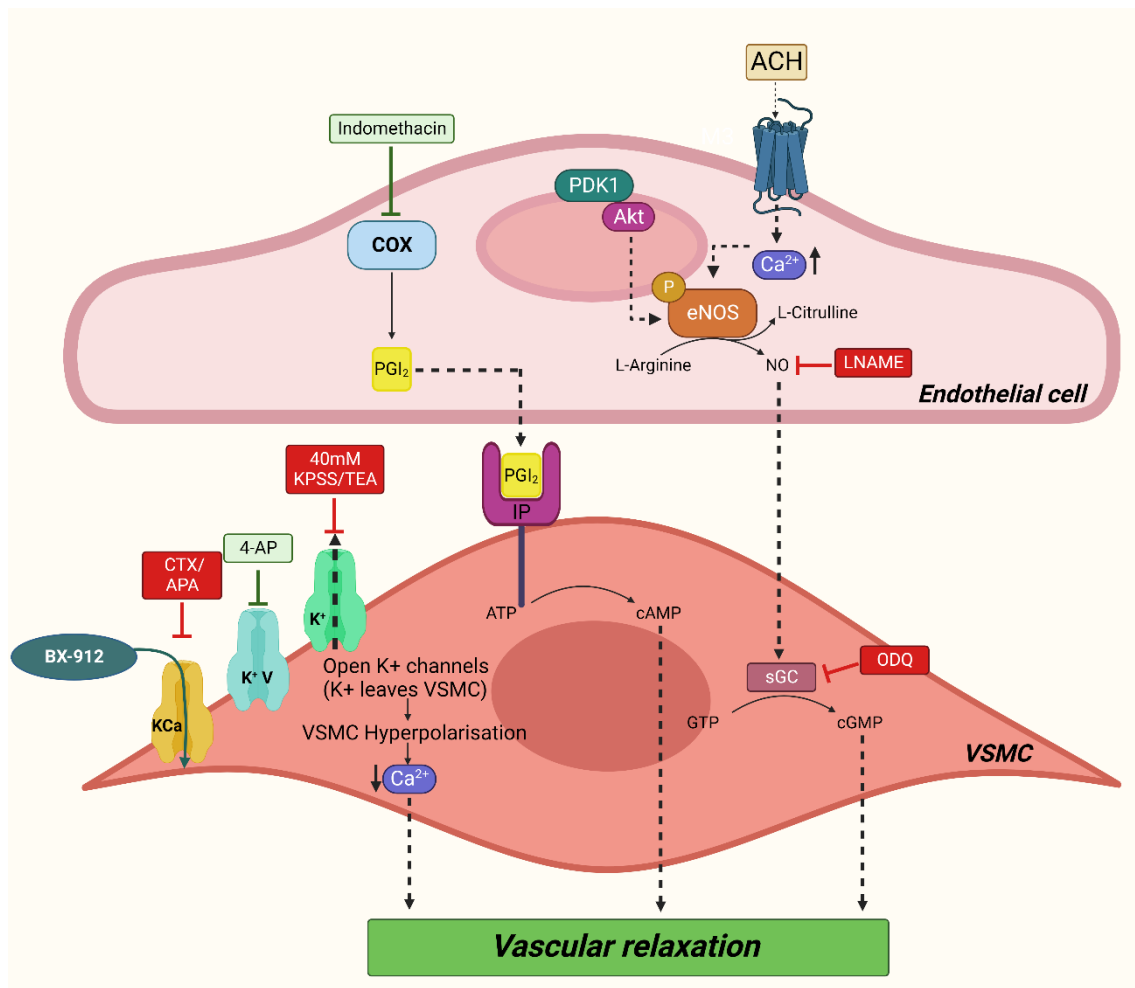


Figure 4.3. Graphical illustration of targeted pathways by each drug used to identify the signalling cascade BX uses to induce vascular relaxation. Inhibitory drugs were administered prior to a cumulative DRC to BX. This diagram demonstrates the inhibited component and how it relates to the overall relaxation response and the known role of PDK1 on the PDK1/Akt/eNOS/NO pathway. **Abbreviations.** 4-AP, 4-aminopyridine; ACH, acetylcholine; APA, apamin; ATP, adenosine triphosphate; Ca^{2+} , calcium, cAMP, cyclic adenosine monophosphate; cGMP, cyclic guanosine monophosphate; COX, cyclooxygenase; CTX, charybdotoxin; eNOS, endothelial nitric oxide synthase; GTP, guanosine 5'-triphosphate; IP, prostaglandin I2 receptor; KPSS, potassium physiological salt solution; L-NAME, N(ω)-nitro-L-arginine methyl ester; NO, nitric oxide; ODO, 1H- [1,2,4] oxadiazolo [4,3-a] quinoxaline-1-one; PDK1, Phosphoinositide-dependent Kinase-1; PGI, prostaglandin I2; sGC, soluble guanylyl cyclase; TEA, tetraethylammonium and VSMC, vascular smooth muscle cell. This diagram was adapted from [114]. Created with BioRender.com.

4.4.3.1 Effects of mechanical denudation on BX-induced relaxation.

Vessels were subjected to mechanical denudation to remove endothelial cells from the vascular lumen to identify if BX-induced vasodilation was endothelial-dependent. Results showed that mechanical denudation had no significant effect on BX-induced relaxation compared to the BX group at any dose in CD thoracic aorta vessels and CD of interlobar arteries. Interlobar arteries showed no shift in LogEC₅₀ nor statistical significance in AUC in the denuded (DEN) group of interlobar arteries compared to the BX group in either a CD or AD. The statistical significance showed that in the DEN group in CD mesenteric arteries, relaxation was enhanced compared to the BX group at dose 10⁻⁵ [M] (-68.2 ± 12.6 vs -43.9 ± 7.8 %; *p*<0.05), (figure 4.4). An AD did not affect BX-induced relaxation in the presence of mechanical denudation, supported by no significance observed in LogEC₅₀ or AUC, as illustrated in table 4.4E.

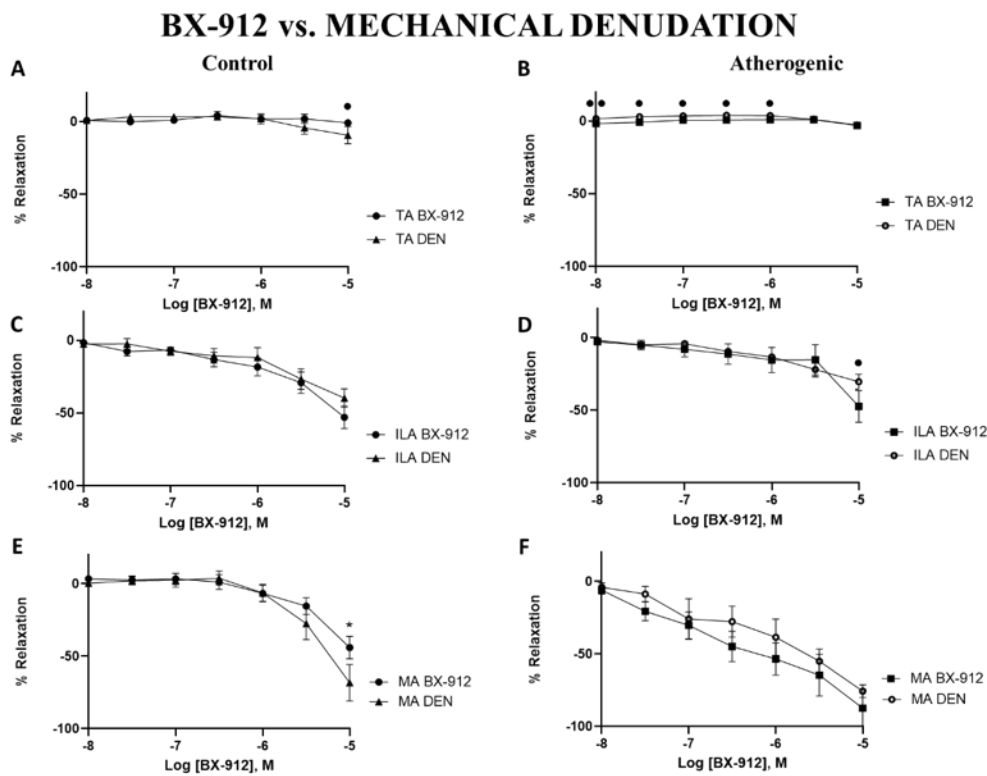


Figure 4.4. Mechanistic evaluation of endothelial dependency via mechanical denudation on BX-induced vasodilation (n=4-15). A, C and E represent mechanical denudation prior to a cumulative DRC to BX in DEN vs. BX vessels, A. TA, C. ILA, and E. MA represent mechanical denudation prior to a cumulative DRC to BX in CD and B. TA, D. ILA, and F. MA represent the response to DEN vs. BX in an AD. All data is represented as Mean ± SEM, and statistical analysis was performed using a one-way ANOVA followed by a Dunnett's post hoc test. * (*p*<0.05), **(*p*<0.01), *** (*p*<0.001), † (*p*<0.0001). Effect size (*d*) and Cohen's *d* values are taken as •*d*=0.2-0.5 (small effect), ••*d*=0.5-0.8 (medium effect), and •••*d*≥0.8 (large effect).

Abbreviations: AD, atherogenic diet; CD, control diet; DEN, denuded; ILA, interlobar artery; MA, mesenteric artery; [M], Molar; n, sample size; TA, thoracic aorta.

4.4.3.2 Effect of L-NAME to assess eNOS dependency on BX-induced vasodilation.

To understand if BX-induced vasodilation was eNOS dependent, following pre-constriction, the vessel was incubated with $10^{-3.0}$ [M] L-NAME to inhibit eNOS and the subsequent production of NO. The L-NAME group had a significant effect on enhancing relaxation compared to the BX group in CD thoracic aorta at doses $10^{-5.5}$ [M] (-8.6 ± 2.5 vs 2.0 ± 3.1 %; $p < 0.05$) and 10^{-5} [M] (-14.5 ± 3.9 vs -0.8 ± 2.2 %; $p < 0.01$) as illustrated in (figure 4.5A). Analysis showed that a medium effect (*Cohen's d*) was observed in enhancing relaxation in the L-NAME group of AD thoracic aorta compared to the BX group at doses $10^{-5.5}$ [M] (-4.0 ± 1.0 vs 0.9 ± 1.7 %; $d = 0.59$) and 10^{-5} [M] (-9.2 ± 1.4 vs -3.1 ± 1.9 %; $d = 0.67$), (figure 4.5B). The L-NAME group did not affect relaxation compared to the BX group in CD interlobar and mesenteric arteries, (figure 4.5C and D). L-NAME in an AD had an effect (*Cohen's d*) in both interlobar and mesenteric arteries. The L-NAME group inhibited relaxation compared to the BX group in interlobar arteries, and a small effect (*Cohen's d*) was observed at 10^{-8} $d = -0.39$, $10^{-7.5}$ $d = -0.42$, 10^{-7} $d = -0.41$, $10^{-6.5}$ $d = -0.34$, 10^{-6} $d = -0.34$ and 10^{-5} [M] $d = -0.33$, (figure 4.5D). These same results were observed in mesenteric arteries at doses $10^{-7.5}$ $d = -0.21$, 10^{-7} $d = -0.27$, $10^{-6.5}$ $d = -0.33$ and 10^{-6} [M] $d = -0.32$, (figure 4.5F).

BX-912 vs. L-NAME

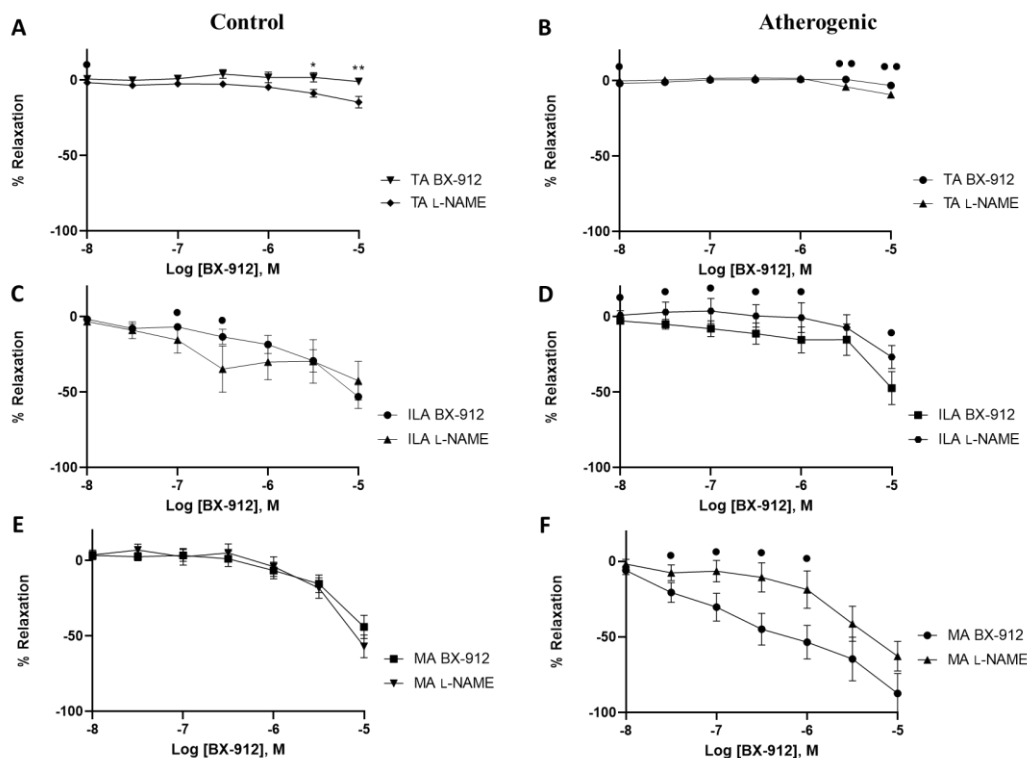


Figure 4.5. Mechanistic evaluation of BX-induced vasodilation in the presence of eNOS-inhibition, L-NAME (n=5-15). A, C and E represent L-NAME inhibition prior to a cumulative DRC to BX in L-NAME vs. BX vessels. A. TA, C. ILA, and E. MA represent L-NAME inhibition prior to a cumulative DRC to BX in CD and B. TA, D. ILA, and F. MA represent the response to L-NAME vs BX in an AD. All data is represented as Mean \pm SEM, and statistical analysis was performed using a one-way ANOVA followed by a Dunnett's post hoc test. * ($p < 0.05$), ** ($p < 0.01$), *** ($p < 0.001$), † ($p < 0.0001$). Effect size (d) and Cohen's d values are taken as • $d = 0.2-0.5$ (small effect), ** $d = 0.5-0.8$ (medium effect), and *** $d \geq 0.8$ (large effect). **Abbreviations:** AD, atherogenic diet; CD, control diet; ILA, interlobar artery; L-NAME, L-NG-Nitroarginine Methyl Ester; MA, mesenteric artery; [M], Molar; n, sample size; TA, thoracic aorta.

4.4.3.3 ODQ pre-incubation has a slight effect on reducing BX-induced relaxation.

ODQ was used to inhibit NO-stimulated sGC-induced vasodilation. In interlobar arteries, the ODQ group reduced vasodilation compared to the BX group in both a CD at 10^{-5} [M] (-24.9 ± 14.2 vs -53.0 ± 7.8 %; $p < 0.05$), (figure 4.6C) and AD at 10^{-5} [M] (-20.0 ± 8.1 vs -47.2 ± 10.9 %; $p < 0.05$), (figure 4.6D). Surprisingly, the ODQ group did not affect vasodilation in mesenteric arteries in a CD compared to the BX group, (figure 4.6E); however, in mesenteric arteries from AD, the ODQ group reduced vasodilation compared to the BX group at doses $10^{-6.5}$ [M] (-4.5 ± 5.6 vs -44.9 ± 10.6 %; $p < 0.05$) and 10^{-6} [M] (-0.8 ± 10.3 vs -53.5 ± 11.1 %; $p < 0.05$), (figure 4.6E and F). Additionally, in

mesenteric arteries, the ODQ group did not affect LogEC₅₀, or AUC, compared to the BX group in either a CD or AD, table 4.4.

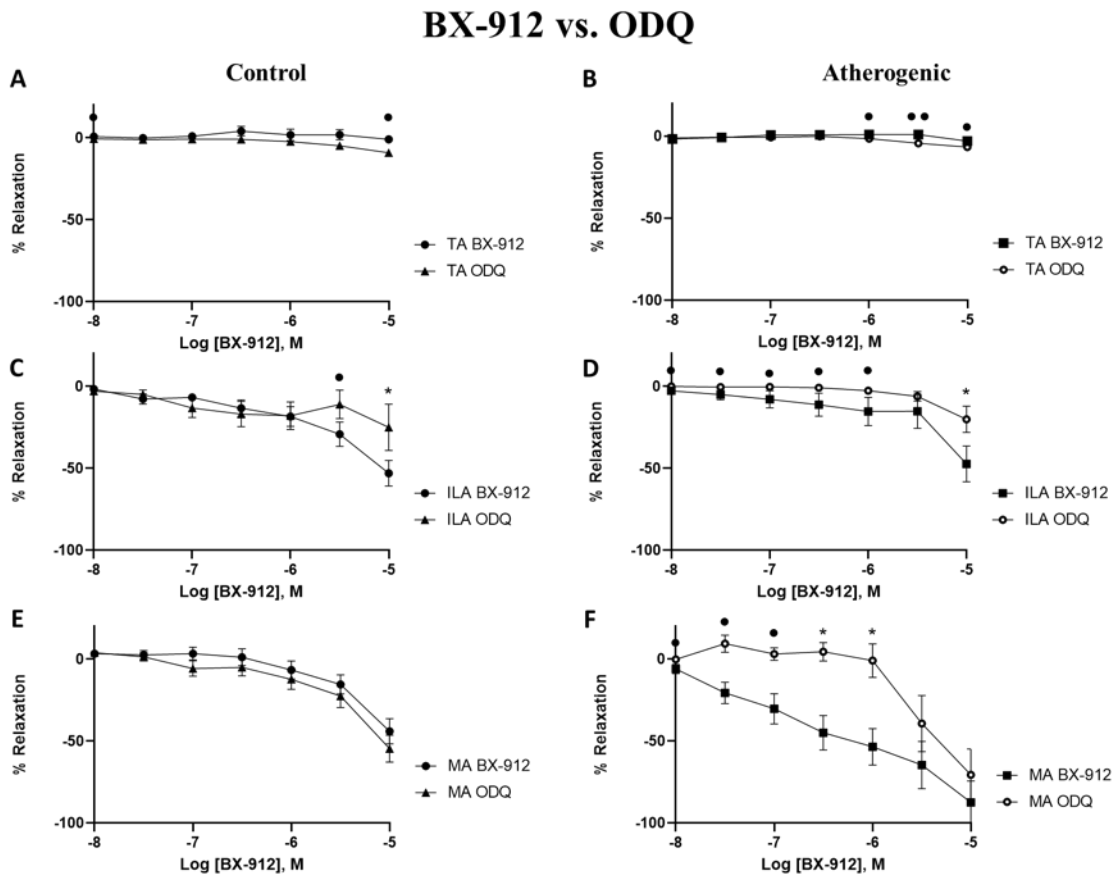


Figure 4.6. BX dose-response curve graphs of CD and AD, thoracic aorta, interlobar arteries, and mesenteric arteries incubated with ODQ ($n=5-15$). A. TA, C. ILA, and E. MA represent ODQ inhibition prior to a cumulative DRC to BX in CD and B. TA, D. ILA, and F. MA represent the response to ODQ vs BX in an AD. MA. All data is represented as Mean \pm SEM, and statistical analysis was performed using a one-way ANOVA followed by a Dunnett's post hoc test. * ($p<0.05$), **($p<0.01$), *** ($p<0.001$), † ($p<0.0001$). Effect size (d) and Cohen's d values are taken as • $d=0.2-0.5$ (small effect), •• $d=0.5-0.8$ (medium effect), and ••• $d\geq 0.8$ (large effect). **Abbreviations:** AD, atherogenic diet; CD, control diet; ILA, interlobar artery; MA, mesenteric artery; [M], Molar; n , sample size; ODQ, 1H- [1,2,4] oxadiazolo [4,3-a] quinoxaline-1-one; TA, thoracic aorta.

4.4.3.4 KPSS Inhibits the vasodilatory effects of BX in ILA and mesenteric arteries.

Vascular KPSS pre-incubation followed by a DRC is used to identify non-specific K⁺ channel-dependent relaxation, (figure 4.7). Thoracic aorta, interlobar, and mesenteric arteries were pre-constricted with 40mM KPSS prior to a cumulative DRC to BX (10^{-8} to 10^{-5} [M]). The KPSS group did not affect relaxation in CD of thoracic aorta compared to the BX group; however, KPSS enhanced relaxation in thoracic aorta compared to the BX group in an AD at dose 10^{-5} [M], (figure 4.7B). In CD of interlobar arteries, the KPSS group induced no shift in LogEC₅₀ compared to the BX group, table 4.4. Despite this, KPSS inhibited BX-induced vasodilation compared to the BX group at doses 10^{-6} , $10^{-5.5}$ and at 10^{-5} [M], (figure 4.7C). The KPSS group reduced AUC compared to the BX group (27.2 ± 5.0 vs 55.0 ± 11.1 %, $p < 0.05$). Interestingly, an AD relaxation was only suppressed in the KPSS group of interlobar arteries at dose 10^{-5} [M], (figure 4.7D); an AD in interlobar arteries induced a shift in LogEC₅₀ in KPSS-treated vessels that were not observed in the CD, table 4.4. In mesenteric arteries, KPSS inhibited relaxation in a CD at doses 10^{-6} , $10^{-5.5}$ and 10^{-5} [M] compared to the BX group, (figure 4.7E). The inhibitory effect of KPSS was observed at additional doses in an AD of mesenteric arteries 10^{-7} , $10^{-6.5}$, 10^{-6} , $10^{-5.5}$ and 10^{-5} [M] compared to the BX group, (figure 4.7F). KPSS also reduced AUC compared to the BX group (66.6 ± 12.6 vs 249.2 ± 51.7 %, $p < 0.05$) and caused a shift in LogEC₅₀ (-5.6 ± 0.1 vs -6.2 ± 0.18 %, $p < 0.01$). For statistically significant p values and effect size (*Cohen's d*) values obtained for each dose, please refer to table 4.5.

BX-912 vs. 40mM KPSS

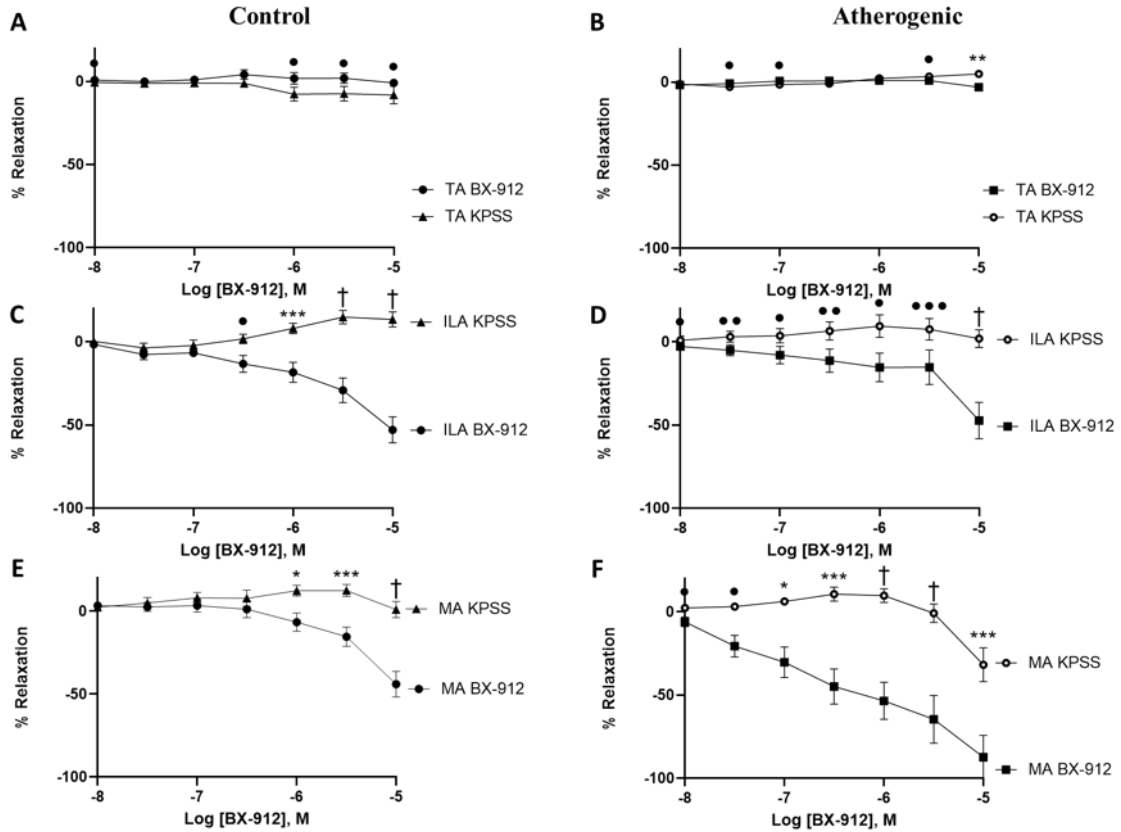


Figure 4.7. BX dose-response curve graphs of CD and AD, thoracic aorta, interlobar arteries, and mesenteric arteries pre-constricted with 40mM KPSS, (n=4-15). A, TA, C, ILA, and E. MA represent 40mM pre-constricted vessels prior to a cumulative DRC to BX in CD and B, TA, D, ILA, and F, MA represent the response to 40mM KPSS vs BX in an AD. All data is represented as Mean \pm SEM, and statistical analysis was performed using a one-way ANOVA followed by a Dunnett's post hoc test. * ($p < 0.05$), ** ($p < 0.01$), *** ($p < 0.001$), † ($p < 0.0001$). Effect size (d) and Cohen's d values are taken as * $d = 0.2-0.5$ (small effect), ** $d = 0.5-0.8$ (medium effect), and *** $d \geq 0.8$ (large effect). **Abbreviations:** AD, atherogenic diet; CD, control diet; ILA, interlobar artery; KPSS, potassium physiological salt solution; MA, mesenteric artery; [M], Molar; n, sample size; TA, thoracic aorta.

Table 4.5. The effect of KPSS inhibited K⁺ channels on BX mediated relaxation in CD/AD of thoracic aorta, interlobar arteries and mesenteric arteries.

BX-912 [M]	Conc	CD (LKB1 vs 40 [mM] KPSS)			AD (LKB1 vs 40 [mM] KPSS)		
		TA	ILA	MA	TA	ILA	MA
10 ⁻⁸		d= 0.26	p=ns	p=ns	p=ns	d= -0.45	d= -0.31
10 ^{-7.5}		p=ns	p=ns	p=ns	d= 0.24	d= -0.53	d= -0.38
10 ⁻⁷		p=ns	p=ns	p=ns	d= 0.27	d= -0.48	p= 0.041
10 ^{-6.5}		p=ns	d= -0.22	p=ns	p=ns	d= -0.55	p= 0.002
10 ⁻⁶		d= 0.20	p= 0.0006	p= 0.0483	p=ns	d= -0.39	p <0.0001
10 ^{-5.5}		d= 0.21	p <0.0001	p= 0.0004	d= -0.25	d= -0.82	p <0.0001
10 ⁻⁵		d= 0.23	p <0.0001	p <0.0001	p= 0.008	p <0.0001	p =0.001

Statistical significance is taken at ($p < 0.05$), and effect size (d) and Cohen's d values are taken as $d = 0.2 - < 0.5$ (small effect), $d = 0.5 - < 0.8$ (medium effect), and $d = \geq 0.8$ (large effect).

Abbreviations: AD, atherogenic diet; Conc, concentration; CD, control diet; d , Cohen's d ; ILA, interlobar artery; KPSS, potassium physiological salt solution; MA, mesenteric artery; [M], Molar; n , sample size; $p = ns$, non-significant; TA, thoracic aorta.

4.4.3.5 K⁺ channel Inhibitor effect on BX-induced relaxation

Given the inhibitory effects of KPSS in both interlobar and mesenteric arteries in response to cumulative doses of BX represented in (figure 4.8). Identification of the specific K⁺ channel involved in BX induced vasodilation was important to understand the signalling cascade. Multiple drug inhibitions to block specific K⁺ channel pathways were used. CTX and Apamin were used to inhibit K_{Ca} channels, TEA was used to non-selectively inhibit K⁺ channels, and 4-AP was used to inhibit voltage-gated K⁺ channels. The results of interlobar artery drug incubations are shown in (figure 4.8). Results demonstrated that the CTX group significantly reduced relaxation compared to the BX group at doses 10^{-6.5}, 10⁻⁶, 10^{-5.5} and 10⁻⁵ [M], (figure 4.8A). Incubation with APA enhanced BX-induced relaxation at dose 10⁻⁵ [M] (-87.8 ± 2.4 vs -53.0 ± 7.8 %, $p < 0.01$), (figure 4.8C). Pre-incubation with TEA and 4-AP had no significant effect on relaxation compared to the BX group, (figure 4.8B and C).

Control ILA

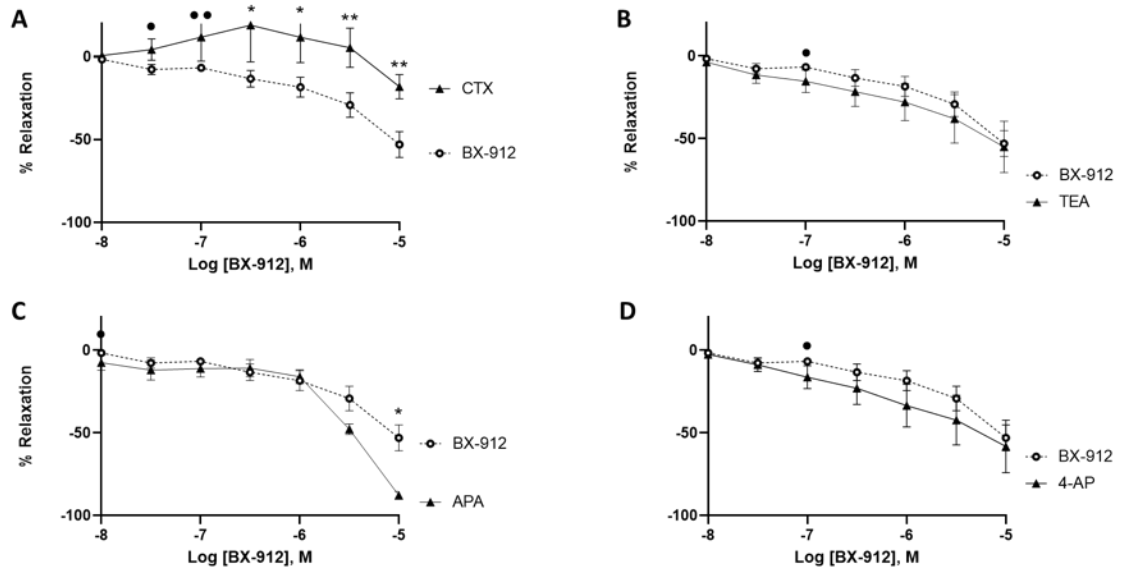


Figure 4.8. BX dose-response curve graphs of CD, interlobar arteries pre-incubated with various K⁺ channel inhibitors (n=3-15). Vessels were pre-incubated with **A.** CTX, **B.** TEA, **C.** APA, or **D.** 4-AP. All data is represented as Mean ± SEM, and statistical analysis was performed using a one-way ANOVA followed by a Dunnett's post hoc test. * (p<0.05), ** (p<0.01), *** (p<0.001), † (p<0.0001). Effect size (d) and Cohen's d values are taken as •d=0.2-0.5 (small effect), **d=0.5-0.8 (medium effect), and ***d≥0.8 (large effect). **Abbreviations:** 4-AP, 4-Aminopyridine; APA, Apamin; CTX, Charybdotoxin; CD, control diet; ILA, interlobar artery; [M], Molar; n, sample size; TEA, Tetraethylammonium; TA, thoracic aorta.

Table 4.6 Log EC₅₀ and AUC for Inhibition of K⁺ channels of CD-fed rabbit interlobar and mesenteric arteries (CTX, TEA, APA, and 4-AP) followed by a DRC to BX.

ILA– BX DRC	n	Log EC ₅₀ ± SEM	p vs BX	d vs BX	AUC ± SEM	p vs BX	d vs BX
(CD) BX	16	-5.89 ± 0.1			54.96 ± 11.1		
(CD) CTX	3	-5.59 ± 0.1	n/s	-	40.10 ± 28.7	n/s	-
(CD) TEA	3	-6.00 ± 0.2	n/s	-	71.68 ± 27.7	n/s	-
(CD) APA	3	-5.51 ± 0.04	n/s	-	72.56 ± 9.2	n/s	-
(CD) 4-AP	3	-6.12 ± 0.2	n/s	-	77.05 ± 28.9	n/s	-
MA – BX DRC	n	Log EC ₅₀ ± SEM	p vs BX	d vs BX	AUC ± SEM	p vs BX	d vs BX
(CD) BX	14	-5.72 ± 0.1			39.27 ± 6.9		
(CD) CTX	3	-6.50 ± 0.5	n/s	d= 0.49	77.39 ± 37.8	n/s	d= -0.39
(CD) TEA	3	-5.82 ± 0.3	n/s	-	18.72 ± 8.0	n/s	d= 0.22
(CD) APA	3	-6.26 ± 0.4	n/s	d= 0.34	69.75 ± 26.4	n/s	d= -0.32
(CD) 4-AP	3	-6.29 ± 0.5	n/s	d= 0.36	72.04 ± 13.1	n/s	d= -0.35

All data is represented as Mean ± SEM, and statistical analysis was performed using a one-way ANOVA followed by a Dunnett's post hoc test. Statistical significance is taken at (p<0.05), and effect size (d) and Cohen's d values are taken as d=0.2-<0.5 (small effect), d=0.5-<0.8 (medium effect), and d=≥0.8 (large effect). **Abbreviations:** AUC, area under the curve; DRC, dose-response curve; CD, control diet; AD, atherogenic diet; ILA, interlobar artery; MA, mesenteric artery; CTX, charybdotoxin; TEA, tetraethylammonium; APA, apamin; 4-AP, 4-Aminopyridine; Ca²⁺, calcium; n/s, non-significant; n, sample size.

Control MA

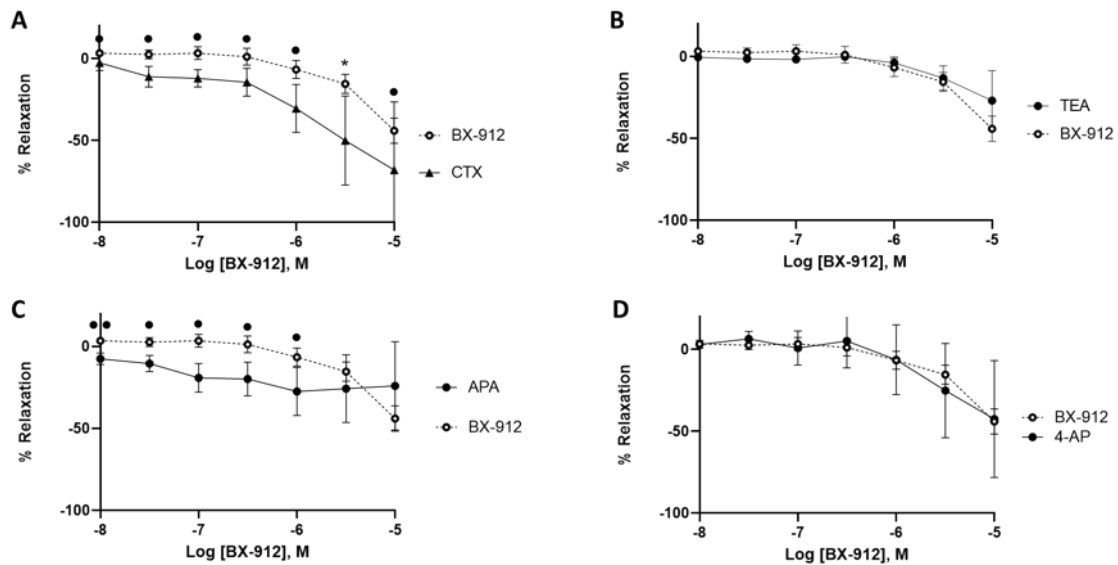


Figure 4.9. BX dose-response curve graphs of CD, mesenteric arteries pre-incubated with various K⁺ channel inhibitors (n=3-15). Vessels were pre-incubated with A. CTX, B. TEA, C. APA, or D. 4-AP. All data is represented as Mean \pm SEM, and statistical analysis was performed using a one-way ANOVA followed by a Dunnett's post hoc test. * ($p < 0.05$), ** ($p < 0.01$), *** ($p < 0.001$), † ($p < 0.0001$). Effect size (d) and Cohen's d values are taken as • $d = 0.2-0.5$ (small effect), •• $d = 0.5-0.8$ (medium effect), and ••• $d \geq 0.8$ (large effect). **Abbreviations:** 4-AP, 4-Aminopyridine; APA, Apamin; CTX, Charybdotoxin; CD, control diet; ILA, interlobar artery; [M], MA, mesenteric artery; Molar; n, sample size; TEA, Tetraethylammonium; TA, thoracic aorta.

In mesenteric arteries incubated with specific K⁺ channel inhibitors, (figure 4.9), the CTX group enhanced relaxation compared to the BX group at dose $10^{-5.5}$ [M] (-14.5 ± 3.9 vs -0.8 ± 2.2 %, $p < 0.01$) and showed a small effect (Cohen's d), at dose $10^{-5.5}$ [M] ($d = 0.22$), (figure 4.9A). In mesenteric arteries, the TEA, APA, and 4-AP groups did not affect relaxation compared to the BX group, (figure 4.9B, C and D). Surprisingly, CTX $d = 0.49$, APA $d = 0.34$ and 4-AP $d = 0.36$ generated a small effect (Cohen's d) on shifting the LogEC₅₀ compared to the BX group. Additionally, the CTX $d = -0.39$, APA $d = -0.32$ and 4-AP $d = -0.35$ groups generated a small effect (Cohen's d) on increasing AUC compared to the BX group, whilst TEA only reduced AUC $d = 0.22$, table 4.6.

4.4.3.6 COX-2 inhibition by indomethacin enhances BX-induced vasodilation.

To determine COX-dependent relaxation, vessels were pre-constricted with Phen (interlobar arteries) and Ciraz (mesenteric arteries) and then further incubated with $10^{-6.0}$ [M] INDO. Results illustrated in (figure 4.10) showed that the INDO group enhanced relaxation in interlobar arteries compared to the BX group at doses $10^{-7.5}$, 10^{-7} , $10^{-6.5}$, 10^{-6} , $10^{-5.5}$ and 10^{-5} [M]. It also caused a shift in LogEC₅₀ (-6.7 ± 0.4 vs -5.9 ± 0.1 %, $p < 0.05$) and elevated AUC (194.1 ± 22.2 vs 55.0 ± 11.1 %, $p < 0.0001$) compared to the BX group. The INDO group did not affect BX-induced relaxation in mesenteric arteries. Surprisingly, the INDO-treated mesenteric arteries induced a significant shift in LogEC₅₀ compared to the BX group, despite a lack of effect at each BX dose (-6.3 ± 0.4 vs -5.7 ± 0.1 %, $p < 0.05$).

Control BX-912 vs. INDO

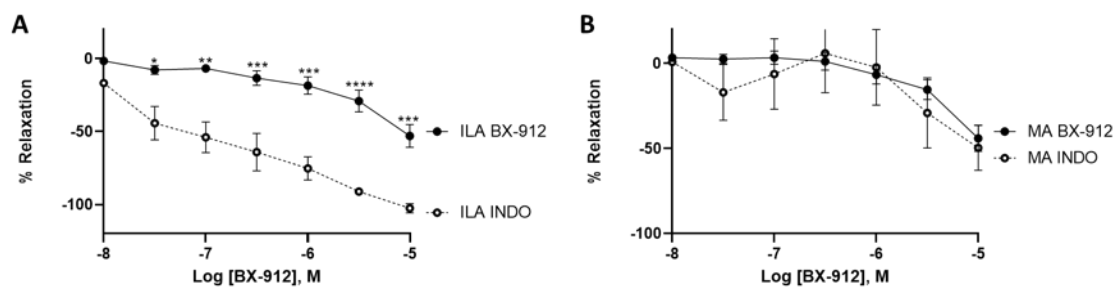


Figure 4.10. Effect of COX-2 inhibition by Indomethacin on BX-induced relaxation DRC, ($n=3-15$). **A.** Interlobar artery BX vs INDO, **B.** Mesenteric artery BX vs INDO. All data is represented as Mean \pm SEM, and statistical analysis was performed using a one-way ANOVA followed by a Dunnett's post hoc test. * ($p < 0.05$), ** ($p < 0.01$), *** ($p < 0.001$), † ($p < 0.0001$). **Abbreviations:** CD, control diet; ILA, interlobar artery; INDO, indomethacin; MA, mesenteric artery; [M], Molar; n, sample size.

4.5 Discussion

It is reported that, for the first time, BX is a direct inducer of vascular relaxation. Interlobar arteries were used as our primary vessel given the disease, we are targeting results in renal microvascular vasoconstriction. Thoracic aorta and mesenteric arteries were used to determine vessel specificity. Our previous studies have demonstrated a role for vessel specificity in disease, highlighting the importance of vessel specific treatment options. Some of the key findings of this study include a) BX-induced vascular relaxation in a vessel-specific manner; b) an AD increases BX-induced relaxation in mesenteric arteries, c) BX-induced vasodilation is endothelial and eNOS independent; d) ODQ inhibits BX-induced relaxation at high doses; e) KPSS inhibits BX-induced relaxation in CD/AD interlobar arteries and mesenteric arteries; f) CTX reduces BX relaxation in interlobar arteries and g) INDO enhances BX-induced relaxation in interlobar arteries.

BX is a potent and selective inhibitor of PDK1. Currently, a significant amount of literature illustrates the vasodilatory pathway of PDK1 and its involvement in the Akt/eNOS/NO pathway [115]. However, the role of PDK1 inhibition in vascular function is becoming more elucidated. Interestingly, although BX-induced PDK1 inhibition had not been identified as a vasodilator before now, other forms of PDK1 inhibition, either through genetic deletion or direct/indirect pharmaceutical inhibition, have shown relaxation effects [108-110, 116, 117]. These results highlight that in addition to PDK1 activation, there is a role for PDK1 inhibition in vasoactivity.

a) BX is a vasodilator.

To determine the effect of BX and variations in vascular response, vessels were subjected to a cumulative DRC to BX. The results presented in this study suggest that BX induces vasorelaxation and, therefore, could be a promising treatment in the prevention of CIAKI. The results showed that BX had little to no effect on inducing relaxation in the thoracic aorta but a positive vasodilatory effect in interlobar and mesenteric arteries. This therapeutic approach is important because increased vasodilation in large arteries, particularly for prolonged periods, can increase the risk of adverse side effects, including hypotension and syncope [87]. Interestingly, although a causative relationship was not identified, a retrospective study demonstrated that hypotension duration and severity determined by changes in mean arterial pressure was a risk factor for AKI development [118]. Although that study did not investigate the direct effects of CDDP on AKI, it does highlight the importance of vessel-specific vasodilation in AKI. The small artery vasodilatory response is a specific and highly

targeted approach. It can be applied to diseases resulting from peripheral artery constriction, such as CIAKI, peripheral artery disease and Raynaud's phenomenon. It may be important to understand the protein variances to determine the reason for the lack of vasodilation observed in thoracic aorta and to assist in determining the direct mechanism of action of BX.

a) BX-induced vasodilation is unaffected by an atherogenic diet

Endothelial dysfunction is a crucial vascular pathology associated with CIAKI [8], potentially linked to reduced renal blood flow and increased vascular resistance associated with diminished GFR [70-72]. The AD was used to induce endothelial dysfunction as patients with cancer also present with endothelial dysfunction and cancer treatment-related cardiac dysfunction [119]. Intriguingly, an AD did not affect the relaxation effects of BX in thoracic aorta and interlobar arteries; however, it significantly increased relaxation in mesenteric arteries. Given the little knowledge about the mechanisms governing PDK1 inhibition on relaxation and the lack of understanding of BX involvement in the vasculature, providing a theoretical explanation of the mechanism causing this is challenging. It is speculated that PDK1 inhibition could result in mTORC inactivation. This has been linked to increased vasodilatory properties [120]. Furthermore, AD has been shown to cause endothelial dysfunction through reduced eNOS phosphorylation and subsequent NO production [33, 34]. As AD did not affect BX-induced relaxation in interlobar and mesenteric arteries, this drug could also be used in patients with endothelial dysfunction and heart disease to increase vasodilation during CDDP treatment.

b) BX-induced relaxation is endothelial and eNOS independent.

Typically, PDK1 activation is associated with increased eNOS through stimulation of the PI3K/PDK1/Akt/eNOS pathway, as shown in (figure 4.3). This shows an eNOS-dependent vasoprotective role in PDK1 activation [115]. This study showed that mechanical denudation and eNOS inhibition with L-NAME did not affect interlobar or mesenteric arteries in either a CD/AD following a cumulative DRC to BX (10^{-8} to 10^{-5} [M]). This study highlights a vasoprotective role for PDK1 inhibition in an endothelial-independent manner. Another drug similar to BX, quercetin, has demonstrated vasodilatory abilities [109] and has been suggested to be mediated via the eNOS/NO pathway, at least in part. This was concluded, given that eNOS inhibition or mechanical denudation of the endothelium diminished quercetin relaxation response [109]. In addition to restoring eNOS, quercetin decreased inducible nitric oxide synthase [117]. Mechanical denudation of vessels eliminates the endothelium and, therefore, the

96

eNOS/NO pathway of vasodilation. This data suggests that not all PDK1 inhibitors function through the eNOS pathway, as BX is independent of this pathway.

PDK1 knockdown in mice has been shown to reduce eNOS at serine 1177 and 1179 [121]; this supports our study, which suggests that BX stimulated vasodilation is eNOS independent, given that eNOS inhibition by L-NAME in their study also had no impact on relaxation. Together this indicates that PDK1 activation through targeting of endothelial and eNOS-dependent mechanisms and PDK1 inhibition through its direct effect on VSMCs are both vasoprotective effects. This could be particularly beneficial given the association between CDDP administration and endothelial dysfunction. This study suggests that the mechanism of BX-induced vasodilation directly targets VSMC and therefore bypasses the endothelium altogether to induce relaxation. This suggests that renal blood flow and GFR could be restored irrespective of endothelial damage.

c) ODQ pre-incubation reduced BX-induced relaxation in interlobar arteries.

To determine the involvement of the NO/sGC signalling cascade, before a cumulative DRC to BX, vessels were pre-incubated with the sGC inhibitor ODQ. This showed that pre-incubation with the ODQ reduced BX-induced relaxation at the last dose of a BX DRC in both a CD and an AD of interlobar arteries. Although BX has not been used in functional evaluations, quercetin, a PDK1 inhibitor, has been used in vascular function studies. Their study showed that incubation with both L-NAME and ODQ significantly decreased the vasorelaxation effects of quercetin [122]. ODQ reduced relaxation aligns with the results of this study; however, L-NAME in our study did not affect BX suggesting the involvement of other mechanisms in BX-mediated vasodilation. Further investigations are required to determine the mechanism of ODQs inhibition of the relaxation effects of BX and the direct involvement of PDK1 inhibition. For a graphical representation of the mechanism of ODQ, please refer to (figure 4.3).

d) Pre-constriction with 40mM KPSS inhibited BX-mediated relaxation.

K⁺ channels play a critical role in maintaining and regulating VSMC vasoactivity. Activating K⁺ channels on endothelial cells results in K⁺ efflux, stimulating VSMC membrane hyperpolarisation and is a critical vasodilatory mechanism [96]. To determine the involvement of K⁺ channels on BX-mediated relaxation, vessels were pre-constricted with KPSS resulting in non-selective inhibition of potassium channels [114]. Results demonstrated that constriction with 40mM KPSS reduced BX-induced vasodilation in the CD/AD of interlobar and mesenteric arteries. This suggests that BX-induced relaxation is partially mediated through K⁺ channels. It is unclear as to the

mechanism of the PDK1 inhibition in K⁺ channel-induced relaxation; however, it is possible that BX resulted in an increased conductance to K⁺ ions [123].

e) Calcium-activated potassium channels partially mediate BX-induced relaxation

The specific K⁺ channels assessed here include voltage-gated potassium channels (K(V)) and KCa (including large - (BK(Ca)), intermediate - (IKCa), and small-conductance (SK(Ca)) KCa channels). To determine the involvement of specific K⁺ channels, before BX DRC, vessels were incubated with K⁺ channel blockers. In both interlobar and mesenteric arteries, APA, TEA, and 4-AP had no effect in reducing BX vasodilation compared to BX. Interestingly, CTX significantly reduced relaxation in the interlobar arteries compared to BX; however, this effect did not occur in the mesenteric arteries. This suggests that the degree of vasodilation is not only vessel specific but that its mechanism of action may vary within the different vasculature segments. In the interlobar arteries, BX acts via KCa channels.

Given that most pharmacological inhibitors of PDK1 act through an eNOS-dependent mechanism, little information exists linking PDK1 activation/inhibition and its function to stimulation of KCa channels. Surprisingly, a reduction in mTORC activity has been associated with increased protein levels of potassium channels and their associated proteins [124]. Notably, PDK1-stimulated Akt activity is essential for mTORC activity, suggesting that BX-induced relaxation could result from reduced mTORC activity increasing potassium channel activity. For visual representation of BX and the K⁺ channels, please refer to (figure 4.3).

f) COX inhibition by indomethacin enhanced BX-induced relaxation.

Prostacyclin-induced vasorelaxation is stimulated by COX-2 and is considered an essential vasodilatory pathway [125]. COX-1 and COX-2 work counteractively in the vascular system, with COX-1 activity responsible for the production of thromboxane, a potent vasoconstrictor, whilst COX-2 is responsible for producing the vasodilation-inducing compound prostacyclin [110]. Previously, a study has demonstrated that the anti-hypertensive nature of non-selective COX inhibitors is attributed predominantly to reduced endothelial dysfunction [126]. In this study, BX-induced relaxation is shown to be endothelial-independent. The results of this study demonstrated that pre-incubation of interlobar arteries with INDO, a non-specific COX inhibitor, enhanced relaxation compared to the BX group, suggesting the potential of a COX-2/PDK1 crosstalk relationship or the addition of INDO provides an additive effect to relaxation induced

by BX. A previous study showed that administration of INDO enhanced acetylcholine-mediated relaxation, highlighting the potential of a cooperative mechanism between COX-2 and PDK1 inhibition resulting in enhanced relaxation [126]. Mesenteric artery vasodilation stimulated by BX was unaffected by the addition of INDO pre-incubation. Provided the often-uniform results between interlobar and mesenteric arteries observed throughout this study, it would be interesting to observe if increased sample size and Power influenced the vasoreactivity to COX inhibition in mesenteric arteries that was observed in interlobar arteries.

4.6 Limitations

Drug specificity is one of the critical limitations of this study. It is possible that the off-target effects of the drugs used in this study could explain the results observed in this study. The small sample size observed in the K⁺ channel section of this study is a limitation of this thesis. An increased sample size would increase the Power of the study and give a greater statistical representation of the function of BX in K⁺ channels. A limitation of this study was that experiments were performed *in vitro* rather than *in vivo*.

4.7 Future studies

This study has established the involvement of the K⁺ channels; however, a larger study is required to confirm the involvement of specific K⁺ channels. Interestingly, given previous literature showing that the addition of PDK1 inhibitors enhances ACH-mediated relaxation, it would be beneficial to determine if BX also has enhancement properties in addition to its direct relaxation effects. Treatment of KCa KO mice with BX may further confirm the results obtained in this study. Additionally, using an alternative PDK1 inhibitor may help confirm any off-target effects mediating the relaxation effects of BX. It is also critical to progress with the use of BX alone *in vivo* to determine the systemic effects.

4.8 Conclusion

This study has elucidated the general mechanism of action of BX as a vasodilator and that an AD does not reduce BX-mediated vasodilation. Results determined that BX-mediated was endothelial, eNOS and COX independent, however was at least partially mediated through KCa channels. Inhibition of sGC by ODQ partially reduced BX-induced vasodilation in a vessel specific manner, and further studies are required to confirm these results. This study provides evidence that BX displays properties that positively correlate with a potential treatment against reduced renal blood flow associated with CIAKI.

Chapter 5: Identification of a CDDP dose that induces vascular dysfunction and pathological kidney damage.

5.1 Abstract

Background: Cisplatin (CDDP) is a potent chemotherapy used to treat a broad range of solid tumours that induces nephrotoxicity and often manifests as acute kidney injury (AKI). Currently, a well-established cisplatin-induced acute kidney injury (CIAKI) mouse model exists, with a single high CDDP dose administered and mice euthanised 72 hours post-intraperitoneal (IP) injection. However, the dose varies, ranging from 10-30mg/kg [127]. This study aimed to identify a physiologically relevant CDDP dose to induce vascular injury (determined via vasodilation dose-response curves to either acetylcholine (ACH) or sodium nitroprusside (SNP) or vasoconstriction dose-response curves to angiotensin II (ANGII), morphological damage, increased cell stress and pro-inflammatory biomarkers whilst not causing irreversible kidney damage. **Method:** Male C57BL6J mice (10–12-week-old) (n=4) were administered a dose of either 6.25mg/kg of CDDP (CDDP6.25) or 12.5mg/kg of CDDP (CDDP12.5) and euthanised 72 hours following. Sham mice received an equivalent volume of saline. Vessels were removed for isometric tension analysis. Cumulative DRC to ACH or SNP was performed in the abdominal aorta, and ANGII-mediated vasoconstriction was assessed in the iliac arteries. Kidneys were harvested and fixed in 4% paraformaldehyde for immunohistochemical analysis. Statistical procedures also used *Cohen's d* analysis. **Results:** CDDP12.5 showed a reduced effect size (*Cohen's d*) ACH-mediated relaxation compared to the SHAM group at doses 10^{-6} $d=-0.54$, $10^{-5.5}$ $d=-0.89$ and 10^{-5} [M] $d=-0.96$, however, relaxation was not reduced by the CDDP6.25 group. A significant increase in ANGII-mediated vasoconstriction was also observed compared to the SHAM group at doses $10^{-7.5}$, ($p<0.01$) and 10^{-7} , ($p<0.05$). In addition, a significant increase in tubular and glomerular periodic acid Schiff (PAS) stain was observed in the CDDP12.5 group and an increased tubular expression of tumour necrosis factor-alpha (TNF-a), glucose-regulated protein 78 (GRP78) and T cell immunoglobulin mucin domain-1/kidney injury molecule-1 (TIM-1/KIM-1) occurred in both CDDP groups. Tubular, glomerular and interlobar artery (ILA) expression of intracellular adhesion molecule 1 (ICAM-1), vascular cell adhesion molecule 1 (VCAM-1) and E-selectin were enhanced in the CDDP (6.25 and 12.5) groups compared to the SHAM.

Discussion: Decreased ACH-induced relaxation is suggestive of endothelial dysfunction, a well-established vascular pathology associated with CDDP treatment. The CDDP (6.25 12.5) groups synonymously increased cell stress and injury biomarkers, suggesting that the CDDP6.25 group induced some renal damage. The results of pro-inflammatory biomarkers suggest that the CDDP12.5 group caused a higher level of renal injury. **Conclusion:** Although the CDDP6.25 group induced a significant upregulation in protein expression associated with renal injury, the CDDP12.5 group caused a greater degree of vascular dysfunction combined with pathological damage. This suggests that 12.5mg/kg is a more suitable dose of CDDP for future CIAKI studies using this model.

5.2 Introduction

CDDP is a highly potent and effective antineoplastic agent used as a first-line treatment for a broad range of blood, solid and soft tissue cancers, including leukemia, lymphomas, breast, testicular, ovarian, head and neck, and cervical cancers, and sarcomas [47]. Despite its anticancer properties, its use is clinically restricted by nephrotoxicity, and its dose-limiting side effect manifests as AKI [1]. AKI is defined as a rapid decline in glomerular filtration rate (GFR), resulting in the accumulation of waste products, including serum blood urea nitrogen (sBUN) and creatinine (sCr) [67]. Despite the extent of pre-clinical studies producing a wide range of potential pharmaceutical interventions targeting oxidative stress, inflammation, and apoptotic mechanisms, the current standard of care is intravenous (IV) isotonic saline administration and the use of the osmotic diuretic mannitol [128]. This treatment aims to increase fluid content in combination with inducing diuresis to promote renal clearance of platinum (Pt) and reduce renal exposure and the toxic effects caused by Pt accumulation in proximal tubule epithelial cells (PTEC) [129]. It has been established that PTEC contains a 5-fold increase in Pt concentration compared to systemic circulation. This has been attributed to the upregulation of CDDP influx transporters, copper transporter 1 and organic cation transporter 2 and reduced efflux transporter multidrug and toxin extrusion, located on the basolateral and brush border membranes of PTEC cells [1].

The five-day CDDP model of inducing AKI is a widely and commonly used experimental protocol with a 72-hour post-CDDP IP injection endpoint [36-39]. C57BL6/J mice are one of the most used strains for this specific model; however, the CDDP dose has a high variability throughout the literature. Published CDDP doses in this model vary from 10-30mg/kg [127], all of which vary in degree of damage and

degree of amelioration in response to pharmacological interventions. This study aimed to determine a close to clinically relevant CDDP dose that induced a significant increase in pathological biomarkers and a significant reduction in vascular function of CIAKI without inducing irreversible kidney damage. In this study, we investigated the ability of CDDP (6.25 and 12.5) to induce AKI.

Functional and pathological *ex vivo* experiments were completed to determine the ideal dose that induces pathologies and cell stress. CIAKI is a highly complex condition; however, it is often initially associated with reduced renal blood flow within three hours of CDDP infusion in patients. This often unknowingly precedes reductions in GFR [67, 68]. Endothelial dysfunction resulting from CDDP reduced endothelial nitric oxide synthase (eNOS) phosphorylation, stimulating reduced NO bioavailability. This is one of the key signalling cascades resulting in increased vascular resistance and reduced renal blood flow, ultimately resulting in diminished GFR, implicating these two factors in CIAKI development [70-72]. Increasing renal blood flow and decreasing vascular resistance through enhanced vasodilation [74] is a theoretically beneficial strategy to mitigate CIAKI. VSMC toxicity and endothelial dysfunction are other known pathophysiological mechanisms associated with CIAKI. An *in vitro* study demonstrated that pre-incubation of isolated rat thoracic aorta rings for six hours with 200 μ M of CDDP decreased contractile function of thoracic aorta, induced vascular wall damage and promoted VSMC cytotoxicity [130].

Immunohistochemical analysis of many specific biomarkers has previously been used to identify multiple pathways and molecular mechanisms in CIAKI. KIM-1 is a novel and recently exposed blood, urinary and tissue early biomarker to indicate acute kidney injury [131]. Increased sBUN and sCr, in addition to reduced GFR and creatinine clearance, are the current clinical indicators and diagnostic measurements of CIAKI, however often manifest later in disease progression, thus clinical diagnosis is not rapid, highlighting an urgency for a preventative option favourable to a treatment approach. KIM-1 has been identified as an early biomarker of AKI and could become preferential to the current biomarkers [132].

ICAM-1, VCAM-1 and E-Selectin are molecules that play a critical role in cell-cell and cell-basement membrane interaction. Additionally, they exert prominent involvement in inflammation, with their expression induced by pro-inflammatory proteins. Further, these molecules contribute to cellular adhesion, particularly to the vascular endothelium, and their expression positively correlates with tumour progression [133]. Upregulation

of messenger ribonucleic acid (mRNA) and protein expression of ICAM-1, VCAM-1 and E-Selectin is well documented in models of CIAKI [134, 135]. Although these biomarkers are well known to be upregulated in PTEC following CDDP treatment, their effects on glomeruli and interlobar artery expression are not well established. Investigations could provide more information on potential interrelationships between the tubules, interlobar arteries and the manifestation of CIAKI, in addition to the upregulation of pro-inflammatory biomarkers. Additionally, CDDP treatment results in enhanced expression of endoplasmic reticulum (ER)-stress-mediated apoptotic proteins, including GRP78 [136].

GRP78 is a central ER chaperone protein. Its role as an ER chaperone protein contributes to its widely known role as a master ER-stress regulation protein [137]. Its upregulation is associated with the ER stress response, a pro-survival mechanism to avoid cellular dysfunction and eventual ER-stress-induced apoptotic pathways [138].

The pro-inflammatory cytokine TNF- α is produced by macrophages and monocytes in response to acute inflammation [139]. Increased serum and urinary concentration of TNF- α is associated with CIAKI [1].

This study aimed to use vascular reactivity and histological analysis of renal tissue to determine an effective CDDP dose to induce vascular dysfunction and upregulation of proteins associated with cell stress in CIAKI.

5.3 Methods

5.3.1 Materials/Chemicals

Chemicals: Please refer to Chapter 2, section 2.13 solutions for purchasing information for the following chemicals: CDDP, human angiotensin II, acetylcholine chloride, sodium nitroprusside, 9,11-dideoxy-11 α ,9 α -epoxymethanoprostaglandin F_{2 α} (U46619), and paraformaldehyde (PFA). For purchasing details for periodic acid-Schiff (PAS) staining system and DAB substrate kit please refer to Chapter 2, sections 2.8.2 and 2.8.1 respectively. **Antibodies:** For details on antibodies used, including catalogue number, clonality, and concentration, please refer to Chapter 2, table 2.2. KREBS pH 7.4 and 40mM KPSS (for instructions on formulation, please refer to Chapter 2, section 2.13, subsection 2.13.2 general chemicals. To compare *in vitro* doses of CDDP of other publications, the *in vivo* doses used in this study were converted to concentration from mg/kg. The average blood volume of a mouse is 80ml per kg. The average weight for a 10–12-week-old mouse was taken using our data, showing an average of 20.37g. This weight suggests that the average total blood volume for mice in this study was 1.6ml.

For a 6.25mg/kg dose of CDDP in a 20g mouse, 0.125mg of CDDP in 1.6 ml is required, yielding a concentration of 260 μ M. For 12.5mg/kg, the mass of CDDP is doubled, and thus the concentration is doubled, presenting a concentration of 520 μ M.

5.3.2 Animals/Experimental Protocol

For animal purchase, housing, and treatment regimen information, please refer to Chapter 2, section 2.1 Animals/experimental regimens, subsection 2.1.2 CIAKI (five-day model). For details on monitoring during the experiment period, please refer to section 2.2 monitoring, 2.2.1 mice monitoring. For information on the anaesthetisation and culling, please refer to section 2.3. For mouse dissection protocol is illustrated in section 2.4. For reference, SHAM-treated mice, CDDP (6.25 and 12.5), were administered 0.9% saline. For ANGII DRC, CDDP-treated mice received CDDP dissolved in a vehicle of 1:9 dimethylformamide: phosphate buffered saline (DMF: PBS).

5.3.3 Isometric tension analysis

For the isometric tension procedure, please refer to Chapter 2, section 2.6 isometric tension analysis. For additional information, please refer to table 2.1. For information on drugs used for functional analysis, please refer to section 2.6.2, Mouse drug stimulations.

5.3.4 Tissue Processing/Histological and Immunohistochemical analysis

Tissue processing details are described in Chapter 2, General methods, section 2.7. For information on histology, please refer to section 2.8. For specific details on immunohistochemistry, please refer to section 2.8.1. and table 2.2 for further information on antibodies used for staining, including clonality, supplier, catalogue and concentrations used in specific vessel types. Please refer to 2.8.2 for the description of the PAS stain protocol. For an explanation of the semi-quantification used for immunohistochemical analysis, please refer to section 2.9.

5.3.5 Data/Statistical Analysis

Statistical analyses are detailed in Chapter 2, General methods section 2.12. For analysis of variance (ANOVA) details, please refer to section 2.12.1 and for information on *Cohen's d* analysis, please refer to section 2.12.2. For *Cohen's d*, the analysis of effect size values are compared to CDDP. Positive *d* values indicate a reduction compared to SHAM, and negative *d* values represent an increase compared to SHAM.

5.4 Results

5.4.1 CDDP 6.25 and 12.5 mg/kg has opposing effects on aortic relaxation.

To determine the effect of CDDP on ACH-mediated relaxation, abdominal aorta was harvested from SHAM, CDDP, (6.25 or 12.5)-treated mice and assessed for function. LogEC₅₀ and area under the curve (AUC) were calculated, comparing each CDDP dose group to the SHAM group, table 5.1. Results showed that the CDDP12.5 group, had a medium effect (*Cohen's d*) on reducing ACH-mediated relaxation compared to the SHAM group at dose 10⁻⁶ [M] and a large effect at doses 10^{-5.5} and 10⁻⁵ [M]. Additionally, the CDDP 12.5 group generated a small effect (*Cohen's d*) on shifting the LogEC₅₀ compared to the SHAM group (-7.2 ± 0.2 % vs -6.7 ± 0.2 %, p=ns, *d*=0.39) and in reducing the AUC (84.2 ± 7.3 % vs 102.8 ± 19.4 %, p=ns, *d*=0.28). Surprisingly, the CDDP6.25 group showed a medium effect (*Cohen's d*) in increased relaxation compared to the SHAM group at 10⁻⁵, (-76.2 ± 17.3 % vs -59.1 ± 6.7 %, p=ns, *d*=0.62) and the AUC, (144.6 ± 97.9 % vs 102.8 ± 19.4 %, p=ns, *d*=-0.51). The CDDP6.25 group had no effect, statistically or on effect size (*Cohen's d*), in shifting the LogEC₅₀ compared to SHAM. *Effect size (Cohen's d)* showed that increased relaxation following stimulation with ACH occurred at all doses except 10⁻⁷ [M] in the CDDP6.25 compared to the SHAM group, with effect sizes ranging from *d*=0.38-*d*=0.78. For statistically significant p values and effect size (*Cohen's d*) values obtained for each dose, please refer to table 5.1.

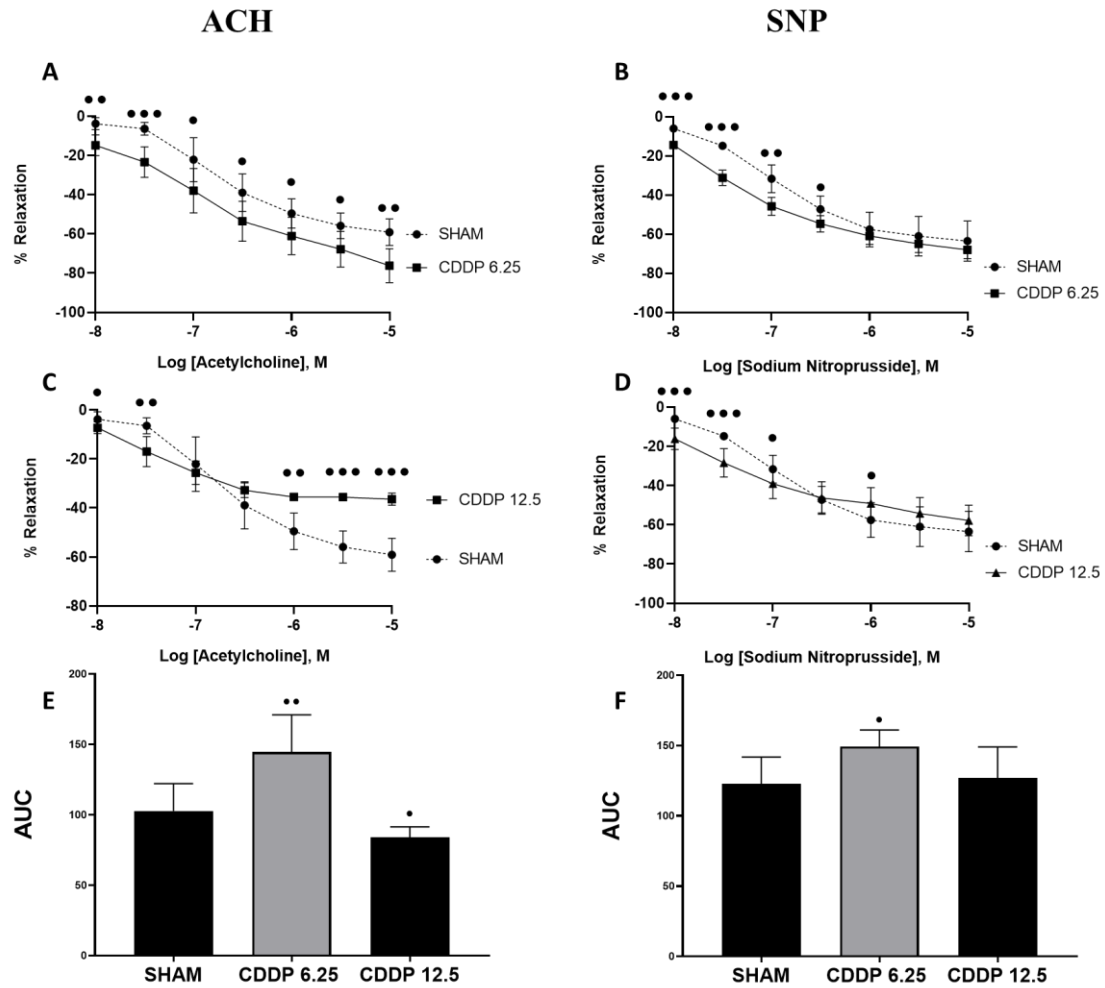


Figure 5.1. CDDP effect on vasodilation to cumulative doses of ACH and SNP (10^{-8} to 10^{-5} [M]), ($n=4$). **A.** ACH, SHAM vs CDDP 6.25, **B.** SNP, SHAM vs CDDP 6.25. **C.** ACH, SHAM vs CDDP 12.5, **D.** SNP, SHAM vs CDDP 12.5. **E.** ACH bar graph of AUC, **F.** SNP bar graph of AUC. All data is represented as Mean \pm SEM, and statistical analysis was performed using a one-way ANOVA followed by a Dunnett's post hoc test. * ($p < 0.05$), ** ($p < 0.01$), *** ($p < 0.001$), † ($p < 0.0001$). Effect size (d) and Cohen's d values are taken as • $d = 0.2-0.5$ (small effect), •• $d = 0.5-0.8$ (medium effect), and ••• $d \geq 0.8$ (large effect). **Abbreviations:** AUC; area under the curve; CDDP, cisplatin; CDDP 6.25, cisplatin 6.25mg/kg; CDDP 12.5, cisplatin 12.5mg/kg; d , Cohen's d ; M, Molar; n , sample size.

Table 5.1. Effect of CDDP (6.25 and 12.5) groups on vascular function, determined through cumulative dose-response curve to acetylcholine and sodium nitroprusside (10^{-8} to 10^{-5} [M]).

Drug Conc [M]	ACH		SNP	
	CDDP6.25	CDDP12.5	CDDP6.25	CDDP12.5
10^{-8}	d= 0.78	d= 0.31	d= 1.43	d= 0.95
$10^{-7.5}$	d= 0.95	d= 0.95	d= 1.84	d= 0.90
10^{-7}	d= 0.37	p=ns	d= 0.55	d= 0.27
$10^{-6.5}$	d= 0.39	p=ns	d= 0.30	p=ns
10^{-6}	d= 0.38	d= -0.54	p=ns	d=-0.2
$10^{-5.5}$	d= 0.43	d= -0.89	p=ns	p=ns
10^{-5}	d= 0.62	d= -0.96	p=ns	p=ns

Statistical significance is taken at ($p < 0.05$), and effect size (d) and Cohen's d values are taken as $d = 0.2 - < 0.5$ (small effect), $d = 0.5 - < 0.8$ (medium effect), and $d = \geq 0.8$ (large effect).

Abbreviations: ACH, acetylcholine; CDDP, cisplatin; CDDP6.25, cisplatin 6.25mg/kg; CDDP12.5, cisplatin 12.5mg/kg; Conc, concentration; d , Cohen's d ; [M], Molar; n , sample size; SNP; sodium nitroprusside.

5.4.2 CDDP does not affect SNP-stimulated vasodilation.

CDDP is known to cause vascular smooth muscle cell (VSMC) toxicity [130]. To determine the effect of CDDP on VSMC function, abdominal aorta was isolated *ex vivo* and assessed for vasodilatory abilities to cumulative doses of SNP (10^{-8} to 10^{-5} [M]). Despite the current theory that CDDP induces toxicity to VSMCs, this study did not support this. Cohen's d analysis of effect size exhibited that an effect on relaxation occurred at almost all doses. Mice treated with CDDP6.25 showed a large effect (Cohen's d) at doses 10^{-8} , and $10^{-7.5}$ [M] and a medium and small effect (Cohen's d) were observed at 10^{-6} and $10^{-6.5}$ [M], respectively, compared to the SHAM group, (figure 5.1). The same enhancement in relaxation was observed in CDDP12.5 treated mice compared to the SHAM group. A small effect (Cohen's d) was seen at doses 10^{-7} and reduced relaxation at 10^{-6} [M]. SNP doses induced a large effect (Cohen's d) in the CDDP12.5 treated mice compared to the SHAM group at doses 10^{-8} and $10^{-7.5}$ [M]. CDDP6.25 induced a small effect (Cohen's d) on AUC compared to the SHAM group (149.2 ± 11.9 % vs 122.9 ± 19.0 %, $p = ns$, $d = -0.38$). CDDP at either dose did not shift

the LogEC₅₀. For statistically significant p values and effect size (*Cohen's d*) values obtained for each dose, please refer to *table 5.1*.

5.4.3 Effect of CDDP on ANGII-induced vasoconstriction compared to SHAM mice

The role of ANGII and, more specifically, its receptors is a widely investigated therapeutic mechanism in ameliorating CIAKI. Angiotensin receptor blockers (ARBs) have shown both amelioration and exacerbation of CIAKI [140-143]. However, the correlation between AKI and the vasoconstrictive response of CDDP to ANGII remains largely unexplained. To elucidate the impact of CDDP on ANGII-induced vasoconstriction, iliac arteries from mice treated with CDDP were excised and assessed for vasoconstrictive effects to cumulative doses of ANGII (doses 10⁻⁸ to 10⁻⁵ [M]). Results showed that the CDDP12.5 group significantly increased vasoconstrictive response to ANGII compared to the SHAM group at doses 10^{-7.5} [M] (25.9 ± 4.7 % vs 8.3 ± 2.9 %, *p*<0.01) and 10⁻⁷ [M] (29.3 ± 6.5 % vs 14.5 ± 5.4 %, *p*<0.05), (figure 5.2). Analysis of effect size (*Cohen's d*) demonstrated that either a small, medium, or large effect was obtained at each of the remaining doses. As described in table 5.2, CDDP12.5 had no significant effect on LogEC₅₀ or AUC in response to ANGII stimulation. However, a small effect (*Cohen's d*) was determined compared to the SHAM for LogEC₅₀ (-6.5 ± 0.2 % vs -7.0 ± 0.4 %, *p*=ns, *d*=0.29) and a large effect (*Cohen's d*) for AUC as shown in 9figure 5.2B), (25.9 ± 4.7 % vs 8.3 ± 2.9 %, *p*=ns, *d*=-1.06).

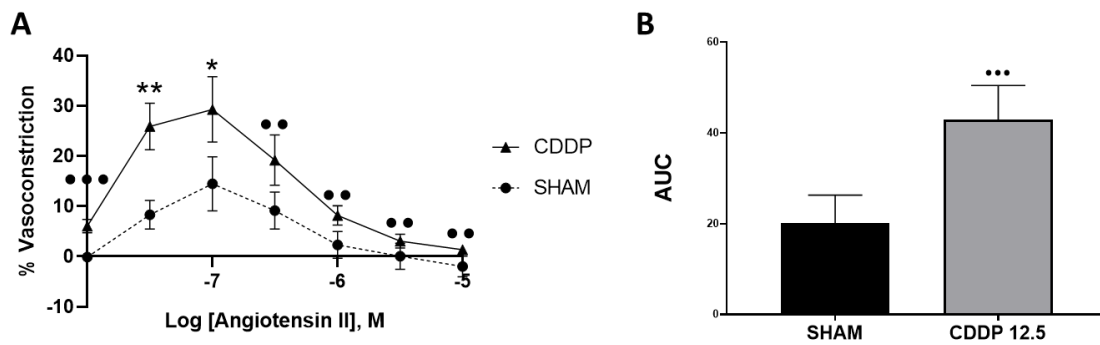


Figure 5.2. Effect of Angiotensin II-induced vasoconstriction in the SHAM and CDDP12.5 groups (n=3-4). **A.** IP Injection of CDDP12.5 significantly increased ANGII-induced vasoconstriction compared to SHAM at doses 10^{-7} and $10^{-7.5}$ [M]. **B.** AUC graph representing that the CDDP12.5 group had a significantly larger AUC compared to the SHAM treatment. All data is represented as Mean \pm SEM, and statistical analysis was performed using a one-way ANOVA followed by a Dunnett's post hoc test. * ($p < 0.05$), ** ($p < 0.01$), *** ($p < 0.001$), † ($p < 0.0001$). Effect size (d) and Cohen's d values are taken as * $d = 0.2-0.5$ (small effect), ** $d = 0.5-0.8$ (medium effect), and *** $d \geq 0.8$ (large effect). **Abbreviations:** AUC, area under the curve; CDDP, cisplatin; CDDP 6.25, cisplatin 6.25mg/kg; CDDP 12.5, cisplatin 12.5mg/kg; d , Cohen's d ; M, Molar; n , sample size.

5.4.4 Weight differences

All mice were normalised to 100% for the determination of % weight difference. Weights were monitored and recorded daily from days 0-4 for either the CDDP (6.25 or 12.5) groups. Results shown in (figure 5.3) demonstrated that SHAM mice gained weight % from days 0-4 whilst both CDDP (6.25 and 12.5), lost weight, (figure 5.3). Mice treated with CDDP6.25 significantly reduced weight compared to the SHAM group by day four of the study ($97.2 \pm 1.3\%$ vs $102.3 \pm 1.2\%$, $p < 0.05$). Mice treated with CDDP12.5 showed reduced weight compared to the SHAM group at days three (95.2 ± 1.6 vs 100.0 ± 1.8 , $p < 0.05$) and four (92.4 ± 3.1 vs 102.3 ± 1.2 , $p < 0.0001$). A significant difference between % weight loss occurred on day four between the two CDDP doses, which showed that a more substantial weight loss % occurred in CDDP12.5 treated mice compared to the CDDP6.25 group (92.4 ± 3.1 vs 97.2 ± 1.3 , $p < 0.05$).

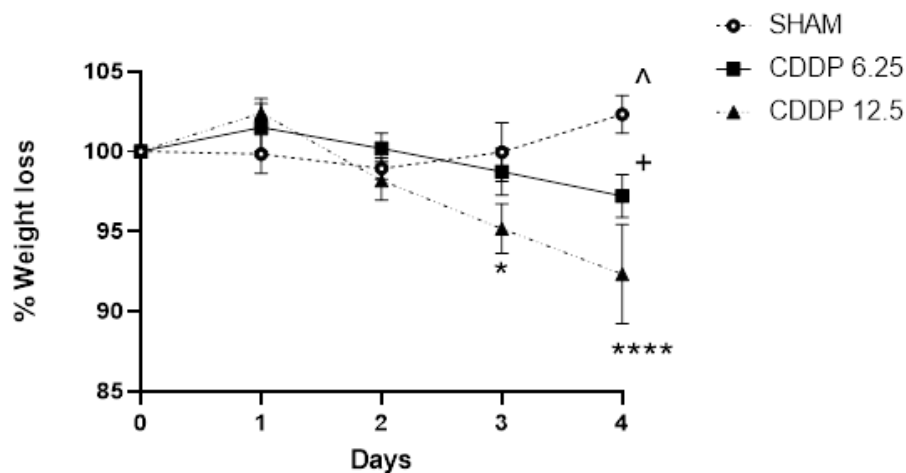


Figure 5.3. Percentage (%) weight loss of CDDP (6.25 and 12.5) treated mice (n=3-4). Daily changes in mouse weights were monitored to determine the weight % lost from day 0 before the commencement of treatment until day 4 (date of euthanasia). All data is represented as Mean \pm SEM, and statistical analysis was performed using a one-way ANOVA followed by a Dunnett's post hoc test. * ($p < 0.05$), ** ($p < 0.01$), *** ($p < 0.001$), † ($p < 0.0001$). (^ = CDDP6.25 vs SHAM, + = CDDP12.5 vs CDDP6.25, * = CDDP12.5 vs SHAM). **Abbreviations:** CDDP, cisplatin; CDDP6.25, cisplatin 6.25mg/kg; CDDP12.5, cisplatin 12.5mg/kg; n, sample size; %, percentage.

Table 5.2. LogEC₅₀ and AUC of SHAM vs CDDP (6.25 and 12.5) treated mice.

AA- ACH	n	Log EC ₅₀ \pm SEM	p vs SHAM	d vs SHAM	AUC \pm SEM	p vs SHAM	d vs SHAM
SHAM	4	-6.69 \pm 0.2			102.8 \pm 19.4		
CDDP 6.25	4	-6.68 \pm 0.2	p=ns	p=ns	144.6 \pm 97.9	p=ns	d=-0.51
CDDP 12.5	4	-7.15 \pm 0.2	p=ns	d=0.39	84.16 \pm 7.3	p=ns	d=0.28
AA- SNP	n	Log EC ₅₀ \pm SEM	p vs SHAM	d vs SHAM	AUC \pm SEM	p vs SHAM	d vs SHAM
SHAM	4	-6.86 \pm 0.03			122.9 \pm 19.0		
CDDP 6.25	4	-7.06 \pm 0.1	p=ns	p=ns	149.2 \pm 11.9	p=ns	d=-0.38
CDDP 12.5	4	-6.94 \pm 0.2	p=ns	p=ns	127.0 \pm 22.0	p=ns	p=ns
IA- ANGII	n	Log EC ₅₀ \pm SEM	p vs SHAM	d vs SHAM	AUC \pm SEM	p vs SHAM	d vs SHAM
SHAM	3	-7.02 \pm 0.4			20.10 \pm 6.2		
CDDP 12.5	4	-6.50 \pm 0.2	p=ns	d=0.29	42.90 \pm 7.6	p=ns	d=-1.06

Statistical significance is taken at ($p < 0.05$), and effect size (d) and Cohen's d values are taken as $d = 0.2 - < 0.5$ (small effect), $d = 0.5 - < 0.8$ (medium effect), and $d = \geq 0.8$ (large effect).

Abbreviations: AA, abdominal aorta; IA, iliac artery; ACH, acetylcholine; ANGII, angiotensin II; AUC, area under the curve; CDDP, cisplatin; CDDP6.25, cisplatin 6.25mg/kg; CDDP12.5, cisplatin 12.5mg/kg; n, sample size; SEM, standard error of the mean; SNP, sodium nitroprusside.

5.4.5 CDDP-induced pathological damage.

Pathological damage indicated by morphological hallmarks, including cast formation, are valuable indicators of kidney damage leading to dysfunction. To determine the degree of pathological damage induced by CDDP (6.25 or 12.5), kidney sections (including tubules, glomeruli, and interlobar arteries) were stained from CDDP-treated mice with PAS. PTECs remain a significant focus for kidney damage; results of this study showed that CDDP6.25 did not affect tubular PAS expression. The CDDP12.5 group showed a significant elevation in positive PAS expression in the tubules compared to the SHAM group, (figure 5.4D) (4.7 ± 1.1 % vs 1.0 ± 0.4 %, $p < 0.01$). CDDP6.25 did not affect glomerular PAS positive expression but induced a significant difference following CDDP12.5 treatment compared to the SHAM group (2.0 ± 0.3 % vs 1.0 ± 0.2 , $p < 0.05$), (figure 5.4H). Analysis of interlobar arteries from CDDP-treated mice showed that CDDP6.25 had a small effect (*Cohen's d*) on reducing positive PAS staining in the endothelium compared to the SHAM group (0.4 ± 0.1 % vs 1.1 ± 0.4 %, $p = \text{ns}$, $d = 0.38$), (figure 5.4L). The CDDP12.5 group had a dose-dependent increase in positive PAS staining in the medial (1.7 ± 0.3 % vs 0.7 ± 0.3 %, $p < 0.05$) and adventitial layers as indicated by a medium effect (*Cohen's d*) (1.7 ± 0.4 % vs 0.8 ± 0.3 %, $p = \text{ns}$, $d = -0.65$) compared to the SHAM group.

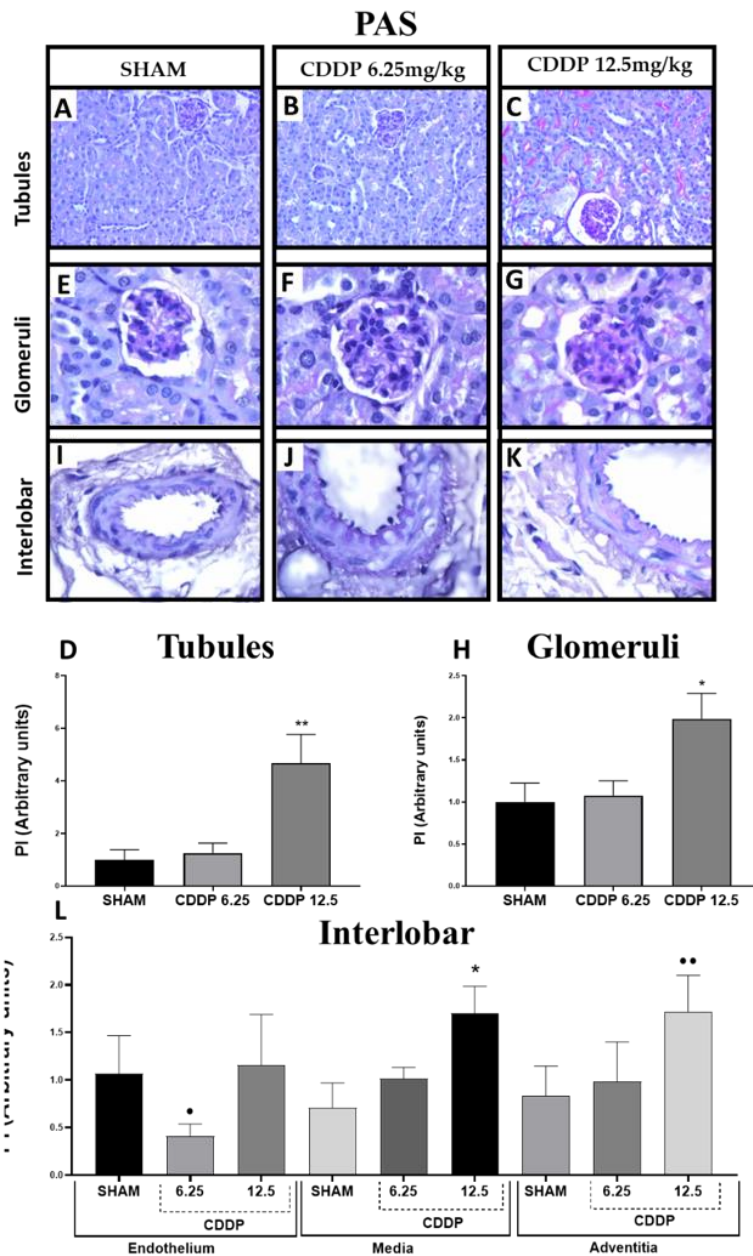


Figure 5.4. Histochemical analysis using periodic acid Schiff (PAS) stain of kidney structures, including tubules, glomeruli and interlobar arteries in mice treated with SHAM, CDDP (6.25 or 12.5), ($n=3-4$). Images taken using Leica software of PAS-stained tissues are shown in A-C. SHAM, CDDP 6.25 and CDDP 12.5-stained tubules at 40x magnification E-G. SHAM, CDDP6.25, CDDP12.5-stained glomeruli at 100x magnification, and I-K. SHAM, CDDP6.25 and CDDP12.5 stained interlobar arteries at 100x magnification. Graphs of semi-quantified analysis of tissues are shown in D. tubules, H. glomeruli and L. interlobar arteries. All data is represented as Mean \pm SEM, and statistical analysis was performed using a one-way ANOVA followed by a Dunnett's post hoc test. * ($p<0.05$), **($p<0.01$), *** ($p<0.001$), † ($p<0.0001$). Effect size (d) and Cohen's d values are taken as • $d=0.2-0.5$ (small effect), •• $d=0.5-0.8$ (medium effect), and ••• $d\geq 0.8$ (large effect). **Abbreviations:** CDDP, cisplatin; CDDP6.25, cisplatin 6.25mg/kg; CDDP12.5, cisplatin 12.5mg/kg; d , Cohen's d ; PAS, periodic acid Schiff; PI, proportional intensity; n , sample size.

5.4.6 Immunohistochemical analysis determined that CDDP treatment enhances tubular expression of TNF- α , GRP78 and Tim-1/Kim-1.

The development of CIAKI is associated with increased tubular expression of TNF α , GRP78 and TIM-1/KIM-1 in patients and pre-clinical models of CIAKI [1, 132, 144]. These markers were used in paraffin-embedded kidney tissues harvested from CDDP (6.25 and 12.5) treated mice to determine a dose suitable to induce increased expression of these proteins compared to the SHAM group to indicate cell stress. Both CDDP6.25 (8.9 ± 2.3 % vs 1.0 ± 0.5 %, $p < 0.03$) and CDDP12.5 groups (9.3 ± 1.0 % vs 1.0 ± 0.5 %, $p < 0.05$) increased TNF- α expression compared to the SHAM group, (figure 5.5E). This was also observed in tissues stained for KIM-1, CDDP6.25 (1.8 ± 0.1 % vs 1.0 ± 0.1 %, $p < 0.01$) and CDDP12.5 groups (1.8 ± 0.1 % vs 1.0 ± 0.1 %, $p < 0.01$), (figure 5.5O). Interestingly, GRP78 stained tubules demonstrated that CDDP6.25 (2.6 ± 0.9 % vs 0.5 ± 0.3 %, $p = \text{ns}$, $d = -0.84$) and CDDP12.5 groups (2.6 ± 0.9 % vs 0.5 ± 0.3 %, $p = \text{ns}$, $d = -0.90$) induced a large effect (*Cohen's d*) compared to the SHAM group, (figure 5.5J).

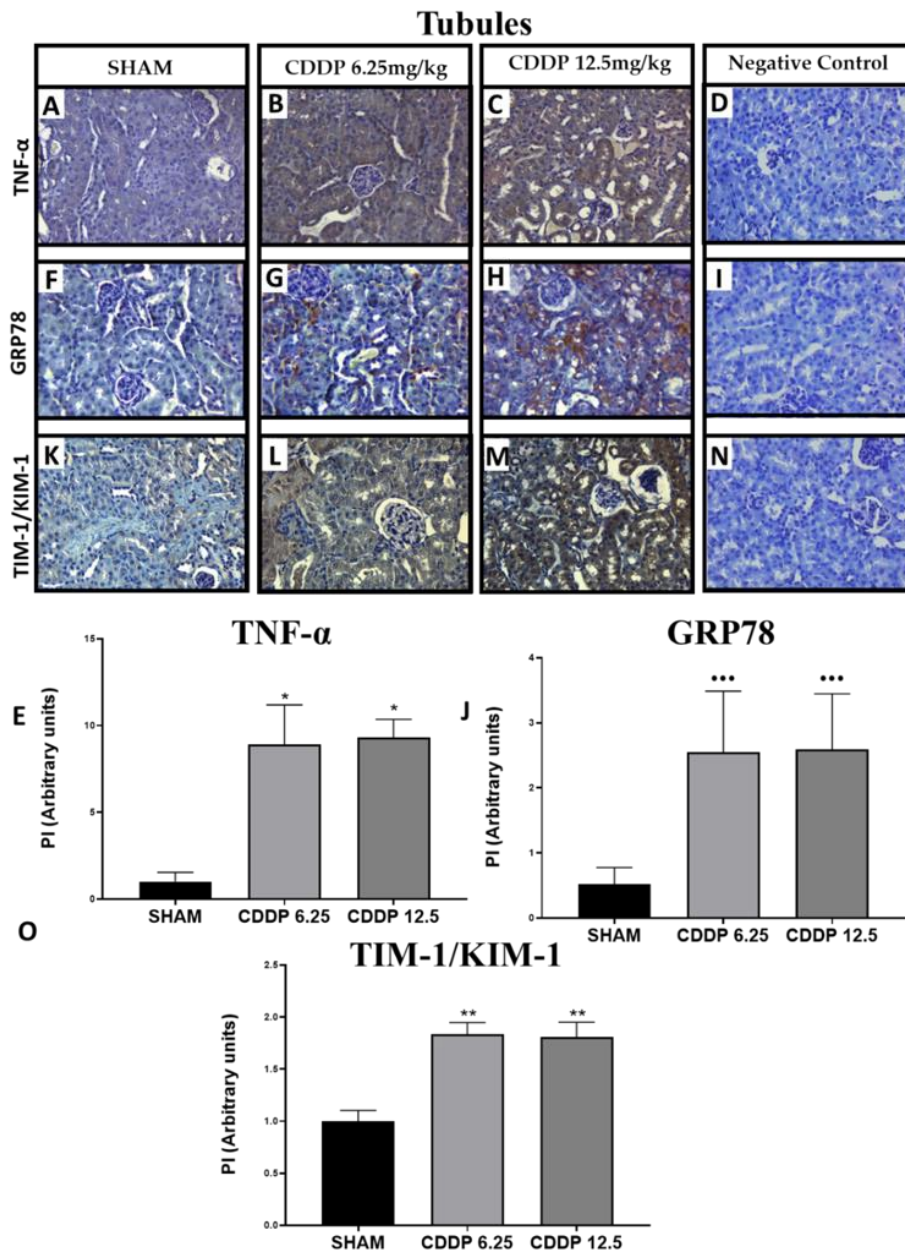


Figure 5.5. Immunohistochemical tubular expression of *TNF- α* , a pro-inflammatory biomarker, *GRP78*, an ER stress marker and *TIM-1/KIM-1*, a kidney injury biomarker ($n=3-4$). Images of SHAM, CDDP6.25, CDDP12.5 and negative control for tubules stained with **A-D**. *TNF- α* , **F-I**. *GRP78* and **K-N**. *TIM-1/KIM-1* (all taken at 40x magnification). Graphical representations of semi-quantified data are illustrated in **E**. *TNF- α* , **J**. *GRP78* and **O**. *TIM-1/KIM-1*. All data is represented as Mean \pm SEM, and statistical analysis was performed using a one-way ANOVA followed by a Dunnett's post hoc test. * ($p<0.05$), **($p<0.01$), *** ($p<0.001$), † ($p<0.0001$). Effect size (d) and Cohen's d values are taken as • $d=0.2-0.5$ (small effect), ** $d=0.5-0.8$ (medium effect), and *** $d\geq 0.8$ (large effect). **Abbreviations:** CDDP, cisplatin; CDDP6.25, cisplatin 6.25mg/kg; CDDP12.5, cisplatin 12.5mg/kg; d , Cohen's d ; *GRP78*, glucose-regulated protein 78; *TIM-1/KIM-1*; T cell immunoglobulin mucin domain-1/kidney injury molecule-1; *TNF- α* , tumour necrosis factor α ; n , sample size; PI, proportional intensity.

5.4.7 Pro-inflammatory markers ICAM-1, VCAM-1 and E-Selectin expression are upregulated by CDDP.

ICAM-1, VCAM-1, and E-Selectin are essential pro-inflammatory proteins that are upregulated following treatment with CDDP and are indicators of endothelial cell stress. Tubules, glomeruli and interlobar arteries were stained using primary antibodies to ICAM-1, VCAM-1 and E-Selectin, stained with DAB and analysed for colour intensity and proportional area to generate proportional intensity, representing the degree of protein expression in tissue sections.

Results showed that CDDP had a dose-dependent increase in ICAM-1 expression in the tubules compared to the SHAM group, CDDP6.25 ($5.3 \pm 1.7\%$ vs $1.0 \pm 0.3\%$, $p < 0.04$) and CDDP12.5 groups ($6.9 \pm 1.8\%$ vs $1.0 \pm 0.3\%$, $p < 0.05$), (figure 5.6E). Although CDDP6.25 had a significant increase in ICAM-1 expression compared to the SHAM group in the glomeruli ($3.8 \pm 0.9\%$ vs $1.0 \pm 0.4\%$, $p < 0.001$), CDDP12.5 showed a small effect (*Cohen's d*) in reduced ICAM-1 compared to the SHAM group ($2.1 \pm 1.5\%$ vs $1.0 \pm 0.4\%$, $p = \text{ns}$, $d = -0.34$), (figure 5.6J). However, no difference between the two CDDP doses was observed. ICAM-1 expression was significantly upregulated compared to the SHAM group in the endothelium of mice treated with CDDP12.5 ($2.6 \pm 0.5\%$ vs $1.0 \pm 0.1\%$, $p < 0.05$). This was also observed in the adventitial layer ($18.6 \pm 7.0\%$ vs $1.0 \pm 0.7\%$, $p < 0.05$). The medial layer showed a medium effect (*Cohen's d*) in the CDDP12.5 group compared to the SHAM group ($2.7 \pm 1.5\%$ vs $1.0 \pm 0.6\%$, $p = \text{ns}$, $d = -0.5$). Analysis showed a medium effect (*Cohen's d*) in the CDDP6.25 treated mice compared to the SHAM group in the endothelium ($2.0 \pm 0.6\%$ vs $1.0 \pm 0.1\%$, $p = \text{ns}$, $d = -0.5$) and the medial layer ($2.1 \pm 0.6\%$ vs $1.0 \pm 0.6\%$, $p = \text{ns}$, $d = -0.6$). In the adventitial layer, CDDP6.25 significantly upregulated ICAM-1 expression compared to the SHAM group ($5.2 \pm 0.7\%$ vs $1.0 \pm 0.5\%$, $p < 0.05$). No significant difference occurred between the two CDDP doses was observed at any vascular layer, (figure 5.6O).

ICAM-1

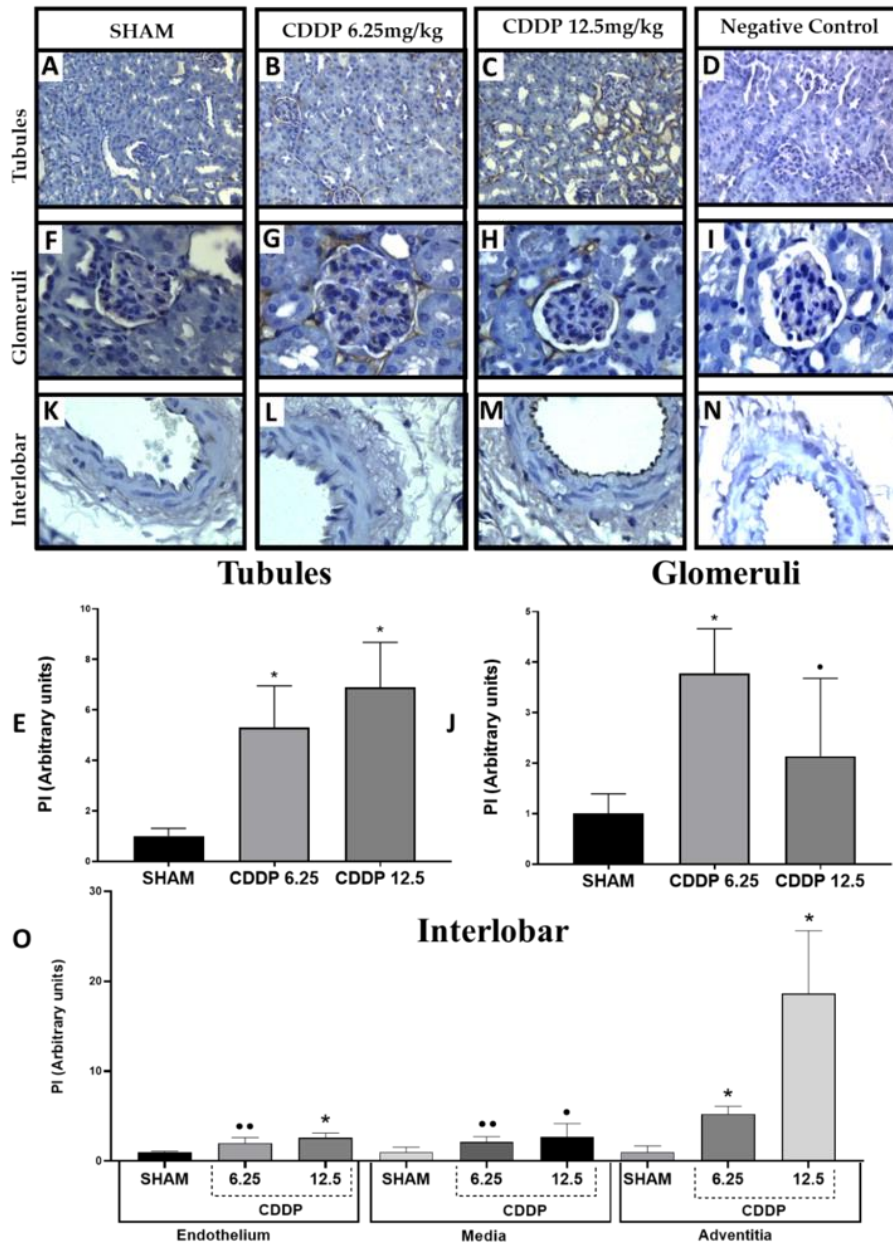


Figure 5.6. Immunohistochemical staining analysis of ICAM-1 expression in kidney structures, including tubules, glomeruli and interlobar arteries in mice treated with SHAM, CDDP (6.25 or 12.5), (n=3-4). Images taken using Leica software are shown A-D. SHAM, CDDP6.25, CDDP12.5, and negative control-stained tubules at 40x magnification F-I. SHAM, CDDP6.25, CDDP12.5 and negative control-stained glomeruli at 100x magnification, K-N. SHAM, CDDP6.25, CDDP12.5, and negative control stained interlobar arteries at 100x magnification. Graphs of semi-quantified analysis of tissues are shown in E. tubules, J. glomeruli and O. interlobar arteries. All data is represented as Mean \pm SEM, and statistical analysis was performed using a one-way ANOVA followed by a Dunnett's post hoc test. * ($p < 0.05$), ** ($p < 0.01$), *** ($p < 0.001$), \dagger ($p < 0.0001$). Effect size (d) and Cohen's d values are taken as * $d = 0.2-0.5$ (small effect), ** $d = 0.5-0.8$ (medium effect), and *** $d \geq 0.8$ (large effect). **Abbreviations:** CDDP, cisplatin; CDDP6.25, cisplatin 6.25mg/kg; CDDP12.5, cisplatin 12.5mg/kg; d , Cohen's d ; ICAM-1, intracellular adhesion molecule 1; n , sample size; PI, proportional intensity.

5.4.8 VCAM-1 was upregulated in the tubules, glomeruli, and interlobar arteries of CDDP-treated mice

Expression of VCAM-1 was unaffected by CDDP6.25 compared to the SHAM group in the tubules (Figure 5.7E). However, CDDP12.5 increased tubular VCAM-1 expression compared to the SHAM group (3.3 ± 0.5 % vs 1.0 ± 0.3 %, $p < 0.01$). The glomerular analysis illustrated that CDDP6.25 (3.4 ± 0.4 % vs 0.2 ± 0.1 %, $p < 0.01$) and CDDP12.5 groups (2.4 ± 0.5 % vs 0.2 ± 0.1 %, $p < 0.01$) increased VCAM-1 protein expression significantly compared to the SHAM group, (figure 5.7J). CDDP resulted in significantly enhanced VCAM-1 expression by CDDP (6.25 and 12.5) in interlobar arteries, (figure 5.7O). Endothelial (13.5 ± 2.1 % vs 1.0 ± 0.2 %, $p < 0.001$) and medial (3.4 ± 0.9 % vs 1.0 ± 0.2 %, $p < 0.05$) expression of VCAM-1 was significantly enhanced by CDDP6.25 compared to the SHAM group. However, adventitial VCAM-1 expression showed a large effect (*Cohen's d*) compared to the SHAM group (5.5 ± 2.1 % vs 1.0 ± 0.4 %, $p = \text{ns}$, $d = -1.09$). VCAM-1 expression was significantly increased in the CDDP12.5 group compared to the SHAM group in the endothelium (7.7 ± 1.9 % vs 1.0 ± 0.2 %, $p < 0.05$), media (3.7 ± 1.0 % vs 1.0 ± 0.2 %, $p < 0.05$) and adventitial layers (4.2 ± 0.6 % vs 1.0 ± 0.4 %, $p < 0.01$).

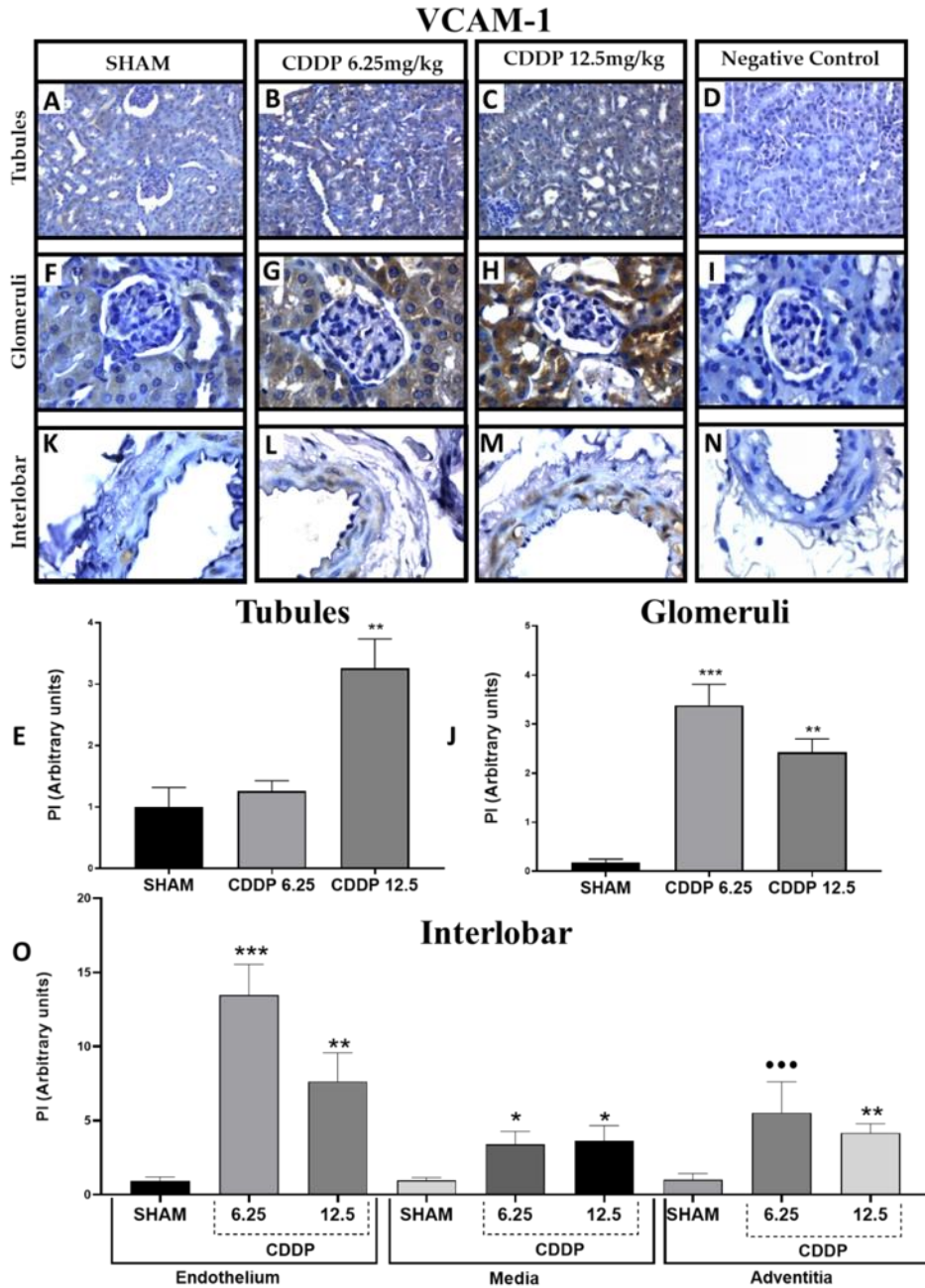


Figure 5.7. Immunohistochemical staining analysis of VCAM-1 expression in renal structures, including tubules, glomeruli and interlobar arteries in mice treated with SHAM, CDDP (6.25 or 12.5), (n=3-4). A-D. SHAM, CDDP6.25, CDDP12.5, and negative control-stained tubules at 40x magnification F-I. SHAM, CDDP6.25, CDDP12.5 and negative control-stained glomeruli at 100x magnification, K-N. SHAM, CDDP6.25, CDDP12.5, and negative control stained interlobar arteries at 100x magnification. Graphs of semi-quantified analysis of tissues are shown in E. tubules, J. glomeruli and O. interlobar arteries. All data is represented as Mean \pm SEM, and statistical analysis was performed using a one-way ANOVA followed by a Dunnett's post hoc test. * ($p < 0.05$), ** ($p < 0.01$), *** ($p < 0.001$), † ($p < 0.0001$). Effect size (d) and Cohen's d values are taken as •d=0.2-0.5 (small effect), ••d=0.5-0.8 (medium effect), and •••d \geq 0.8 (large effect). **Abbreviations:** CDDP, cisplatin; CDDP6.25, cisplatin 6.25mg/kg; CDDP12.5, cisplatin 12.5mg/kg; d, Cohen's d; n, sample size; PI, proportional intensity; VCAM-1, Vascular Cell Adhesion Molecule 1.

5.4.9 CDDP-induced E-Selectin upregulation following CDDP treatment.

Tubular expression of E-Selectin following treatment with CDDP was dose-dependent. CDDP6.25 (3.1 ± 0.1 % vs 1.0 ± 0.4 %, $p < 0.01$) and CDDP12.5 groups (3.4 ± 0.6 % vs 1.0 ± 0.4 %, $p < 0.01$) enhanced E-selectin expression, this was not observed between the CDDP doses, (figure 5.8E). Glomerular expression of E-Selectin was upregulated in both CDDP6.25 (7.4 ± 1.1 % vs 1.0 ± 0.4 %, $p < 0.001$) and CDDP12.5 groups compared to the SHAM group (3.1 ± 0.3 % vs 1.0 ± 0.4 %, $p < 0.01$), (figure 5.8J). In the CDDP6.25 group, endothelial (14.6 ± 2.9 % vs 1.0 ± 0.1 %, $p < 0.001$), medial (5.2 ± 1.2 % vs 1.0 ± 0.3 %, $p < 0.01$) and adventitial (4.1 ± 0.1 % vs 1.0 ± 0.3 %, $p < 0.05$) expression of E-selectin was significantly upregulated in all three vascular layers compared to the SHAM group. Medial (2.2 ± 0.3 % vs 1.0 ± 0.3 %, $p < 0.05$) and adventitial (3.9 ± 1.1 % vs 1.0 ± 0.3 %, $p < 0.05$) expression of E-Selectin was also upregulated in the CDDP12.5 group compared to the SHAM group, (figure 5.8O). Additionally, endothelial expression of E-Selectin had a medium effect (Cohen's d), (4.3 ± 1.7 % vs 1.0 ± 0.1 %, $p = \text{ns}$, $d = -0.79$) compared to the SHAM group.

E-Selectin

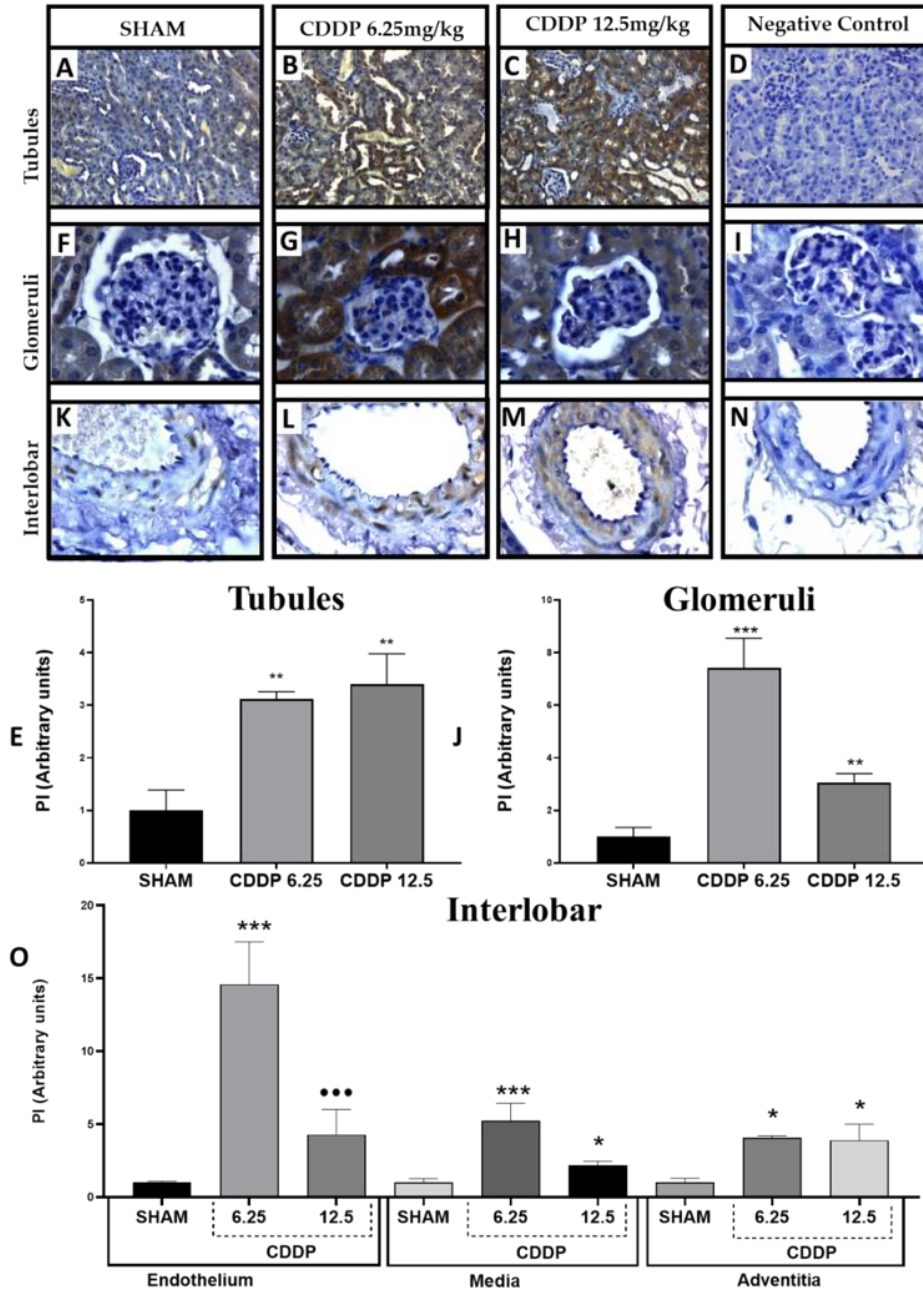


Figure 5.8. Immunohistochemical staining analysis of E-Selectin expression in kidney structures, including tubules, glomeruli and interlobar arteries in mice treated with SHAM, CDDP (6.25 or 12.5), (n=3-4). A-D. SHAM, CDDP6.25, CDDP12.5, and negative control-stained tubules at 40x magnification F-I. SHAM, CDDP6.25, CDDP12.5 and negative control-stained glomeruli at 100x magnification, K-N. SHAM, CDDP6.25, CDDP12.5, and negative control stained interlobar arteries at 100x magnification. Graphs of semi-quantified analysis of tissues are shown in E. tubules, J. glomeruli and O. interlobar arteries. All data is represented as Mean \pm SEM, and statistical analysis was performed using a one-way ANOVA followed by a Dunnett's post hoc test. * ($p < 0.05$), ** ($p < 0.01$), *** ($p < 0.001$), † ($p < 0.0001$). Effect size (d) and Cohen's d values are taken as • $d = 0.2-0.5$ (small effect), •• $d = 0.5-0.8$ (medium effect), and ••• $d \geq 0.8$ (large effect). **Abbreviations:** CDDP, cisplatin; CDDP6.25, cisplatin 6.25mg/kg; CDDP12.5, cisplatin 12.5mg/kg; d , Cohen's d ; n , sample size; PI, proportional intensity.

5.5 Discussion

The significant findings observed in this study include a) the CDDP 12.5 group demonstrated an effect (*Cohen's d*) in reduced ACH-mediated relaxation compared to the SHAM group, b) CDDP increases ANGII-mediated vasoconstriction compared to the SHAM group, c) CDDP12.5 increased positive PAS staining, d) Both CDDP doses increased tubular expression of TNF- α , GRP78 and TIM-1/KIM-1 and e) The CDDP12.5 group increased pro-inflammatory biomarkers ICAM-1, VCAM-1, and E-Selectin.

The CIAKI mouse model (euthanasia 72 hours after CDDP injection) is used extensively for assessing many pharmaceutical interventions against CIAKI. However, there remains no accord on a CDDP dose to induce AKI and its associated pathological damage, including vascular dysfunction, with doses in mouse models within the 10-30mg/kg range.

a) The CDDP 12.5 group demonstrated an effect (Cohen's d) in reduced ACH-mediated relaxation compared to the SHAM group.

Firstly, vascular function was assessed through a DRC to cumulative doses of either ACH to determine ACH-stimulated relaxation and SNP to measure endothelial-independent NO-mediated relaxation. Impaired vascular function is a highlighted pathophysiology involved in CIAKI [64]. This vasodilatory response is impaired by damaged or dysfunctional endothelium. CDDP is known to cause endothelial dysfunction, resulting in increased vascular resistance, and reduced renal blood flow and, consequently, decreased GFR [67, 70-73]. This study investigated the effects of two doses, CDDP (6.25 and 12.5) on ACH-mediated relaxation.

The CDDP12.5 group showed reduced ACH-mediated relaxation compared to SHAM, evidenced by a medium-large effect (*Cohen's d*), highlighting evidence of endothelial dysfunction. However, the CDDP6.25 group demonstrated a small-medium effect (*Cohen's d*) on enhanced relaxation at almost all doses of ACH compared to SHAM-treated mice. This suggests that a CDDP12.5 dose induced endothelial dysfunction, which could be attributed to either reduced NO bioavailability caused by CDDP-reduced eNOS expression or increased ROS generated by eNOS uncoupling. A study investigating the renoprotective effects of propofol on CDDP-induced endothelial injury demonstrated that propofol reduced nitrotyrosine overexpression, an indicator of ROS. Furthermore, propofol reduced CDDP-induced eNOS uncoupling, restoring NO production [145].

Interestingly, the CDDP6.25 group did not induce endothelial dysfunction suggesting that it may be a subtoxic dose at the four-day point. A previous study has linked CDDP incubation in Sprague Dawley rats with decreased contractility in thoracic aorta, vascular wall damage and cytotoxicity towards smooth muscle cells [130]. Thoracic aorta was harvested, endothelial denuded, and then incubated in 200 μ M CDDP for 6 hours before contractile studies. These results demonstrated that in an isolated acute setting, CDDP treatment does cause VSMC toxicity and subsequent functional impairment [130]. Surprisingly, the results of our study revealed that in 72 hours following treatment with CDDP (6.25 and 12.5), VSMC function was unaffected compared to the SHAM group, (figure 5.1C and D).

A study by Jiang et al. investigated *in vitro* the effect of 200 μ M CDDP on the toxicity to VSMC in the absence of systemic circulation and endothelium. Comparatively, our study was an *ex vivo* assessment of approximately 260 and 520 μ M plasma circulating CDDP. Our *in vivo* model could suppress CDDP toxicity caused by the systemic nature of the study, which may explain the reduced VSMC toxicity observed.

b) CDDP increases ANGII-mediated vasoconstriction compared to the SHAM group

The role of the renin-angiotensin-aldosterone system in CIAKI is a widely studied area due to its role in maintaining and regulating blood pressure and fluid balance through hormones such as aldosterone and ANGII [146]. A diverse array of CIAKI studies have reported the effects of CDDP on ANGII and its receptors. Interestingly, angiotensin II type 1 receptor (AT1R)/angiotensin II type 2 receptor (AT2R) receptor deletion, inhibition and activation have presented both protective and harmful effects to CIAKI [1]. Increased AT1R expression is widely reported to enhance the vasoconstrictive and ultimately hypertensive effects induced by ANGII in addition to oxidative stress and inflammation [147]. Aortic studies presented here showed that CDDP12.5-treated mouse iliac arteries had increased vasoconstriction to cumulative doses of ANGII compared to the SHAM group. The CDDP6.25 group was not assessed for ANGII-induced vasoconstriction.

Furthermore, it would be essential to determine if AT1R receptor expression is also upregulated. Tanaka et al. investigated the effects of CDDP treatment in patients with bladder cancer and demonstrated that AT1R receptor expression was upregulated following CDDP treatment [148]. Increased AT1R may also occur in this study

following CDDP treatment, explaining the enhanced vasoconstrictive effects observed in (figure 5.2A).

A study investigated the gender disparity of mean arterial pressure (MAP) in rats following cumulative doses of ANGII. This showed that CDDP treatment abolished gender variations in MAP in rats [149]. However, they did not report the direct effects of graded ANGII infusion in SHAM vs CDDP-treated rats which could have been valuable. Given that CDDP enhances ANGII-mediated vasoconstriction functionally, it is crucial to understand further the mechanisms inducing these effects and the interrelationship between ANGII receptors and CIAKI. This is particularly important for patients with pre-existing hypertension being treated with ARBs to better understand the impact of their comorbidities prior to the commencement of CDDP treatment to ensure renal preservation.

Literature has suggested that a single high dose of CDDP ranging from doses 8-14 mg/kg of CDDP induces a dose-dependent reduction in weight loss (%) in mice [127]. This was shown in (figure 5.3), which illustrates that although the CDDP6.25 group showed a degree of weight loss compared to the SHAM group, it was not observed to the same degree as the CDDP12.5 group. Interestingly, on average, the CDDP12.5 group induced a ~10% loss in % body weight on day four compared to the SHAM group and ~5% after CDDP6.25. Cachexia is a critical and often dose-limiting side effect of many anticancer agents, significantly decreasing cancer patient survivability [150]. It is defined as a >5% unintentional weight loss; given this, it may be useful to monitor food and water consumption more diligently in addition to body composition analysis to identify if weight loss occurs due to CDDP resulting in inadequate food intake or through other means such as cachexia. Although this is an important measurement and typically CDDP is known to cause a dose-dependent reduction in weight loss and is a result confirmed in this study, there is no current precise relationship explored between weight loss and kidney damage. This data has helped identify the dose of CDDP to be used for future CIAKI models, as the CDDP12.5 group induced a more significant weight loss than the CDDP6.25 group. This could suggest a greater degree of toxicity was observed. A study investigating the pathological changes that occur over time and a correlation with weight loss could prove a helpful tool for assessing the degree of renal damage occurring *in vivo*.

c) CDDP12.5 increases positive PAS staining

Histological analysis using PAS stain (figure 5.4) indicates that CDDP (6.25 and 12.5) groups had a higher degree of positive PAS staining than SHAM. This increased positive PAS staining correlates with a heightened glycogen content in renal tissues. In renal injury, intratubular cast formation is a crucial aetiology. Cast formation caused by acute tubular necrosis often presents as granular casts and is made up of previously sloughed cells resulting in tubular lumen obstruction [151]. CDDP (6.25 and 12.5) groups had increased PAS-positive evidence of cast formation in the tubules compared to the SHAM group.

Tubular, and glomerular PAS staining was increased following CDDP treatment with CDDP12.5 compared to the SHAM group; however, tubular, and glomerular expression was unaffected in the CDDP6.25 group. This correlates with the increase in inflammatory biomarkers observed throughout this study. This suggests that although PAS stain is typically used as a method of identification of morphological characteristics and assessed using a graded scoring system, it may also be a useful semi-quantitative analysis for models of AKI with evidence of cast formation resulting from acute tubular necrosis.

Positive PAS staining is significantly increased in the medial and adventitial layer of interlobar arteries from mice treated with CDDP12.5 only. ICAM-1 expression increases in a dose-dependent manner only in the adventitial layer of interlobar arteries. VCAM-1 expression is significantly increased in the endothelial, medial and adventitial layers of interlobar arteries from both CDDP groups, however, this effect is not dose-dependent. This further suggests the potential of PAS as a pathological stain. Further identification of PAS in the vasculature and, more significantly, the role of glycogen accumulation in these cells in disease settings could be beneficial in understanding not only the role of the renal vasculature in CIAKI but also other diseases such as diabetic nephropathy and interstitial glomerulonephritis.

d). CDDP increased tubular expression of TNF- α , GRP78 and TIM-1/KIM-1

The upregulation of cell stress markers is a well-established result of CDDP treatment. Three key biomarkers were assessed specifically in PTECs, as shown in (figure 5.5). TNF- α , GRP78 and KIM-1 are proteins known to be upregulated by CDDP treatment in models of CIAKI. [132, 144]. Results showed that both CDDP groups enhanced tubular expression of inflammatory biomarker TNF- α , ER-stress marker GRP78 and kidney injury molecular TIM-1/KIM-1 compared to SHAM. This was an interesting result; we

expected to observe a potential dose-dependent increase in these biomarkers. However, this was not observed. CDDP (6.25 and 12.5) groups induced upregulation of TNF- α , GRP78 and KIM-1 compared to the SHAM group, and no difference was observed between the two doses. This suggests no pathological difference in these three proteins in the two doses. Additional pro-inflammatory biomarkers were investigated to determine a pathological variance between the doses.

e) CDDP12.5 increased ICAM-1, VCAM-1, and E-Selectin expression.

To further establish the pathological doses that induce cell stress, we investigated pro-inflammatory markers ICAM-1 and VCAM-1, which are also known to increase following CDDP treatment [134, 135]. Tubular, glomerular and interlobar artery expression of these biomarkers were assessed. Results showed that CDDP increased ICAM-1 and VCAM-1. Tubular expression of ICAM-1 was upregulated by both CDDP (6.25 and 12.5) groups compared to the SHAM group, (figure 5.6E); however, VCAM-1 expression was upregulated by CDDP12.5 compared to the SHAM group; however, VCAM-1 expression was unaffected by the CDDP6.25 group. ICAM-1 and VCAM-1 were significantly upregulated in glomeruli by CDDP6.25 compared to the SHAM group, and VCAM-1 was significantly upregulated by CDDP12.5. Surprisingly, the CDDP12.5 group did not considerably affect ICAM-1 expression in the glomeruli; however, it did have a small effect (*Cohen's d*) compared to the SHAM group.

Understanding the involvement of CDDP in renal microvasculature is an understudied area. Given the link postulated between vascular injury and CIAKI pathogenesis, investigating blood vessels from a functional aspect in addition to inflammatory mechanisms may be beneficial to target the impaired renal hemodynamic observed in the condition. A study examining CDDP on vascular toxicity and, more specifically, CAM expression showed that in human vein endothelial cells incubated with 0-10 μ g/ml of CDDP for 24 hours or 4 μ g/ml of CDDP for up to 36 hours, mRNA, and protein expression of ICAM-1 but not VCAM-1 or E-Selectin were upregulated in endothelial cells [152]. Our study showed that in addition to a dose-dependent increase in ICAM-1 expression in endothelial cells following CDDP treatment, both VCAM-1 and E-Selectin were significantly upregulated in the CDDP6.25 compared to the SHAM group. VCAM-1 in endothelial cells was also significantly increased by the CDDP12.5 group compared to the SHAM group. Analysis of effect size showed that for E-Selectin, a large effect (*Cohen's d*) was observed in endothelial cells compared to the SHAM group. Recently, endothelial cells have been gaining attention, specifically in regulating renal inflammation in various kidney diseases [153], which may provide potential

insight into their involvement in CIAKI. However, the effect of pro-inflammatory markers on the medial and adventitial layers remains widely unknown in CIAKI pathogenesis.

Interestingly, CAM expression in the medial layer of blood vessels has also become a target of cardiovascular-related research suggesting ICAM-1 and VCAM-1 are expressed and play an inflammatory role in VSMCs. CDDP upregulated ICAM-1, VCAM-1, and E-Selectin in the medial layer of ILA, suggesting a CDDP-induced inflammatory response. This was consistently observed by both doses of CDDP, implying that CDDP (6.25 and 12.5) may be inducing an acute inflammatory response.

E-Selectin is an endothelial-specific cell surface biomarker of inflammation [154]. Increased mRNA expression of renal E-Selectin has been demonstrated in response to a single 20mg/kg CDDP injection [135]. Immunohistochemistry in our experiments enabled a location-based analysis for E-Selectin expression following CDDP treatment. Endothelial cells are located within the tubular network, glomeruli, and ILA. The results of this study displayed that an inflammatory response is occurring in endothelial cells at all three locations. E-Selectin expression was also increased by CDDP in the medial and adventitial layers of interlobar arteries.

Unpredictably, CDDP6.25 increased relaxation at higher ACH doses, suggesting that a lower dose of CDDP may stimulate vascular relaxation during cell stress. This is also observed in exercise, where oxidative stress and vascular function are increased [155]. PAS staining showed that the CDDP6.25 group had no effect compared to the SHAM group in tubular or glomerular positive PAS expression. Tubular expression of VCAM-1 was not significantly upregulated by the CDDP6.25 group; however, it was upregulated in the CDDP12.5 group compared to the SHAM. However, further studies are required to understand the vasoprotective effects of low-dose CDDP.

5.6 Limitations

A single dose must be decided to test pharmaceutical interventions to prevent CIAKI. The greatest importance was placed on vascular function and protein expression in PTECs. The low sample size used may have hindered the generation of statistical significance. Analysis of effect (*Cohen's d*) size was used better to understand the statistical relevance despite the lack of statistical significance. Although many of the antibodies used for immunohistochemical staining are monoclonal, and one is KO validated, some are polyclonal, and there is the possibility for non-specific binding. IHC analysis is semi-quantitative and is an estimate rather than an exact measurement.

Tissues are often subjected to harsh fixation chemicals such as formalin or glutaraldehyde. In this study, 4% PFA was used due to the cross-linking nature induced by PFA; if over-fixed, this can lead to either tissue damage, protein degradation or impenetrability of antibodies during staining.

5.7 Future directions

It may be beneficial to future investigations to harvest abdominal aorta from *in vivo* treated mice at varying time points from the initial CDDP injection to identify if the same acute toxicity caused by CDDP occurred at varying time points to determine whether the systemic environment allows for either prevention or repair of VSMC toxicity. It is surprising that, based on the magnitude of CIAKI studies, a lack of foundational CIAKI mouse model studies exist. A larger scale dosing study to generate a dose-relationship curve to determine doses that induce minimal CIAKI is needed. Assessing doses at intervals of 3mg/kg from 3-30mg/kg could be useful to understand the effects of CDDP dose on CIAKI development. The assessment of renal perfusion to determine the function of renal interlobar arteries and involvement of the vascular network in CIAKI is a critical future progression for future CIAKI studies. It is a method that our laboratory is developing, and the process of its development is outlined in Appendix A of this thesis.

5.8 Conclusion

Given the toxic effects on the vasculature induced by CDDP and increased tubular damage, this study concluded that the CDDP12.5 group caused physiologically relevant pathological damage to renal tissue and, subsequently, the vasculature, indicated by vascular function studies compared to both the CDDP6.25 and the SHAM groups. Therefore, CDDP12.5 was recognised as a more suitable dose for future CIAKI studies.

Chapter 6: BX-912 mitigates cisplatin-induced AKI through improved renal blood flow and reduced inflammation: A pilot study.

6.1 Abstract

Background: Cisplatin-induced acute kidney injury (CIAKI)¹¹ is a prevalent condition with a high mortality rate in cancer patients treated with cisplatin (CDDP)¹². The current and most effective treatments include pre-hydration therapy and diuretic mannitol. CIAKI is a reduction in glomerular filtration rate (GFR)¹³ stimulated by reduced renal blood flow attributed to CDDP-induced endothelial dysfunction. BX-912 (BX) is a highly selective and potent adenosine triphosphate (ATP)-competitive inhibitor of phosphoinositide-dependent kinase 1(PDK1). BX has been targeted as an anticancer therapy due to its inhibitory effect on the phosphoinositide 3-kinases (PI3K)/PDK1/Akt/mammalian target of rapamycin (mTORC) pro-survival pathway. BX has demonstrated a novel function as a vasodilator in small arteries in our laboratory (Chapter 4). More broadly, PDK1 inhibition is associated with blocking downstream nuclear factor kappa B (NF- κ B) signalling. NF- κ B is a crucial transcription factor for inflammatory cytokines and chemokines, and its transcriptional inhibition has been correlated with CIAKI prevention. Multiple inhibitors of PDK1 have illustrated mitigating effects against CIAKI providing adequate theoretical justification for using BX in the prevention of CIAKI. **Animals/Methods:** To investigate the preventative effects of BX against CIAKI, BX, 5mg/kg (BX5), BX, 0.5mg/kg (BX0.5), and BX, 0.05mg/kg (BX0.05) were intraperitoneally (IP) injected into 10-12wk old C57BL/6J mice on days 0-4. A single 12.5mg/kg dose of CDDP was given via IP injection on day one. Mice were euthanised 72 hours following the CDDP injection. Kidneys were removed for histopathological and genomic analysis. Abdominal aorta was removed for isometric tension studies. **Results:** BX significantly improved acetylcholine (ACH) relaxation in the BX0.5 group at doses 10^{-5} [M], ($p<0.05$) and BX0.05, 10^{-5} [M], ($p<0.0001$) compared to the CDDP group. Additionally, BX reduced angiotensin II (ANGII)-mediated vasoconstriction in the BX5 group at dose $10^{-7.5}$ [M], ($p<0.05$), BX0.5 at dose 10^{-7} [M], ($p<0.01$) and the BX0.05 group at dose, $10^{-7.5}$ [M], ($p<0.01$) compared to the CDDP group. Histopathological analysis revealed that the BX0.05

¹¹ CIAKI, cisplatin-induced acute kidney injury

¹² CDDP, cisplatin

¹³ GFR, glomerular filtration rate

group reduced periodic acid Schiff (PAS) stain expression in tubules, ($p<0.05$). In the BX0.5 group, there was reduced tubular VCAM-1, ($p<0.05$) and kidney injury molecule 1 (KIM-1), ($p<0.05$). Tubular and glomerular expression of KIM-1 was significantly downregulated by the BX0.05 group, ($p<0.05$ and $p<0.001$) compared to the CDDP group. Tubular expression of intracellular adhesion molecule 1 (ICAM-1), vascular cell adhesion molecule 1 (VCAM-1), glucose-regulated protein 78 (GRP78) and E-Selectin were all downregulated by the BX0.05 group compared to the CDDP group, ($p<0.05$). Interestingly, mRNA expression of transmembrane glycoprotein nmb (Gpnmb) was significantly downregulated in the BX0.05 group compared to CDDP ($p<0.05$). A medium effect (Cohen's d) demonstrated downregulation in NOX4 expression in the BX0.05 group compared to the CDDP group $d=0.5$. **Discussion:** BX enhanced ACH-mediated relaxation compared to the CDDP group. This is a beneficial therapeutic effect for the prevention of CIAKI; however, further studies are required to determine the molecular mechanisms involved in the vasodilatory-enhancing effects of BX *in vivo*. Results showed that BX significantly reduced ANGII-mediated vasoconstriction. Currently, there is no evidence to elucidate a relationship between PDK1 inhibition and ANGII vasoconstriction, however, it could be a useful to determine the role of BX in ANGII-mediated vasoconstriction, which requires further study. BX-induced renoprotection may be partially mediated through reduced renal protein expression of CIAKI-associated biomarkers ICAM-1, VCAM-1, and E-Selectin however, further studies to determine the mechanisms associated with protein downregulation induced by BX are required. The renoprotective effects of BX may be partially mediated by reduced mRNA expression of nicotinamide adenine dinucleotide phosphate (NADPH) oxidase 4 (NOX4) expression. Treatment of NOX4 deficient mice could elucidate the role of NOX4 in the renoprotective effects of BX and any potential off-target effects. **Conclusion:** This pilot study provides evidence that BX could inhibit CIAKI. A larger animal study is warranted to confirm these results.

6.2 Introduction

CDDP is a platinum-based antineoplastic agent. It causes inter and intrastrand DNA crosslinks, inhibiting DNA replication [156]. Despite its identification as an anticancer agent in the 1960s, it was not until the late 1970s that it was commercially available as the first food and drug administration (FDA)-approved platinum-derived treatment for cancer [56]. CDDP is used to treat a broad range of cancers, including breast [42], cervical [42], oesophageal [43], bladder [44], small cell lung [45] and testicular cancers [46]. Although it has a long list of systemic side-effects, its dose-limiting factor is nephrotoxicity [52, 57-63] which manifests as acute kidney injury (AKI) in approximately 35% of patients. AKI is defined as a rapid decline in GFR linked to reduced renal blood flow and enhanced vascular resistance [67]. CIAKI incidence is high, highlighting the urgency for treatment. In two studies, CIAKI presented in 23.8% of patients in the first week of receiving a CDDP-based regimen [157] and up to 30% in a cohort study targeted at identifying epidemiological statistics of CIAKI in paediatrics [158]. Understanding the pathophysiology and, more specifically, the molecular mechanisms involved in the development of CIAKI is underway. However, despite this, CIAKI prevalence and incidence remains high, attributed to the absence of pharmacologically preventative options [32].

BX is a highly selective and potent ATP-competitive inhibitor of (PDK1) that currently use has been predominantly targeted as an anticancer therapy due to its inhibition of the PDK1/Akt pathway [102]. BX pre-clinical use has a broad spectrum of therapeutic potential. BX has shown beneficial effects as an anticancer agent [103], PDK1 activity attenuation and chemotaxis in response to vascular injury [106], and inhibition of *in vitro* osteoblast differentiation and maturation [105]. It has also demonstrated a novel function as a vasodilator in small arteries, as denoted in Chapter 4 of this thesis. BX incubation has also been shown to reduce NF- κ B DNA binding in some cell lines [159], and more broadly, PDK1 inhibition is associated with blocking downstream NF- κ B signalling [160]. NF- κ B is a crucial transcription factor for inflammatory cytokines and chemokines [161], and its transcriptional inhibition has been correlated with CIAKI amelioration [38]. In a CDDP-induced nephrotoxicity study showing the preventative effects of celecoxib on renal injury attenuation, it was noted that the selective cyclooxygenase-2 (COX-2) inhibitor, also had PDK1 inhibitory properties [162]. As such, the COX-2 inhibitor is a promising nephroprotective agent [163]. It is unclear whether the protective effects are attributed directly to COX-2 or PDK1 inhibition;

however, this study provides an excellent theoretical background for using BX in CIAKI mitigation.

The PI3K/Akt/mTORC pathway and subsequent suppression of autophagy are associated with the nephrotoxic effects of CIAKI. Pharmacological inhibition of mTORC by rapamycin or indirect mTORC inhibition through inhibited Akt phosphorylation has displayed renoprotective effects against CIAKI [111]. PDK1 is a requirement for Akt activation [164], and its downstream signalling cascade includes mTORC and the uncoordinated-51-like kinases 1 (ULK1) phosphorylated suppression of autophagy [165]. Additionally, treatment with imatinib, a tyrosine kinase inhibitor that results in downstream PI3K/Akt/mTORC pathway inhibition [166], has also shown beneficial effects in preventing CDDP-induced nephrotoxicity [167]. Taken together, indirect inhibition of the PI3K/Akt/mTORC pathway by imatinib and rapamycin presented a novel opportunity in the prevention of CIAKI. Interestingly, it has been suggested that the preservation of vasculature is beneficial in CIAKI amelioration [113]. Given the vasodilatory role of BX described in Chapter 4, extrapolated to improve renal blood flow and its potential anti-inflammatory properties linked to its role as a PDK1 inhibitor, highlighted its potential as a preventative treatment for CIAKI.

To determine the effects of BX in preventing CIAKI through enhanced vasodilation to reduce vascular resistance and improve GFR, three different doses of BX (5, 0.5 and 0.05) were used. Abdominal aorta and iliac arteries were harvested from mice and assessed for vascular function through vasodilation response to the cumulative dose of either ACH or SNP or vasoconstrictive response to ANGII. In addition to vascular function studies, histopathological damage was assessed through PAS staining to determine cast formation indicated by positive PAS stain, immunohistochemistry (IHC) analysis of protein expression of pro-inflammatory biomarkers, ICAM-1, VCAM-1, and E-Selectin, in addition to KIM-1, a biomarker of kidney injury and GRP78, an indicator of endoplasmic reticulum (ER) stress. Scanning electron microscopy (SEM) was used to determine platinum content and accumulation in renal tissues. Nephrotoxicity real-time (RT²) polymerase chain reaction (PCR) was performed to analyse changes in gene expression associated with nephrotoxicity and further elucidate potential mechanisms of BX in CIAKI.

6.3 Materials

Chemicals: Refer to Chapter 2, section 2.13 solutions, for purchasing information for the following chemicals: KREBS, Paraformaldehyde (PFA), McDowell and Trump

Fixative, CDDP, BX, Dimethylformamide (DMF), 9,11-Dideoxy-11 α ,9 α -epoxymethanoprostaglandin F_{2 α} (U46619), acetylcholine Chloride (Ach), Sodium Nitroprusside (SNP), Osmium Tetroxide, Hexamethyldisilazane (HMDS), ImmPRESS™ Anti-Rabbit IgG: made in goat KIT, DAB Substrate Kit, Periodic Acid-Schiff (PAS) Staining system. **Antibodies:** For information on antibodies used in this chapter, please refer to Chapter 2: General Methods, Table 2.2. This table identifies the antibody, clonality and catalogue number for each antibody. For antibody concentrations, refer to the section in the table titled "BX in CDDP-induced AKI".

6.4 Methods

6.4.1 Animals/Experimental Protocol

For animal purchase, housing, and treatment regimen information, please refer to Chapter 2, section 2.1 Animals/experimental regimens, subsection 2.1.2 CIAKI (5-day model). Variations to this include the inclusion of an *in vivo* drug administration protocol. On days 0-4, mice received an intraperitoneal (IP) injection of either BX (5, 0.5 or 0.05 mg/kg) formulated as described in Chapter 2, section 2.6.2 Mouse Drug formulations. For details on monitoring during the experiment period, please refer to section 2.2 monitoring, 2.2.1 mice monitoring. For information on the anaesthetisation and culling, please refer to section 2.3. For mouse dissection protocol is illustrated in section 2.4.

6.4.2 EchoMRI

For information on the timing and procedure of EchoMRI, please refer to Chapter 2, General methods, section 2.5 EchoMRI.

6.4.3 Isometric Tension

For the Isometric tension procedure, refer to Chapter 2, section 2.6 isometric tension. For additional information, please refer to table 2.1. For information on drugs used for functional analysis, please refer to section 2.6.2, Mouse drug stimulations.

6.4.4 Tissue Processing/Histochemical and Immunohistochemical staining/Analysis.

Tissue processing details are described in Chapter 2, General methods, section 2.7. For information on histology, please refer to section 2.8. For specific details on immunohistochemistry, refer to section 2.8.1. and table 2.2. for antibodies used for staining, including clonality, supplier, catalogue and concentrations used in specific vessel types. Please refer to 2.8.2 for the description of the PAS stain protocol. For an

explanation of the semi-quantification used for immunohistochemical analysis, please refer to section 2.9.

6.4.5 SEM analysis

Please refer to Chapter 2, section 2.10 SEM metal composition analysis

6.4.6 RT²-PCR Analysis

For information on RT² profiler PCR array, refer to Chapter 2, General Methods, section 2.11. For specific details, please refer to sections 2.11.1 ribonucleic acid (RNA) isolation protocol and 2.11.2 complementary deoxyribonucleic acid (cDNA) synthesis protocol and for RT² profiler PCR array protocol, please refer to section 2.11.3.

6.4.7 Data/Statistical Analysis

Statistical analyses are detailed in Chapter 2, General methods section 2.12. For analysis of variance (ANOVA) details, please refer to section 2.12.1 and for information on *Cohen's d* analysis, please refer to section 2.12.2. For *Cohen's d*, the calculation of effect and size values are compared to CDDP. Positive *d* values indicate a reduction compared to CDDP, and negative values represent an increase compared to CDDP.

6.5 Results

6.5.1 BX, increased ACH, and SNP-mediated relaxation compared to CDDP treatment alone.

To determine the effect of BX on vascular function, abdominal aorta harvested from BX and CDDP-treated mice were assessed for ACH-mediated and SNP-mediated relaxation, (figure 6.1A and B). Results demonstrated that BX5 had an increase in relaxation which revealed a dose-dependent increase in effect size ranging from a small effect (*Cohen's d*), (0.22) at 10⁻⁸ [M] to a large effect (*Cohen's d*), (0.85) at 10⁻⁵ [M]. Surprisingly, the BX0.5 group improved ACH-mediated vascular relaxation compared to the CDDP group at 10⁻⁵ [M] (-62.4 ± 5.3 % vs -38.0 ± 6.34 %, *p*<0.05). The BX0.05 group significantly improved ACH-induced relaxation compared to the CDDP group from doses 10⁻⁸ [M] (-15.3 ± 3.7 % vs -4.8 ± 3.4 %, *p*<0.01) to 10⁻⁵ [M] (-78.5 ± 8.1 % vs -38.0 ± 6.4 %, *p*<0.0001). In addition, the BX0.05 group also showed a significant difference in area under the curve (AUC) compared to the CDDP group (164.2 ± 17.2 vs 73.8 ± 25.6, *p*<0.05). An increase in AUC was observed, supported by a medium effect (*Cohen's d*) in mice treated with BX5 *d*=-0.59 and BX0.5 *d*=-0.65 compared to CDDP. Interestingly no shift in LogEC₅₀ was observed in any BX dose compared to CDDP treatment alone, table 6.2.

SNP was used to assess vascular smooth muscle cell (VSMC) function and demonstrated that BX improved vascular function in all three doses (*Cohen's d* effect). However, it was only significant in the BX0.05 group at dose at $10^{-6.5}$ [M] (-60.4 ± 9.4 % vs 33.1 ± 6.8 %, $p < 0.05$) compared to the CDDP group. Further, an increase in LogEC_{50} and AUC was noted at each BX groups (5, 0.5 and 0.05) (table 6.2). For statistically significant p values and effect size (*Cohen's d*) values obtained for each ACH and SNP dose, please refer to table 6.1.

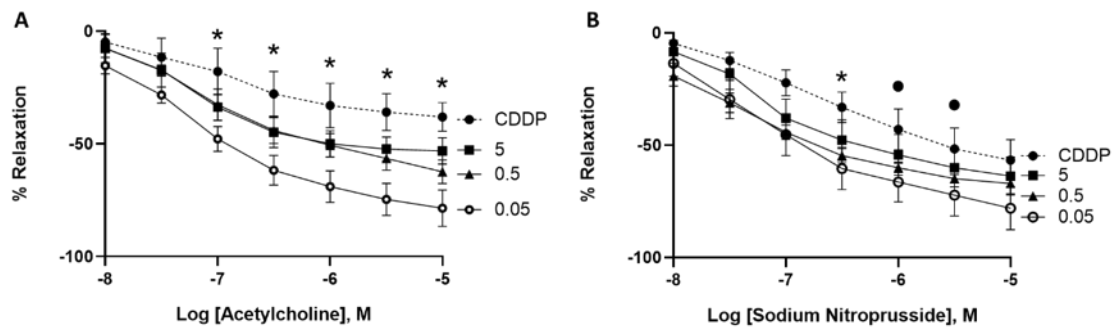


Figure 6.1. Isometric tension analysis results of CDDP and CDDP + BX treated mice (n=3-4). (A) ACH and (B) SNP (doses 10^{-5} to 10^{-8} [M]) -induced vascular relaxation of abdominal aorta in CDDP and CDDP + BX (5, 0.5 and 0.05) treated mice. All data is represented as mean \pm standard error of the mean (SEM), and statistical analysis was performed using a one-way ANOVA followed by a Dunnett's post hoc test. * ($p < 0.05$), ** ($p < 0.01$), *** ($p < 0.001$), † ($p < 0.0001$). Effect size (d) and Cohen's d values are taken as • $d = 0.2-0.5$ (small effect), •• $d = 0.5-0.8$ (medium effect), and ••• $d \geq 0.8$ (large effect). For p values and Cohen's d values of effect size, please refer to table 6.1 **Abbreviations:** ACH; acetylcholine, SNP; sodium nitroprusside and CDDP; cisplatin; BX5, 5mg/kg of BX-912; BX0.5, 0.5 mg/kg of BX-912; BX0.05, 0.05 mg/kg of BX-912; [M], Molar; n, sample size.

Table 6.1. Effect of BX in vivo treatment on the prevention of cisplatin-induced vascular dysfunction. This was determined by a dose-response curve to cumulative doses of ACH and SNP

ACH/SNP Conc [M]	Acetylcholine (ACH)			Sodium nitroprusside (SNP)		
	BX5	BX0.5	BX0.05	BX5	BX0.5	BX0.05
10^{-8}	d= 0.22	d= 0.3	d= 0.94	d= 0.35	d= 1.51	d= 0.44
$10^{-7.5}$	d= 0.24	d= 0.27	d= 0.76	d= 0.35	d= 1.28	d= 0.62
10^{-7}	d= 0.59	d= 0.51	p= 0.004	d= 0.63	d= 1.05	d= 0.69
$10^{-6.5}$	d= 0.65	d= 0.61	p= 0.001	d= 0.52	d= 0.89	p= 0.023
10^{-6}	d=0.66	d= 0.67	p= 0.0005	d= 0.32	d= 0.54	d= 0.67
$10^{-5.5}$	d= 0.77	d= 0.92	p= 0.0002	d= 0.24	d= 0.41	d= 0.61
10^{-5}	d= 0.85	p= 0.024	p <0.0001	d= 0.20	d= 0.32	d= 0.64

Statistical significance is taken at ($p < 0.05$), and effect size (d) and Cohen's d values are taken as $d = 0.2 - < 0.5$ (small effect), $d = 0.5 - < 0.8$ (medium effect), and $d = \geq 0.8$ (large effect).

Abbreviations: ACH, acetylcholine; BX5, 5 mg/kg of BX-912; BX0.5, 0.5 mg/kg of BX-912; BX0.05, 0.05 mg/kg of BX-912; CDDP, cisplatin; Conc, concentration; d = Cohen's d ; [M], Molar; SNP, sodium nitroprusside.

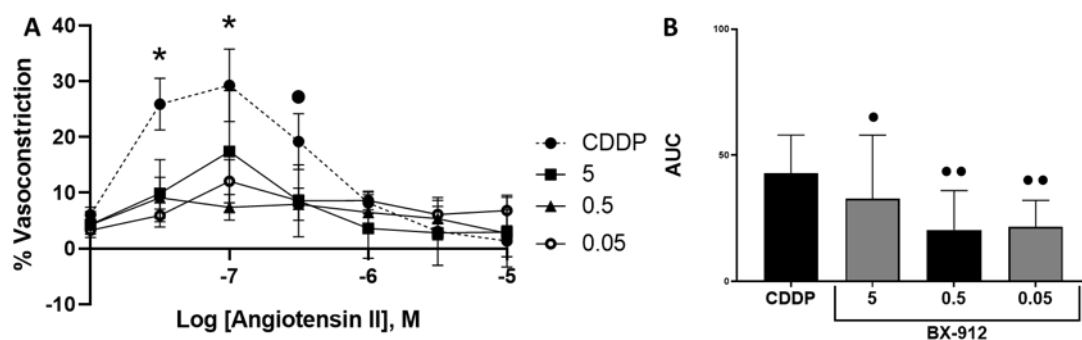
Table 6.2. LogEC₅₀ and AUC of CDDP and CDDP + BX (5, 0.5 and 0.05) treated mice.

AA- ACH	n	Log EC₅₀ ± SEM	p vs CDDP	d vs CDDP	AUC ± SEM	p vs CDDP	d vs CDDP
<i>CDDP</i>	3	-6.73 ± 0.3			73.76 ± 25.6		
<i>CDDP + BX5</i>	3	-7.05 ± 0.01	p=ns	d= 0.27	114.1 ± 18.5	p=ns	d= -0.59
<i>CDDP + BX0.5</i>	4	-6.78 ± 0.2	p=ns	p=ns	118.1 ± 13.7	p=ns	d= -0.65
<i>CDDP + BX0.05</i>	4	-6.90 ± 0.01	p=ns	p=ns	164.2 ± 17.2	p= 0.02	d= -1.26
AA- SNP	n	Log EC₅₀ ± SEM	p vs CDDP	d vs CDDP	AUC ± SEM	p vs CDDP	d vs CDDP
<i>CDDP</i>	4	-6.57 ± 0.1	p=ns		96.39 ± 18.7		
<i>CDDP + BX5</i>	4	-6.93 ± 0.1	p=ns	d= 0.24	127.5 ± 23.3	p=ns	d= -0.41
<i>CDDP + BX0.5</i>	4	-6.96 ± 0.1	p=ns	d=0.26	148.9 ± 6.9	p=ns	d= -0.80
<i>CDDP + BX0.05</i>	4	-6.93 ± 0.1	p=ns	d= 0.24	159.9 ± 25.0	p=ns	d= -0.81
IA- ANGII	n	Log EC₅₀ ± SEM	p vs CDDP	d vs CDDP	AUC ± SEM	p vs CDDP	d vs CDDP
<i>CDDP</i>	3	-6.50 ± 0.2			73.76 ± 25.6		
<i>CDDP + BX5</i>	4	-6.98 ± 0.4	p=ns	d= 0.35	114.1 ± 18.5	p=ns	d=0.30
<i>CDDP + BX0.5</i>	4	-6.37 ± 0.5	p=ns	p=ns	118.1 ± 13.7	p=ns	d=0.76
<i>CDDP + BX0.05</i>	4	-5.86 ± 0.8	p=ns	d= -0.40	164.2 ± 17.2	p=ns	d=0.77

All data is represented as Mean ± SEM, and statistical analysis was performed using a one-way ANOVA followed by a Dunnett's post hoc test. Statistical significance is taken at (p<0.05), and effect size (d) and Cohen's d values are taken as d=0.2-<0.5 (small effect), d=0.5-<0.8 (medium effect), and d=≥0.8 (large effect). **Abbreviations:** AA, abdominal aorta; IA, iliac artery; ACH, acetylcholine; SNP, sodium nitroprusside; ANGII, angiotensin II; SEM, standard error of the mean; CDDP, cisplatin; AUC, area under the curve; n, sample size

6.5.2 BX reduced ANGII-induced vasoconstriction in CDDP-treated mice.

The vascular response to ANGII in CIAKI is incompletely understood, with most ANGII studies occurring in renal epithelial tissue. A DRC to ANGII from doses (10^{-8} to 10^{-5} [M]) in iliac arteries was completed *ex vivo* to elucidate the impact of BX on ANGII-induced vasoconstriction compared to the CDDP group, (figure 6.2). Isometric tension analysis showed that concomitant treatment of CDDP with BX significantly reduced ANGII-induced vasoconstriction in groups BX5, $10^{-7.5}$ [M] (9.9 ± 6.0 % vs 25.9 ± 4.7 %, $p < 0.05$), BX0.5 $10^{-7.5}$ [M] (9.1 ± 3.7 % vs 25.9 ± 4.7 %, $p < 0.05$) and 10^{-7} [M] (7.4 ± 2.3 % vs 29.3 ± 6.5 %, $p < 0.01$) and BX0.05, $10^{-7.5}$ [M] (25.9 ± 4.7 % vs 6.0 ± 1.2 %, $p < 0.01$) compared to the CDDP group. Analysis of AUC demonstrated that an effect size according to *Cohen's d* was generated compared to CDDP for BX5, $d = 0.3$, BX0.5,



$d = 0.76$ and BX0.05, $d = 0.77$ BX treated groups. For statistically significant p values and effect size (*Cohen's d*) values obtained for each ANGII dose, please refer to table 6.3.

Figure 6.2. BX reduced ANGII-induced vasoconstriction in CDDP + BX treated mice compared to CDDP alone ($n = 4$). Separate rings obtained from mice treated with either CDDP alone or in combination with BX (5, 0.5 or 0.05) were subjected to **A.** a cumulative DRC to determine if BX reduced ANGII-induced vasoconstriction. **B.** Representative AUC graph indicating AUC for each treatment. All data is represented as Mean \pm SEM, and statistical analysis was performed using a one-way ANOVA followed by a Dunnett's post hoc test. * ($p < 0.05$), ** ($p < 0.01$), *** ($p < 0.001$), \dagger ($p < 0.0001$). Effect size (d) and *Cohen's d* values are taken as • $d = 0.2 - 0.5$ (small effect), •• $d = 0.5 - 0.8$ (medium effect), and ••• $d \geq 0.8$ (large effect). For p values and *Cohen's d* values of effect size, please refer to table 6.3 Abbreviations: AUC, Area Under Curve; CDDP, cisplatin; d , *Cohen's d*; BX5, 5mg/kg of BX-912; BX0.5, 0.5mg/kg of BX-912; BX0.05, 0.05mg/kg of BX-912; [M], Molar; n , sample size.

Table 6.3. Effect of BX in vivo treatment on ANGII-induced vasoconstriction compared to CDDP alone.

ANGII Conc [M]	CDDP + BX5	CDDP + BX0.5	CDDP + BX0.05
10^{-8}	$d= 0.28$	$d= 0.33$	$d= 0.59$
$10^{-7.5}$	$p= 0.03$	$p= 0.02$	$p= 0.01$
10^{-7}	$d= 0.44$	$p= 0.01$	$d= 1.23$
$10^{-6.5}$	$d= 0.51$	$d= 0.62$	$d= 0.61$
10^{-6}	$d= 0.40$	$p= ns$	$p= ns$

Statistical significance is taken at ($p<0.05$), and effect size (d) and Cohen's d values are taken as $d=0.2-<0.5$ (small effect), $d=0.5-<0.8$ (medium effect), and $d=\geq 0.8$ (large effect). **Abbreviations:** ANGII, angiotensin II; BX5, 5mg/kg of BX-912; BX0.5, 0.5 mg/kg of BX-912; BX0.05, 0.05 mg/kg of BX-912; CDDP, cisplatin; Conc, concentration; $d=$ Cohen's d ; [M], Molar.

6.5.3 Effect of CDDP and CDDP + BX on body composition.

In Chapter 5, a significant reduction in body weight following CDDP treatment was shown. To determine the effects of BX on alterations in body composition, mice were given a pre-and post-treatment EchoMRI to determine Δ Fat loss %, Δ Lean loss %, Δ Free water %, and Δ Total water %. Firstly, results illustrated that CDDP increased Δ Fat loss % compared to control (CON) (56.2 ± 7.6 vs -4.1 ± 7.0 , $p<0.001$). CDDP also increased Δ Lean loss % (9.4 ± 1.8 vs -2.6 ± 0.2 , $p<0.01$) and Δ Total water % (10.8 ± 1.8 vs -1.0 ± 2.2 , $p<0.05$) compared to CON (figure 6.3). Adding BX (5, 0.5 or 0.05) to CDDP did not reduce Δ Fat loss %, Δ Lean loss % or Δ Total water % compared to CDDP alone. Surprisingly, BX0.05 significantly reduced free water % compared to CDDP.

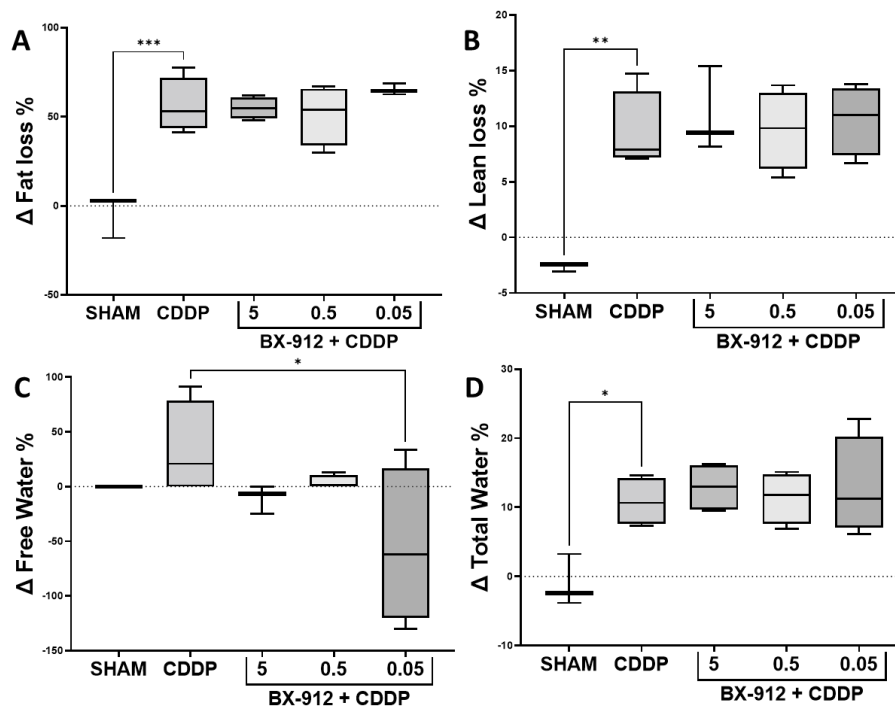


Figure 6.3. Effect of CDDP and BX + CDDP on mouse body composition analysis, (n=3-4). **A.** Δ Fat loss %, **B.** Δ Lean loss %, **C.** Δ Free water %, and **D.** Δ Total water %. All data is represented as Mean \pm SEM, and statistical analysis was performed using a one-way ANOVA followed by a Dunnett's post hoc test. * ($p < 0.05$), ** ($p < 0.01$), *** ($p < 0.001$), † ($p < 0.0001$). **Abbreviations:** BX5, 5mg/kg of BX-912; BX0.5, 0.5mg/kg of BX-912; BX0.05, 0.05mg/kg of BX-912; CDDP, cisplatin; CON, control; n, sample size.

6.5.4 BX reduces tubular PAS staining.

An increase in PAS histological staining is used to indicate renal damage. Increased positive PAS staining is associated with renal injury following CDDP treatment. The BX0.05 group reduced positive tubular PAS staining indicative of reduced tubular injury compared to the CDDP group, (figure 6.4F), (0.1 ± 0.1 % vs 1 ± 0.3 %, $p < 0.05$). Results showed that both the BX5 and BX0.5 groups produced a small effect *Cohen's d*) in reducing tubular injury compared to the CDDP group ($d = 0.27$ and $d = 0.29$). Despite the reduced histological damage in proximal tubule epithelial cells (PTEC) by BX, glomerular damage was not improved by BX at any dose (figure 6.4L). The BX0.05 group reduced positive PAS staining in the endothelium and medial layers of interlobar arteries $d = 0.48$ and $d = 0.45$ compared to the CDDP group. Although BX0.05 did not affect the adventitial layer, BX0.5 had a small effect (*Cohen's d*), $d = 0.21$ (figure 6.4R).

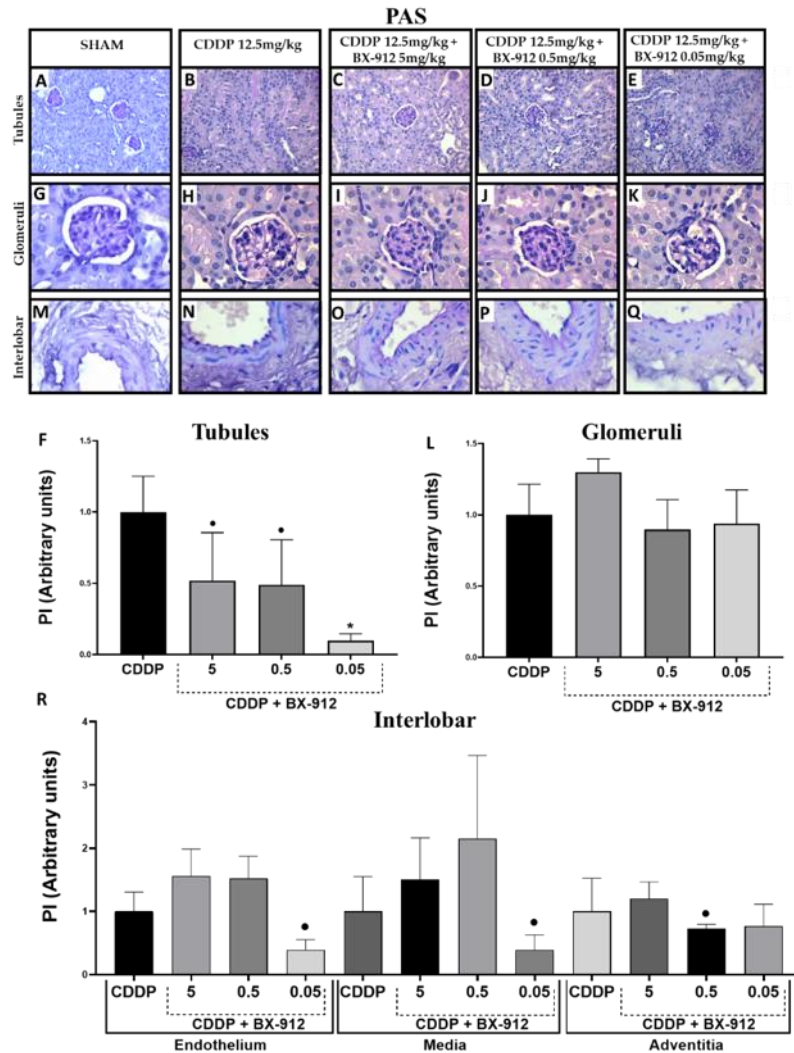


Figure 6.4. Histological analysis of PAS-stained mouse kidney tubules, glomeruli and interlobar arteries, (n=3-4). 40x magnification Images of paraffin-embedded kidney sections were taken from mice treated with CDDP and various doses of BX + CDDP. **A-E.** Kidney tubules (SHAM, CDDP 12.5, CDDP 12.5 + BX (5, 0.5 and 0.05.)) **F.** Graph representing tubular PAS positive expression of mice treated with CDDP or CDDP + BX (5, 0.5 and 0.05). **H-L.** Renal glomeruli were taken at 100x magnification under immersion oil (SHAM, CDDP 12.5, CDDP 12.5 + BX (5, 0.5 and 0.05.)) **L.** Graph representing PAS positive expression in Glomeruli of CDDP or CDDP + BX (5, 0.5 and 0.05) treated mice. Images **M-Q.** Renal interlobar arteries were taken at 100x magnification under immersion (SHAM, CDDP 12.5, CDDP 12.5 + BX (5, 0.5 and 0.05.)) **R.** Graph of PAS-positive expression in the endothelium, media, and adventitial layers of interlobar arteries in CDDP or CDDP + BX (5, 0.5 and 0.05) treated mice. All data is represented as Mean \pm SEM, and statistical analysis was performed using a one-way ANOVA followed by a Dunnett's post hoc test. * ($p < 0.05$), ** ($p < 0.01$), *** ($p < 0.001$), \dagger ($p < 0.0001$). Effect size (d) and Cohen's d values are taken as $\bullet d = 0.2-0.5$ (small effect), $\bullet\bullet d = 0.5-0.8$ (medium effect), and $\bullet\bullet\bullet d \geq 0.8$ (large effect). **Abbreviations:** BX5, 5mg/kg of BX-912; BX0.5, 0.5mg/kg of BX-912; BX0.05, 0.05mg/kg of BX-912; CDDP, cisplatin; d = Cohen's d ; n , sample size; PAS, periodic acid Schiff; PI, proportional intensity.

6.5.5 BX reduces KIM-1 in tubules and glomeruli of CDDP-treated mice.

KIM-1 is a valuable biomarker for PTEC injury in humans with acute renal failure [131] and glomerular injury in proteinuria kidney disease [168]. Adjunct BX and CDDP-treated mice showed reduced KIM-1 expression in renal tubules compared to CDDP alone in the BX0.5 group ($0.7 \pm 0.1\%$ vs $1.3 \pm 0.05\%$, $p < 0.05$) and BX0.05 group ($0.7 \pm 0.2\%$ vs $1.3 \pm 0.05\%$, $p < 0.05$) (figure 6.5G). However, the BX5 group increased KIM-1 tubular expression, generating a small effect (*Cohen's d*), $d = 0.24$. Interestingly, BX0.05 reduced KIM-1 glomerular expression compared to CDDP ($0.1 \pm 0.02\%$ vs $0.6 \pm 0.05\%$, $p < 0.001$); but not at any of the other doses (figure 6.5N). In addition, a small effect (*Cohen's d*) was observed, showing reduced KIM-1 expression in the interlobar arteries in the BX0.05 compared to CDDP in the endothelium $d = 0.48$ and medial layers $d = 0.45$. A small effect size (*Cohen's d*) was also observed in the adventitial layer but only in the BX0.5 group (figure 6.5U).

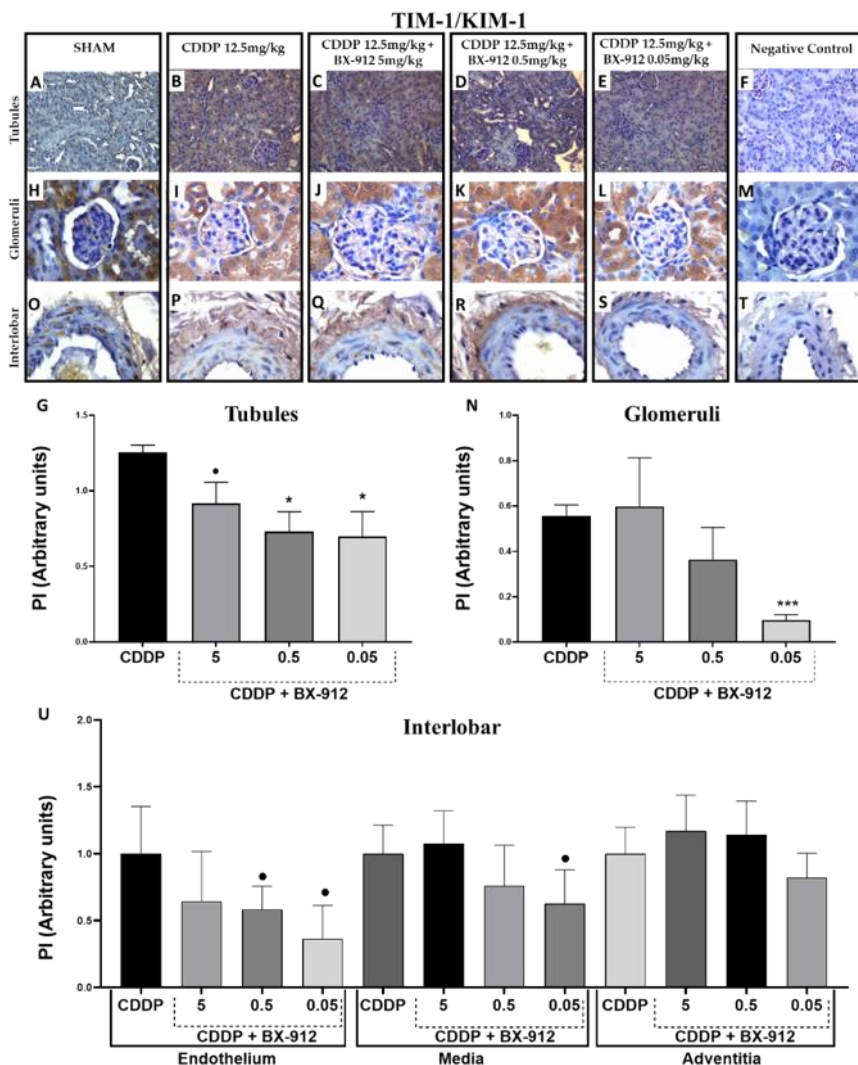


Figure 6.5. Immunohistochemical Analysis of KIM-1-stained mouse kidney tubules, glomeruli and interlobar arteries (n=3-4). 40x magnification Images of paraffin-embedded kidney sections were taken from mice treated with CDDP and various doses of BX + CDDP. **A-F.** Kidney tubules (SHAM, CDDP 12.5, CDDP 12.5 + BX (5, 0.5 and 0.05) and negative control). **G.** Graph representing tubular KIM-1 expression of mice treated with SHAM, CDDP 12.5, CDDP 12.5 + BX (5, 0.5 and 0.05) and negative control. **H-M.** Renal glomeruli were taken at 100x magnification under immersion oil (SHAM, CDDP, CDDP 12.5 + BX (5, 0.5 and 0.05) and negative control). **N.** Graph representing KIM-1 expression in glomeruli of CDDP or CDDP + BX (5, 0.5 and 0.05) treated mice. **O-T** Interlobar artery images were taken at 100x magnification under immersion oil (SHAM, CDDP 12.5, CDDP 12.5 + BX (5, 0.5 and 0.05)). **U.** Graph representing KIM-1 expression in interlobar arteries of CDDP or CDDP + BX (5, 0.5 and 0.05) treated mice. All data is represented as Mean \pm SEM, and statistical analysis was performed using a one-way ANOVA followed by a Dunnett's post hoc test. * ($p < 0.05$), ** ($p < 0.01$), *** ($p < 0.001$), \dagger ($p < 0.0001$). Effect size (d) and Cohen's d values are taken as • $d = 0.2-0.5$ (small effect), •• $d = 0.5-0.8$ (medium effect), and ••• $d \geq 0.8$ (large effect). **Abbreviations:** BX5, 5mg/kg of BX-912; BX0.5, 0.5mg/kg of BX-912; BX0.05, 0.05mg/kg of BX-912; CDDP, cisplatin; d = Cohen's d ; TIM-1/KIM-1, T cell immunoglobulin mucin domain-1/kidney injury molecule-1; n , sample size; PI, proportional intensity.

6.5.6 Inflammatory biomarkers are reduced in BX compared to CDDP treated mice.

6.5.6.1 Tubules

ICAM-1, VCAM-1 and E-Selectin are biomarkers of endothelial activation, a pro-inflammatory state upregulated in various inflammatory diseases, including CIAKI [169]. The BX0.05 group significantly reduced tubular expression of ICAM-1 (0.5 ± 0.1 % vs 1.0 ± 0.2 %, $p < 0.05$), (figure 6.6G), VCAM-1 (0.7 ± 0.1 % vs 1.1 ± 0.03 %, $p < 0.05$), (figure 6.7G) and E-Selectin (0.7 ± 0.1 % vs 1 ± 0.03 %, $p < 0.05$), (figure 6.8G), compared to the CDDP group. Additionally, the BX0.5 group showed reduced tubular VCAM-1 expression compared to CDDP (0.8 ± 0.1 % vs 1.1 ± 0.03 %, $p < 0.05$) and a small effect (*Cohen's d*) was noted in tubular ICAM-1 for both the BX5 $d = 0.25$ and BX0.5 $d = 0.26$ groups.

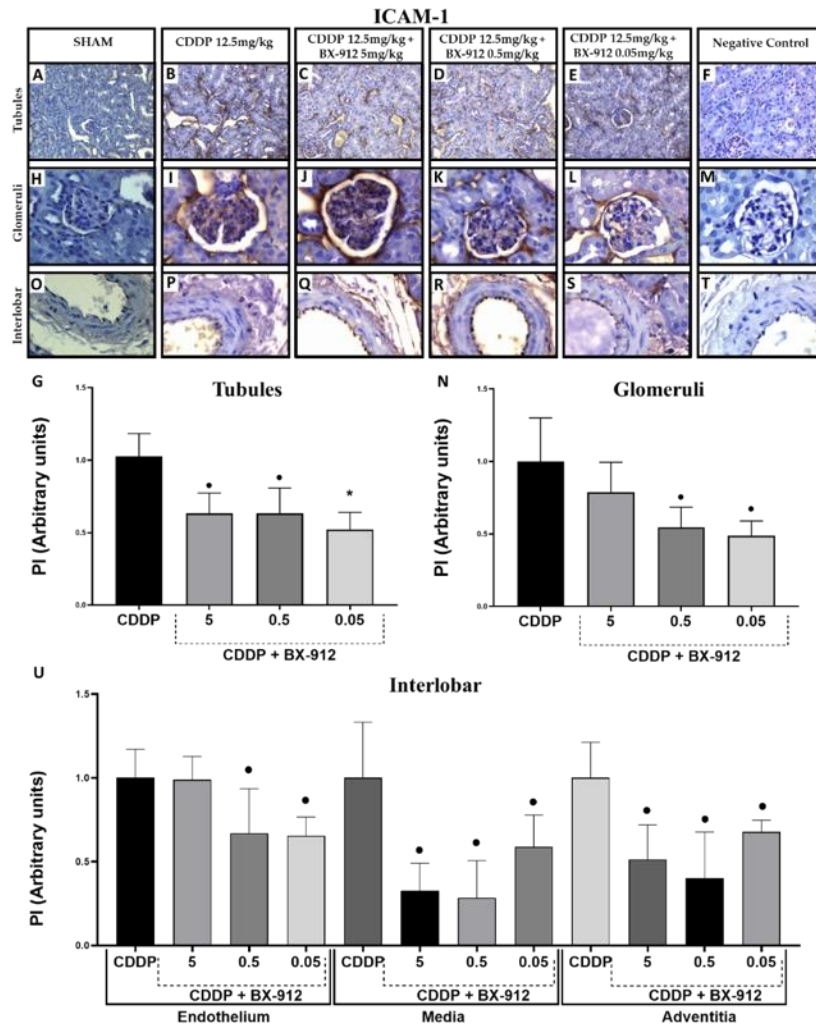


Figure 6.6. Immunohistochemical Analysis of ICAM-1-stained mouse kidney tubules, glomeruli and interlobar arteries (n=3-4). 40x magnification Images of paraffin-embedded kidney sections were taken from mice treated with CDDP and various doses of BX + CDDP. **A-F.** Kidney tubules (SHAM, CDDP 12.5, CDDP 12.5 + BX (5, 0.5 and 0.05) and negative control). **G.** Graph representing tubular ICAM-1 expression of mice treated with SHAM, CDDP 12.5, CDDP 12.5 + BX (5, 0.5 and 0.05) and negative control. **H-M.** Renal glomeruli were taken at 100x magnification under immersion oil (SHAM, CDDP 12.5, CDDP 12.5 + BX (5, 0.5 and 0.05) and negative control). **N.** Graph representing ICAM-1 expression in glomeruli of CDDP or CDDP + BX (5, 0.5 and 0.05) treated mice. **O-T** Interlobar artery images were taken at 100x magnification under immersion oil (SHAM, CDDP 12.5, CDDP 12.5 + BX (5, 0.5 and 0.05)). **U.** Graph representing ICAM-1 expression in interlobar arteries of CDDP or CDDP + BX (5, 0.5 and 0.05) treated mice. All data is represented as Mean \pm SEM, and statistical analysis was performed using a one-way ANOVA followed by a Dunnett's post hoc test. * ($p < 0.05$), ** ($p < 0.01$), *** ($p < 0.001$), \dagger ($p < 0.0001$). Effect size (d) and Cohen's d values are taken as $\bullet d = 0.2-0.5$ (small effect), $\bullet\bullet d = 0.5-0.8$ (medium effect), and $\bullet\bullet\bullet d \geq 0.8$ (large effect). **Abbreviations:** BX5, 5mg/kg of BX-912; BX0.5, 0.5mg/kg of BX-912; BX0.05, 0.05mg/kg of BX-912; CDDP, cisplatin; d = Cohen's d ; ICAM-1, intracellular adhesion molecule 1; n , sample size; PI, proportional intensity.

6.5.6.2 Glomeruli

A small effect (*Cohen's d*) in reduced ICAM-1 expression in the glomeruli of BX0.5 $d=0.26$ and BX0.05 $d=0.29$ groups were noted, compared to CDDP (figure 6.6N). Glomerular E-Selectin expression in BX-treated mice had a small effect (*Cohen's d*) in all three BX groups, BX5 $d=0.26$, BX0.5 $d=0.31$ and BX0.05 $d=0.41$ compared to CDDP, (figure 6.8N). Surprisingly glomerular expression of VCAM-1 in the BX0.5 group was increased compared to CDDP, evidenced by a large effect (*Cohen's d*), $d=-0.99$ (figure 6.7N). The other BX groups had no statistical difference or effect size compared to CDDP. Based on the reduced ICAM-1 and E-Selectin expression, the increased VCAM-1 expression in the glomeruli was surprising.

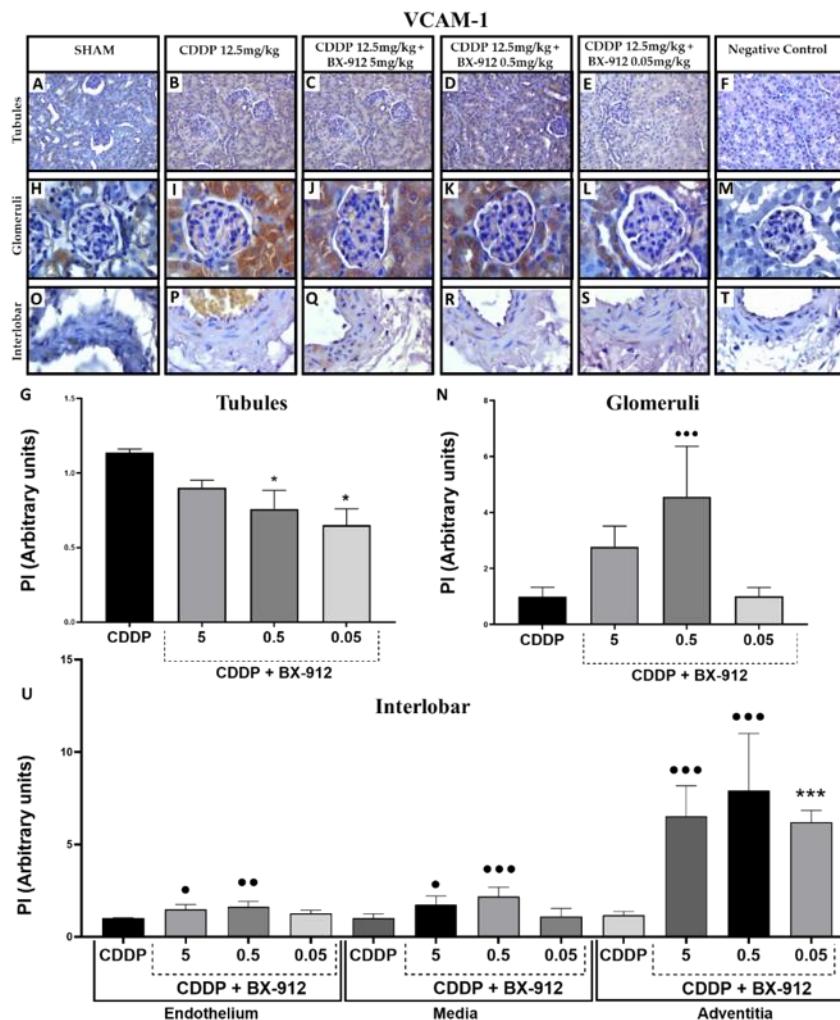


Figure 6.7. Immunohistochemical analysis of kidneys stained for VCAM-1 of mouse kidney tubules, glomeruli and interlobar arteries (n=3-4). 40x magnification Images of paraffin-embedded kidney sections were taken from mice treated with CDDP and various doses of BX + CDDP. **A-F.** Kidney tubules (SHAM, CDDP 12.5, CDDP 12.5 + BX (5, 0.5 and 0.05) and negative control). **G.** Graph representing tubular VCAM-1 expression of mice treated with SHAM, CDDP 12.5, CDDP 12.5 + BX (5, 0.5 and 0.05) and negative control. **H-M.** Renal glomeruli were taken at 100x magnification under immersion oil (SHAM, CDDP 12.5, CDDP 12.5 + BX (5, 0.5 and 0.05) and negative control). **N.** Graph representing VCAM-1 expression in glomeruli of CDDP or CDDP + BX (5, 0.5 and 0.05 mg/kg) treated mice. Images **O-T.** Renal interlobar arteries were taken at 100x magnification under immersion oil (SHAM, CDDP 12.5, CDDP 12.5 + BX (5, 0.5 and 0.05) U. Graph of VCAM-1 expression in the endothelium, media, and adventitial layers of interlobar arteries in CDDP or CDDP + BX (5, 0.5 and 0.05) treated mice. All data is represented as Mean \pm SEM, and statistical analysis was performed using a one-way ANOVA followed by a Dunnett's post hoc test. * ($p < 0.05$), ** ($p < 0.01$), *** ($p < 0.001$), † ($p < 0.0001$). Effect size (d) and Cohen's d values are taken as • $d = 0.2-0.5$ (small effect), •• $d = 0.5-0.8$ (medium effect), and ••• $d \geq 0.8$ (large effect). **Abbreviations:** BX5, 5 mg/kg of BX-912; BX0.5, 0.5 mg/kg of BX-912; BX0.05, 0.05 mg/kg of BX-912; CDDP, cisplatin; d = Cohen's d ; n , sample size; PI, proportional intensity; VCAM-1, vascular cell adhesion molecule 1.

6.5.6.3 Interlobar arteries

The ribbon tool was selected using Micro Computer Imaging Device 6.0 program (MCID) Software (Interfocus, UK). The endothelial layer was traced independently of the other vascular layers to identify the specific expression of pro-inflammatory markers within the endothelium, including ICAM-1, VCAM-1, and E-Selectin. These were measured in the endothelium, media, and adventitia of paraffin-embedded kidney interlobar arteries, (figure 6.6U, figure 6.7U and figure 6.8U), respectively, after treatment with BX (5, 0.5 and 0.05). A small effect (*Cohen's d*) in reduced ICAM-1 expression was observed following treatment with BX in the three vascular layers. In the BX5 group, a small effect (*Cohen's d*) was observed for ICAM-1 expression in the media and adventitia. In the endothelium, media, and adventitia of the BX0.5 group, a small effect (*Cohen's d*) in each layer was observed compared to CDDP. In the BX0.05 group, a small effect (*Cohen's d*) was obtained for the endothelium, media and adventitia compared to the CDDP group, (figure 6.6U). VCAM-1 expression demonstrated a small effect (*Cohen's d*) on increased expression in the CDDP group compared to the BX5 group in the endothelium and media, whilst a large effect (*Cohen's d*) was observed in the adventitia. A medium effect (*Cohen's d*) was observed in the endothelium and media, and a large effect (*Cohen's d*) was seen in the adventitia of the BX0.5 group compared to CDDP. The only effect observed in the BX0.05 group compared to the CDDP group was in the adventitia ($6.2 \pm 0.7\%$ vs $1.0 \pm 0.2\%$, $p < 0.01$) (figure 6.7U). Interlobar analysis of E-Selectin expression demonstrated a small effect (*Cohen's d*) in the BX0.05 group in the medial layer (figure 6.8U).

Table 6.4. Effect of BX on expression of ICAM-1, VCAM-1 and E-Selectin in vascular layers of interlobar arteries.

	Vessel layer	BX5	BX0.5	BX0.05
ICAM-1	Endothelium	p=ns	d=0.21	d=0.22
	Media	d=0.37	d=0.38	d=0.27
	Adventitia	d=0.39	d=0.47	d=0.26
VCAM-1	Endothelium	d=-0.31	d=-0.56	p=ns
	Media	d=-0.40	d=-0.81	p=ns
	Adventitia	d=-1.5	d=-1.5	p<0.01
E-Selectin	Endothelium	p=ns	p=ns	p=ns
	Media	p=ns	p=ns	d=0.2
	Adventitia	p=ns	p=ns	p=ns

Statistical significance is taken at ($p < 0.05$), and effect size (d) and Cohen's d values are taken as $d = 0.2 - < 0.5$ (small effect), $d = 0.5 - < 0.8$ (medium effect), and $d = \geq 0.8$ (large effect).

Abbreviations: BX5, 5mg/kg of BX-912; BX0.5, 0.5mg/kg of BX-912; BX0.05, 0.05mg/kg of BX-912; d = Cohen's d .

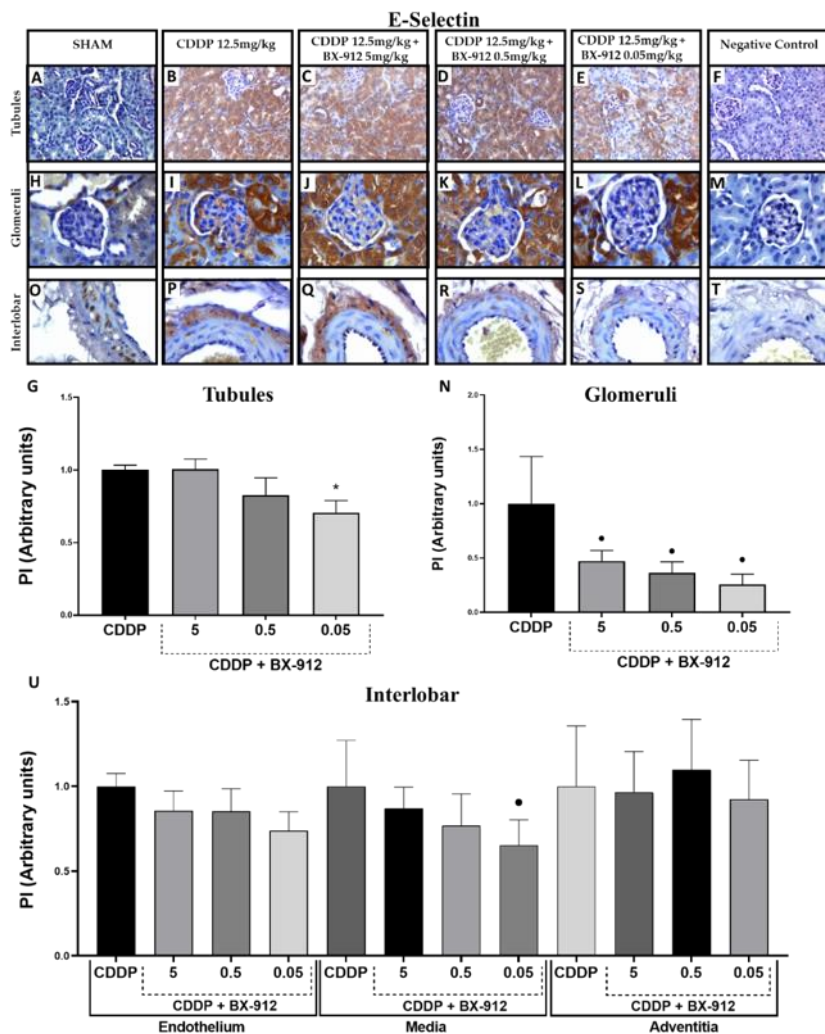


Figure 6.8. Immunohistochemical analysis of kidneys stained for E-Selectin of mouse kidney tubules, glomeruli and interlobar arteries (n=3-4). 40x magnification Images of paraffin-embedded kidney sections were taken from mice treated with CDDP and various doses of BX + CDDP. **A-F.** Kidney tubules (SHAM, CDDP 12.5, CDDP 12.5 + BX (5, 0.5 and 0.05) and negative control). **G.** Graph representing tubular E-Selectin expression of mice treated with SHAM, CDDP 12.5, CDDP 12.5 + BX (5, 0.5 and 0.05) and negative control. **H-M.** Renal glomeruli were taken at 100x magnification under immersion oil (SHAM, CDDP 12.5, CDDP 12.5 + BX (5, 0.5 and 0.05) and negative control). **N.** Graph representing E-Selectin expression in glomeruli of CDDP or CDDP + BX (5, 0.5 and 0.05) treated mice. Images **O-T.** Renal interlobar arteries were taken at 100x magnification under immersion oil (SHAM, CDDP 12.5, CDDP 12.5 + BX (5, 0.5 and 0.05) **U.** Graph of E-Selectin expression in the endothelium, media, and adventitial layers of interlobar arteries in CDDP or CDDP + BX (5, 0.5 and 0.05) treated mice. All data is represented as Mean \pm SEM, and statistical analysis was performed using a one-way ANOVA followed by a Dunnett's post hoc test. * ($p < 0.05$), ** ($p < 0.01$), *** ($p < 0.001$), \dagger ($p < 0.0001$). Effect size (d) and Cohen's d values are taken as • $d = 0.2-0.5$ (small effect), •• $d = 0.5-0.8$ (medium effect), and ••• $d \geq 0.8$ (large effect). **Abbreviations:** BX5, 5mg/kg of BX-912; BX0.5, 0.5mg/kg of BX-912; BX0.05, 0.05mg/kg of BX-912; CDDP, cisplatin; d = Cohen's d ; n , sample size; PI, proportional intensity.

6.5.7 Tubular GRP78 expression is reduced following concomitant administration of BX at various doses.

GRP78 is a protein biomarker for ER stress-induced apoptosis and is elevated in response to CDDP treatment [144]. Immunohistochemical staining of kidney sections following concomitant CDDP and BX, results showed that the BX5 and 0.05 groups did not affect GRP78 expression compared to the CDDP group. Interestingly, the BX0.05 group showed a statistically significant reduction in GRP78 expression in the tubules (0.4 ± 0.1 % vs 1.0 ± 0.1 %, $p < 0.05$), (figure 6.9G). Despite the effects of the BX0.05 group in the tubules, the same effects did not occur in the glomeruli. The BX0.05 group had a small effect (*Cohen's d*) showing an increase in GRP78 expression compared to the CDDP group (1.6 ± 0.4 % vs 1.3 ± 0.1 %, $p = \text{ns}$, $d = -0.22$). In addition, the BX0.5 group showed a significant reduction in GRP78 glomerular expression compared to CDDP (0.9 ± 0.1 % vs 1.3 ± 0.1 %, $p < 0.05$), (figure 6.9N). Our previous studies had noted that CDDP 12.5 mg/kg increased GRP78 expression in interlobar arteries. The only significant effect observed in GRP78 expression in the interlobar arteries occurred in the adventitial layer of the BX0.05 group compared to the CDDP group (0.9 ± 0.2 % vs 1.0 ± 0.4 %, $p < 0.05$), (figure 6.9U). Surprisingly, the BX5 group had a small effect (*Cohen's d*) in increasing GRP78 expression in the endothelial $d = -0.21$ and adventitial layers $d = -0.27$ compared to the CDDP group.

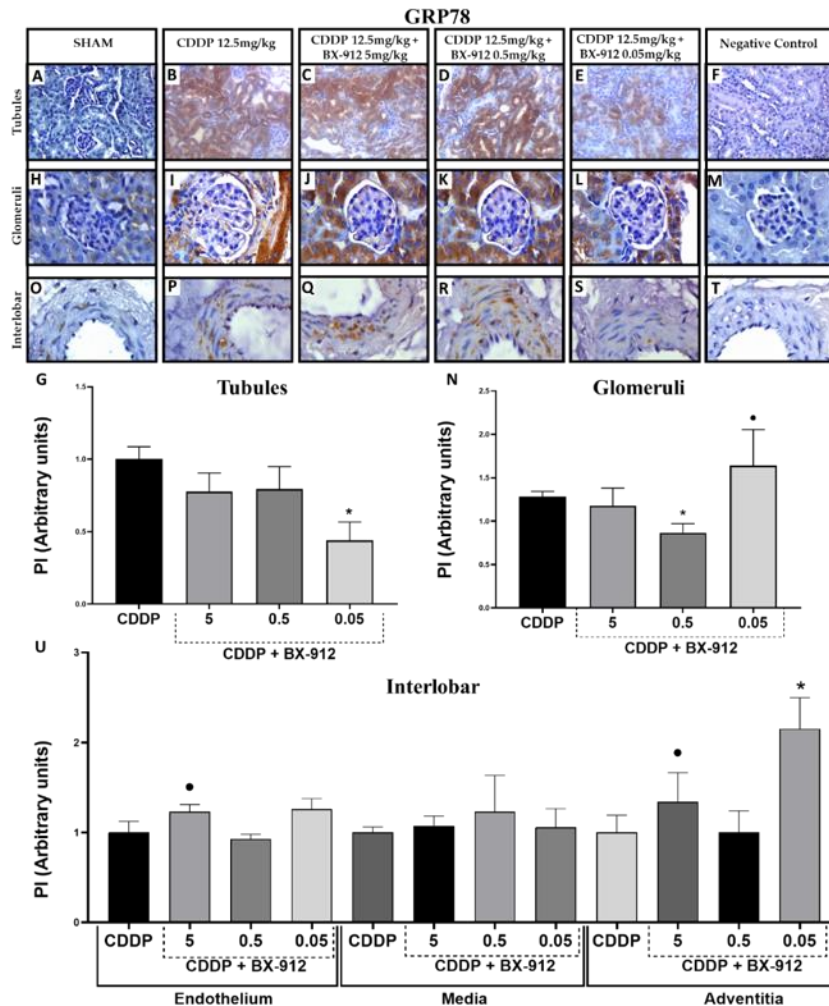


Figure 6.9. Immunohistochemical analysis of kidneys stained for GRP78 in mouse kidney tubules, glomeruli and interlobar arteries ($n=3-4$). 40x magnification images of paraffin-embedded kidney sections were taken from mice treated with CDDP and various doses of BX + CDDP. **A-F.** Kidney tubules (SHAM, CDDP 12.5, CDDP 12.5 + BX (5, 0.5 and 0.05) and negative control). **G.** Graph representing tubular GRP78 expression of mice treated with SHAM, CDDP 12.5, CDDP 12.5 + BX (5, 0.5 and 0.05) and negative control. **H-M.** Renal glomeruli were taken at 100x magnification under immersion oil (SHAM, CDDP 12.5, CDDP 12.5 + BX (5, 0.5 and 0.05) and negative control). **N.** Graph representing GRP78 expression in glomeruli of CDDP or CDDP + BX (5, 0.5 and 0.05) treated mice. **O-T.** Renal interlobar arteries were taken at 100x magnification under immersion oil (SHAM, CDDP 12.5, CDDP 12.5 + BX (5, 0.5 and 0.05)). **U.** Graph of GRP78 expression in the endothelium, media, and adventitial layers of interlobar arteries in CDDP or CDDP + BX (5, 0.5 and 0.05) treated mice. All data is represented as Mean \pm SEM, and statistical analysis was performed using a one-way ANOVA followed by a Dunnett's post hoc test. * ($p < 0.05$), ** ($p < 0.01$), *** ($p < 0.001$), † ($p < 0.0001$). Effect size (d) and Cohen's d values are taken as • $d=0.2-0.5$ (small effect), •• $d=0.5-0.8$ (medium effect), and ••• $d \geq 0.8$ (large effect). **Abbreviations:** BX5, 5mg/kg of BX-912; BX0.5, 0.5mg/kg of BX-912; BX0.05, 0.05mg/kg of BX-912; CDDP, cisplatin; d = Cohen's d ; GRP78, glucose regulation protein 78; n , sample size. PI, proportional intensity.

6.5.8 Effect of BX on the platinum accumulation in renal glomeruli following CDDP treatment.

Platinum accumulation is considered a primary step in renal toxicity exhibited by CDDP. The effect of BX on platinum accumulation was determined in the CDDP group, (figure 6.10A) and the BX0.05 group (figure 6.10B). Analysis of effect size showed that the BX0.05 group demonstrated a small effect (*Cohen's d*) in reducing % weight concentration compared to the CDDP group (0.7 ± 0.1 vs 1.0 ± 0.3 , $p=ns$, $d=0.27$), (figure 6.10C).

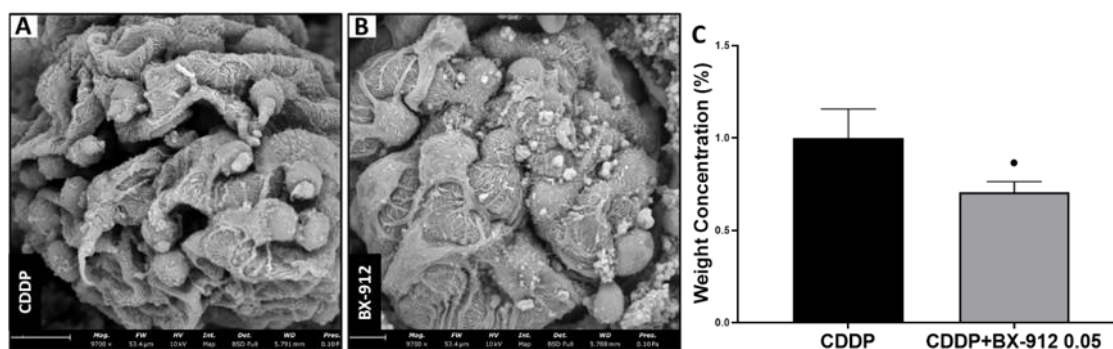


Figure 6.10. Element Identification (EID) X-Ray analysis using SEM of Glomeruli from CDDP and BX + CDDP treated mice (n=3). Effect size (*d*) and Cohen's *d* values are taken as * $d=0.2-0.5$ (small effect), ** $d=0.5-0.8$ (medium effect), and *** $d \geq 0.8$ (large effect). Abbreviations: CDDP, cisplatin; n, sample size.

6.5.9 Mouse nephrotoxicity gene expression in CDDP + BX0.05 treated mice.

RT² Profiler PCR analysis showed alterations to 19 genes associated with nephrotoxicity in the BX0.05 group compared to the CDDP group. Of these genes, glycoprotein nmb-like protein (Gpnmb), also known as Osteoactivin (OA) (figure 6.11D), was significantly downregulated by the BX0.05 group compared to the CDDP group (0.5 ± 0.1 vs 1.0 ± 0.1 , $p < 0.05$). The remainder of the genes demonstrated a small to large effect (*Cohen's d*) size, shown in (figure 6.11). One of the most promising genes affected by BX0.05 was NOX4 which showed a medium effect (*Cohen's d*) compared to the CDDP group $d=0.5$. Additionally, in the total of 84 genes, 19 genes were up/downregulated; however, 65 genes were unaffected by the addition of BX treatment (for a list of unaffected genes, refer to appendix B).

Under- expressed Genes vs CDDP

Over- expressed Genes vs CDDP

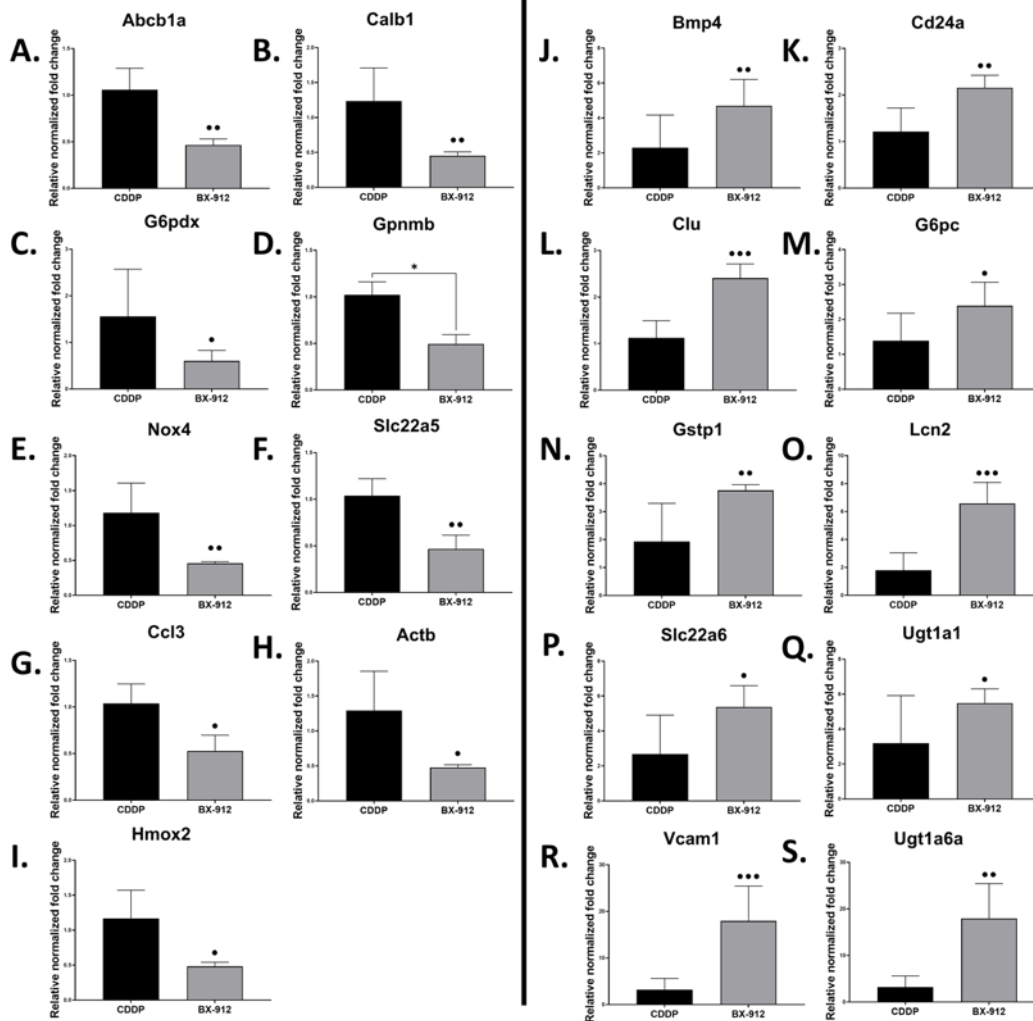


Figure 6.11. Relative fold regulation of genetic response using RT² Profiler PCR in kidneys of mice treated with either CDDP or CDDP + BX0.05, (n=3). A.-J. Graphs representing genes downregulated by BX0.05 compared to CDDP. K.-S. Graphs of genes upregulated by BX0.05 compared to CDDP. All data is represented as Mean \pm SEM, and statistical analysis was performed using a student's t-test. * ($p < 0.05$), ** ($p < 0.01$), * ($p < 0.001$), † ($p < 0.0001$). Effect size (d) and Cohen's d values are taken as * $d = 0.2-0.5$ (small effect), ** $d = 0.5-0.8$ (medium effect), and *** $d \geq 0.8$ (large effect). Abbreviations: *Abcb1a*, ATP-binding cassette, sub-family B (MDR/TAP), member 1A; *Actb*, Actin beta; *Bmp4*, Bone morphogenetic protein 4; *Calb1*, calbindin 1; *Ccl3*, chemokine (C-C motif) ligand 3; *Cd24a*, CD24a antigen; *Clu*, Clusterin; *G6pc*, glucose-6-phosphatase catalytic; *G6pdx*, glucose-6-phosphate dehydrogenase X-linked; *Gpnmb*, glycoprotein (transmembrane) nmb; *Gstp1*, glutathione S-transferase, pi 1; *Hmox2*, heme oxygenase (decycling) 2; *Lcn2*, lipocalin 2; *n*, sample size; *Nox4*, NADPH oxidase 4; *Slc22a5*, solute carrier family 22 (organic cation transporter), member 5; *Slc22a6*, solute carrier family 22 (organic cation transporter), member 6; *Ugt1a1*, UDP glucuronosyltransferase 1 family, polypeptide A1; *Ugt1a6a*, UDP glucuronosyltransferase 1 family, polypeptide A6A and *Vcam1*, vascular cell adhesion molecule 1**

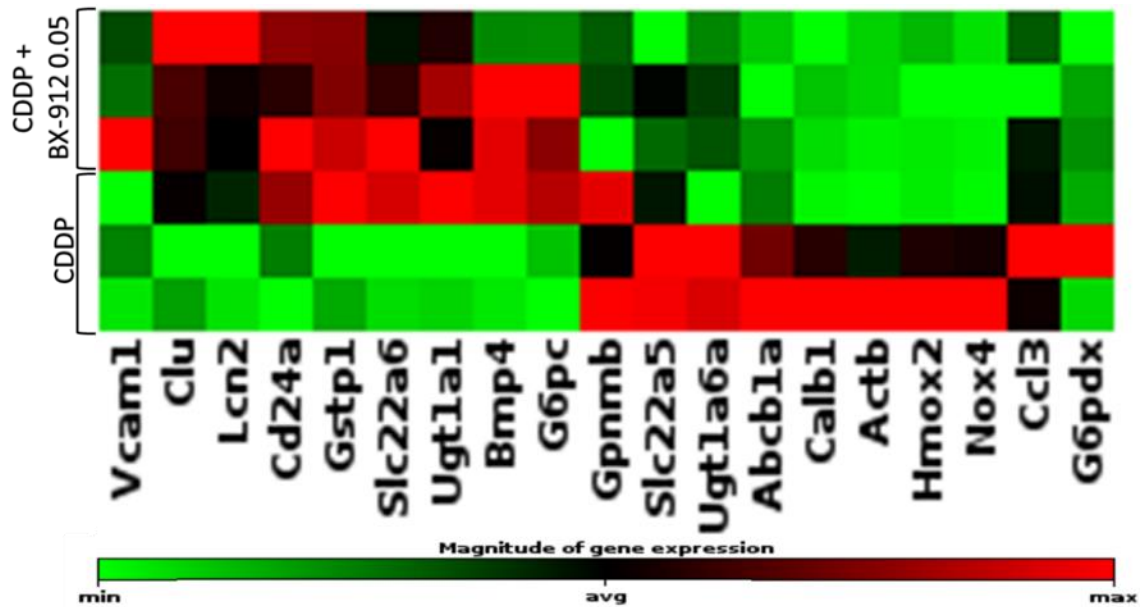


Figure 6.12. Clustergram illustrating the gene expression of CDDP vs CDDP + BX0.05 ($n=3$). **Abbreviations:** *Abcb1a*, ATP-binding cassette, sub-family B (MDR/TAP), member 1A; *Actb*, Actin beta; *Bmp4*, Bone morphogenetic protein 4; *Calb1*, calbindin 1; CDDP, cisplatin; *Ccl3*, chemokine (C-C motif) ligand 3; *Cd24a*, CD24a antigen; *Clu*, Clusterin; *G6pc*, glucose-6-phosphatase catalytic; *G6pdx*, glucose-6-phosphate dehydrogenase X-linked; *Gpnmb*, glycoprotein (transmembrane) *nmb*; *Gstp1*, glutathione S-transferase, pi 1; *Hmox2*, heme oxygenase (decycling) 2; *Lcn2*, lipocalin 2; *Nox4*, NADPH oxidase 4; *Slc22a5*, solute carrier family 22 (organic cation transporter), member 5; *Slc22a6*, solute carrier family 22 (organic cation transporter), member 6; *Ugt1a1*, UDP glucuronosyltransferase 1 family, polypeptide A1; *Ugt1a6a*, UDP glucuronosyltransferase 1 family, polypeptide A6A and *Vcam1*, vascular cell adhesion molecule 1.

6.6 Discussion

The study in this chapter aimed to determine the effects of BX in preventing CIAKI. In this study, it was observed that a) BX enhances ACH/SNP-mediated relaxation vs CDDP, b) BX reduces ANGII -induced vasoconstriction vs CDDP, c) reduced positive PAS staining immunohistochemical expression of key biomarkers associated with CIAKI, including ICAM-1, VCAM-1 E-selectin and GRP78, and d) BX reduced renal Gpnmb and NOX4 expression.

CIAKI is associated with reduced renal perfusion and, subsequently, GFR, initiated by intrarenal vascular damage [67]. To the best of our knowledge, the use of BX in models of vascular function and renal diseases has yet to be evaluated. BX is an identified PDK1 inhibitor. The mechanistic role of both BX and PDK1 inhibition in vasodilation or vasoconstriction are not clearly defined throughout the literature. However, it has been used and shown effective in the prevention and treatment of cancer [170], pulmonary arterial hypertension [108] and asthma [171].

a) BX enhances ACH/SNP-mediated relaxation vs CDDP.

Results from this study showed that CDDP + BX0.5 and BX0.05 preserves endothelial and VSMC function compared to CDDP treatment alone. This enhanced relaxation could improve blood flow to prevent the reduced GFR leading to CIAKI manifestation. Blood vessel relaxation is mainly due to functional eNOS, and CDDP treatment interferes with this by causing eNOS uncoupling leading to endothelial dysfunction and reactive oxygen species (ROS) production [145]. Nitric oxide (NO), produced by eNOS, is an essential vasoprotective molecule in maintaining endothelial function. In a healthy endothelium, following eNOS-induced NO production, NO activates soluble guanylyl cyclase, a soluble enzyme within VSMCs, resulting in cyclic guanosine monophosphate production and subsequent vascular relaxation [172]. The enhanced ACH-mediated relaxation induced by BX could reduce endothelial dysfunction associated with CDDP treatment [8, 69, 145]. This is likely attributable to increased eNOS and NO bioavailability and, in turn, enhanced renal blood flow. Although enhanced Akt and eNOS phosphorylation is typically associated with increased PDK1 activity, these results highlight a potential role for PDK1 inhibition in improved eNOS and NO-mediated relaxation or a potential off-target effect of BX independent of PDK1 inhibition. Our previous evaluation of BX in rabbit vasculature determined an endothelial-independent mechanism for vasodilation; however, an assessment of the

effects of BX on ACH-mediated relaxation was not performed. Therefore, a mechanistic evaluation is required to determine the direct impact of BX on eNOS expression and activity.

Noteably, our previous studies also demonstrated that CDDP did not cause impaired VSMC function compared to CON; however, this study elucidated that BX enhanced VSMC function. This finding could prove beneficial in treating other disorders involving smooth muscle dysfunction. Further vascular investigations, including IHC or RT² profiler PCR of each vascular layer, could provide a pharmacological mechanistic discovery to outline any vascular protective effects of BX.

b) BX reduces ANGII -induced vasoconstriction vs CDDP

Interestingly, adding BX to CDDP reduced the vasoconstrictive response to ANGII compared to CDDP. Current literature provided no insight into either BX or PDK1 inhibitions role in the response of ANGII. It has been shown that PDK1 is activated downstream of AT1R receptor agonism, resulting in cell adhesion [173]. Still, there is no evidence suggesting the potential for a PDK1 inhibitor to function as an angiotensin receptor blocker (ARB). Previous studies investigated the use of ANGII receptor antagonists in preventing CIAKI with non-consistent findings throughout the literature. The ARB losartan, a potent AT1R receptor antagonist and an anti-hypertensive agent, has been used to treat various vascular-related disorders [174]. In a CIAKI model, losartan restored serum blood urea nitrogen (sBUN) and serum creatinine (sCr), demonstrating improved pathological damage [175]. Selective AT1R receptor inhibition has been shown to be beneficial in preventing CIAKI [176]. The AT1R receptor antagonists' candesartan and telmisartan both showed beneficial and harmful effects against CIAKI [140-143]. It is unclear whether BX acts as an ARB or via a different mechanism. Based on previous studies, it is possible that BX-mediated reduction in ANGII-induced vasoconstriction could be a contributing factor to the prevention of CIAKI observed in this study.

c) BX reduced PAS staining of ICAM-1, VCAM-1, E-selectin and GRP78.

CDDP causes a significant degree of pathological renal damage associated with CIAKI. Positive PAS staining correlated with increased cast formation, and its reduction was used to indicate less renal damage. However, this pathological damage was attenuated by BX, identified through reduced PAS staining in renal tubules and interlobar arteries. However, it did not affect glomerular PAS staining. In addition, enhanced histological

evaluations of essential biomarker proteins, including KIM-1 and GRP78, were used to correlate these results. KIM-1 is responsible for eliminating debris resulting from AKI from the tubular lumen [2], and its expression is positively associated with AKI, with its expression low in healthy tissue [131]. Given this, reduced KIM-1 expression was used as a criterion for reduced kidney injury. Reduced KIM-1 in this study demonstrates the renoprotective role of BX and indirectly indicates a reduction in apoptosis. GRP78 is an essential ER chaperone protein, and its overexpression is associated with the development of AKI [144].

Interestingly, BX reduced GRP78 expression in the renal tubules, indicating reduced ER stress. Surprisingly, GRP78 was not reduced in the glomeruli or the interlobar arteries despite the tubular effects. Given the dense vascular nature of the glomeruli and the elevated GRP78 expression observed in the interlobar arteries, it is unsurprising that GRP78 expression remained high. This suggests that the renoprotective effects of the BX groups in the tubules may be attributed, at least in part, to the inhibition of CDDP-induced ER stress. However, further identification of the role of GRP78 in the vasculature of CIAKI will help to clarify the effects observed in this study. ICAM-1, VCAM-1 and E-Selectin are cellular adhesion molecules that play an essential role in the inflammatory response. Upregulation of these adhesion molecules is well documented in models of CIAKI [134, 135]. ICAM-1, VCAM-1 and E-Selectin expressions were downregulated by BX. Tubular expression of these biomarkers was reduced in the BX groups compared to the CDDP group. Previous literature has highlighted the involvement of the PI3K/Akt/NF- κ B pathway in inflammation [177]. PDK1 is a crucial requirement for Akt activation and the subsequent induction of NF- κ B signalling, which stimulates pro-inflammatory protein activation. Therefore, inhibition of Akt and thus NF- κ B could explain the reduced ICAM-1, VCAM-1 and E-Selectin observed in this study.

Use of the NF- κ B inhibitor, JSH-23 provided ameliorative effects in CIAKI; however, it did not affect ICAM-1 expression reversal following a 25mg/kg injection of CDDP. This suggests that ICAM-1 expression may be NF- κ B independent. Based on the unclear role of NF- κ B inhibition on ICAM-1 expression in CIAKI, investigations into ICAM-1, VCAM-1 and E-Selectin and the effect of BX on its reduction are essential. This will help determine if this response is mediated via inhibition of the

PI3K/Akt/mTORC/NF- κ B pathway or a different mechanism, which could be beneficial to establish the anti-inflammatory mechanism of BX.

d) BX reduced renal Gpnmb and NOX4 expression.

To identify the potential pharmacological mechanistic effects of BX, an RT² Profiler Nephrotoxicity PCR gene analysis assay was performed on the BX0.05 group as it demonstrated the highest renoprotective qualities. PCR results illustrated that Gpnmb expression was downregulated in the BX0.05 group in kidney tissue compared to the CDDP group. Gpnmb is a gene shown to be highly upregulated in both rat and mouse models of AKI not induced by CDDP and has been shown to cause negative regulation of macrophage inflammation [178]. Based on its inflammatory role, it has been suggested as a potential biomarker of AKI [179]. In addition, through immunoblotting or flow cytometry it was noted in another study that CDDP did not affect the enhanced expression of Gpnmb, although no data was provided to support this [180]. While the role of Gpnmb in models of AKI, particularly in IRI and other nephrotoxicity models, is well studied, its role in CIAKI remains unclear. This highlights a further limitation in using generalised assays, such as the Qiagen mouse nephrotoxicity kit.

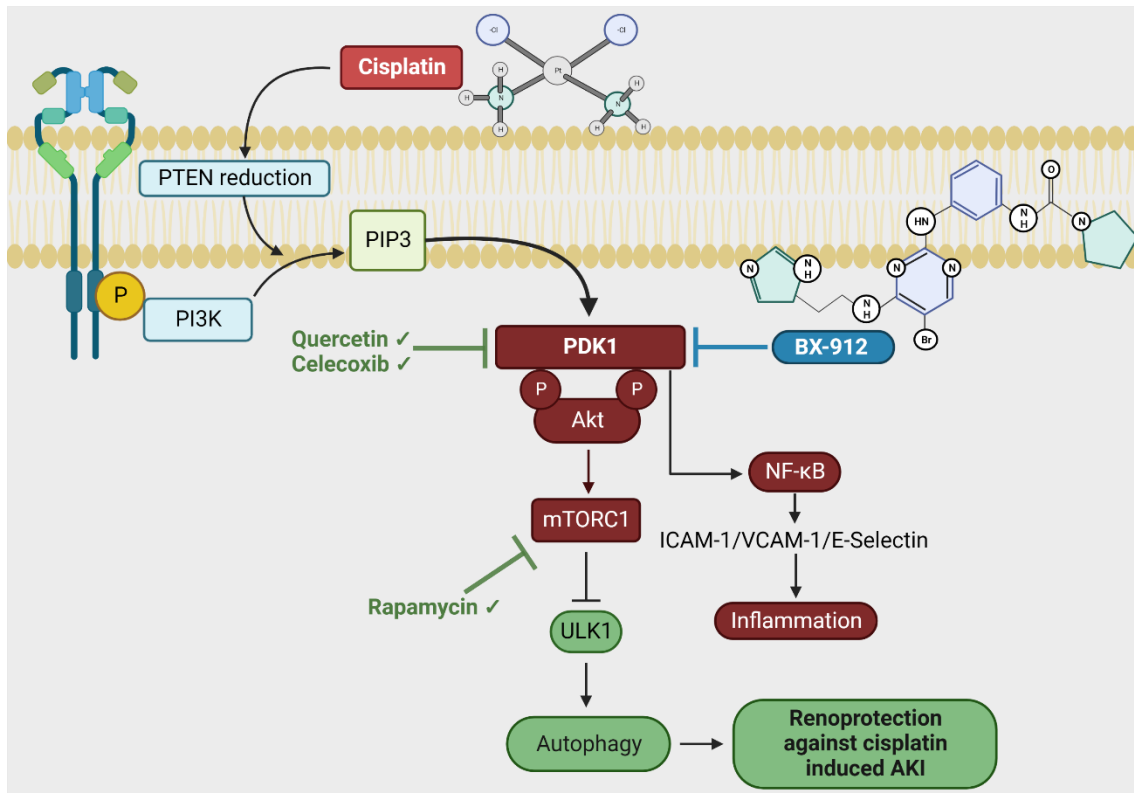
In addition to Gpnmb, the analysis of other genes with a 2-fold regulation demonstrated up or downregulation, illustrated as either a small, medium, or large effect (*Cohen's d*) size. Interestingly, in addition to Gpnmb, not all genes are principally associated with the nephrotoxic effects of CDDP, such as Bmp4; however, these results could elucidate a potential mechanism of action for BX. The downregulation of G6pdx and NOX4 induced by BX treatment may significantly contribute to the renoprotective effects observed in this study. G6pdx, the gene that encodes glucose-6-phosphate dehydrogenase, which is responsible for producing NADPH oxidase and its family of enzymes, including NOX4, was downregulated by BX. NADPH oxidases are a family of enzymes, including NOX4, that are responsible for the production of ROS and have critical roles in immunity, cell growth and signalling. The overproduction of NOX enzymes is associated with the pathogenesis of many diseases [181], including CIAKI.

A publication by Meng et al. illustrated that disruption of NOX4 led to the recovery of renal function, reduced renal damage and decreased inflammation. This study showed a reduction in KIM-1 protein and gene expression levels in renal tissues of CDDP-treated Nox4-deficient mice [182]. Reduced tubular injury score of PAS-stained tissues was also observed. Conclusions made by this study indicate that NOX4

knockdown attenuated CDDP-induced renal damage, highlighting its renoprotective effects against CIAKI. [182]. Reduction in NOX4 was also observed in a study by Jo et al. that investigated the effect of orexin a (OXA); this study aimed to reduce NOX4 and, subsequently, the elevation of ROS. Results demonstrated renoprotective capabilities against CIAKI [183]. This highlights a key role for NOX4 in the pathogenesis of CIAKI. Results of NOX4 analysis in this study also indicated that the BX0.05 group had a medium effect (*Cohen's d*) in reduced NOX4 mRNA expression compared to the CDDP group. This could explain the renoprotective effects observed in this study. Further analysis of oxidative stress biomarkers linked to NOX4 may help delineate its precise involvement in renal tissue. In addition, the effects of NOX4 in renal tissue and NOX4 downregulation could contribute to the vascular function results observed in this study. Research has shown that NOX4 inhibition by ursolic acid prevents eNOS uncoupling in mice following doxorubicin treatment, increasing NO levels and reducing the production of ROS [184]; it is possible that NOX4 inhibition could induce the same effects following CDDP treatment. Given the reduced NOX4 expression induced by BX in renal tissue, it is possible to suggest that BX could prevent eNOS uncoupling through NOX4 inhibition, resulting in increased NO bioavailability and accounting for the increased vasodilatory response to ACH. Immunohistochemical results showed that BX reduced KIM-1 expression in renal tissue and reduced kidney injury. Interestingly,

NOX-1/4 inhibition by GKT137831 reduced ATN through evidence of reduced immunostaining of KIM-1. It is possible that the reduced NOX4 expression -induced by BX could explain the reduced KIM-1 expression observed in this study. Treatment with the NOX4 inhibitor GKT137831 has additionally been shown to decrease the activation of Akt, mTORC and NF- κ B [185]. The downregulation of NOX4 in this study may be inhibiting the activity of NF- κ B, explaining the reduced expression of ICAM-1, VCAM-1, and E-selectin.

Figure 6.13. Hypothesised pathway of the renoprotective mechanism of BX. We hypothesise that the renoprotective properties of BX are at least partially attributed to the inhibition of the PDK1/Akt/mTORC pathway. Inhibition of this pathway results in the activation of ULK1 - induced autophagy, a renoprotective mechanism. **Abbreviations:** ICAM-1, Intracellular adhesion molecule 1; mTORC1, mammalian target of rapamycin complex 1; NF- κ B, Nuclear



factor kappa B; P, Phosphorylation; PDK1, Phosphoinositide-dependent kinase-1; PI3K, Phosphoinositide 3-kinases; PIP3, phosphatidylinositol-3, 4, 5-triphosphate; PTEN, phosphate and tensin homolog deleted on chromosome 10; ULK1, Unc-51 like autophagy activating kinase and VCAM-1, Vascular cell adhesion molecule 1. **Created with BioRender.com.**

In summary, it is hypothesised that the renoprotective mechanism of BX may partly be mediated through its inhibition of the PDK1/Akt/mTORC pathway. Two other pharmaceutical agents with PDK1 inhibitory properties demonstrated renoprotective

mechanisms to support this hypothesis. The flavonoid Quercetin (formal name: 2-(3,4-dihydroxyphenyl)-3,5,7-trihydroxy-4H-1-benzopyran-4-one) elicits a variety of protective effects, including anti-inflammatory, anti-oxidant, and anti-tumour. In addition, it has also exhibited renoprotective effects against CIAKI, mediated through Mincle/Syk/NF- κ B inhibition [39]. The non-steroidal anti-inflammatory and COX-2 inhibitor celecoxib has also displayed nephroprotective effects against CIAKI through reduced ferroptosis [163]. Although neither of these studies specifies that the renoprotective mechanism of these drugs is attributed to PDK1 inhibition, they have both demonstrated PDK1 inhibitory properties throughout the literature. They could support the results of BX if PDK1 inhibition is involved.

In addition to the potential renoprotective effects of quercetin and celecoxib against CIAKI through inhibited PDK1, it may also be mediated via inhibition of downstream signalling molecule mTORC. Activating mTORC by Akt, a protein that requires PDK1 for its activation; thus, the subsequent inhibition of PDK1 inhibits the PDK1/Akt/mTORC signalling cascade. Rapamycin is a pharmacological mTORC inhibitor; interestingly, analysis of vascular injury induced by CDDP showed that rapamycin perfluorocarbon nanoparticles preserved vasculature in response to CDDP treatment. This is suggested to be linked to the inhibition of mTORC signalling, ultimately enhancing autophagy and reducing inflammation [113]. In addition, the use of rapamycin nanoparticles alleviated CIAKI, which was not noted following treatment with rapamycin administered via injection [8]. The renoprotective qualities of rapamycin were supported by another study that aimed to determine its effect on autophagy in CIAKI by assessing the accumulation of the autophagosome microtubule-associated protein light chain 3 II (LC3-II). It was concluded that CDDP and rapamycin treatment enhanced autophagy compared to CDDP treatment alone. Elevations in sBUN and sCr were also ameliorated by rapamycin compared to CDDP. H&E staining illustrated reduced pathological scoring of tubular damage. Taken together, this highlights mTORC inhibition as a renoprotective strategy against CIAKI. Further studies are required to elucidate the specific involvement of the Akt/mTOR/ULK1 pathway and the potential inducement of autophagy by BX. Given the renoprotective effects of rapamycin and the subsequent mTORC inhibition that results from PDK1 inhibition, it is plausible to suggest that the renoprotective effects of BX could be partly

due to increased autophagy, stimulated by inhibition of the PDK1/Akt/mTORC signalling cascade.

6.7 Future Studies

The most critical future study of this thesis is to repeat this study in a larger sample size to ensure the validity of these results. Using G Power 3.1, a power analysis was used to determine the required sample. The mean and standard deviation of the CDDP and BX groups were inputted to produce the effect size. This was used to generate the total required sample size by internal calculation by the software. It was determined that an n=12 is the required sample size to achieve an 80% chance (power of 0.8) of reaching a 30% difference between CDDP and BX0.05 groups.

Although PDK1 deficient mice are embryonically fatal, there has been the development of PDK1 partial knockdown mice. This could be useful to delineate the direct effect of PDK1 reduction in mitigating CIAKI in an *in vivo* model. However, mice produced as a partial knockout present with a significantly reduced size and weight which could be detrimental when CDDP is administered. The progression of this study is to repeat this experiment in a tumour-bearing model. Tumour degradation has been implicated as a contributing factor in CIAKI in patients and therefore is essential to include for clinical relevance [1].

The NOX4 knockout mouse model can be used to confirm if the renoprotective effects displayed in this study are a direct result of NOX4 inhibition, partially mediated by NOX4 inhibition, or independent of NOX4 and the result of off-target drug effects of BX.

6.8 Limitations

This discussion assumes that vascular function and dysfunction are systemically similar. In our laboratory it has been shown that this is not the case and that different vascular beds show differing vascular dysfunctions. The use of mouse kidney interlobar arteries was attempted; however, this remains a technical limitation as they are too small. Ideally, pressure measurement from as close to the kidney as possible would provide greater insight into interlobar arteries function, a method we began developing throughout the CIAKI model study. Details of this method are described in Appendix C. This method needs to be developed further and fine-tuned before it can be used as a publishable methodology, however, provided promising results so far. The small sample

size is an essential limitation of the study. Using analysis of effect (*Cohen's d*) size through interpreting the magnitude of a correlation is a helpful tool. A greater sample size could have resulted in the obtainment of statistical analysis abolishing the requirement for *other forms of statistical interpretation*. Antibody specificity is another limitation of this study. Although the best quality antibodies were sought for this study, some are polyclonal in clonality, some are monoclonal, and are not all knockout validated. It is technically challenging to guarantee the absolute specificity of antibodies, considering structural similarities with other antigens.

The limitations of the RT² profiler PCR array for nephrotoxicity were the sample size and the variety of genes it investigates. Genetic upregulation and downregulation resulting in the development of nephrotoxicity vary depending on the agent-inducing disease development. For instance, nephrotoxicity induced by calcineurin inhibitors may cause up and downregulation of different genes to CDDP. Some genes in this catalogued array are not well understood in the context of CIAKI, whilst other vital proteins, such as CDDP transporters, were not included. If repeated, a customised assay should be considered to target specific CIAKI-related genes or next generation sequencing should be considered.

6.9 Conclusion

BX displayed both vascular and renoprotective effects against CDDP. Histopathological studies showed reduced expression of positive PAS staining, KIM-1, ICAM-1, VCAM-1, E-Selectin and GRP78 in renal tissue. PCR analysis discovered a broad range of genes up-downregulated following CDDP treatment that could be useful to determine the mechanism of action of BX if repeated. This pilot study provided evidence to support further studies of BX for the prevention of CIAKI.

Chapter 7: General Discussion and Conclusions.

7.1 Major Findings

Cisplatin-induced acute kidney injury (CIAKI) is a highly prevalent, debilitating and sometimes life-threatening condition associated with cisplatin (CDDP) treatment in cancer patients. Multiple acute kidney injury (AKI) episodes are also associated with a significantly increased mortality risk. Despite the broad array and widespread pre-clinical publications highlighting the importance of this research, an adequate preventative treatment remains unavailable, with 30-40% of patients still presenting with CIAKI despite current interventions. CIAKI is characterised by decreased renal perfusion, associated with increased afferent arteriole vasoconstriction [88], resulting in a reduced glomerular filtration rate (GFR) [67]. Therefore, identifying novel vasodilators to stimulate renal blood flow to improve or prevent reductions in GFR could be a valuable target in the prevention of CIAKI. This thesis was split into three critical studies divided into four chapters. *Study 1*. Identification of novel vasodilators and their mechanism of action (Chapters 3 and 4). *Study 2*. Determination of a CDDP dose to induce pathologies associated with CIAKI (Chapter 5). *Study 3*. Assessment of the drug identified in study 1, in the model established in study 2, to determine its preventative effects against CIAKI (Chapter 6).

Study 1 assessed two novel potential vasodilators (LKB1 and BX) and investigated their mechanism of action. It was decided that BX-912 (BX) provided a more clinically relevant effect on vascular relaxation, and additionally, its endothelial-independent vasodilatory mechanism provided theoretical potential due to CDDP-induced endothelial damage. Study 2 aimed to establish a dose relevant CIAKI model. Current literature uses a broad range of CDDP doses, 10-30 mg/kg [127], to induce CIAKI. This study aimed to identify a CDDP dose to induce a reversible degree of pathological kidney damage and vascular dysfunction. Finally, study 3 used BX (identified in chapter 4) to prevent vascular dysfunction and pathological renal damage associated with CIAKI. Figure 7.1 summarises the significant findings elucidated by each chapter of this thesis.

significant findings from thesis chapters

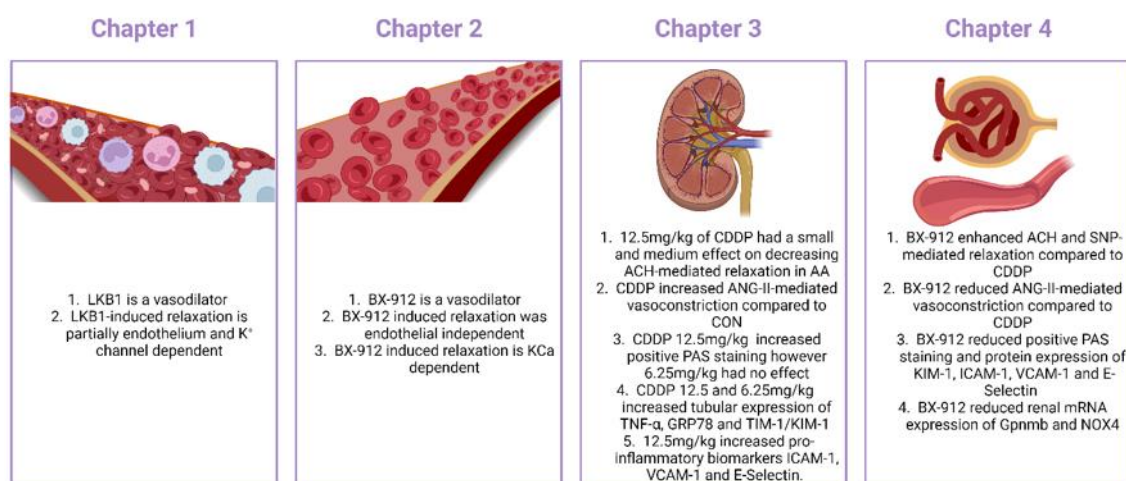


Figure 7.1. Graphical representation outlining the critical findings of this thesis.
Abbreviations: AA, abdominal aorta; ACH, acetylcholine; ANGII, angiotensin II; CDDP, cisplatin; CON, control; Gpnmb, transmembrane glycoprotein nmb; GRP78, glucose-regulated protein 78; ICAM-1, intracellular adhesion molecule 1; KCa, calcium-activated potassium channel; mRNA, messenger ribonucleic acid; NOX4, NADPH oxidase 4; PAS, periodic acid Schiff's stain; SNP, sodium nitroprusside; TIM-1/KIM-1, T cell immunoglobulin and mucin domain 1/kidney injury molecule 1; TNF- α , tumour necrosis factor α ; VCAM-1, vascular cell adhesion molecule 1. **Figure created with BioRender.com**

7.1.1 Chapter 3. LKB1, identification as a novel vasodilator.

The aim of Chapter 3 was to identify if LKB1 was a vasodilator and elucidate its mechanism of action. Results of **Chapter 3** demonstrated that the potent proviral integration site for Moloney murine leukemia virus-1 (PIM1) kinase inhibitor LKB1 is a vasodilator. Dose-response curves (DRC) to LKB1 from (10^{-8} to 10^{-5} [M]) induced vasodilation in interlobar and mesenteric arteries; however, vasodilation did not occur in thoracic aorta. A mechanistic evaluation of LKB1-induced vasodilation revealed it was partially endothelium-dependent, evidenced by reduced relaxation response to mechanically denuded vessels and pre-incubated vessels with the endothelial nitric oxide synthase (eNOS) inhibitor L-N^G-nitro arginine methyl ester (L-NAME). Similarly, the literature shows alternative drugs with PIM1 inhibitory properties (quercetin and rapamycin) also demonstrated vasodilatory effects mediated through endothelial mechanisms [8, 92, 116, 122].

Interestingly, pre-constriction with 40mM potassium physiological salt solution (KPSS) pH 7.4, as a non-selective potassium (K^+) channel inhibitor) also reduced LKB1-mediated vasodilation. This study concluded that LKB1 is a vasodilator in some vessel types and that two mechanisms partially mediate LKB1-induced relaxation. Further investigations into the role of specific K^+ channels are essential to identify the underlying mechanism of action of LKB1.

7.1.2 Chapter 4. BX-912: a potential treatment for reduced renal blood flow and vascular resistance in cisplatin-induced acute kidney injury through its function as a vasodilator.

In Chapter 4, the vasorelaxation properties of the selective phosphoinositide-dependent kinase 1 (PDK1) inhibitor BX were determined in addition to its mechanism of action. It was concluded that BX was a vasodilator in interlobar and mesenteric arteries; however, relaxation did not occur in thoracic aorta. Mechanical denudation and pre-incubation with the eNOS inhibitor L-NAME did not affect BX-induced relaxation, suggesting that vasorelaxation was endothelial-independent. BX-induced relaxation was markedly reduced in interlobar and mesenteric vessels pre-constricted with 40mM KPSS. Pre-constriction with 40 mM KPSS non-selectively inhibited all K^+ channels. Furthermore, it was elucidated that calcium-activated K^+ (KCa) channels were at least partially responsible for the relaxation effects of BX, given KCa inhibition with charybdotoxin reduced relaxation in interlobar arteries. This same effect was not observed in mesenteric arteries; however, it could be attributed to the low sample size.

7.1.2.1 The PI3k/Akt/mTORC pathway.

The findings in this study demonstrated similar effects in BX and LKB1. These drugs did not affect relaxation in the thoracic aorta but induced vasodilation in the interlobar and mesenteric arteries. Treatment with the PIM1 kinase inhibitor SMI-4a considerably downregulated phosphoinositide 3-kinases (PI3k), Akt and mTORC phosphorylation, resulting in autophagy activation [186]. Furthermore, BX also reduces the PDK1/Akt/mammalian target of the rapamycin (mTORC) signalling pathway by inhibiting PDK1 phosphorylated Akt activation [102]. This subsequently inhibits mTORC activity. Therefore, it is possible that LKB1 and BX are inhibitors of the Akt/mTORC signalling cascade and may induce vasodilation by triggering the same downstream signalling

through mTORC inhibition. Further, research studying this pathway could explain the similarities in the vascular responses observed in Chapters 3 and 4.

7.1.2.2 LKB1 vs BX to mitigate CIAKI.

Interestingly, mechanistically both LKB1 (through PIM-1 kinase inhibition) and BX (through PDK-1 inhibition) presented the solid theoretical potential to mitigate CIAKI. These chapters aimed to identify a vasodilator to use in a mouse model of CIAKI. This increased vasodilation aimed to reduce vascular resistance and subsequently increase GFR associated with CIAKI. Results of the vasodilator studies from chapters 3 and 4 showed that whilst both demonstrated vasodilation abilities, there was at least a partial variance in the mechanism of action. LKB1 induced relaxation in an endothelial and eNOS-dependent manner; however, BX induced relaxation in an endothelial-independent manner. Reduced GFR is associated with endothelial dysfunction and afferent arteriole vasoconstriction. Reduced eNOS and nitric oxide (NO) caused by CDDP results in endothelial dysfunction. It is well established that CDDP causes endothelial dysfunction, resulting in afferent arteriole vasoconstriction and subsequently reduced GFR. The results of this study showed that LKB1-induced relaxation was at least partially mediated through endothelial mechanisms. It was unclear whether LKB1 had the potential to overcome the endothelial dysfunction induced by CDDP. However, BX-mediated relaxation was endothelial independent; therefore, BX would induce vasodilation by bypassing the endothelium was a more suitable approach (rationale for **Chapter 5**).

7.1.3 Chapter 5. Identification of a CDDP dose that induces vascular dysfunction and pathological kidney damage.

The aim of chapter 5 was to determine a CDDP dose to induce significantly, however, reversible kidney damage. Two doses of CDDP (6.25 and 12.5 mg/kg) were assessed, and various *ex vivo* studies were completed to determine their pathological effects. Isometric tension analysis of acetylcholine (ACH) or sodium nitroprusside (SNP) DRC followed by analysis of effect size, that showed that the CDDP12.5 group had a small effect *Cohen's d*) on reduced ACH-mediated relaxation compared to the SHAM group. However, this reduction was not observed in the CDDP6.25 group. This suggests that the CDDP6.25 did not induce vascular dysfunction or that the degree of toxicity induced may have enabled a recovery period prior to *ex vivo* experimentation. Results of this study showed that the CDDP12.5 group increased angiotensin II (ANGII)-mediated

vasoconstriction compared to the SHAM group. Periodic acid Schiff's (PAS) staining in this study indicates cast formation associated with renal damage. Results demonstrated that the CDDP12.5 group increased tubular and glomerular positive PAS staining compared to the SHAM group; however, the CDDP6.25 group had no effect compared to the SHAM. Tubular expression of tumour necrosis factor α (TNF- α) and T cell immunoglobulin and mucin domain 1/kidney injury molecule 1 (TIM-1/KIM-1) were significantly upregulated by both CDDP groups compared to the SHAM, and no significant difference was observed between doses. Analysis of effect (*Cohen's d*) size determined that the CDDP (6.25 and 12.5) groups significantly increased tubular glucose-regulated protein 78 (GRP78) expression. Surprisingly, the lack of difference between the CDDP (6.25 and 12.5) groups in these proteins made it a poor criterion for determining a pathological CDDP dose; therefore, additional biomarkers were used to allow better separation of the pathological effects of doses. Pro-inflammatory biomarkers intracellular adhesion molecule 1 (ICAM-1), vascular cell adhesion molecule 1 (VCAM-1) and E-Selectin in renal tissues were assessed and demonstrated that the CDDP12.5 group had a more significant overall increase in these biomarkers compared to the CDDP6.25 group. The vascular function studies and histology experiments showed that the CDDP12.5 group had a more significant overall pathological effect on inducing renal damage than the CDDP6.25 group. Therefore, it was concluded that in future CIAKI studies using this model, the CDDP12.5 was a more suitable dose compared to CDDP6.25.

7.1.4 Chapter 6. BX-912 mitigates cisplatin-induced AKI through improved renal blood flow and reduced inflammation: A pilot study.

Following the identification of BX in **chapter 4** as a vasodilator, three doses of BX (5, 0.5 and 0.05 mg/kg) were administered to mice in addition to CDDP to observe their renoprotective effects. ACH/SNP mediated relaxation was enhanced in the abdominal aorta of BX and CDDP-treated mice compared to CDDP alone. It is not clear why BX enhanced ACH-mediated relaxation. However, given the results of previous vascular function studies in **chapter 4**, which detailed that BX-mediated relaxation was endothelial-independent and KCa channel dependent, this was an unexpected finding. This requires further investigation in order to understand the effects of BX and, more specifically, its effects on the endothelium.

CDDP-induced vascular smooth muscle cell (VSMC) toxicity is well established throughout the literature [130]; however, the results obtained in **chapter 5** failed to provide evidence that 12.5 mg/kg CDDP group-induced vascular toxicity. However, BX enhanced the relaxation of VSMC compared to CDDP. Based on results obtained in chapter 4, this is possibly attributed to VSMC hyperpolarisation mediated through BX-induced activation of KCa channels; however, further research is required to confirm this hypothesis.

Iliac arteries harvested from CDDP and CDDP + BX treated mice showed that BX reduced ANGII-mediated vasoconstriction. It is unclear whether the cause of the reduced constriction is a result of BX acting as an angiotensin receptor blocker (ARB) or via an alternate intracellular mechanism. However, future studies are required to understand the effects of BX on ANGII, and the expression of ANGII receptors angiotensin II type 1 and type 2 could help understand these results.

Histological studies demonstrated that BX reduced positive PAS staining and, therefore, kidney damage, indicative of reduced cast formation. These results were corroborated through immunohistochemical analysis of essential proteins involved in the pathogenesis of CIAKI. KIM-1, GRP78, ICAM-1, VCAM-1 and E-Selectin were all reduced in kidneys in the BX0.05 group. Although a reduction in these biomarkers is evident, further research is required to identify the cause of these reductions. Mechanistic signalling of PDK1, the functional enzyme inhibited by BX and inhibition of its signalling cascade could explain the reduced expression of ICAM-1, VCAM-1, and E-Selectin through inhibition of nuclear factor kappa B (NF- κ B).

Additionally, preliminary studies of messenger RNA (mRNA) gene expression demonstrated that transmembrane glycoprotein nmb (Gpnmb) expression was significantly reduced by BX0.05 group compared to the CDDP group. Additionally, NOX4 expression was downregulated, evidenced by a medium effect (*Cohen's d*) suggesting that BX displayed anti-inflammatory properties. A larger-scale study is required to confirm these results. This study does not confirm whether the renoprotective effects directly result from increased vasodilation, reduced inflammatory proteins or a combination of both. However, it does provide evidence to support the hypothesis that BX is a potential treatment to prevent CIAKI; however, larger replication studies are required to confirm these results.

7.2 Future Directions

This thesis elucidates three key novel areas that require investigation. These include identifying two novel vasodilators, LKB1 and BX, and the anti-inflammatory effects of BX in reducing kidney damage induced by CDDP. Although this thesis has elucidated some key novel areas, future studies are required further to understand the vasodilatory mechanisms of the two drugs and to determine the renoprotective mechanism of BX following CDDP treatment. One of the general future directions of this work is to repeat these experiments in female animals to identify the effects of hormonal influence on disease manifestation and effects.

This section details the specific future directions of each chapter below.

7.2.1 Chapter 3. LKB1, identification as a novel vasodilator.

LKB1 and, subsequently, PIM1 kinase inhibition in disease is a possible therapeutic target. However, there are studies critical for future LKB1 research. Identifying the specific LKB1 mechanism of action is an important *ex vivo* study required prior to its use *in vivo*. Results obtained in Chapter 3, suggest that LKB1 is a vasodilator, and that it is vessel specific. In fact, vasodilation occurred in interlobar and mesenteric arteries; however, it had little to no effect in the thoracic aorta. Next generation sequencing experiments could be used to further understand the variance in vessel reactivity. Preliminary investigations in our laboratory have shown that in *ex vivo* isometric tension studies, LKB1 induced vasodilation in the abdominal aorta of mice. This suggests that vasodilation may not be species-specific; therefore, using LKB1 in mouse disease models such as CIAKI and in isolated human arteries, are potential future directions.

However, LKB1 has not been used in an *in vivo* model; therefore, to ensure its safety, a full-scale toxicology analysis would be required before using LKB1 in pre-existing animal projects such as the CIAKI project used in this study. This animal study will be developed following the OECD Guidelines Test No. 425: Acute Oral Toxicity: Up and Down procedure [187].

7.2.2 Chapter 4. BX-912: a potential treatment for reduced renal blood flow and vascular resistance in cisplatin-induced acute kidney injury through its function as a vasodilator.

Results from Chapter 4 elucidated that BX is vessel specific as it induced vasodilation in smaller arteries but not aorta. The study concluded that BX-mediated vasodilation is at least partially mediated through KCa; however, an increased sample size is essential to validate this and the involvement of other K⁺ channels. Further studies are required to determine the mechanism of action leading to enhanced BX-mediated relaxation, stimulated by cyclooxygenase (COX) inhibition, and further, why this result occurred in interlobar arteries and was not observed in mesenteric arteries.

7.2.3 Chapter 5. Identification of a CDDP dose that induces vascular dysfunction and pathological kidney damage.

It is well documented that CDDP results in increased renal expression of inflammatory biomarkers ICAM-1, VCAM-1 and E-Selectin. Multiple reported pathways resulting in the upregulation of these proteins have been outlined in other animal models of inflammatory disease; however, no specific mechanisms are detailed in models of CIAKI. This is primarily attributed to the nature of preventative CIAKI research and the complexity of CIAKI pathophysiology. Increased signalling by TNF- α and NF- κ B have been attributed to increased expression of ICAM-1, VCAM-1, and E-Selectin. It is well established that CDDP upregulates the expression of these inflammatory proteins; therefore, pharmacological interventions are targeted to reduce this inflammatory cascade. However, it may be useful to identify the signalling cascades leading to the upregulation of ICAM-1, VCAM-1, and E-Selectin, to determine potential therapeutic targets.

7.2.4 Chapter 6. BX-912 mitigates cisplatin-induced AKI through improved renal blood flow and reduced inflammation: A pilot study.

The initial study on BX in the prevention of CIAKI is preliminary; therefore, a larger-scale study is required to confirm these results and build on the knowledge elucidated by this study. This study needs to be repeated to ensure reproducibility and validity. Due to the low sample size (n=3-4), the chance of achieving statistical significance is low. Therefore, based on the data obtained, a Power analysis was performed using the software (G Power 3.1). The mean and standard deviation of the CDDP and BX groups were used. The software determined that an n=12 is the required sample size to achieve

an 80% chance (power of 0.8) of reaching a 30% difference between CDDP and BX (5, 0.5 and 0.05) groups. In this study, it will also be essential to proceed with a total organ harvest on animals treated with BX alone and in combination with CDDP. CDDP is known to cause other systemic toxicities besides nephrotoxicity, including ototoxicity, myelosuppression, neurotoxicity, and cardiotoxicity [56, 188]. Thus, it is vital to ensure BX does not contribute to these systemic toxicities and identify any BX-specific adverse effects or toxicities.

7.3 Limitations of the thesis

One of the fundamental limitations of this thesis, particularly regarding Chapter 5 and Chapter 6, *in vivo* mouse studies, is the low sample size (n=3-4). An increased sample size is required to increase the power of the study and therefore increase the chance of statistical significance.

To confirm the specificity of pharmacological agents and to identify any potential off-target effects, genetically modified animals, mainly genetic knockout mice (^{-/-}) are commonly used. Research has demonstrated that PDK1^{-/-} mice are embryonically fatal at 9.5 days gestation resulting from abnormalities, particularly neurologically. Remarkably, a hypomorphic PDK1 model has been developed, reducing PDK1 activity in mice by 25-50%, which are embryonically viable and fertile. However, despite the viability, these mice present with an approximate 30% reduced birth size/weight compared to their wild-type counterparts, which is worsened with age; size percentage increasing to a 45% reduction by six months of age [189]. This could prove harmful for mice that are additionally subjected to CDDP treatment, which results in further body weight loss, as shown by the EchoMRI analysis in Chapter 6 (figure 3). This together could reduce the survivability of mice in combination with their overall welfare, potentially hindering the outcomes of the study. This indicates that in addition to PDK1 genetic knockout mice, genetic modification reducing PDK1 activity may not be a suitable option to confirm the results observed in the PDK1 pharmacological inhibition study. Repetition with a different potent and specific PDK1 inhibitor, such as BX-795, to determine whether the same results are noted could be a suitable alternative. Furthermore, although some mTORC depletion mice have shown to be viable and could prove helpful to confirm the degree of involvement of mTORC in both LKB1 and BX-induced vasodilation, attempts at total mTORC deletion proved embryonically fatal

[190]. This suggests that using GMOs for this study requires further development to complement pharmacological investigation.

7.3.1 Scanning Electron Microscopy

CDDP, more specifically the platinum atoms following CDDP metabolism, travel through the bloodstream, accumulate in proximal tubule epithelial cells (PTECs) and is suggested to initiate and contribute to increased reactive oxygen species formation and subsequent pathological kidney damage. It was essential to determine the potential effects of BX on renal platinum clearance and, thus, the prevention of CDDP accumulation. The SEM methodology was chosen preferentially to other forms of metal analysis, such as inductively coupled plasma (ICP), as it can only analyse samples in liquid form and therefore requires sample digestion. There can be no structural delineation and identification of specific PTEC tubular expressions. However, this specific structural analysis is possible if samples are prepared correctly for SEM. Cutting the section transversely would provide better tubule cross-sections. The kidneys in the SEM experiments were cut on a sagittal plane, whilst for immunohistochemistry (IHC), kidneys were embedded and cut transversely. The cutting plane was less critical for glomerular analysis due to its spherical shape; however, orientation is vital for cutting tubular structures. Cutting transversely provided a clear circular tubular structure for IHC analysis and could prove beneficial for future SEM experiments. In this study, the sagittal sections resulted in inadequate PTEC presentation and Glomeruli were analysed for platinum content instead. Glomerular Pt content is widely understudied compared to PTECs and whole kidney platinum content and could provide valuable additional understanding of the cause of glomerular damage induced by CDDP. When repeated, it is essential to alter the orientation to better identification PTECs for Pt analysis.

7.3.2 Real-time polymerase chain reaction

Identification of the exact mechanism of action of BX and its renoprotective effects observed in Chapter 6 is unclear. The PCR nephrotoxicity analysis aimed to provide a more precise and widespread mechanistic understanding based on an array of 84 potential genes. The only gene that yielded a greater than 2-fold increase and a significant p-value was Gpmb. Due to the low Power, the study failed to achieve statistical significance in many genes despite the fold change in both over and under-expressed genes. KIM-1 was not one of the 84 genes investigated. Recently KIM-1 has

been highlighted as a critical early biomarker for AKI and has been suggested to replace the current clinical biomarkers sBUN and sCr [131]. Some of the genes in the generalised nephrotoxicity kit have not been investigated significantly in CIAKI, such as that of *Gpnmb*, the only significantly affected gene by BX. This could be a novel finding and could be interesting to investigate further. Nephrotoxicity cannot be a generalised classification for the effects of genetic expression. Not all drugs induce kidney gene expression in the same manner; however, this kit provides a reasonable basis for a large-scale genetic test; however, it should be repeated or followed up with other evaluations, such as next-generation sequencing.

In preparation for repetition, a few alterations would be made to the experimental design. Given that some of these genes are not explicitly associated with CIAKI, a vehicle-treated group is required to delineate the exact effect of CDDP on each gene and to create a baseline to compare variances in the BX group to. The increased sample size is also vital to aid in power and statistical analysis and could alter the results observed in this pilot study. Additionally, since the analysis of genes showed an apparent alteration in specific genes, a subsequent analysis should be performed using a customised plate with those genes in addition to KIM-1.

7.4 Conclusions

In this thesis it is concluded that LKB1 is a novel vasodilator whereby its relaxation effects are partially mediated through endothelial-dependent and K^+ channel pathways. The degree of involvement of each of these mechanisms is not clear, and further studies are required to elucidate this further. It was determined that BX is a novel small-vessel vasodilator, with preliminary *ex vivo* studies demonstrating that BX-mediated vasodilation is endothelial-independent and is at least partially mediated via KCa channels. Results of the CIAKI dose-finding study reported that the CDDP 12.5 group induced a greater degree of overall kidney damage and vascular dysfunction than the 6.25 CDDP group. Further studies are required to determine if 6.25 is a subtherapeutic dose or if there was a degree of recoverability to explain the reduced toxicity. The final study determined that BX displayed renoprotective qualities in a model of CIAKI. BX enhanced vascular function and reduced ANGII-mediated vasoconstriction, and significantly reduced renal expression of key biomarkers associated with CIAKI pathogenesis, including KIM-1, GRP78, ICAM-1, VCAM-1, and E-Selectin. This thesis

presents multiple novel discoveries and provides important preliminary data to justify future studies aimed to solidify the results presented here.

References

- [1] K. R. McSweeney, L. K. Gadanec, T. Qaradakhi, B. A. Ali, A. Zulli, and V. Apostolopoulos, "Mechanisms of cisplatin-induced acute kidney injury: Pathological mechanisms, pharmacological interventions, and genetic mitigations," *Cancers*, vol. 13, no. 7, p. 1572, 2021.
- [2] W. Yin, S. M. Naini, G. Chen, D. M. Hentschel, B. D. Humphreys, and J. V. Bonventre, "Mammalian target of rapamycin mediates kidney injury molecule 1-dependent tubule injury in a surrogate model," *Journal of the American Society of Nephrology*, vol. 27, no. 7, pp. 1943-1957, 2016.
- [3] S.-J. Huang *et al.*, "The renoprotective effect of curcumin against cisplatin-induced acute kidney injury in mice: involvement of miR-181a/PTEN axis," *Renal Failure*, vol. 42, no. 1, pp. 350-357, 2020.
- [4] M. J. Mitchell, M. M. Billingsley, R. M. Haley, M. E. Wechsler, N. A. Peppas, and R. Langer, "Engineering precision nanoparticles for drug delivery," *Nature Reviews Drug Discovery*, vol. 20, no. 2, pp. 101-124, 2021.
- [5] T. Lan *et al.*, "Dual-Responsive Curcumin-Loaded Nanoparticles for the Treatment of Cisplatin-Induced Acute Kidney Injury," *Biomacromolecules*, 2022.
- [6] N. Andrianova *et al.*, "Rapamycin is not protective against ischemic and cisplatin-induced kidney injury," *Biochemistry (Moscow)*, vol. 84, no. 12, pp. 1502-1512, 2019.
- [7] M. Jiang, Q. Wei, G. Dong, M. Komatsu, Y. Su, and Z. Dong, "Autophagy in proximal tubules protects against acute kidney injury," *Kidney international*, vol. 82, no. 12, pp. 1271-1283, 2012.
- [8] Q. Zhou *et al.*, "Safety Profile of Rapamycin Perfluorocarbon Nanoparticles for Preventing Cisplatin-Induced Kidney Injury," *Nanomaterials*, vol. 12, no. 3, p. 336, 2022.
- [9] X. Duan, C. He, S. J. Kron, and W. Lin, "Nanoparticle formulations of cisplatin for cancer therapy," *Wiley*

Interdisciplinary Reviews: Nanomedicine and Nanobiotechnology, vol. 8, no. 5, pp. 776-791, 2016.

- [10] X. Chen, P. B. Comish, D. Tang, and R. Kang, "Characteristics and biomarkers of ferroptosis," *Frontiers in Cell and Developmental Biology*, vol. 9, p. 637162, 2021.
- [11] J. Yang *et al.*, "Targeting cell death: pyroptosis, ferroptosis, apoptosis and necroptosis in osteoarthritis," *Frontiers in Cell and Developmental Biology*, vol. 9, p. 3861, 2022.
- [12] Z. Hu *et al.*, "VDR activation attenuate cisplatin induced AKI by inhibiting ferroptosis," *Cell Death & Disease*, vol. 11, no. 1, pp. 1-11, 2020.
- [13] L. Zhou *et al.*, "Polydatin Attenuates Cisplatin-Induced Acute Kidney Injury by Inhibiting Ferroptosis," (in eng), *Oxid Med Cell Longev*, vol. 2022, p. 9947191, 2022.
- [14] J. Hu, W. Gu, N. Ma, X. Fan, and X. Ci, "Leonurine alleviates ferroptosis in cisplatin-induced acute kidney injury by activating the Nrf2 signalling pathway," *British Journal of Pharmacology*, 2022.
- [15] M. Conrad *et al.*, "Regulation of lipid peroxidation and ferroptosis in diverse species," *Genes & development*, vol. 32, no. 9-10, pp. 602-619, 2018.
- [16] D.-H. Kim *et al.*, "Farnesoid X receptor protects against cisplatin-induced acute kidney injury by regulating the transcription of ferroptosis-related genes," *Redox Biology*, vol. 54, p. 102382, 2022.
- [17] Y. Bao *et al.*, "DNA demethylase Tet2 suppresses cisplatin-induced acute kidney injury," *Cell death discovery*, vol. 7, no. 1, pp. 1-11, 2021.
- [18] L. Wen *et al.*, "Selective EZH2 inhibitor zld1039 alleviates inflammation in cisplatin-induced acute kidney injury partially by enhancing RKIP and suppressing NF- κ B p65 pathway," *Acta Pharmacologica Sinica*, pp. 1-14, 2021.
- [19] F. ALTINDAĞ, "Silymarin ameliorates cisplatin-induced nephrotoxicity by downregulating TNF- α and NF- κ B and by

- upregulating IL-10," *Journal of Experimental and Clinical Medicine*, vol. 39, no. 1, pp. 216-220, 2022.
- [20] S. Liu *et al.*, "Baicalein-loaded silk fibroin peptide nanofibers protect against cisplatin-induced acute kidney injury: Fabrication, characterization and mechanism," *International Journal of Pharmaceutics*, vol. 626, p. 122161, 2022.
- [21] W.-H. Lin *et al.*, "Renoprotective Effect of *Pediococcus acidilactici* GKA4 on Cisplatin-Induced Acute Kidney Injury by Mitigating Inflammation and Oxidative Stress and Regulating the MAPK, AMPK/SIRT1/NF- κ B, and PI3K/AKT Pathways," *Nutrients*, vol. 14, no. 14, p. 2877, 2022.
- [22] W. Gong *et al.*, "The novel STING antagonist H151 ameliorates cisplatin-induced acute kidney injury and mitochondrial dysfunction," *American Journal of Physiology-Renal Physiology*, vol. 320, no. 4, pp. F608-F616, 2021.
- [23] M.-G. Gwon, H. Gu, J. Leem, and K.-K. Park, "Protective effects of 6-Shogaol, an active compound of ginger, in a murine model of cisplatin-induced acute kidney injury," *Molecules*, vol. 26, no. 19, p. 5931, 2021.
- [24] S. Luo *et al.*, " β -Hydroxybutyrate against Cisplatin-Induced acute kidney injury via inhibiting NLRP3 inflammasome and oxidative stress," *International Immunopharmacology*, vol. 111, p. 109101, 2022.
- [25] J. Fan *et al.*, "A novel 3-phenylglutaric acid derivative (84-B10) alleviates cisplatin-induced acute kidney injury by inhibiting mitochondrial oxidative stress-mediated ferroptosis," *Free Radical Biology and Medicine*, vol. 194, pp. 84-98, 2023.
- [26] H. Qi, F. Deng, Y. Wang, H. Zhang, Y. S. Kanwar, and Y. Dai, "Myo-Inositol Supplementation Alleviates Cisplatin-Induced Acute Kidney Injury via Inhibition of Ferroptosis," *Cells*, vol. 12, no. 1, p. 16, 2023.
- [27] İ. İlhan *et al.*, "Irbesartan decreased mitochondrial stress related apoptosis in cisplatin induced acute kidney injury via

- regulating BCL-2/BAX signaling," *Molecular Biology Reports*, pp. 1-9, 2022.
- [28] P. Thongnuanjan *et al.*, "Protective effect of panduratin a on cisplatin-induced apoptosis of human renal proximal tubular cells and acute kidney injury in mice," *Biological and Pharmaceutical Bulletin*, vol. 44, no. 6, pp. 830-837, 2021.
- [29] F. Shahbazi *et al.*, "Effect of silymarin administration on cisplatin nephrotoxicity: report from a pilot, randomized, double-blinded, placebo-controlled clinical trial," *Phytotherapy Research*, vol. 29, no. 7, pp. 1046-1053, 2015.
- [30] G. N. Barber, "STING: infection, inflammation and cancer," *Nature Reviews Immunology*, vol. 15, no. 12, pp. 760-770, 2015.
- [31] F. Gialama and N. Maniadakis, "Comprehensive overview: efficacy, tolerability, and cost-effectiveness of irbesartan," *Vascular Health and Risk Management*, vol. 9, p. 575, 2013.
- [32] C.-y. Fang *et al.*, "Natural products: Potential treatments for cisplatin-induced nephrotoxicity," *Acta Pharmacologica Sinica*, vol. 42, no. 12, pp. 1951-1969, 2021.
- [33] A. Zulli and D. L. Hare, "High dietary methionine plus cholesterol stimulates early atherosclerosis and late fibrous cap development which is associated with a decrease in GRP78 positive plaque cells," *International journal of experimental pathology*, vol. 90, no. 3, pp. 311-320, 2009.
- [34] A. Tacey *et al.*, "The effect of an atherogenic diet and acute hyperglycaemia on endothelial function in rabbits is artery specific," *Nutrients*, vol. 12, no. 7, p. 2108, 2020.
- [35] S. Rai, D. L. Hare, and A. Zulli, "A physiologically relevant atherogenic diet causes severe endothelial dysfunction within 4 weeks in rabbit," *International journal of experimental pathology*, vol. 90, no. 6, pp. 598-604, 2009.
- [36] C. N. Sharp *et al.*, "Repeated administration of low-dose cisplatin in mice induces fibrosis," in *Am J Physiol Renal Physiol*, vol. 310no. 6), 2016, pp. F560-8.

- [37] J. Qi, Q. Xue, L. Kuang, L. Xie, R. Luo, and X. Nie, "Berberine alleviates cisplatin-induced acute kidney injury by regulating mitophagy via PINK 1/Parkin pathway," *Translational andrology and urology*, vol. 9, no. 4, p. 1712, 2020.
- [38] A. Ozkok, K. Ravichandran, Q. Wang, D. Ljubanovic, and C. L. Edelstein, "NF- κ B transcriptional inhibition ameliorates cisplatin-induced acute kidney injury (AKI)," *Toxicology letters*, vol. 240, no. 1, pp. 105-113, 2016.
- [39] R. Z. Tan *et al.*, "Quercetin protects against cisplatin-induced acute kidney injury by inhibiting Mincle/Syk/NF- κ B signaling maintained macrophage inflammation," *Phytotherapy Research*, vol. 34, no. 1, pp. 139-152, 2020.
- [40] L. Graham and J. M. Orenstein, "Processing tissue and cells for transmission electron microscopy in diagnostic pathology and research," *Nature protocols*, vol. 2, no. 10, pp. 2439-2450, 2007.
- [41] M. J. Dykstra, P. C. Mann, M. R. Elwell, and S. V. Ching, "Suggested standard operating procedures (SOPs) for the preparation of electron microscopy samples for toxicology/pathology studies in a GLP environment," *Toxicologic pathology*, vol. 30, no. 6, pp. 735-743, 2002.
- [42] S. Wang, J. Xie, J. Li, F. Liu, X. Wu, and Z. Wang, "Cisplatin suppresses the growth and proliferation of breast and cervical cancer cell lines by inhibiting integrin β 5-mediated glycolysis," (in eng), *Am J Cancer Res*, vol. 6, no. 5, pp. 1108-17, 2016.
- [43] Z. Li, P. Zhang, Q. Ma, D. Wang, and T. Zhou, "Cisplatin-based chemoradiotherapy with 5-fluorouracil or pemetrexed in patients with locally advanced, unresectable esophageal squamous cell carcinoma: A retrospective analysis," in *Mol Clin Oncol*, vol. 6no. 5), 2017, pp. 743-7.
- [44] S. Hussain *et al.*, "A study of split-dose cisplatin-based neoadjuvant chemotherapy in muscle-invasive bladder cancer," *Oncology letters*, vol. 3, no. 4, pp. 855-859, 2012.

- [45] B. A. Chan and J. I. G. Coward, "Chemotherapy advances in small-cell lung cancer," (in eng), *Journal of thoracic disease*, vol. 5 Suppl 5, no. Suppl 5, pp. S565-S578, 2013.
- [46] L. H. EINHORN and J. DONOHUE, "Cis-Diamminedichloroplatinum, Vinblastine, and Bleomycin Combination Chemotherapy in Disseminated Testicular Cancer," *Annals of Internal Medicine*, vol. 87, no. 3, pp. 293-298, 1977.
- [47] A. Brown, S. Kumar, and P. B. Tchounwou, "Cisplatin-based chemotherapy of human cancers," *Journal of cancer science & therapy*, vol. 11, no. 4, 2019.
- [48] A. Yimit, O. Adebali, A. Sancar, and Y. Jiang, "Differential damage and repair of DNA-adducts induced by anti-cancer drug cisplatin across mouse organs," *Nature communications*, vol. 10, no. 1, pp. 1-11, 2019.
- [49] L. P. Rybak, D. Mukherjea, S. Jajoo, and V. Ramkumar, "Cisplatin ototoxicity and protection: clinical and experimental studies," *The Tohoku journal of experimental medicine*, vol. 219, no. 3, pp. 177-186, 2009.
- [50] L. P. Rybak, C. A. Whitworth, D. Mukherjea, and V. Ramkumar, "Mechanisms of cisplatin-induced ototoxicity and prevention," (in eng), *Hear Res*, vol. 226, no. 1-2, pp. 157-67, Apr 2007.
- [51] M. H. Park *et al.*, "Neuropeptide Y improves cisplatin-induced bone marrow dysfunction without blocking chemotherapeutic efficacy in a cancer mouse model," *BMB reports*, vol. 50, no. 8, p. 417, 2017.
- [52] J. Sastry and S. J. Kellie, "Severe neurotoxicity, ototoxicity and nephrotoxicity following high-dose cisplatin and amifostine," *Pediatric hematology and oncology*, vol. 22, no. 5, pp. 441-445, 2005.
- [53] O. Kanat, H. Ertas, and B. Caner, "Platinum-induced neurotoxicity: A review of possible mechanisms," *World journal of clinical oncology*, vol. 8, no. 4, p. 329, 2017.

- [54] S. R. McWhinney, R. M. Goldberg, and H. L. McLeod, "Platinum neurotoxicity pharmacogenetics," *Molecular cancer therapeutics*, vol. 8, no. 1, pp. 10-16, 2009.
- [55] S. Amptoulach and N. Tsavaris, "Neurotoxicity caused by the treatment with platinum analogues," *Chemotherapy research and practice*, vol. 2011, 2011.
- [56] S. Dasari and P. B. Tchounwou, "Cisplatin in cancer therapy: molecular mechanisms of action," (in eng), *European journal of pharmacology*, vol. 740, pp. 364-378, 2014.
- [57] N. Pabla and Z. Dong, "Cisplatin nephrotoxicity: mechanisms and renoprotective strategies," *Kidney international*, vol. 73, no. 9, pp. 994-1007, 2008.
- [58] N. A. G. dos Santos, M. A. C. Rodrigues, N. M. Martins, and A. C. dos Santos, "Cisplatin-induced nephrotoxicity and targets of nephroprotection: an update," *Archives of toxicology*, vol. 86, no. 8, pp. 1233-1250, 2012.
- [59] J. j. Xing *et al.*, "Ginsenoside Rb3 provides protective effects against cisplatin-induced nephrotoxicity via regulation of AMPK-/mTOR-mediated autophagy and inhibition of apoptosis in vitro and in vivo," *Cell proliferation*, p. e12627, 2019.
- [60] J. Hoek *et al.*, "Nephrotoxicity as a Dose-Limiting Factor in a High-Dose Cisplatin-Based Chemoradiotherapy Regimen for Head and Neck Carcinomas," in *Cancers (Basel)*, vol. 8no. 2), 2016.
- [61] X.-j. Mi *et al.*, "The protective effects of maltol on cisplatin-induced nephrotoxicity through the AMPK-mediated PI3K/Akt and p53 signaling pathways," *Scientific Reports*, vol. 8, no. 1, p. 15922, 2018/10/29 2018.
- [62] F. Ashrafi *et al.*, "The Role of Magnesium Supplementation in Cisplatin-induced Nephrotoxicity in a Rat Model: No Nephroprotectant Effect," in *Int J Prev Med*, vol. 3no. 9), 2012, pp. 637-43.
- [63] Y. Qin *et al.*, "cAMP signalling protects proximal tubular epithelial cells from cisplatin-induced apoptosis via

- activation of Epac," *British journal of pharmacology*, vol. 165, no. 4b, pp. 1137-1150, 2012.
- [64] A. Ozkok and C. L. Edelstein, "Pathophysiology of cisplatin-induced acute kidney injury," (in eng), *Biomed Res Int*, vol. 2014, p. 967826, 2014.
- [65] C. N. Sharp, M. A. Doll, J. Megyesi, G. B. Oropilla, L. J. Beverly, and L. J. Siskind, "Subclinical kidney injury induced by repeated cisplatin administration results in progressive chronic kidney disease," *American Journal of Physiology-Renal Physiology*, vol. 315, no. 1, pp. F161-F172, 2018.
- [66] Y. Fu *et al.*, "Chronic effects of repeated low-dose cisplatin treatment in mouse kidneys and renal tubular cells," *American Journal of Physiology-Renal Physiology*, vol. 317, no. 6, pp. F1582-F1592, 2019.
- [67] D. P. Basile, M. D. Anderson, and T. A. Sutton, "Pathophysiology of acute kidney injury," *Comprehensive Physiology*, 2012.
- [68] P. D. Sánchez-González, F. J. López-Hernández, J. M. López-Novoa, and A. I. Morales, "An integrative view of the pathophysiological events leading to cisplatin nephrotoxicity," *Critical reviews in toxicology*, vol. 41, no. 10, pp. 803-821, 2011.
- [69] D. J. Vaughn, S. C. Palmer, J. R. Carver, L. A. Jacobs, and E. R. Mohler, "Cardiovascular risk in long-term survivors of testicular cancer," *Cancer*, vol. 112, no. 9, pp. 1949-1953, 2008.
- [70] J. A. Winston and R. Safirstein, "Reduced renal blood flow in early cisplatin-induced acute renal failure in the rat," (in eng), *Am J Physiol*, vol. 249, no. 4 Pt 2, pp. F490-6, Oct 1985.
- [71] H. Matsushima, K. Yonemura, K. Ohishi, and A. Hishida, "The role of oxygen free radicals in cisplatin-induced acute renal failure in rats," *Journal of Laboratory and Clinical Medicine*, vol. 131, no. 6, pp. 518-526, 1998.

- [72] C. Bagnis *et al.*, "Erythropoietin enhances recovery after cisplatin-induced acute renal failure in the rat," *Nephrology Dialysis Transplantation*, vol. 16, no. 5, pp. 932-938, 2001.
- [73] R. Carroll, "Chapter 11: Renal System and Urinary Tract," *Elsevier's Integrated Physiology*, pp. 117-137, 2007.
- [74] R. Ramanlal and V. Gupta, "Physiology, Vasodilation," 2020.
- [75] V. Asati, D. K. Mahapatra, and S. K. Bharti, "PIM kinase inhibitors: Structural and pharmacological perspectives," *European journal of medicinal chemistry*, vol. 172, pp. 95-108, 2019.
- [76] X. Zhang, M. Song, J. K. Kundu, M.-H. Lee, and Z.-Z. Liu, "PIM kinase as an executional target in cancer," *Journal of Cancer Prevention*, vol. 23, no. 3, p. 109, 2018.
- [77] S. Renard *et al.*, "Pim-1: a new biomarker in pulmonary arterial hypertension," *Pulmonary circulation*, vol. 3, no. 1, pp. 74-81, 2013.
- [78] Y. Tursynbay *et al.*, "Pim-1 kinase as cancer drug target: an update," *Biomedical reports*, vol. 4, no. 2, pp. 140-146, 2016.
- [79] Z. Wang *et al.*, "Pim-1: a serine/threonine kinase with a role in cell survival, proliferation, differentiation and tumorigenesis," *Journal of veterinary science*, vol. 2, no. 3, pp. 167-179, 2001.
- [80] Y.-J. Ha *et al.*, "PIM-1 kinase is a novel regulator of proinflammatory cytokine-mediated responses in rheumatoid arthritis fibroblast-like synoviocytes," *Rheumatology*, vol. 58, no. 1, pp. 154-164, 2019.
- [81] G. A. Borillo *et al.*, "Pim-1 kinase protects mitochondrial integrity in cardiomyocytes," *Circulation research*, vol. 106, no. 7, pp. 1265-1274, 2010.
- [82] R. F. Fan *et al.*, "PIM-1 kinase inhibitor SMI-4a exerts antitumor effects in chronic myeloid leukemia cells by enhancing the activity of glycogen synthase kinase 3 β ," *Molecular Medicine Reports*, vol. 16, no. 4, pp. 4603-4612, 2017.

- [83] R. PAULIN, J. MELOCHE, A. COURBOULIN, C. LAMBERT, E. DUMAS DE LA ROQUE, and S. BONNET, "Pim-1 Reverses Both Human And Experimental Pulmonary Arterial Hypertension," in *C18. NOVEL INSIGHTS INTO THE PATHOGENESIS OF PULMONARY ARTERIAL HYPERTENSION*: American Thoracic Society, 2010, pp. A4024-A4024.
- [84] R. Fu *et al.*, "Pim-1 as a therapeutic target in lupus nephritis," *Arthritis & Rheumatology*, vol. 71, no. 8, pp. 1308-1318, 2019.
- [85] R. Paulin *et al.*, "Signal transducers and activators of transcription-3/pim1 axis plays a critical role in the pathogenesis of human pulmonary arterial hypertension," *Circulation*, vol. 123, no. 11, pp. 1205-1215, 2011.
- [86] R. Paulin, J. Meloche, M. H. Jacob, M. Bissierier, A. Courboulin, and S. Bonnet, "Dehydroepiandrosterone inhibits the Src/STAT3 constitutive activation in pulmonary arterial hypertension," *American Journal of Physiology-Heart and Circulatory Physiology*, vol. 301, no. 5, pp. H1798-H1809, 2011.
- [87] W. Wieling, R. D. Thijs, N. Van Dijk, A. A. Wilde, D. G. Benditt, and J. G. Van Dijk, "Symptoms and signs of syncope: a review of the link between physiology and clinical clues," *Brain*, vol. 132, no. 10, pp. 2630-2642, 2009.
- [88] O. F. P. dos Santos, M. A. Boim, E. J. Barros, and N. Schor, "Role of platelet activating factor in gentamicin and cisplatin nephrotoxicity," *Kidney international*, vol. 40, no. 4, pp. 742-747, 1991.
- [89] T. Wallerath *et al.*, "Resveratrol, a polyphenolic phytoalexin present in red wine, enhances expression and activity of endothelial nitric oxide synthase," *Circulation*, vol. 106, no. 13, pp. 1652-1658, 2002.
- [90] K. L. Gordish and W. H. Beierwaltes, "Resveratrol induces acute endothelium-dependent renal vasodilation mediated through nitric oxide and reactive oxygen species

- scavenging," *American Journal of Physiology-Renal Physiology*, vol. 306, no. 5, pp. F542-F550, 2014.
- [91] J.-L. Hsu *et al.*, "Pim-1 knockdown potentiates paclitaxel-induced apoptosis in human hormone-refractory prostate cancers through inhibition of NHEJ DNA repair," *Cancer letters*, vol. 319, no. 2, pp. 214-222, 2012.
- [92] P.-G. Li, L. Sun, X. Han, S. Ling, W.-t. Gan, and J.-W. Xu, "Quercetin induces rapid eNOS phosphorylation and vasodilation by an Akt-independent and PKA-dependent mechanism," *Pharmacology*, vol. 89, no. 3-4, pp. 220-228, 2012.
- [93] M. Chen *et al.*, "Pim1 kinase promotes angiogenesis through phosphorylation of endothelial nitric oxide synthase at Ser-633," *Cardiovascular Research*, vol. 109, no. 1, pp. 141-150, 2016.
- [94] D. H. Kim *et al.*, "SIRT1 activation by resveratrol ameliorates cisplatin-induced renal injury through deacetylation of p53," *American Journal of Physiology-Renal Physiology*, vol. 301, no. 2, pp. F427-F435, 2011.
- [95] O. F. Pavão dos Santos, M. A. Boim, E. J. Barros, E. Pirotzky, P. Braquet, and N. Schor, "Effect of platelet-activating factor antagonist BN 52063 on the nephrotoxicity of cisplatin," *Lipids*, vol. 26, no. 12Part2, pp. 1324-1328, 1991.
- [96] T. Kitazono, F. M. Faraci, H. Taguchi, and D. D. Heistad, "Role of potassium channels in cerebral blood vessels," *Stroke*, vol. 26, no. 9, pp. 1713-1723, 1995.
- [97] A. A. Quyyumi and M. Ozkor, "Vasodilation by hyperpolarization: beyond NO," vol. 48, ed: Am Heart Assoc, 2006, pp. 1023-1025.
- [98] P. M. Price *et al.*, "Dependence of cisplatin-induced cell death in vitro and in vivo on cyclin-dependent kinase 2," *Journal of the American Society of Nephrology*, vol. 17, no. 9, pp. 2434-2442, 2006.
- [99] A. C. Cameron *et al.*, "Comprehensive characterization of the vascular effects of cisplatin-based chemotherapy in

- patients with testicular cancer," *Cardio Oncology*, vol. 2, no. 3, pp. 443-455, 2020.
- [100] H. Cardinal, M. Dieudé, and M.-J. Hébert, "Endothelial dysfunction in kidney transplantation," *Frontiers in Immunology*, vol. 9, p. 1130, 2018.
- [101] P. Maione *et al.*, "Treating advanced non-small cell lung cancer in the elderly," *Therapeutic advances in medical oncology*, vol. 2, no. 4, pp. 251-260, 2010.
- [102] R. I. Feldman *et al.*, "Novel small molecule inhibitors of 3-phosphoinositide-dependent kinase-1," *Journal of Biological Chemistry*, vol. 280, no. 20, pp. 19867-19874, 2005.
- [103] S. Maegawa *et al.*, "Phosphoinositide-dependent protein kinase 1 is a potential novel therapeutic target in mantle cell lymphoma," *Experimental Hematology*, vol. 59, pp. 72-81. e2, 2018.
- [104] Y. Chinen *et al.*, "3-Phosphoinositide-Dependent Protein Kinase 1 (PDPK1) Is a Pivotal Cell Signaling Mediator in Multiple Myeloma," *Blood*, vol. 124, no. 21, p. 4728, 2014.
- [105] Y. Bai *et al.*, "Effects of inhibiting PDK-1 expression in bone marrow mesenchymal stem cells on osteoblast differentiation in vitro," *Molecular medicine reports*, vol. 23, no. 2, pp. 1-1, 2021.
- [106] D. S. Weber, L. M. Sullivan, J. R. Bennett, and C. McCarthy, "Activation of PDK1 mediates VSMC migration and may contribute to vascular remodeling following injury," ed: Wiley Online Library, 2013.
- [107] E. M. Sturm *et al.*, "Phosphoinositide-dependent protein kinase 1 (PDK1) mediates potent inhibitory effects on eosinophils," *European journal of immunology*, vol. 45, no. 5, pp. 1548-1559, 2015.
- [108] R. Di, Z. Yang, P. Xu, and Y. Xu, "Silencing PDK1 limits hypoxia-induced pulmonary arterial hypertension in mice via the Akt/p70S6K signaling pathway," (in eng), *Experimental and therapeutic medicine*, vol. 18, no. 1, pp. 699-704, 2019.

- [109] A. Perez *et al.*, "The flavonoid quercetin induces acute vasodilator effects in healthy volunteers: Correlation with beta-glucuronidase activity," *Pharmacological research*, vol. 89, pp. 11-18, 2014.
- [110] L. I. Brueggemann, A. R. Mackie, B. K. Mani, L. L. Cribbs, and K. L. Byron, "Differential effects of selective cyclooxygenase-2 inhibitors on vascular smooth muscle ion channels may account for differences in cardiovascular risk profiles," *Molecular pharmacology*, vol. 76, no. 5, pp. 1053-1061, 2009.
- [111] D. Zhang *et al.*, "Protein kinase C δ suppresses autophagy to induce kidney cell apoptosis in cisplatin nephrotoxicity," *Journal of the American Society of Nephrology*, vol. 28, no. 4, pp. 1131-1144, 2017.
- [112] B. R. Webster *et al.*, "Phosphoinositide-dependent kinase-1 and protein kinase C δ contribute to endothelin-1 constriction and elevated blood pressure in intermittent hypoxia," *Journal of Pharmacology and Experimental Therapeutics*, vol. 344, no. 1, pp. 68-76, 2013.
- [113] H. Pan, Z. Motawe, J. Breslin, and S. Wickline, "Preservation of vasculature is beneficial in mitigating cisplatin induced acute kidney injury," *European Heart Journal*, vol. 43, no. Supplement_2, p. ehac544. 3017, 2022.
- [114] L. K. Gadanec *et al.*, "Diminazene aceturate uses different pathways to induce relaxation in healthy and atherogenic blood vessels," *Biochemical Pharmacology*, p. 115397, 2022.
- [115] T. Kobayashi, K. Taguchi, S. Nemoto, T. Nogami, T. Matsumoto, and K. Kamata, "Activation of the PDK-1/Akt/eNOS pathway involved in aortic endothelial function differs between hyperinsulinemic and insulin-deficient diabetic rats," *American Journal of Physiology-Heart and Circulatory Physiology*, vol. 297, no. 5, pp. H1767-H1775, 2009.
- [116] R. L. Edwards, T. Lyon, S. E. Litwin, A. Rabovsky, J. D. Symons, and T. Jalili, "Quercetin reduces blood pressure in

- hypertensive subjects," *The Journal of nutrition*, vol. 137, no. 11, pp. 2405-2411, 2007.
- [117] O. Dagher, P. Mury, N. Thorin-Trescases, P. E. Noly, E. Thorin, and M. Carrier, "Therapeutic potential of quercetin to alleviate endothelial dysfunction in age-related cardiovascular diseases," *Frontiers in Cardiovascular Medicine*, vol. 8, p. 658400, 2021.
- [118] L.-w. Lehman, M. Saeed, G. Moody, and R. Mark, "Hypotension as a risk factor for acute kidney injury in ICU patients," in *2010 Computing in Cardiology*, 2010, pp. 1095-1098: IEEE.
- [119] C. Ching, D. Gustafson, P. Thavendiranathan, and J. E. Fish, "Cancer therapy-related cardiac dysfunction: is endothelial dysfunction at the heart of the matter?," *Clinical Science*, vol. 135, no. 12, pp. 1487-1503, 2021.
- [120] C. E. Van Skike and V. Galvan, "A perfect sTORm: the role of the mammalian target of rapamycin (mTOR) in cerebrovascular dysfunction of Alzheimer's disease: a mini-review," *Gerontology*, vol. 64, no. 3, pp. 205-211, 2018.
- [121] Y.-J. Jin *et al.*, "Protein kinase N2 mediates flow-induced endothelial NOS activation and vascular tone regulation," *The Journal of clinical investigation*, vol. 131, no. 21, 2021.
- [122] T.-Y. Yuan *et al.*, "Vasorelaxant effect of quercetin on cerebral basilar artery in vitro and the underlying mechanisms study," *Journal of Asian natural products research*, vol. 20, no. 5, pp. 477-487, 2018.
- [123] J. E. Brayden, J. M. Quayle, N. B. Standen, and M. T. Nelson, "Role of potassium channels in the vascular response to endogenous and pharmacological vasodilators," *Journal of Vascular Research*, vol. 28, no. 1-3, pp. 147-153, 1991.
- [124] F. Niere and K. F. Raab-Graham, "mTORC1 is a local, postsynaptic voltage sensor regulated by positive and negative feedback pathways," *Frontiers in cellular neuroscience*, vol. 11, p. 152, 2017.

- [125] N. S. Kirkby *et al.*, "Cyclooxygenase-2 selectively controls renal blood flow through a novel PPAR β / δ -dependent vasodilator pathway," *Hypertension*, vol. 71, no. 2, pp. 297-305, 2018.
- [126] M. E. Widlansky *et al.*, "Short-and long-term COX-2 inhibition reverses endothelial dysfunction in patients with hypertension," *Hypertension*, vol. 42, no. 3, pp. 310-315, 2003.
- [127] M. Perše, "Cisplatin mouse models: treatment, toxicity and translatability," *Biomedicines*, vol. 9, no. 10, p. 1406, 2021.
- [128] P. Sainamthip, S. Saichaemchan, B. Satirapoj, and N. Prasongsook, "The Effect of Intravenous Mannitol Combined With Normal Saline in Preventing Cisplatin-Induced Nephrotoxicity: A Randomized, Double-Blind, Placebo-Controlled Trial," *JCO Global Oncology*, vol. 8, p. e2100275, 2022.
- [129] D. J. Crona, A. Faso, T. F. Nishijima, K. A. McGraw, M. D. Galsky, and M. I. Milowsky, "A systematic review of strategies to prevent cisplatin-induced nephrotoxicity," *The oncologist*, vol. 22, no. 5, pp. 609-619, 2017.
- [130] Y. Jiang *et al.*, "Effects of cisplatin on the contractile function of thoracic aorta of Sprague-Dawley rats," *Biomedical reports*, vol. 2, no. 6, pp. 893-897, 2014.
- [131] W. K. Han, V. Bailly, R. Abichandani, R. Thadhani, and J. V. Bonventre, "Kidney Injury Molecule-1 (KIM-1): a novel biomarker for human renal proximal tubule injury," *Kidney international*, vol. 62, no. 1, pp. 237-244, 2002.
- [132] D. M. Tanase *et al.*, "The predictive role of the biomarker kidney molecule-1 (KIM-1) in acute kidney injury (AKI) cisplatin-induced nephrotoxicity," *International journal of molecular sciences*, vol. 20, no. 20, p. 5238, 2019.
- [133] D. O'hanlon, H. Fitzsimons, J. Lynch, S. Tormey, C. Malone, and H. Given, "Soluble adhesion molecules (E-selectin, ICAM-1 and VCAM-1) in breast carcinoma," *European Journal of Cancer*, vol. 38, no. 17, pp. 2252-2257, 2002.

- [134] B. Humanes *et al.*, "Cisplatin-induced renal inflammation is ameliorated by cilastatin nephroprotection," *Nephrology Dialysis Transplantation*, vol. 32, no. 10, pp. 1645-1655, 2017.
- [135] J.-Y. Kim, J. Jo, J. Leem, and K.-K. Park, "Kahweol ameliorates cisplatin-induced acute kidney injury through pleiotropic effects in mice," *Biomedicines*, vol. 8, no. 12, p. 572, 2020.
- [136] E. Bahar, J.-Y. Kim, H.-S. Kim, and H. Yoon, "Establishment of acquired cisplatin resistance in ovarian cancer cell lines characterized by enriched metastatic properties with increased twist expression," *International Journal of Molecular Sciences*, vol. 21, no. 20, p. 7613, 2020.
- [137] M. Wang, S. Wey, Y. Zhang, R. Ye, and A. S. Lee, "Role of the unfolded protein response regulator GRP78/BiP in development, cancer, and neurological disorders," *Antioxidants & redox signaling*, vol. 11, no. 9, pp. 2307-2316, 2009.
- [138] R. V. M. Manalo and P. M. B. Medina, "The endoplasmic reticulum stress response in disease pathogenesis and pathophysiology," *Egyptian Journal of Medical Human Genetics*, vol. 19, no. 2, pp. 59-68, 2018.
- [139] H. T. Idriss and J. H. Naismith, "TNF α and the TNF receptor superfamily: Structure-function relationship (s)," *Microscopy research and technique*, vol. 50, no. 3, pp. 184-195, 2000.
- [140] S. Malik, K. Suchal, N. Gamad, A. K. Dinda, D. S. Arya, and J. Bhatia, "Telmisartan ameliorates cisplatin-induced nephrotoxicity by inhibiting MAPK mediated inflammation and apoptosis," *European journal of pharmacology*, vol. 748, pp. 54-60, 2015.
- [141] A. Hosoda *et al.*, "Telmisartan Exacerbates Cisplatin-Induced Nephrotoxicity in a Mouse Model," *Biological and Pharmaceutical Bulletin*, vol. 43, no. 9, pp. 1331-1337, 2020.
- [142] I. O. Sherif, L. A. Al-Mutabagani, A. M. Alnakhli, M. A. Sobh, and H. E. Mohammed, "Renoprotective effects of angiotensin receptor blocker and stem cells in acute kidney

- injury: involvement of inflammatory and apoptotic markers," *Experimental Biology and Medicine*, vol. 240, no. 12, pp. 1572-1579, 2015.
- [143] S. Okui *et al.*, "Cisplatin-induced acute renal failure in mice is mediated by chymase-activated angiotensin-aldosterone system and interleukin-18," *European journal of pharmacology*, vol. 685, no. 1-3, pp. 149-155, 2012.
- [144] Y. Chai *et al.*, "Dexmedetomidine alleviates cisplatin-induced acute kidney injury by attenuating endoplasmic reticulum stress-induced apoptosis via the α 2AR/PI3K/AKT pathway," *Molecular medicine reports*, vol. 21, no. 3, pp. 1597-1605, 2020.
- [145] M. Zhu, J. Chen, H. Yin, H. Jiang, M. Wen, and C. Miao, "Propofol protects human umbilical vein endothelial cells from cisplatin-induced injury," *Vascular pharmacology*, vol. 61, no. 2-3, pp. 72-79, 2014.
- [146] J. H. Fountain and S. L. Lappin, "Physiology, renin angiotensin system," 2017.
- [147] C. Liu *et al.*, "Increased AT1 receptor expression mediates vasoconstriction leading to hypertension in Snx1^{-/-} mice," *Hypertension Research*, vol. 44, no. 8, pp. 906-917, 2021.
- [148] N. Tanaka *et al.*, "Cis-dichlorodiammineplatinum Upregulates Angiotensin II Type 1 Receptors through Reactive Oxygen Species Generation and Enhances VEGF Production in Bladder Cancer CDDP Upregulates AT1R and Enhances VEGF Production," *Molecular cancer therapeutics*, vol. 9, no. 11, pp. 2982-2992, 2010.
- [149] A. Dehghani, S. Saberi, and M. Nematbakhsh, "Cisplatin-induced nephrotoxicity alters blood pressure response to angiotensin II administration in rats," *Advanced biomedical research*, vol. 5, 2016.
- [150] J. M. Garcia *et al.*, "Inhibition of cisplatin-induced lipid catabolism and weight loss by ghrelin in male mice," *Endocrinology*, vol. 154, no. 9, pp. 3118-3129, 2013.

- [151] M. A. Perazella, S. G. Coca, M. Kanbay, U. C. Brewster, and C. R. Parikh, "Diagnostic value of urine microscopy for differential diagnosis of acute kidney injury in hospitalized patients," *Clinical Journal of the American Society of Nephrology*, vol. 3, no. 6, pp. 1615-1619, 2008.
- [152] M. Yu *et al.*, "Cisplatin up-regulates ICAM-1 expression in endothelial cell via a NF- κ B dependent pathway," vol. 99, no. 2, pp. 391-397, 2008.
- [153] J. C. Oates, D. L. Russell, and J. P. Van Beusecum, "Endothelial cells: potential novel regulators of renal inflammation," *American Journal of Physiology-Renal Physiology*, vol. 322, no. 3, pp. F309-F321, 2022.
- [154] S. Ma *et al.*, "E-selectin-targeting delivery of microRNAs by microparticles ameliorates endothelial inflammation and atherosclerosis," *Scientific reports*, vol. 6, no. 1, pp. 1-11, 2016.
- [155] A. Almeida *et al.*, "Nephroprotective effect of exercise training in cisplatin-induced renal damage in mice: influence of training protocol," *Brazilian Journal of Medical and Biological Research*, vol. 55, 2022.
- [156] J. M. Wagner and L. M. Karnitz, "Cisplatin-induced DNA damage activates replication checkpoint signaling components that differentially affect tumor cell survival," *Molecular pharmacology*, vol. 76, no. 1, pp. 208-214, 2009.
- [157] M. Yanishi and H. Kinoshita, "Urinary L-type fatty acid-binding protein is a predictor of cisplatin-induced acute kidney injury," *BMC nephrology*, vol. 23, no. 1, pp. 1-6, 2022.
- [158] K. R. McMahon *et al.*, "Epidemiologic characteristics of acute kidney injury during cisplatin infusions in children treated for cancer," *JAMA network open*, vol. 3, no. 5, pp. e203639-e203639, 2020.
- [159] B. Kloo *et al.*, "Critical role of PI3K signaling for NF- κ B-dependent survival in a subset of activated B-cell-like diffuse large B-cell lymphoma cells," *Proceedings of the*

- National Academy of Sciences*, vol. 108, no. 1, pp. 272-277, 2011.
- [160] M. J. Hossen, J. Y. Cho, and D. Kim, "PDK1 in NF- κ B signaling is a target of *Xanthium strumarium* methanolic extract-mediated anti-inflammatory activities," *Journal of Ethnopharmacology*, vol. 190, pp. 251-260, 2016.
- [161] T. Liu, L. Zhang, D. Joo, and S.-C. Sun, "NF- κ B signaling in inflammation," *Signal transduction and targeted therapy*, vol. 2, no. 1, pp. 1-9, 2017.
- [162] S. Arico *et al.*, "Celecoxib induces apoptosis by inhibiting 3-phosphoinositide-dependent protein kinase-1 activity in the human colon cancer HT-29 cell line," *Journal of Biological Chemistry*, vol. 277, no. 31, pp. 27613-27621, 2002.
- [163] G. M. Suddek, A. E. El-Kenawi, A. Abdel-Aziz, and H. A. El-Kashef, "Celecoxib, a selective cyclooxygenase-2 inhibitor, attenuates renal injury in a rat model of cisplatin-induced nephrotoxicity," *Chemotherapy*, vol. 57, no. 4, pp. 321-326, 2011.
- [164] C. Dangelmaier, B. K. Manne, E. Liverani, J. Jin, P. Bray, and S. P. Kunapuli, "PDK1 selectively phosphorylates Thr (308) on Akt and contributes to human platelet functional responses," *Thrombosis and haemostasis*, vol. 112, no. 03, pp. 508-517, 2014.
- [165] C. H. Jung, M. Seo, N. M. Otto, and D.-H. Kim, "ULK1 inhibits the kinase activity of mTORC1 and cell proliferation," *Autophagy*, vol. 7, no. 10, pp. 1212-1221, 2011.
- [166] K. Airiau, F. Mahon, M. Josselin, M. Jeanneteau, and F. Belloc, "PI3K/mTOR pathway inhibitors sensitize chronic myeloid leukemia stem cells to nilotinib and restore the response of progenitors to nilotinib in the presence of stem cell factor," *Cell death & disease*, vol. 4, no. 10, pp. e827-e827, 2013.
- [167] Y. Tanihara, S. Masuda, T. Katsura, and K.-i. Inui, "Protective effect of concomitant administration of imatinib on cisplatin-induced nephrotoxicity focusing on renal organic

- cation transporter OCT2," *Biochemical pharmacology*, vol. 78, no. 9, pp. 1263-1271, 2009.
- [168] X. Zhao *et al.*, "Glomerular expression of kidney injury molecule-1 and podocytopenia in diabetic glomerulopathy," *American journal of nephrology*, vol. 34, no. 3, pp. 268-280, 2011.
- [169] S.-J. Hwang *et al.*, "Circulating adhesion molecules VCAM-1, ICAM-1, and E-selectin in carotid atherosclerosis and incident coronary heart disease cases: the Atherosclerosis Risk In Communities (ARIC) study," *Circulation*, vol. 96, no. 12, pp. 4219-4225, 1997.
- [170] C. Raimondi and M. Falasca, "Targeting PDK1 in cancer," *Current medicinal chemistry*, vol. 18, no. 18, pp. 2763-2769, 2011.
- [171] R. Fang *et al.*, "PDK 1/Akt/PDE 4D axis identified as a target for asthma remedy synergistic with β 2 AR agonists by a natural agent arctigenin," *Allergy*, vol. 70, no. 12, pp. 1622-1632, 2015.
- [172] P. Vanhoutte, H. Shimokawa, M. Feletou, and E. Tang, "Endothelial dysfunction and vascular disease—a 30th anniversary update," *Acta physiologica*, vol. 219, no. 1, pp. 22-96, 2017.
- [173] J. W. Wright, S. Mizutani, and J. W. Harding, "Pathways involved in the transition from hypertension to hypertrophy to heart failure. Treatment strategies," *Heart failure reviews*, vol. 13, no. 3, pp. 367-375, 2008.
- [174] A. Sacerdote *et al.*, "Effects of chronic treatment with losartan on blood pressure, endothelin-like immunoreactivity and nitric oxide in normotensive rats," *Journal of hypertension*, vol. 13, no. 12 Pt 2, pp. 1670-1673, 1995.
- [175] S. Saleh, A. A. Ain-Shoka, E. El-Demerdash, and M. M. Khalef, "Protective effects of the angiotensin II receptor blocker losartan on cisplatin-induced kidney injury," *Chemotherapy*, vol. 55, no. 6, pp. 399-406, 2009.

- [176] J. Zhang *et al.*, "Competing actions of type 1 angiotensin II receptors expressed on T lymphocytes and kidney epithelium during cisplatin-induced AKI," *Journal of the American Society of Nephrology*, vol. 27, no. 8, pp. 2257-2264, 2016.
- [177] Y. Zhao *et al.*, "Role of PI3K in the Progression and Regression of Atherosclerosis," *Frontiers in Pharmacology*, vol. 12, p. 632378, 2021.
- [178] N. Li, J. Chen, P. Wang, H. Fan, S. Hou, and Y. Gong, "Major signaling pathways and key mediators of macrophages in acute kidney injury," *Molecular medicine reports*, vol. 23, no. 6, pp. 1-12, 2021.
- [179] L. Zhou *et al.*, "Glycoprotein non-metastatic melanoma protein b (Gpnmb) is highly expressed in macrophages of acute injured kidney and promotes M2 macrophages polarization," *Cellular immunology*, vol. 316, pp. 53-60, 2017.
- [180] X. Qian, E. Mills, M. Torgov, W. J. LaRochelle, and M. Jeffers, "Pharmacologically enhanced expression of GPNMB increases the sensitivity of melanoma cells to the CR011-vcMMAE antibody-drug conjugate," *Molecular oncology*, vol. 2, no. 1, pp. 81-93, 2008.
- [181] A. Panday, M. K. Sahoo, D. Osorio, and S. Batra, "NADPH oxidases: an overview from structure to innate immunity-associated pathologies," *Cellular & molecular immunology*, vol. 12, no. 1, pp. 5-23, 2015.
- [182] X.-M. Meng *et al.*, "NADPH oxidase 4 promotes cisplatin-induced acute kidney injury via ROS-mediated programmed cell death and inflammation," *Laboratory Investigation*, vol. 98, no. 1, p. 63, 2018.
- [183] J. Jo, J.-Y. Kim, and J. Leem, "Protective Effects of Orexin A in a Murine Model of Cisplatin-Induced Acute Kidney Injury," *Journal of Clinical Medicine*, vol. 11, no. 23, p. 7196, 2022.
- [184] H. Mu *et al.*, "Ursolic acid prevents doxorubicin-induced cardiac toxicity in mice through eNOS activation and

- inhibition of eNOS uncoupling," *Journal of cellular and molecular medicine*, vol. 23, no. 3, pp. 2174-2183, 2019.
- [185] Q. D. Zhao *et al.*, "NADPH oxidase 4 induces cardiac fibrosis and hypertrophy through activating Akt/mTOR and NFκB signaling pathways," *Circulation*, vol. 131, no. 7, pp. 643-655, 2015.
- [186] W. Jiang, Y. Chen, X. Song, Y. Shao, Z. Ning, and W. Gu, "Pim-1 inhibitor SMI-4a suppresses tumor growth in non-small cell lung cancer via PI3K/AKT/mTOR pathway," *OncoTargets and therapy*, vol. 12, p. 3043, 2019.
- [187] OECD, *Test No. 425: Acute Oral Toxicity: Up-and-Down Procedure*. 2022.
- [188] R. Oun, Y. E. Moussa, and N. J. Wheate, "The side effects of platinum-based chemotherapy drugs: a review for chemists," *Dalton transactions*, vol. 47, no. 19, pp. 6645-6653, 2018.
- [189] M. A. Lawlor *et al.*, "Essential role of PDK1 in regulating cell size and development in mice," *The EMBO journal*, vol. 21, no. 14, pp. 3728-3738, 2002.
- [190] D. A. Guertin *et al.*, "Ablation in mice of the mTORC components raptor, rictor, or mLST8 reveals that mTORC2 is required for signaling to Akt-FOXO and PKCα, but not S6K1," *Developmental cell*, vol. 11, no. 6, pp. 859-871, 2006.
- [191] J. Czogalla, F. Schweda, and J. Loffing, "The mouse isolated perfused kidney technique," *JoVE (Journal of Visualized Experiments)*, no. 117, p. e54712, 2016.

Appendix A: Establishing the method- Renal Perfusion

The role of the vascular network in the development of CIAKI is in its infancy [113]. CDDP treatment is associated with reduced renal blood flow and increased vascular resistance, contributing to reduced GFR. Currently, understanding the functional capacity of renal microvasculature is unknown, particularly pre-clinically. Abdominal aorta and iliac arteries were harvested from CDDP-treated mice and assessed for vascular function. Isolation of mouse renal microvasculature (interlobar arteries) for isometric tension analysis was a technical limitation of this study and therefore stimulated the development of this method as a determinant of renal microvascular function. Abdominal aorta and iliac arteries, anatomically closest to the renal arteries, were used in isometric tension studies to help understand the renal vascular involvement in CIAKI (Chapters 5 and 6). The Zulli laboratory developed the system in (Figure A1) during my candidature. This system measured fluid pressure changes to determine the resistance-pressure relationship of kidneys in response to CDDP treatment. This appendix describes the processes undertaken to establish a method for renal perfusion.



Figure A1. Renal perfusion setup with a graphical representation of the mouse. The main key features in the setup include **A.** KREBS/Drug well, **B.** tubes perfusing KREBS A to kidney, **C.** peristaltic pump, **D.** pressure sensor, **E.** microtube inserted into thoracic aorta and towards the renal artery, and **F.** heated plate maintained at 37°C.

Initially, different internal tube diameters (1.27 x 0.97, 2.5 x 1.5 and 0.7x 3mm) were tested to determine variations in the time taken for fluid to reach the beginning and end

of the system and pressure readings. The dead volume (tubing volume) was calculated by filling the tubing with KREBS from the pump pinch rotor to the end of tube E. The expelled liquid was collected and measured to determine the total volume of the tubing. This is important for measuring total volume for pressure calculations.

To determine the effect of the addition of drugs, the time was measured from the addition of drugs to KREBS (well A) to the endpoint of tube E by using food colouring. Therefore, a response will not be immediately seen in the real-time trace after the addition of drugs.

Once these two values were identified, we then altered the motor settings of the peristaltic pump using the software developed by (Zultek Engineering, Melbourne, Australia). By altering both the RPM and the step delay, the pressures were adjusted to read 10mmHg.

Once connected, the pressure rose to 80mmHg (only one kidney was evaluated for pressure). During the dissection period, the abdominal aorta was tied using a suture string and cut off as close to the left renal artery as possible. Then right renal, suprarenal, superior mesenteric and celiac arteries were tied as close to the abdominal aorta as possible (Figure A2).

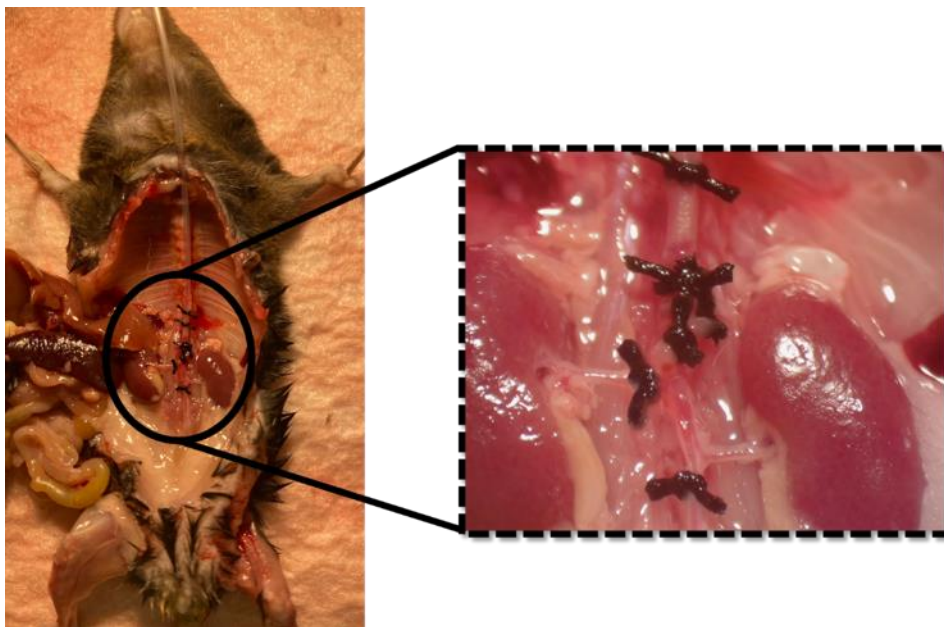


Figure A2. Illustration of the suture placement and tubing location to prepare the animal for renal perfusion. These sutures are tied to inhibit fluid leakage from any aortic branches that would impact the pressure readings.

Once vessels were securely sutured, a small flexible tube with a similar external diameter (0.8mm) to the internal aorta diameter was inserted into the highest point of the thoracic aorta. The tubing was cut at an angle to ease feeding into the aorta. It was imperative to go slowly and be gentle as the sharp point of the tubing could easily puncture the aortic wall. The tubing was then secured with sutures tied around the aorta to hold the tube in place and to prevent any backflow around the tubing.

After this, the software was run, and a baseline pressure was recorded at around 20-30mmHg. It was necessary for the pressure reading not to be excessive as a baseline. The recorded reading is as close to the kidney as possible, however does not account for the reduced lumen diameter inside the kidney and, thus, the increased pressure. If the baseline readings were high, the interlobar arterial pressure would be even more significant again, increasing the risk of vessel rupture. Once a stable baseline reading was observed, U46619 (2×10^{-5} [M]) was added to the perfusion solution to initiate constriction. As determined earlier, a time was calculated for us to expect to see the constriction response on the software. Figure A3 shows the tracing software and a visual representation of an actual graph obtained in this study. After the U46619 response, once the pressure had stabilised, the kidney was infused with 10^{-5} [M] BX (the dose that induced the best vasodilatory response identified in Chapter 4). This enabled us to see the direct effect of BX on changes in blood pressure.

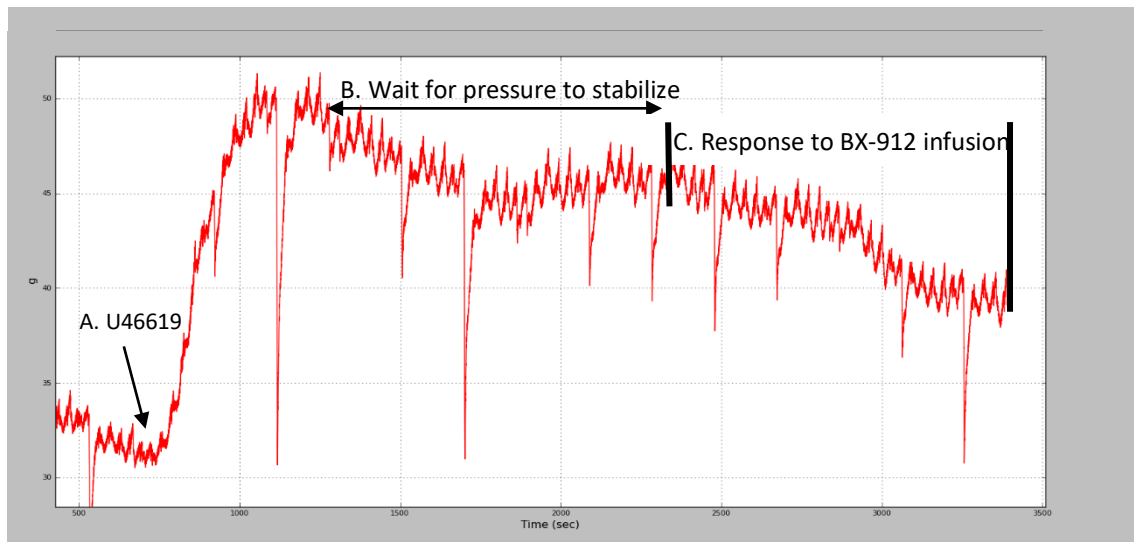


Figure A3. Real-time reading using MediDaq software to view the response of BX in the kidney. The figure above represents a real-time reading of infusion A. Administration of the vasoconstrictor U46619 B. Period to allow the vessel to stabilise and plateau, C. DRC response to infusion of BX.

Benefits of this study

Perfecting this model will enable a more clinically relevant assessment of renal function for models of CIAKI. Although vascular function can be inferred without removing interlobar arteries and subjecting them to vascular function studies (which proved too technically challenging for this study), it is impossible to confirm that AA and ILA are functionally the same. This study enables proximity to the kidney pressure assessment.

Challenges faced.

The continual challenge that repeatedly arose during the development of this model was leakage in the system resulting in impaired pressure readings by the sensor. Food colouring was added to the perfusing solution to allow for easier identification of any leakage and enable rectification. However, the leaking could not be stopped. Interestingly, Czogalla et al. published a study providing a detailed *ex vivo* protocol for renal perfusion [191]. This is a significantly more complex setup involving total isolation of the kidney from the mouse and placed into a temperature-regulated fluid solution. They cannulate multiple aspects of the renal circuit, including the ureter and veins.

Conclusion

This system is a new development from our laboratory, and refining the methodology is necessary. Further refinements in the perfusion pump may also eliminate potential vascular rupture caused by high pressure in the microvasculature. This is an important method that could help elucidate the role of the renal vascular network in the pathogenesis of CIAKI.

Appendix B: Genes unaffected by BX-912 administration in RT² profiler PCR experiments in Chapter 6

Below is the list of genes that were not affected compared to cisplatin in RT² profiler PCR experiments. These genes were outside the 2-fold parameters and did not obtain statistical significance.

Genes unaffected by administration of BX-912 0.05mg/kg compared to CDDP in kidneys			
A2m	Cst3	Gpx8	Odc1
Aass	Ctss	Gstk1	Rgn
Abcc2	Cxcl10	Havcr1	Rtn4
Aldh1a1	Cxcl3	Hmox1	Scd1
Angptl4	Cyp2c54	Hsp90aa1	Slc22a1
Anxa5	Cyp2d22	Idh1	Socs3
Atf3	Ccn1	Igfbp1	Sod2
Bhmt	Egf	Igfbp3	Sod3
Bmp1	Fgb	Ipmk	Spp1
Btg2	Fmo2	Klk1	Sprr1a
Cat	Fn1	Lgals3	Timp1
Ccnd1	Gadd45a	Mcm6	Tmsb10
Ccng1	Gamt	Mgp	Tnfrsf12a
Ccs	Gatm	Mt1	Uchl1
Cd44	Gc	Nphs2	Ugt1a1
Cdkn1a	Ghr	Nqo1	Vim
Cp	Glul	Oat	